NASA CR 135313
PWA - 5543

HIGH FREQUENCY DYNAMIC ENGINE SIMULATION

By J. A. Schuerman, K. E. Fischer, and P. W. McLaughlin

UNITED TECHNOLOGIES CORPORATION
Pratt & Whitney Aircraft Group
Commercial Products Division
East Hartford, Connecticut 06108

Prepared for

NATIONAL AERONAUTICS AND SPACE ADMINISTRATION
NASA Lewis Research Center
Contract NAS3-20292

NASA CR 135313
PWA - 5543

HIGH FREQUENCY DYNAMIC ENGINE SIMULATION

By J. A. Schuerman, K. E. Fischer, and P. W. McLaughlin

UNITED TECHNOLOGIES CORPORATION
Pratt & Whitney Aircraft Group
Commercial Products Division
East Hartford, Connecticut 06108

Prepared for

NATIONAL AERONAUTICS AND SPACE ADMINISTRATION
NASA Lewis Research Center
Contract NAS3-20292

1. Report No.	2. Government Accession No.	3. Recipient's Catalog No.
NASA CR-135313		

4. Title and Subtitle	5. Report Date
High Frequency Dynamic Engine Simulation	July 1977
	6. Performing Organization Code

7. Author(s)	8. Performing Organization Report No.
J. A. Schuerman K. E. Fischer P. W. McLaughlin	PWA-5543
	10. Work Unit No.

9. Performing Organization Name and Address	11. Contract or Grant No.
UNITED TECHNOLOGIES CORPORATION Pratt & Whitney Aircraft Group Commercial Products Division East Hartford, Connecticut 06108	NAS3-20292
	13. Type of Report and Period Covered
12. Sponsoring Agency Name and Address	Contractor Report
National Aeronautics and Space Administration Washington, D. C. 20546	14. Sponsoring Agency Code

15. Supplementary Notes

16. Abstract

A digital computer simulation of a mixed flow, twin spool turbofan engine was assembled to evaluate and improve the dynamic characteristics of the engine simulation to disturbance frequencies of at least 100 Hz. One dimensional forms of the dynamic mass, momentum and energy equations were used to model the engine. A TF30 engine was simulated so that dynamic characteristics could be evaluated against results obtained from testing of the TF30 engine at the NASA Lewis Research Center. Dynamic characteristics of the engine simulation were improved by modifying the compression system model. Modifications to the compression system model were established by investigating the influence of size and number of finite dynamic elements.

Based on the results of this program, high frequency engine simulations using finite dynamic elements can be assembled so that the engine dynamic configuration is optimum with respect to dynamic characteristics and computer execution time. Resizing of the compression system finite elements improved the dynamic characteristics of the engine simulation but showed that additional refinements are required to obtain close agreement between simulation and actual engine dynamic characteristics.

17. Key Words (Suggested by Author(s))	18. Distribution Statement
Turbofan Digital Dynamic Simulation Frequency Response Transient Response Stability Limits Dynamic Element Sizing	

19. Security Classif. (of this report)	20. Security Classif. (of this page)	21. No. of Pages	22. Price*

* For sale by the National Technical Information Service, Springfield, Virginia 22151

FOREWORD

This program was prepared for the National Aeronautics and Space Administration, Lewis Research Center, under Contract NAS3-20292 to assemble and refine a gas turbine engine simulation program. Mr. Carl Daniele was the NASA Program Manager for this effort. Mr. J. A. Schuerman served as Program Manager for Pratt & Whitney Aircraft assisted by Messrs. K. E. Fischer and P. W. McLaughlin.

This report was prepared under the Contractor's reference no. PWA-5543.

TABLE OF CONTENTS

TABLE OF CONTENTS (Cont'd)

LIST OF ILLUSTRATIONS

LIST OF ILLUSTRATIONS (Cont'd)

LIST OF ILLUSTRATIONS (Cont'd)

LIST OF ILLUSTRATIONS (Cont'd)

SUMMARY

A program was conducted under NASA Contract NAS3-20292 to investigate techniques for simulating and evaluating the dynamic characteristics of a mixed flow turbofan engine. A digital computer was used to simulate the engine which was modeled using one dimensional forms of the dynamic mass, momentum, and energy equations and the dynamic response to planar disturbances was evaluated. The TF30 engine was simulated to allow comparison of dynamic characteristics to results obtained from testing of the TF30 engine at the NASA-Lewis Research Center. During these tests, the engine was subjected to planar inlet pressure disturbances which were induced by the NASA-Lewis developed air jet system.

The simulation techniques investigated during this program concentrated on improving the dynamic characteristics of the engine simulation through modification of the compression system model. Improvement of the simulation dynamic characteristics was approached in three steps: First, a baseline engine simulation using overall component performance characteristics and dynamic elements sized to the lengths of the major compression system components was assembled, and the simulation dynamic characteristics were established. During the process of establishing the simulation dynamic characteristics, the importance of the dynamic energy equation was assessed. Second, a separate simulation of the compression system was assembled using blade and vane row performance characteristics. Six dynamic configurations of the compression system were formulated by combining the row performance characteristics to form dynamic elements composed of compressor stages or stage groups. The dynamic characteristics and computer run time were established and an optimum dynamic configuration was selected on the basis of comparison to the dynamic characteristics and computer run time associated with a stage-by-stage simulation. Computer run time improvements associated with algorithms for prediction of the program iterative solutions were also investigated using the optimum dynamic configuration of the compression system. Third, the engine simulation was modified by incorporating the optimum compression system. The dynamic characteristics of the modified engine simulation were then evaluated for improvements associated with modifications to the compression system model.

Three tests were employed to evaluate the dynamic characteristics of the simulations. These were tests of the simulation frequency response (gain and phase versus frequency), transient response (pressure versus time), and limits of system stability. Each of these were used to evaluate one simulation versus another and/or to evaluate the simulations versus test results.

Three methods were used to calculate simulation frequency response and consisted of 1) transfer function, 2) step response, and 3) discrete frequency methods. The transfer function method was different from the other two in the respect that state variables were used to describe the simulation by a high order system of linear differential equations. Solution of the differential equations established the transfer functions describing the frequency response characteristics. The step response and discrete frequency methods employed analysis of the simulation input and output transients to arrive at frequency response characteristics.

The significant results obtained in this study included the following:

- The reduced order analysis of the compression system simulation showed that at 100 Hz, the dynamic characteristic of a stage-by-stage simulation could be obtained with a more simplified dynamic configuration while realizing substantial savings in computer execution time. The analysis showed that the dynamic elements should be uniformly sized to achieve the best frequency response.

- The engine simulation with the modification to the compression system showed improved frequency response characteristics above 50 Hz.

- The transfer function provided better resolution of the high frequency response of the simulation than the transient methods.

- Coupling of the fan bypass and core dynamics has a potentially significant effect on core stream transient operation.

- Stability limits of the modified engine simulation were twice that shown by engine test results.

The results of this program highlight the need to further develop the engine simulation to achieve closer agreement with actual engine dynamic characteristics.

INTRODUCTION

Gas turbine manufacturers must produce engines which operate stably during normal use. During normal operation, the engine is exposed to time variant operating conditions such as gas generator power transients, augmentor transients, and inlet distortion which can potentially produce compression system surge/stall. The equivalent dynamic frequency of these time variant operating conditions can range from less than one to thousands of Hertz. Engine response to the time variant conditions is dependent on the coupled dynamic characteristics of the assembled system of engine components which in turn affects stability.

To maximize the stability of a developed engine, it is necessary to assess engine stability characteristics during the design stage. To accomplish this, reliable analytical capability is required. Computer programs which simulate the low frequency dynamics of engine power transients are being used successfully in support of the design process. In contrast, dynamic simulation of engine operation in a high frequency environment such as time variant inlet distortion, is not as reliable. As a result, the engine design criteria for stability are primarily derived from past experience and established within the framework of uncoupled component characteristics. The earliest that stability of the engine as a dynamic system can be evaluated is during the development stage. Since the cost of the instrumentation and tests is often high, the testing is usually of limited scope, and as a result, the impact on the engine design is minimal.

Simulation of engine dynamics can be achieved using analog, digital or hybrid (analog plus digital) computers. The analog approach provides continuous transient results with a minimum of implementation effort, while requiring large, complex and expensive computing systems whose reliability and accuracy decreases with the size of the program. Digital computation provides the capability to model large systems with a high degree of precision at the expense of computer run time and increased implementation complexity. Hybrid systems have been formulated to simultaneously exploit the advantages of analog and digital computers. In recent years, improved simulation techniques coupled with faster digital processors have made digital simulation of high frequency engine transients the most practical alternative available.

During the years 1970 - 1974, under contract to the Air Force, Pratt & Whitney Aircraft assembled a digital dynamic simulation of the TF30 engine and investigated its dynamic characteristics. As reported in Vol. II of AFAPL-TR-74-107, the simulation used only the mass equation in dynamic form and modeled the compression system using one dynamic element for each compression system component. Evaluation of the simulation dynamics revealed that modifications to the compression system simulation were required to improve the core stream dynamic characteristics. Stage-by-stage modeling of the compression system was suggested as approach for improving the core dynamic characteristics, but was not tried in the engine simulation because of limitations imposed at that time by computer size and run time.

The work discussed in this report has used the improved computational capabilities of the digital computer to further investigate dynamic engine simulations. The objective of the work was to assemble a digital computer simulation of a mixed flow, twin spool turbofan engine and

evaluate the dynamic characteristics of the engine. The goal of the work was to improve the dynamic characteristic of the simulation to disturbance frequencies of at least 100 Hz by modifying the compression system simulation. The engine was modeled using one dimensional forms of the dynamic mass momentum and energy equations and response to planar disturbances was evaluated. The TF30 engine was simulated so that dynamic characteristics could be evaluated against results obtained from testing of the TF30 engine at the NASA Lewis Research Center. During these tests, the engine was subjected to planar inlet pressure disturbances induced by the air jet system developed by the Lewis Research Center.

A three step approach was used in working toward the goal of improving dynamic characteristics of the engine simulation. First, a baseline engine simulation was assembled using dynamic elements sized on the order of the compression system component lengths and the dynamic characteristics established. Second, a separate compression system simulation was assembled by adding dynamics to the compression system simulation used for the distortion modeling of the TF30-P-3 compression system reported in NASA CR-135124. The dynamic element sizing of the simulation was varied by combining compressor row performance characteristics to establish a configuration which produced dynamic characteristics similar to a stage by stage simulation, while minimizing the computer computation time. Third, the engine simulation was modified by introducing the compression system simulation established in the second step. The dynamic characteristics of the modified engine simulation were then reevaluated for improvements. The analysis of simulation dynamics was performed in each of the three steps at engine operating conditions of approximately 8600 and 7600 rpm corrected low spool speed ($N1/\sqrt{\theta_{T2.0}}$).

ENGINE SIMULATION

NASA LEWIS TESTS OF ENGINE DYNAMICS

A TF30-P-3 engine was tested by the NASA Lewis Research Center to investigate engine dynamics. The results obtained from the NASA program were used to evaluate the dynamic characteristics of the engine simulation. Tests were performed in an altitude chamber using the Lewis Research Center developed air jet system described in ref. 1, which induced dynamic pressure conditions at the engine face. The average inlet conditions for the test produced a Reynolds number index of 0.5 at an inlet pressure of 5.07 to 5.45 N/CM^2 abs (7.35 to 7.90 psia). The engine exhaust pressure was set at 1.66 N/CM^2 abs (2.4 psia). As illustrated in Figure 1, high response total pressure instrumentation was installed at the engine inlet (station 2.0), fan first stator passage (station 2.1), fan core stream discharge (station 2.3), fan bypass stream discharge (station 2.3F), low compressor discharge (station 3.0), twelfth stage stator passage (station 3.12) and high compressor discharge (station 4.0).

A portion of the NASA test program was devoted to investigation of the engine dynamic response to spatially uniform (planar) periodic pressure disturbances induced at the engine inlet. By using a frequency sweep test technique described in reference 1, gain and phase characteristics of response to the engine inlet pressure were established for total pressures at the internal engine stations 2.3, 2.3F, 3.0 and 4.0. Gain and phase characteristics acquired at engine power conditions of approximately 8600 and 7600 low spool corrected speed ($N1/\sqrt{\theta_{T2.0}}$) were used for comparison to the dynamic characteristics of the baseline and modified engine simulations. These operating conditions are referred to as OP1 and OP2 respectively, in this report. Engine stability limits were also investigated under the NASA test program. During these tests, discrete frequency inlet pressure oscillations were induced and amplitude was increased until either engine stall/surge was encountered or the amplitude limits of the air jet system were reached. Results of these tests in terms of $P_{T2.0}$ amplitude at stall/surge were used for comparison to the stability limits of the modified engine simulation at approximately 8600 $N1/\sqrt{\theta_{T2.0}}$.

SIMULATION SYSTEM

Pratt & Whitney Aircraft has developed an engine simulation system identified as SOAPP (State of the Art Performance Program). The purpose of the system was to provide the capability to assemble simulations of new engine configurations with simple commands to the system. To implement the system, basic thermodynamic programs were written for each major engine component i. e. compressor, burner, turbine, etc. and filed in a computer library. A second library was also written to file the specific performance characteristics of each component of every engine model. As a result, the simulation system was formulated on a modular concept which provides the flexibility to simulate operation of any configuration of engine (turbojet, turbofan, etc.) or its components (compressors, turbines, ducts, etc.). The system also includes an input/output structure which allows definition of the simulation boundary conditions. The SOAPP system was used to assemble the three simulations discussed in this report.

Baseline Dynamic Engine Simulation

The first step to improving engine simulation dynamic characteristics included assembly of a baseline engine simulation and definition of the dynamic characteristics. The purpose of this step was to establish a baseline of dynamic characteristics against which the influence of compression system model modifications could be assessed. The discussion which follows provides a comparative description of the TF30 engine and the configuration of the baseline engine simulation. This is followed by an evaluation of the importance of the energy equation to simulation dynamic characteristics. This discussion is concluded with a description of the dynamic characteristics derived from the simulation.

Configuration

The TF30-P-3 is a twin spool augmented, turbofan engine which mixes bypass and core gas flows in the afterburner duct. The low pressure spool is composed of a three stage fan and six stage low pressure compressor driven by a three stage turbine. The high pressure spool is composed of a seven stage high pressure compressor driven by a one stage air-cooled turbine. The combustor is a can type surrounded by a secondary chamber which uses high compressor discharge air to cool the burner cans, and dilute the fuel-air mixture. Surge bleeds are incorporated at the seventh and twelfth stages of the compression system.

The dynamic configuration assembled for the baseline engine simulation is compared to a side view of the engine in Figure 2. The configuration is composed of twenty dynamic elements sized on the order of the length dimensions of the major compression system components (i. e. fan, low compressor, high compressor). To achieve the length similarity, the high and low pressure turbines were combined into a single dynamic element, while the fan discharge and afterburner ducts were subdivided into a total of 12 elements. The subdivision of the afterburner duct included separation of the bypass and core gas streams. The main burner was represented by two parallel elements which separated the primary burning and secondary cooling airflows.

The afterburner duct bypass and core flow streams were separated to accomodate the dynamic mixing calculations investigated under the Air Force Contract reported in Vol. II of AFAPL-TR-47-107. The calculation assumes that during transients, the inertial and viscous characteristics of the gas flow induce a lag in the equalization of static pressures in the bypass and core streams. The calculation allows a pressure imbalance to occur during transients and equalizes the pressures during steady state operation. During transients the pressure imbalance changes the flow areas in a direction to equalize the static pressures.

Appendix A describes the methods used to calculate dynamic operation of the modified engine simulation assembled for the third step of this analysis. With the exception of the compression system, the component performance characteristics described in Appendix are the same for the baseline simulation; therefore only the compression system characteristics are described at this point of the discussion.

The performance characteristics of the low and high compressor are defined by the curves illustrated in Figures 3 and 4 which show the compressor inlet corrected airflow and temperature rise correlated with component inlet corrected speed and $\overline{m}$. As illustrated in Figure 5, the $\overline{m}$ values identify lines of constant slope on a standard pressure ratio versus corrected airflow map. The values of m are calculated from the equation

$$\overline{m} = \frac{PR - C_{PR}}{WAC - C_{WAC}} \qquad (1)$$

where

PR = pressure ratio

WAC = corrected inlet flow

C_{PR} and C_{WAC} = the pressure ratio and airflow at the intersection of all $\overline{m}$ lines

The $\overline{m}$ line method of defining maps is used to accomodate the regions of the compressor map where constant speed characteristics are either vertical or horizontal.

The performance of the fan bypass stream was defined in the same $\overline{m}$ line format as the low and high compressors. Total inlet corrected airflow, and bypass stream temperature rise ($\Delta T_T/T_{T\ BYPASS}$) were used to define curves in the format of Figures 3 and 4 respectively. The fan core stream pressure ratio (PR_{CORE}) and temperature ratio (TR_{CORE}) were described as illustrated in Figures 6 and 7 respectively.

Dynamic Energy Equation

Prior to establishing the dynamic characteristics of the baseline engine simulation, the influence of the dynamic energy equation on simulation transient characteristics was investigated. The analysis was made to determine if the energy equation was required, in addition to the dynamic mass and momentum equations, to define the dynamic characteristics of the baseline simulation. To assess the role of the energy equation, two transient test cases were computed for a step increase in engine inlet pressure. In one case only the dynamic mass and momentum equations were used; the second case used dynamic mass, momentum, and energy equations.

The results of the two test cases are illustrated on Figure 8. The figure shows the inlet pressure step ($P_{T2.0}$) and the pressure and temperature at the fan duct discharge station (7.0F) plotted versus time. Comparison of the two cases shows that without the energy equation, the $P_{T2.0}$ step induced an initial decrease in the duct pressure and temperature which was immediately propagated over the period of the first computed time step (DT = .001 seconds). This result was dictated by the fan map characteristics. During the first time step of the transient (.001 seconds), the fan pressure ratio and consequently temperature ratio were reduced. The reduced temperature ratio in turn lowered the fan discharge temperature because the inlet temperature to the engine was held constant during the transient. In the absence of the energy equation, the reduced fan discharge temperature was instantaneously propagated to station 7.0F in the fan duct. Solution of the gas state equation at station 7.0F required a reduction in the pressure level in the presence of the reduced temperature. During subsequent

time steps, increased airflow and pressure levels induced by the step in inlet pressure were propagated through the fan ducts and caused the pressure and temperature rise at station 7.0F.

The case which included the energy equation showed that a 0.003 to 0.004 second time period elapsed before the fan duct discharge pressure and temperature responded; this compared to an estimated propagation time of approximately 0.005 seconds based on sonic velocity, airflow velocity and length of the duct. The initial change in pressure and temperature were in an increasing direction as expected. This result was attributable to inclusion of the energy equation which transported the fan discharge temperature changes through the duct at essentially the airflow velocity. On the basis of this comparison, the energy equation was included in the simulation to achieve the most realistic dynamic characteristics.

Dynamic Characteristics

The dynamic characteristics of the baseline simulation were established in two formats. First, gain and phase plots were defined for response to $P_{T2.0}$ of the total pressures at station 2.3, 2.3F, 3.0 and 4.0. The gain and phase characteristics were compared to similar results from the NASA TF30/air jet testing. Second, pressure time traces were defined for stations 2.3, 2.3F, 3.0 and 4.0 for a step input of $P_{T2.0}$ and fuel flow. These were later used for comparison to the modified engine simulation.

The frequency response, i. e. gain and phase versus frequency of the simulation was evaluated by three methods: transfer functions, direct analysis of the $P_{T2.0}$ step transient response, and amplitude and phase analysis of response to discrete frequency $P_{T2.0}$ sine waves. The capability for all of these analytical methods was consolidated into the engine simulation and could be activated via input.

The transfer function was the first method used for computing response characteristics. This method was implemented by combining a state variable definition of the engine with the routines of Seidel reported in reference 2. As described in reference 3., the state variable method provides a linear description of a system using first order differential equations of the form.

$$\dot{x}(t) = Ax(t) + Bu(t) \text{ where} \qquad (2)$$

x = state vector

u = input vector

A = system matrix

B = input matrix

The system output is described by

$$y(t) = Cx(t) + Du(t) \text{ where} \qquad (3)$$

y = output vector

C = output matrix

D = output/input direct coupling matrix

The matrices in the above expressions consist of partial derivatives which are determined from the simulation by finite differences. Each state and input variable was perturbed individually with all others held constant.

The state variables used for the baseline simulation were the mass, momentum, and energy of each dynamic element, core exhaust area for dynamic mixing and fuel flow for the engine fuel control. The input variable was $P_{T2.0}$ and the output variables were $P_{T2.3}$, $P_{T2.3F}$, $P_{T3.0}$ and $P_{T4.0}$. Formulation of these variables resulted in matrices of the following form for a 62nd order system.

$$A = \begin{vmatrix} \frac{\partial \dot{x}_1}{\partial x_1} & \cdots & \frac{\partial \dot{x}_1}{\partial x_{62}} \\ \vdots & & \vdots \\ \frac{\partial \dot{x}_{62}}{\partial x_1} & \cdots & \frac{\partial \dot{x}_{62}}{\partial x_{62}} \end{vmatrix} \qquad B = \begin{vmatrix} \frac{\partial \dot{x}_1}{\partial u_1} \\ \vdots \\ \frac{\partial \dot{x}_{62}}{\partial u_1} \end{vmatrix} \qquad (4)$$

$$C = \begin{vmatrix} \frac{\partial y_1}{\partial x_1} & \cdots & \frac{\partial y_1}{\partial x_{62}} \\ \vdots & & \vdots \\ \frac{\partial y_4}{\partial x_1} & \cdots & \frac{\partial y_4}{\partial x_{62}} \end{vmatrix} \qquad D = \begin{vmatrix} \frac{\partial y_1}{\partial u_1} \\ \vdots \\ \frac{\partial y_4}{\partial u_1} \end{vmatrix}$$

Using the computer routines of Seidel which were furnished by the NASA Lewis Research Center and reported in reference 2, the matrix algebra was performed for simultaneous solution of equations (2) and (3) to define the transfer functions $\frac{y(t)}{u(t)}$. The resulting gain and phase characteristics of the simulation were obtained from the transfer functions.

The second method for defining simulation frequency response used the pressure versus time characteristics computed for the $P_{T2.0}$ step transient. Using the methods of Levy reported in reference 4 the gain and phase were computed directly from the time response of $P_{T2.3}$, $P_{T2.3F}$, $P_{T3.0}$ and $P_{T4.0}$.

The third method for deriving gain and phase characteristics used direct analysis of a transient induced with discrete frequency sinusoidal $P_{T2.0}$ waves. As illustrated in Figure 9, direct measurement of the input ($P_{T2.0}$) and output ($P_{T2.3}$, $P_{T2.3F}$, $P_{T3.0}$ and $P_{T4.0}$) wave amplitudes and output lag were made from the pressure time traces of the transient. A half wave amplitude of approximately 0.25% $P_{T2.0}$ was used for input and produced smoothly defined output sine waves. The simulation transient was run for a period of time which insured that stabilized output wave amplitudes and lags were reached. The ratio of output over input amplitudes was calculated to define gain, and the lag time was converted to phase angle.

Gain and phase response characteristics were computed for the baseline engine simulation at conditions OP1 and OP2. The average absolute inlet and exhaust pressures were set at 5.34 N/cm^2 (7.75 psia) and 1.65 N/cm^2 (2.4 psia), respectively, at condition OP1 to simulate the conditions of the NASA engine tests. At condition OP2 the inlet and exhaust pressures were 5.44 N/cm^2 (7.89 psia) and 1.65 N/cm^2 (2.4 psia).

The response characteristics derived at OP1 using the three methods discussed above are shown on Figures 10 through 17 and are compared to the engine test results. The gain levels were normalized to steady state compression ratio and plotted in units of decibels versus input frequency in units of Hertz. Phase was plotted in units of degrees versus frequency. Figure 10 shows the gain response of $P_{T4.0}$ to $P_{T2.0}$. The gain levels derived by the transfer function and step response methods are shown over the range of 0.1 to 200 Hz. Gain for the discrete frequency cases are shown as points at 20, 35, 54, 73, and 100 Hz. The gain levels computed by the discrete frequency wave and step response analyses of the induced transients show good agreement. Gain levels computed by the transfer function method were on the order of 1 to 2 db higher than the levels derived from the transients at frequencies up to 50 Hz; at higher frequencies the levels diverged. Comparison of the simulation gain levels to the engine data shows good agreement to 10 Hz, with the simulation levels significantly higher above 10 Hz.

The phase response of $P_{T4.0}$ to $P_{T2.0}$ is shown for the simulation and engine test data on Figure 11. The phase angles computed from induced $P_{T2.0}$ transients (step and discrete frequency) formed a band of results which was up to 30° wide at frequencies up to 100 Hz. The transfer function phase levels were to the lower side of the band in close agreement with discrete frequency results. Comparison to test data shows good agreement (~ 15° Δ phase) up to 10 Hz. Above 10 Hz, the simulation and test data begin to show significant divergence.

Figures 12 through 15 show the gain and phase response for the remaining core flow stations 2.3 and 3.0 at condition OP1. These curves shows results similar to station 4.0. Simulation gain levels determined by the three analytical methods are in close agreement at frequencies up to 50 Hz and in close agreement with test data up to 10-20 Hz. Simulation phase characteristics show banded results to 100 Hz and significant deviation from test data at frequencies above 20 Hz.

The gain characteristics of the simulation and test data at the fan discharge station 2.3F are illustrated in Figure 16 for condition OP1. The simulation gain characteristics computed by all three methods are in good agreement up to a frequency of 65 Hz. All methods predict a response peak at approximately 35 Hz which is close to the 36.6 Hz equivalent frequency estimated for downstream plus return propagation of a pressure disturbance in the fan ducts.

Above 65 Hz, the transfer function method computes response peaks at approximately 74, 118 and 188 Hz which are close to the 36.6 Hz first, second, and fourth harmonics of 73.2, 109.8 and 183 Hz. In contrast, the gains computed from the step and discrete frequency transients show only slight resolution of a peak at 74 Hz and complete attenuation of higher order peaks. The engine data shown in Figure 16 shows response peaks at approximately 32 Hz and 82 Hz. Data was defined to only 100 Hz and it is therefore not known if other peaks would be resolved above this frequency. The close correspondence of the test peaks at 32 and 82 Hz to the estimated equivalent propagation frequency of 36.6 and the first harmonic frequency of 73.2 Hz led to the conclusion that the data was showing a dominating influence of the fan duct dynamics. Comparison of the simulation results to the test data indicated that the transfer function method gave a better description of the actual predominant fan discharge dynamics than was shown by transient computations.

The station 2.3F phase characteristics of the simulation and test data at condition OP1 are shown in Figure 17. As in the case of the core stations, the simulation phase characteristics computed from inlet pressure transients gave a band of results which showed a spread of up to 35° at 100 Hz. The phase derived from transfer functions again fell along the bottom of the band in good agreement with the discrete frequency transients. The transfer function and step transient methods predicted phase peaks at approximately 25 and 62 Hz, however, peak attenuation was again in evidence by 62 Hz. Phase peaks were not identified from the discrete frequency results. It is expected that the phase peaks would not be resolved by additional discrete frequency cases, but would show the smoothing demonstrated by the step transient results above 35 Hz. This expectation is based on the good agreement of the gain levels predicted by the two methods as shown on Figure 16, plus past experience which has shown similar results from both methods. The engine test data and simulation predictions showed good agreement at the 25 Hz peak. Above 40 Hz divergence of engine and simulation characteristics occurred with the second phase peak of the test data occurring at approximately 90 Hz, compared to 62 Hz for the simulation. At condition OP2 simulation gain and phase characteristics were generated using only the transfer function and step response methods. The simulation characteristics are compared to the engine test data on Figures 18 through 25. The results obtained at OP2 generally agreed with the findings at OP1.

In addition to the gain and phase characteristics derived at OP1 and OP2, pressure and rotor speed versus time plots were generated for inlet pressure and fuel flow step transients. The results of these cases are not discussed here because they were used to support the analysis of the compression system simulation and modified engine simulation.

On the basis of the results obtained from the baseline engine simulation, the following conclusions were reached at this point of analysis.

1. Dynamic mass, momentun and energy equations should be used in high frequency engine simulations.

2. Gain characteristics obtained by the transfer function method were representative of simulation transient dynamics at frequencies up to 50 Hz.

3. Phase characteristics obtained from transfer functions were representative of simulation transient results to 100 Hz.

4. The transient method is better than the discrete frequency method of deriving gain and phase characteristics from simulation transients because full sweep information is provided.

5. Simulation core stream response characteristics were representative of the engine at frequencies between 0 and 10-20 Hz.

6. Simulation fan stream response characteristics were representative of the engine at frequencies between 0 and 40-65 Hz.

7. Frequency response results confirmed the need to construct a better simulation of the core airstream.

Modified Compression System Simulation

The second step toward improving the dynamic characteristics of the engine simulation was concentrated on modifying the compression system model. The modification was based on the past experience gained from the Air Force sponsored program. These investigations suggested that stage-by-stage modeling of the compression system should be implemented to improve engine simulation dynamic response in the engine core airstream. The potential for exceeding available computer storage and introducing excessively long run time requirements was recognized as a drawback to implementing a stage-by-stage model.

On the basis of the Air Force studies, modifications to the compression system model were performed within the framework of a separate compression system simulation. Due to the absence of other engine components, the system dynamics were different from the engine, and the data acquired from NASA engine tests could not easily be used as a basis for assessing modifications; instead, a stage-by-stage simulation was assembled and used to establish a basis for assessing modifications.

Modification of the compression system simulation was approached in three steps. First, a stage-by-stage simulation of the fan, low and high compressors was assembled by combining row performance characteristics to create a dynamic element for each stage. The dynamic characteristics and computer run time were then defined at conditions OP1 and OP2. Second, five reduced order simulations were assembled by combining stages to reduce the number of dynamic elements. The dynamic characteristics and computer run times of the reduced order models were compared to the stage-by-stage results to select a configuration for further evaluation in the engine simulation. Third, a further reduction in computer run time was investigated by evaluating four algorithms for prediction of program iterative solutions.

The discussion which follows presents a description of the stage-by-stage simulation and its dynamic characteristics. The reduced order compression system models are then described and followed by a comparative discussion of the dynamic characteristics and run time requirements of the reduced order and stage-by-stage models. The discussion is concluded with a presentation of the predictor algorithm investigation.

Stage-by Stage Simulation

The stage-by-stage simulation was assembled by adding finite element dynamics to the compression system simulation used for the circumferential distortion modeling of the TF30-P-3 as reported in NASA CR-135124. The dynamic configuration is illustrated in Figure 26. Key features of the model included use of rotor and stator row performance characteristics, accounting of bypass ratio effects on radial streamline bending in the fan and airflow separation off of the flow splitter at the low compressor entrance, and use of unsteady aerodynamic effects on airfoil loss characteristics. Due to the absence of other engine com ponents downstream of the compression system, choked nozzles were used to terminate both the core and bypass streams of the simulation. A brief description of the implementation of these effects is provided here and supported with further details in Appendix A.

The steady state performance was described by characteristics of Φ, ψ, and λ. The performance characteristics were derived from rig tests of the compression system and smoothed for data errors. The rotor and stator row static pressure rise map was described by Φ and ψ where

$$\Phi = \frac{W_a\sqrt{\theta_T}}{\delta_T A} \quad \frac{(N/\sqrt{\theta_T})}{(N/\sqrt{\theta_T})}\ \text{DESIGN} \tag{5}$$

$$\psi = \frac{\Delta P_S}{P_S} \left[\frac{(N/\sqrt{\theta_T})\ \text{DESIGN}}{(N/\sqrt{\theta_T})}\right]^2 \tag{6}$$

$$\lambda = \frac{\Delta T_T}{T_T} \left[\frac{(N/\sqrt{\theta_T})\ \text{DESIGN}}{(N/\sqrt{\theta_T})}\right]^2 \tag{7}$$

The total pressure required for calculation of Φ and the static pressure in ψ were related by

$$P_T = P_S\left(1.0 + \frac{\gamma - 1.0}{2.0} M^2\right)^{\frac{\gamma}{\gamma - 1}} \tag{8}$$

The effects of bypass ratio variations on the flow properties of the fan and low compressor were accounted for in the simulation and are illustrated in Figure 27. The location of the streamline dividing the bypass and core airflows is shown for operating conditions of high and low bypass ratio. Under conditions of high bypass, the streamline is located toward the fan hub at the plane of the inlet guide vanes. As flow procedes through the fan toward the splitter, the streamline bends radially in the direction of the fan tip and stagnates on the splitter. At conditions of low bypass ratio, the dividing streamline starts toward the fan tip

at the IGV plane and bends radially toward the hub as the splitter is approached. When the bypass ratio is sufficiently low, the core flow separates from the drooped leading edge of the splitter and reduces the effective flow area through the core stream third stator.

The bypass ratio effects are accounted for in the simulation in three ways. First, the splitting streamline location in the IGV through rotor 3 are computed assuming constant airflow per unit area through the fan. Second, the rotor 3 map ψ values are modified for effects of radial streamline bending. Third, core stator 3 flow area, inlet flow angle, map ψ value, and static pressure are modified to account for effects of flow separation at the splitter.

Unsteady aerodynamic effects were incorporated to account for the deviations from quasi-steady lift characteristics that an airfoil exhibits in a transient flow environment. Airflow separation from an airfoil (stall) occurs at large incidence angles and requires a finite period of time to propogate to the trailing edge. The effect on airfoil performance is shown in Figure 28. The difference in airfoil lift coefficient translates in to deviations in blade and vane loss characteristics for compressor operation as illustrated in Figure 29. The net effect on compressor operation is to effectively modify the compressor map characteristics in a high frequency operating environment. The unsteady effects were incorporated into the compression system simulation as described in Appendix A.

Stage-by-Stage Dynamic Characteristics

The dynamic characteristics of the stage by stage compression system were established for the high compressor discharge station (4.0). Gain and phase plots and pressure-time histories for a step in inlet pressure were defined for $P_{T4.0}$. Both the transfer function and step response methods were used to establish the gain and phase characteristics.

Figures 30 and 31 show gain and phase plots for the simulation at condition OP1. The gain characteristics defined by the transfer function and step response methods are shown in Figure 30 to agree closely up to 120 Hz, beyond which the results diverge. Figure 31 shows good agreement in phase to 200 Hz with no more than 20° spread between the two methods. Figures 32 and 33 show the OP2 gain and phase characteristics derived by the two methods to be in close agreement to 200 Hz. On the basis of the results, the gain and phase characteristics derived by the transfer function method was concluded to be representative of simulation transients to frequencies of at least 120 Hz. The transfer function method was selected for gain and phase evaluation of the reduced order models because the method appeared to give better resolution of fan high frequency response characteristics in the baseline engine simulation. The pressure-time histories of response to the step in inlet pressure are shown and discussed with results from the reduced order simulations.

Description Of Reduced Order Compression System Simulations

Five reduced order compression system simulations were assembled and evaluated for the potential of reducing computer runtime while retaining the dynamic characteristics of the stage-by-stage simulation. Each of the reduced order simulations used the row performance characteristics, and bypass ratio effects implemented in the stage-by-stage model. The reduced order configurations were established by combining the compressor row performance characteristics into dynamic elements to form stage groups within a single finite element.

The configurations of the five reduced order simulations are summarized in Table I. The five configurations were identified as: 1) fan/low/high lumped, 2) ten similarly sized elements, 3) bleed, 4) fan lumped/compressors staged, and 5) fan staged/compressors lumped.

The configurations fell into two categories; the first 3 configurations resulted in dynamic elements of essentially similar length while the last two resulted in dissimilar lengths. Each of the dynamic configurations is illustrated in Figures 34 through 38, where the dynamic stage groupings are shown as a function of the cumulative length of the compression system. Dynamic element sizing was necessarily constrained by the dimensions of each compressor stage.

Reduced Order Dynamic Characteristics

The dynamic characteristics of each reduced order simulation were evaluated on the basis of gain and phase plots derived by the transfer function method and pressure-time response to a step in inlet pressure ($P_{T2.0}$). Dynamics of the high pressure compressor discharge pressure ($P_{T4.0}$) were evaluated on each basis. The computer execution time for each case was also established to assess the trade-off between dynamic characteristics and computer run time.

The gain and phase characteristics derived from the five reduced order simulations are compared to the stage-by-stage results on Figures 39 through 42. Results at condition OP1 are shown on Figures 39 and 40; results at OP2 are shown on Figures 41 and 42. In general, these figures show that as the order of the simulation is reduced, the gain and phase angle at constant frequency is decreased.

Since the frequency responses of all the reduced order models are similar, it is difficult to determine which one should be used. In order to obtain a qualitative measure of the dynamics of the reduced order models, the gain and phase curves of Figures 39 through 42 were cross-plotted at 100 Hz. Figure 43 shows the deviation from the stage-by-stage simulation gain level in units of decibels plotted as a function of the number of simulation dynamic elements. Two characteristics of the plot are outstanding: first, the stage-by-stage gain level was best maintained when the relative sizing of dynamic elements was similar (4, 6, 10 and 21 element configurations versus the compressor lumped and fan lumped); second, the gain level of the stage-by-stage simulation (21 elements) was essentially retained when the system was reduced to ten dynamic elements of similar relative sizing. A third observation from the plot notes that the compressor lumped and fan lumped points for condition OP1 produced spurious results. These two points failed to reach solutions within the prescribed program iteration tolerances, resulting in poorer calculation precision than the other cases. This tendency toward iteration failures appeared to correlate with systems composed of dissimilar dynamic element sizing.

The crossplot of phase results at 100 Hz is shown on Figure 44. Here, the deviation from the stage-by-stage simulation phase angle is plotted in degrees versus the number of dynamic elements. Again, results were grouped according to similarity of dynamic element sizing, with least phase deviation ($\sim 20°$) shown by the configuration with 10 similarly sized elements. The two points which failed to reach iterative solutions with in program tolerances again showed spurious results.

TABLE I

Summary of Reduced Order Compression System Simulations

	Configuration	Number of Dynamic Elements	Relative Element Length	State Variable System Order	Comments
1.	Fan/low/high lumped	4	Similar	12	Same dynamic configuration as baseline engine simulation
2.	Ten similarly sized elements	10	Similar	30	Approximately half the dynamic elements of the stage-by-stage simulation
3.	Bleed	6	Similar	18	Dynamic element boundaries placed at the component interface and bleed stations
4.	Fan lumped/compressor staged	15	Dissimilar	45	Fan bypass and core stages each combined into one dynamic element
5.	Fan staged/compressor lumped	10	Dissimilar	30	Low and high compressor stages each combined into one dynamic element

Simulation pressure-time response to a step in inlet pressure is illustrated on Figures 45 and 46. Plots of high compressor discharge pressure versus time are shown for the five reduced order and stage-by-stage simulations. Results at condition OP1 are shown on Figure 45. Figure 46 shows OP2 results. On each plot, 63.2% of the pressure change at station 4.0 is identified to give a measure of the effective first order time constant of the simulations.

Here also the responses of all the reduced order models are similar. In order to make a comparison of the step responses results, a crossplot of the time to 63.2% of the compressor discharge pressure rise was made as shown on Figure 47. The crossplot shows once again, that the configurations with dissimilar element sizing gave results outside the family obtained with similar element sizing. Both the bleed and ten element configurations showed a minimal effect on response time, with the ten element configuration showing a response time closest to the stage-by-stage.

Computer Run Time

The impact of the simulation order on computer run time is shown on Figure 48 for the inlet pressure step transient. The case execution time (excluding load time) is plotted versus the number of dynamic elements. The curve shows that by reducing the order of the model from 21 elements to a range of four to ten elements, significant reductions in computed run time can be achieved. As a minimum, the run time reduction is approximately 55% with the ten element configuration. Approximately 10% additional run time reduction can be achieved by further reducing the number of elements from ten to four.

Figure 49 shows the run times required for computation of frequency response by the transfer function method. The results showed that the six element configuration provided the most reduction in run time with a savings of approximately 75% associated with reducing the number of elements from 21 to six. The ten and four element models showed a run time reduction ranging from 62 to 68%, respectively.

On the basis of the trade-offs in simulation dynamic characteristics and computer run time, a configuration was selected for further evaluation of run time improvements. Both the bleed and ten element configurations showed similar results in terms of transient response time and computer run time. Due to the emphasis placed on frequency response improvements, the configuration with ten similarly sized elements was selected over the six element (bleed) model on the basis of its better frequency response characteristics. If model simplification or minimum run time had been emphasized in this work, the four or six element models would have been better choices. The ten element configuration was used to evaluate further run time improvements, using variations in the algorithms for prediction of program iterative solutions.

Predictor Algorithms

Computation of transients in the SOAPP simulation system requires iterative solution of a large number of non-linear equations. The program execution time is partially dependent on how accurately the solution values of independent variables can be predicted. As the accuracy of the predictions improves, the number of iterations required for solution is decreased, and the computation time reduced. Prediction of the independent variable values from solutions at previous time steps is one of the techniques employed in the SOAPP system solution routines.

A study of prediction algorithms was made using the ten element compression system. Four different prediction formulas were evaluated using step and sinusoidal inlet pressure ($P_{T2.0}$) disturbances, and a high compressor discharge pressure-time history as input transients. The $P_{T4.0}$ pressure-time history was derived from a fuel step transient induced into the baseline engine simulation (Figure 50). For the purposes of this study, constant values of the time increment and the iteration tolerance were employed. The parameter used to evaluate the performance of the prediction algorithms was the average number of iterations per solution. The four prediction formulas are derived below.

1. The simplest prediction scheme is the use of values obtained from the most recent solution. For the transient case where the effect of the disturbance has died out, this predictor offers the best performance since none of the independent variables are changing. This is a trivial case but, as will be seen, the response to a step change appears to lend itself quite well to this prediction algorithm.

2. The next level of complexity is represented by a linear predictor of the form:

$$X = at+b$$

where X = independent variable (9)

t = time

If the two past values of 'X' & 't' are known, the coefficients 'a' and 'b' can be calculated such that

$$X = \left(\frac{X_1 - X_2}{t_1 - t_2}\right)t + \left(\frac{X_2 t_1 - X_1 t_2}{t_1 - t_2}\right) \tag{10}$$

For the evenly-spaced time interval case ($t - t_1 = t_1 - t_2$),

This reduces to

$$X = 2X_1 - X_2 \tag{11}$$

3. A quadratic form represents the highest order predictor included in this study

$$X = at^2 + bt + c \tag{12}$$

Again, for equally-spaced time increments, the following formula is obtained

$$X = 3X_1 - 3X_2 + X_3 \tag{13}$$

for $t - t_1 = t_1 - t_2 = t_2 - t_3$

4. An exponential predictor was also investigated in the study. Its form is

$$X = ae^{bt} \tag{14}$$

The equally-spaced form of this predictor is

$$X = X_1^2/X_2 \tag{15}$$

Table II summarizes the results of the study. The results show that higher order predictors, represented by the quadratic form, produce the poorest performance for all three types of input disturbances. For the case of a sinusoidal disturbance, the linear predictor performs better than either the past value or the quadratic forms. The exponential predictor appears to be exactly equivalent to the linear.

This observation is confirmed upon examination of the linearized form of the exponential predictor:

$$\frac{\Delta X}{X} = \left(\frac{2\,\Delta X_1}{X_1}\right) - \left(\frac{\Delta X_2}{X_2}\right) \tag{16}$$

For the case where $X \approx X_1 \approx X_2$, this reduces to the linear predictor formula. Most transient solutions do not exhibit large changes to the independent variables from one point to the next. Therefore, for the small amplitude (1%) sinusoidal disturbance case, it follows that the linear and the exponential predictors perform in a virtually identical manner.

The final result shows that use of past value prediction offers improved performance over the linear form when the transient shows significant "settling out" time after the initial disturbance ($P_{T4.0}$ results).

An overall conclusion drawn from these results is that the minimum degree of prediction applicable to a particular type of transient will yield the fewest number of iterative passes. This stems from the fact that solution tolerances produce errors in the solutions which tend to be amplified by the higher order prediction algorithms. Furthermore, although the set of equations is highly non-linear, the results obtained over a few time increments tend to be linear, which also indicates that this type of prediction should perform best.

Based on the results of this study, the linear predictor will offer the best performance for the general case of an arbitrary time-dependent disturbance. However, certain special cases, such as the step disturbance with a long settling time, will achieve better results with the past value predictor.

TABLE II

Predictor Algorithm Study Results

Predictor Type	Input Disturbance		
	Step $P_{T2.C}$	Sinusoidal $P_{T2.0}$	$P_{T4.0}$
Past value	2.10 iterations/point	2.50	1.52
linear	2.17	2.33	1.76
quadratic	2.88	2.74	1.90
exponential	—	2.33	—
Transient Time	0.025 seconds	0.025	0.150

The results obtained from the analysis of the stage-by-stage and reduced order compression system simulations led to the following conclusions:

1. The frequency response characteristics of dynamic simulations are dictated by the largest dynamic elements. The reduced order compression system simulations which employed dissimilar element sizing (i. e. fan lumped/compressors staged and fan staged/compressors lumped) showed response characteristics similar to lower order systems containing fewer dynamic elements of more uniform sizing.

2. The uniformly sized 10 element compression system model provided the optimum configuration for evaluation in the engine simulation because it essentially retained the frequency response characteristics of the stage-by-stage configuration while offering a significant reduction in computer run time. For other applications where model simplicity or minimum computer run time is emphasized, the four element or bleed configurations represent optimum models.

3. The linear predictor algorithm should be used for computation of transient cases, because it generally required the smallest number of iterations to reach solutions at each time step of a transient.

Modified Engine Simulation

The third and final step toward improvement of simulation dynamic characteristcs was evaluation of the effects of the compression system model modifications on the frequency response and transient response characteristics of the engine simulation. To perform the evaluation, the baseline engine simulation was modified by incorporating the ten element compression system model. The modified engine simulation was used to define gain and phase frequency response characteristics and pressure-time histories of response to steps in inlet pressure and fuel flow. These dynamic characteristics were compared to results obtained from both the baseline engine simulation and NASA engine tests. As a final step in the evaluation, the modified engine simulation was subjected to discrete frequency sinusoidal inlet pressure disturbances of varying amplitudes to determine the stability limits of the simulation. These results were compared to NASA test data for which the inlet pressure amplitude at engine surge/stall was defined.

The following discussion provides a brief description of the dynamic configuration of the modified engine simulation. The dynamic characteristics of the simulation are presented and compared to results obtained from the baseline engine simulation and NASA engine tests. The dynamic characteristics are discussed in terms of frequency response (gain and phase), transient response (pressure versus time), and stability limits.

Configuration

The baseline engine simulation was modified by implementing the ten element compression system model and linear predictor algorithm selected from the reduced order analysis. The resulting dynamic configuration of the modified engine simulation is shown in Figure 51

compared to an engine side-view. The number of dynamic elements was 27, compared to 20 in the baseline simulation. This increase came from six additional elements in the fan, low and high compressors plus separation of the high compressor discharge diffuser from the compression system. The state variable order of the system was 83, which included mass, momentum, and energy for each of the 27 dynamic elements plus fuel flow and core exhaust area. The simulation is described in detail in Appendix A.

Dynamic Characteristics

The dynamic characteristics of the modified engine simulation were established in three formats. First, the frequency response at stations 2.3, 2.3F, 3.0 and 4.0 was derived using both the transfer function and step response methods. The results of these methods were compared to both engine test and baseline simulation results. Second, time histories of response to steps in inlet pressure and fuel flow were computed for stations 2.3, 2.3F, 3.0 and 4.0 and compared to baseline simulation results. Third, discrete frequency inlet pressure sine wave transients of varying amplitudes were induced to determine the stability limits of the simulation. Results were compared to engine test data where the pressure amplitude at surge/stall was defined.

Frequency Response

The main objective of this program was to develop an engine simulation which showed improved frequency response characteristics to at least 100 Hz. To accomplish this, the frequency response characteristics of the simulation were defined using both the step response and transfer function methods. The results obtained from the modified engine simulation were compared to engine test results and baseline simulation results to assess improvements in simulation frequency response characteristics. In addition, frequency response characteristics derived by the two methods were compared to each other to determine which gave the better representation of the actual engine.

The frequency response characteristics computed for the modified engine simulation are shown in Figures 52 through 67 which show response computed by the transfer function and step response methods compared to the engine test data and transfer function characteristics of the baseline engine simulation. Calculation of transfer functions for the modified engine simulation was found to be more difficult than was experienced with the baseline engine simulation. Implementation of variable scaling of the program iteration tolerances and linearization of performance characteristics were required to complete transfer function calculations. With the variable scaling, all iterations were still not within desired tolerances, however, the frequency response results appeared to provide sufficient accuracy for some comparisons. The effects of solutions outside of tolerance bands were most evident in the core stream response characteristics at condition OP1 and in the bypass stream characteristics at both OP1 and OP2. The most common evidence was unusually low gain levels at frequencies up to 10 Hz or a 360° shift in the phase angle.

The influence of the modified compression system model on the engine simulation core stream gain characteristics is shown in Figures 52 through 57 which show that the simulation gain levels were affected at frequencies above 50 Hz. The transfer function and step response gains showed a continuation of roll-off above 50 Hz which was not present in the baseline engine simulation. At 200 Hz the modified simulation gain levels at station 4.0, 3.0, and 2.3 were reduced by an average 18, 9, and 4 decibels respectively.

The transfer function gain levels at condition OP2 (Figures 52 through 54) showed improved resolution of the simulation high frequency response characteristics. The gain response showed resemblence to the NASA test results but appear to be displaced to higher frequencies. The resemblence was characterized by a gain peak which occurred at 80-90 Hz in the simulation, compared to 30-35 Hz in the test data. The simulation gain levels predicted by step response at condition OP2 did not resolve high frequency dynamics as well as the transfer function.

At condition OP1, core stream transfer function results showed the effects of program solutions reached outside the desired iteration tolerance. The gain levels defined at the high compressor discharge (Figure 55) disagreed with step response results over the range of 1 to 40 Hz. Agreement was good over this frequency range at condition OP2. At 100 Hz, the transfer function predicted a gain peak at station 4.0, but no similar peak was seen in the gain response at stations 3.0 and 2.3 (Figures 56 and 57). These results were inconsistent with condition OP2, NASA test data, and fan bypass gain response in the baseline engine simulation. At condition OP2, simulation gain peaks at the three core stations were aligned at a frequency of 80-90 Hz. At both OP1 and OP2 the NASA test data showed alignment of peaks at 30 to 35 Hz and 80 to 94 Hz. All of these examples showed influence of downstream components on the gain characteristics. The gain levels at stations 2.3 and 3.0 were showing influence of the burner and high compressor dynamics. The fan bypass gain peaks shown by the baseline simulation indicated that response was influenced by the fan duct dynamics.

The step response gain levels at condition OP1 (Figures 55 through 57) indicated the same results as condition OP2. The gain characteristic rolled-off to 200 Hz with no consistent prediction of gain peaks. The influence of the compression system modifications on simulation core stream phase is shown in Figures 58 through 63. These curves show that the phase angles were affected over the full spectrum of frequency (1 to 200 Hz). In general, the transfer function predicted more lag for the modified engine simulation than was predicted for the baseline simulation up to the frequency where phase peaks were calculated.

At condition OP2 (Figures 58 through 60) the transfer function phase showed improved resolution of the high frequency response characteristics of the modified simulation. Peaks in phase were consistently predicted at all three core stream stations in a frequency range of 70 to 76 Hz. The phase characteristics showed some resemblence to NASA engine data although again appear to be displaced to higher frequency. The NASA data showed phase peaks at approximately 35 Hz. The NASA test data also showed less lag at the phase peaks.

The core stream phase computed at condition OP2 by the step response method (Figures 58 through 60) showed less lag than transfer function phase; this was consistent with results from the baseline simulation. As in the case of the modified simulation gain, there was no consistent prediction of phase peaks with the step response method.

The core stream phase at condition OP1 is shown in Figures 61 through 63. The high compressor discharge station (Figure 61) again showed the effect of reaching program iterative solutions outside of desired tolerances. The effect was indicated by comparison of transfer function and step response results. Over the range of 1 to 75 Hz, the transfer function phase showed less lag than step response which was counter to other simulation results. The transfer function phase at the high compressor discharge also showed a steep

roll-off in phase angle above 65 Hz which gave some resemblence to engine data at approximately 25 Hz. No corresponding phase response was shown at the upstream stations (3.0 and 2.3), again indicating that the influence of dynamic characteristics of downstream components was not being resolved at the upstream stations.

The step response phase computed for the modified engine simulation at condition OP1 (Figures 61 through 63) indicated results similar to condition OP2. With exception of the high compressor discharge station, the step response phase showed less lag than transfer function phase and made no consistent prediction of phase peaks or steep roll-off.

The frequency response characteristics of the fan bypass stream discharge (station 2.3F) are shown in Figures 64 through 67. Comparison of the transfer function gain levels from the baseline and modified simulations (Figures 64 and 65) showed that response peaks continued to be predicted by the modified simulation, although the levels were generally lower than the baseline simulation above 50 Hz. (The -20 db level at 9 Hz predicted by the modified simulation transfer function at condition OP2, (Figure 64) was probably a result of calculation inaccuracy, not system characteristics). The gain levels computed from step response generally showed the same results as the baseline simulation; response peaks above 30 to 35 Hz were significantly attenuated.

Comparison of transfer function phase results in Figures 66 and 67 show that the modified simulation phase angles showed less lag than the baseline and were closer to engine test levels. (The 360 degree phase shift shown at OP1 was again due to calculation in accuracy). The step response phase indicated less lag than the transfer function predictions, consistent with virtually all other results.

Transient Response

Pressure-time histories at stations 2.3F, 2.3, 3.0 and 4.0 are shown in Figures 68 through 75 for a 1.0% step in inlet pressure. These figures compare results obtained from both the baseline and modified engine simulations. Figure 68 shows that the station 2.3F fan bypass stream discharge pressure at condition OP1 exhibited a stairstep characteristic of response resulting from back and forth disturbance propagation in the fan ducts. Results were similar for both the baseline and modified simulations.

Pressure-time response in the core stream at condition OP1 shown in Figures 69 through 71 reveals the response of the baseline and modified simulations was different. The baseline simulation core stream stations responded in stairstep fashion similar to the fan bypass stream while the modified simulation did not. These results indicated that the baseline simulation coupled the fan bypass and core stream dynamics while the modified simulation did not. Similar results were shown at condition OP2 as illustrated in Figures 72 through 75.

The pressure-time response to a 1.0% fuel flow step is shown in Figures 76 through 79. Figure 76 compares at condition OP1, the baseline and modified simulation response at the high compressor and fan bypass stream discharge stations (4.0 and 2.3F). The results at these stations were similar for both simulations where the pressure at station 4.0 rose sharply over the first 0.01 seconds while the pressure at 2.3F showed significant rise at about 0.02 seconds.

The delay in station 2.3F response indicated propagation of the pressure wave resulting from the fuel pulse rearward into the exhaust system and then forward through the fan bypass ducting to the fan bypass stream discharge.

The pressure-time response at condition OP1 is shown for core stream stations 2.3 and 3.0 in Figure 77. At these stations, results from the two simulations were different. The baseline simulation showed a small rise in pressure over the first 0.01 seconds followed by a second larger rise in pressure starting at approximately 0.02 seconds. These characteristics indicated forward propagation of the pressure wave resulting from the fuel pulse over the first 0.01 seconds followed by coupled response to the fan bypass beginning at approximately 0.02 seconds. The modified simulation response showed that the fan bypass-core coupling was not present; only forward propagating response to the fuel pulse was seen over the first 0.01 seconds. The results at condition OP2 were the same as shown in Figures 78 and 79.

The differences in fan coupling characteristics of the baseline and modified simulations were attributable to the respective simulation methods. The fan representation used in the baseline simulation, provided coupling of the bypass and core stream pressures through the performance characteristic illustrated in Figures 6 and 7. The modified simulation contained no coupling. The performance characteristics of the fan bypass and core stream were described in terms of separate ϕ, ψ and λ characteristics with the splitting streamline computed as a function of bypass ratio. In developing the modified compression system simulation, attempts were made to compute the splitting streamline during transients, however, the use of a constant flow per unit area assumption in the computation appeared to give dynamically unstable results. Transfer functions computed for the simulation showed positive roots of the characteristic equation and confirmed the dynamic instability of the streamline calculation. As a remedy, the streamline location was computed at the initialization point of the transient and held constant for the duration of the transient. As shown by the pressure and fuel flow step transient results, coupling therefore was not present in the modified simulation.

Stability Limits

The stability limits were assessed as a final step in evaluation of the dynamic characteristics of the modified engine simulation. At condition OP1, inlet pressure sign waves of varying amplitude were induced into the simulation to determine the approximate amplitude at which simulation computations became unstable. The results were compared to engine test data where the sine wave amplitude at engine surge/stall was defined.

A comparison of simulation and test results (Figure 80) show that the simulation instabilities occurred at wave amplitudes at least twice as large as the amplitudes which induced surge/stall during the engine test (60% to 70% for the simulation versus 30% for the engine). The instability induced in the simulation occurred in the fan bypass stream. This result is illustrated in Figure 81 where the transient path of operation is shown on the fan map for both stable and unstable cases at 10 Hz. The stable case shows orbiting of the transient operating point in a clockwise direction, compared to the unstable case which shows a rise in pressure followed by a large reduction in airflow to the point the simulation computation became unstable. The airflow characteristic shown for the unstable case is typical of test results experienced by Pratt & Whitney during engine surge cycles.

Figures 82 and 83 show that transient operation of the low and high compressors did not induce the simulation instability. The orbiting of the transient operation is shown to be virtually the same during both the unstable and stable cases, with the orbit larger for the unstable case. No evidence of the airflow reduction characteristic of surge is present. The low compressor excursions (Figure 82) exceeded the steady state surge line derived from rig tests, without inducing instability into the simulation and the high compressor excursions (Figure 83) were well below the steady state surge line.

The results of the NASA engine tests were reported in Reference 1 to show instability originating in the core stream. Pratt & Whitney TF30 experience has also shown this to be the case, with the instabilities usually initiated in the low compressor in the form of rotating stall, and culminated with high compressor surge. (See Reference 5).

The comparison of simulation and engine stability limits led to the following conclusion. The simulation predicted the fan to be component limiting stability while test experience showed the core compression system to be limiting. In this sense the simulation and test results disagreed leading to the conclusion that further modification to the simulation is required to properly predict engine core stream dynamics.

The results which were obtained from frequency response, time history response, and stability evaluation of the simulation suggest areas where further work is required to improve the simulation dynamic characteristics. These areas are identified under the discussion of results, conclusions, and recommendations sections of this report.

DISCUSSION OF RESULTS

The investigations made during this program produced the following key results.

1. Use of the dynamic energy equation in combination with dynamic mass and momentum equations is required to properly simulate the propagation of aerodynamic disturbances through the system. With the energy equation, the simulation showed a delayed response of downstream pressures and temperatures with inlet induced disturbances; without the energy equation, downstream response was immediate and therefore improper.

2. The reduced order analysis of the compression system simulation showed that at 100 Hz., the dynamic characteristics of a stage-by-stage simulation could be obtained with a more simplified dynamic configuration while realizing substantial savings in computer execution time. The analysis showed that the dynamic elements should be uniformly sized to achieve the best high frequency response. Non uniform element sizing caused the system response to be dominated by the lower frequency limitations of large elements. The results of the reduced order analysis should not be interpreted to mean that compression systems never require simulation on a stage-by-stage basis. The requirement is dependent on the maximum frequency of interest in a specific problem. As the maximum frequency of interest becomes higher, the required number of dynamic elements should increase in a manner which maintains a similar relationship between element size and propagation time at the maximum frequency. The real significance of the reduced order analysis was the approach that was used. By example, it illustrated a method which can be used to establish a simulation dynamic configuration which is optimum with respect to frequency response and program execution time.

3. The predictor algorithm analysis showed the linear form to produce the best overall efficiency in computation of simulation transients. The good performance of the algorithm resulted from its characteristics of minimal amplification of errors associated with program iteration tolerances and the tendency toward linearity associated with the small time steps used in transient computations.

4. The transfer function provided better resolution of simulation high frequency response characteristics than the transient methods. This was characterized by the peaks in gain and phase frequency response curves. In cases where the transfer functions were calculated with satisfactory accuracy, core stream response peaks were consistently resolved at all stations and aligned at constant frequency. At the fan bypass station, the transfer function appeared to resolve response peaks associated with the dynamics of the fan downstream ducting.

   The frequency response characteristics obtained from the transfer function and simulation transients may differ because of the nature of their respective solutions. Transfer functions are computed by direct solution of the linear system equations

derived from the nonlinear simulation. Errors result in this method from the iteration tolerances needed to compute the linear system model and from the numerical evaluation of the transfer function which requires raising of numbers to large powers. Transient computations are not free from error because of the tolerances required for iterative solutions at each time step of the transient. The tolerances introduce pseudo dynamics into the transient which are reflected in the frequency response characteristics.

The differences inherent in the two methods of defining simulation frequency response characteristics suggest that the transfer function method can be used to advantage. For example, transfer functions can be used to measure how well simulation transients reflect system response characteristics. The advantage of the transfer function also endorses current applications of the method for analysis of control system operation.

5. Modifications to the compression system model primarily affected frequency response characteristics of the engine simulation above 50 Hz. The effects were most clearly illustrated by the reduced gain levels which showed continued roll-off above 50 Hz. The transfer function response showed gain and phase peaks similar to test data, indicating that the dominant dynamic characteristics of the engine were simulated but appears to be displaced to higher frequencies.

   The low frequency response characteristics of the engine simulation were essentially unaffected by the modifications to the compression system model. In an absolute sense, close agreement between the modified simulation and test data remained confined to a maximum frequency of 10 to 20 Hz in the core stream and 40 to 65 Hz in the bypass stream.

   The simulation frequency response characteristics showed that, although modifications to the compression system model improved resolution of the dominant dynamic characteristics of engine, the approach used in this program was not sufficient to achieve close agreement with test data over the frequency spectrum of 0-200 Hz. The approach used in the program was centered around the influence of compression system dynamic element sizing and results showed that further modifications to the engine simulation are required. Three possibilities can be suggested at this point.

   The reduced order compression system analysis showed that dynamic element sizing should be uniform to achieve the best frequency response characteristics. When the ten element compression system model was incorporated into the engine simulation, the dynamic element sizing of other components was not reduced for compatibility with the compression system. This would suggest that if further modifications were pursued, dynamic element sizing of other engine components should be reduced and evaluated.

   The comparisons of simulation and test frequency response characteristics at the fan bypass station showed agreement at higher frequencies (40 to 65 Hz) than at core stream stations (10 to 20 Hz). The bypass flow system component compo-

sition is dominated by ducting while the core stream is more heavily composed of turbomachinery. These facts could suggest that the dynamics of the ducting were more satisfactorily modeled than the turbomachinery dynamics. The simulations used in this program placed the boundaries of the compression system dynamic elements in the gaps between rotor and stator rows and assumed linear distributions of the flow properties between the element inlet and exit boundaries. This assumption therefore did not account for the reduction in flow area and associated increase in Mach number experienced by the flow as it progresses through the airfoil rows. The effect of the assumption used in this investigation is to compute Mach numbers through the compressors which on the average are too low and in turn make propagation time of disturbances traveling upstream too fast. This would suggest that the description of flow property distributions through the turbomachinery should be modified and the effects on frequency response evaluated.

The engine simulations assembled in this program were composed of dynamic elements representing only the engine components. Testing of the actual engine was performed in an altitude test facility which included inlet ducting of significant length ahead of the engine inlet plane. This ducting potentially influenced the dynamic characteristics of the engine-test facility system. It is expected that the inlet ducting would shift the resonances of the system to lower frequencies, therefore if the ducting ahead of the engine was included in the simulation, the agreement between simulation and test frequency response characteristics might be improved. Addition of the inlet ducting to the simulation is a modification which should also be considered.

6. Comparison of the step transient results from the baseline and modified engine simulations showed that coupling of the fan bypass and core dynamics have a significant effect on core stream transient operation. These effects were illustrated by comparison of the results from the baseline and modified engine simulations. Coupling was present in the baseline simulation where transient results showed that the core pressures responded to disturbances propagated forward through the fan bypass ducts. No coupling was present in the modified simulation, and core response to fan bypass stream disturbances were not shown by simulation transient results.

   These results are significant to the engine design process and underline the importance of the role of the dynamic engine simulation. The results show that dynamic characteristics of the turbofan bypass flow system can potentially play a significant role in the transient operation of the core stream compression system and thereby influence the stability of operation. Design characteristics such as length of the fan ducts, proximity of the flow splitter to the fan, and use and placement of fan airfoil shrouds may all play an important role in setting the compression system stability limits. The capability to accurately simulate the effects of these design characteristics is therefore valuable to the design process.

7. The stability limits of the modified engine simulation were more than twice that shown by engine test results. The simulation results showed that instability originated in the fan bypass stream while test data showed origin in the core stream.

The comparison of simulation and test stability limits also showed that further refinements to the simulation are needed to achieve a reliable estimate of the engine stability limits. Further revisions to element sizing and assupmtions of dynamic element property distribution were proposed above. Fan bypass/core coupling was also proposed as potentially very important to stability of operation. Afinal consideration to be made is that instabilities usually originate in the low compressor of the TF30 engine in the form of rotating stall and culminate in high compressor surge. Rotating stall is a type which introduces circumferential variations in the system flow properties. It is conceivable that to finally achieve good simulation of the stability limits of the engine, the one dimensional modeling used during this program might need expansion to account for the circumferential properties of rotating stall.

8. A variety of tests was required to reveal important dynamic characteristics of the simulation. The dynamic characteristics of the simulations assembled during this program were evaluated using three different tests: 1) frequency response (gain and phase versus frequency), 2) transient response (pressure versus time), and 3) stability limits ($P_{T2.0}$ sine wave amplitude). Results of these tests illustrated by example the importance of each test.

   The frequency response characteristics provided an overall view of the simulation dynamics across the frequency spectrum, and suggested requirements for further refinements to the engine simulation in areas such as dynamic element sizing and distribution of properties across the dynamic elements. Over the frequency range of 0-20 Hz, where the simulation stability was evaluated, the frequency response characteristics of the baseline engine simulation, the modified engine simulation, and test data where in closest agreement.

   The transient response characteristics revealed that fan bypass/core dynamic coupling was present in the baseline engine simulation but absent from the modified engine simulation. The results illustrated that the coupling effect has a potentially important effect on engine stability. These results were not apparent from the frequency response characteristics of the two simulations.

   The stability check provided the final test of simulation accuracy and showed that further simulation refinements are necessary to achieve a reliable prediction of engine stability limits.

9. In the process of developing the simulations used in this program, three problems of a numerical nature were encountered. Two of the problems were associated with computation of frequency response by the matrix method; the third problem was associated with stability of the model formulation.

   The first attempt at computing frequency response characteristics by the matrix method gave results which showed non zero gain levels at frequencies near zero Hz. These results were derived from finite difference perturbations which were one sided; i.e., all in a positive or negative direction. Experiments with the perturbation size and iteration tolerances showed that the low frequency offsets in gain level persisted while results at higher frequencies were repeatable. Further

tests showed that by changing the direction of the perturbation, i.e.., from positive to negative, the direction of the low frequency gain offset also changed while higher frequency results again were repeatable. On the basis of these tests, the finite differences routines of the program were modified to compute the matrix elements from perturbations in both the positive and negative directions. This modification virtually eliminated all offsets in low frequency gain levels as long as all program iterations were completed within input tolerance levels.

All of the frequency response characteristics derived by the matrix method for the baseline engine simulation were successfully computed within the iteration tolerance bands. Two cases computed for the reduced order compression system models reached solutions with some iterations falling outside the prescribed tolerances. Further difficulty was encountered in computing matrices for the modified engine simulation. Scaling of the program tolerances was required to reach completed solutions, and then some iterations were still outside of tolerances. The effects of reaching solutions outside of prescribed tolerance bands were usually shown by offsets in gain and phase levels in the low frequency range. In addition, the case run time was also extended, reflecting the attempts of the program to reach satisfactory solutions. The causes of these iteration problems could not be determined during this contract, however it was observed that the occurences correlated with simulation configurations containing dynamic elements of dissimilar sizing.

The final numerical problem encountered with the simulations was associated with the dynamic formulation of the splitting streamline in the improved compression system model. An assumption of constant airflow per unit area was used to compute the radial location of the streamline separating the core and bypass flows of the fan. Initial attempts to compute streamline locations during transients appeared to be unstable. In this case, the matrix computations proved to be very helpful to the problem because the characteristic equation showed positive roots and confirmed instability. To stabilize transient computations, the simulation was modified to compute streamline location at the initialization point and held constant for the duration of the transient.

CONCLUSIONS

The results obtained from investigation of the dynamic characteristics of the mixed flow turbofan engine digitally simulated under this program have led to the following conclusions:

1. High frequency simulations should incorporate dynamic forms of the mass, momentum and energy equations.

2. High frequency engine simulations using finite dynamic elements can be assembled in a manner where the dynamic configuration is optimum with respect to dynamic characteristics and computer execution time. The dynamic configuration should employ dynamic elements of uniform length. The number of required elements will be dictated by the maximum frequency of concern.

3. Implementation of a linear predictor algorithm improved the execution time of the simulations investigated under this program.

4. The transfer function method provides good definition of system frequency response characteristics. The transfer function method can therefore be used to assess the frequency response characteristics derived from simulation transients and, as a corollary, should not be interpreted as necessarily representative of the frequency response characteristics of simulation transients.

5. Dynamic coupling of the fan bypass and core streams can have a significant influence on core stream operation and stability. Accurate prediction of these effects can be important to the engine design process.

6. Tests of the simulation frequency response, transient response, and stability are all useful in assessing the simulation characteristics. The frequency response characteristics provide an overall view of the dynamic characteristics of the simulation and define the valid frequency range when compared to actual data. The transients are useful in identifying the dynamic coupling between the system components. The stability test provides a final check of the simulation when compared to test data, establishes the credibility of predicted engine stability limits.

7. Resizing the compression system finite elements improved the dynamic characteristics of the engine simulation above 50 Hz but showed that additional refinements are required to obtain close agreement between simulation and actual engine dynamic characteristics. The modified engine simulation showed good bypass stream dynamics to 60 Hz and good core stream dynamics to 20 Hz.

RECOMMENDATIONS

Further development of the turbofan engine simulation assembled during this program is required to obtain close agreement with actual engine dynamic characteristics. On the basis of the findings in this program, it is recommended that refinements be made in the following areas:

1. Formulation and evaluation of equations which properly model the dynamic coupling of the fan bypass and core streams. With these revisions to the fan dynamics characteristics, it is possible that another configuration of the reduced order compression system would be optimized with respect to frequency response and computer run time.

2. Resizing of the dynamic elements of other engine components for compatibility with the reduced order compression system model. The frequency response characteristics of the simulation would be improved but at the expense of increasing the number of dynamic equations.

3. Redefinition of the flow properties across the dynamic elements to recognize the area variations which occur as flow passes through the gaps and airfoils of the turbomachinery. These modifications would probably introduce additional complexity to the simulation.

4. Model the inlet ducting to assess its effect on frequency response. This would also increase the number of dynamic equations.

5. Modeling of rotating stall may be needed but should be implemented as a last resort. Test experience with the TF30 engine has shown low compressor rotating stall to be a common form of initial instability in the compression system. This implies that modeling of this process could finally be required to obtain agreement between simulation and test stability limits, however, this approach should be a last resort because of the substantial complexity that would be added to the simulation.

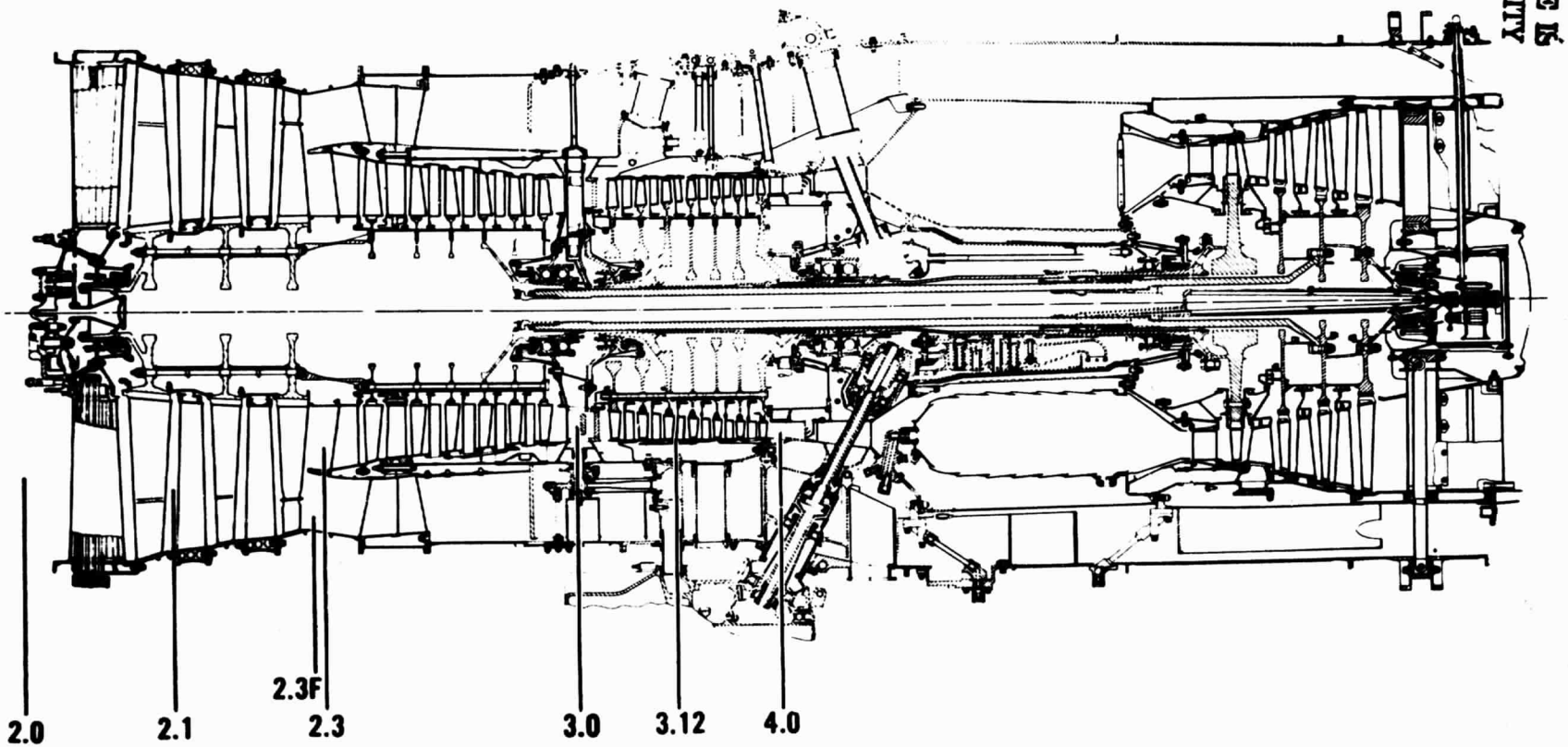

Figure 1 *TF30 Engine Cross Section with High Response Total Pressure Instrumentation Locations*

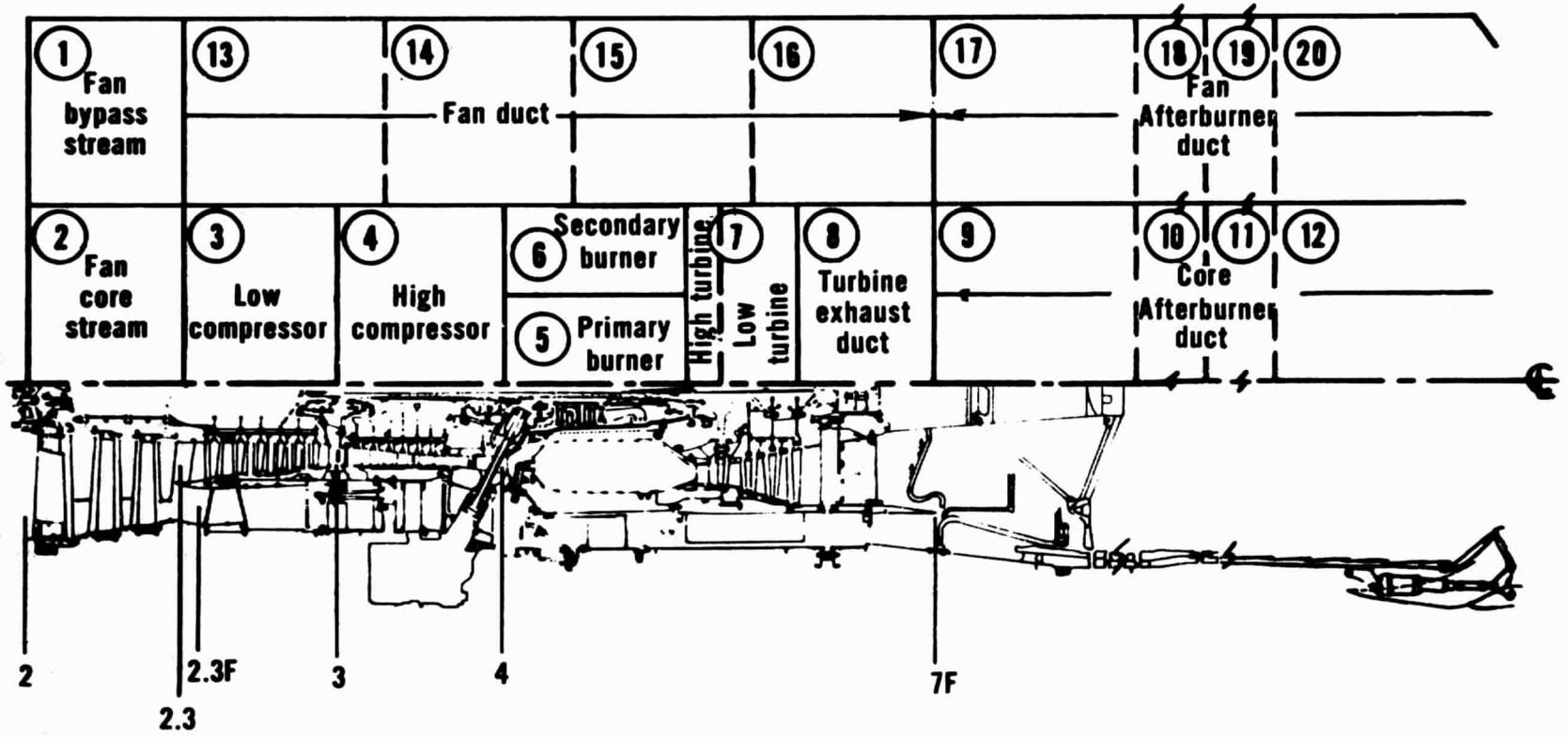

Figure 2 *Configuration of Baseline Engine Simulation*

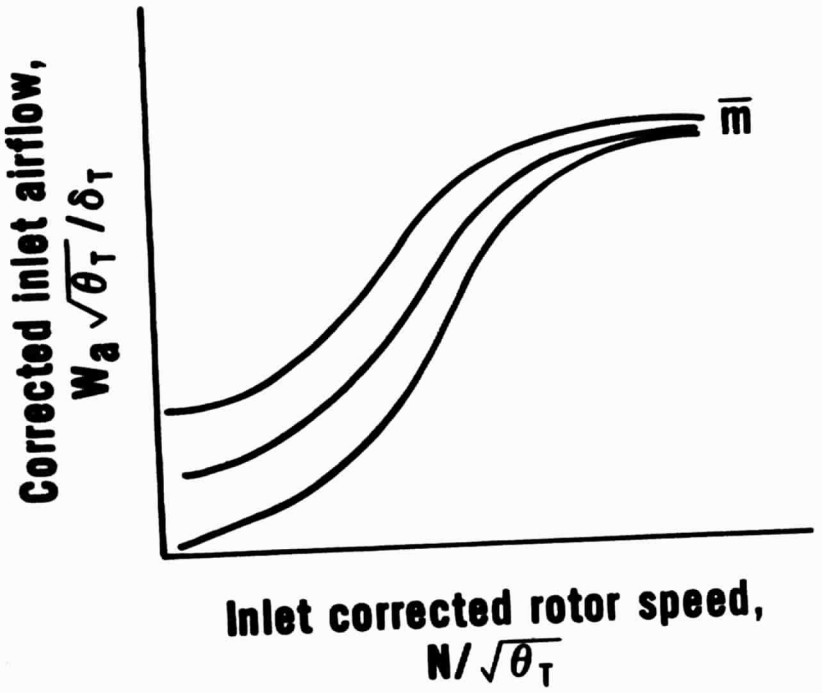

Figure 3 *Compressor Airflow Map*

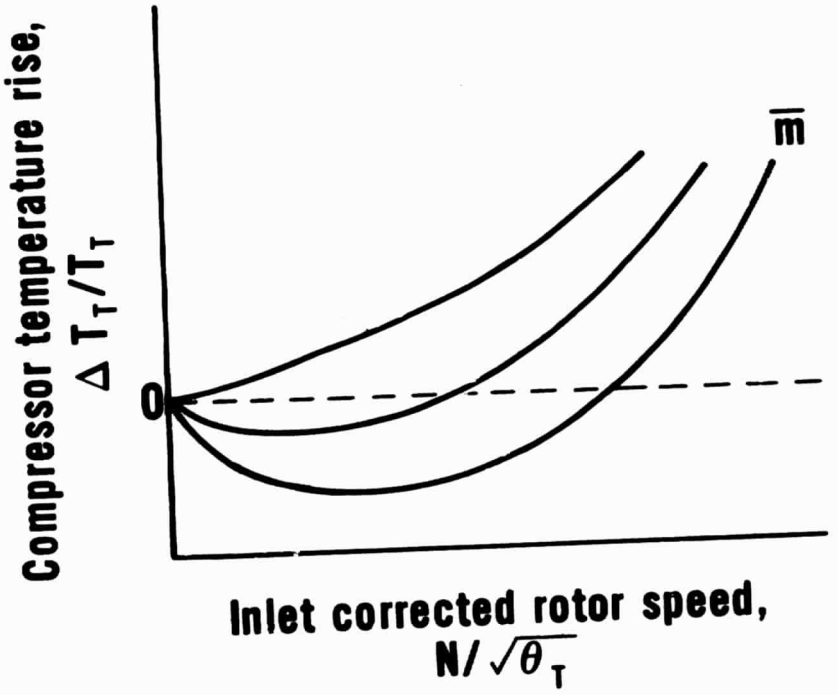

Figure 4 *Compressor Temperature Rise Map*

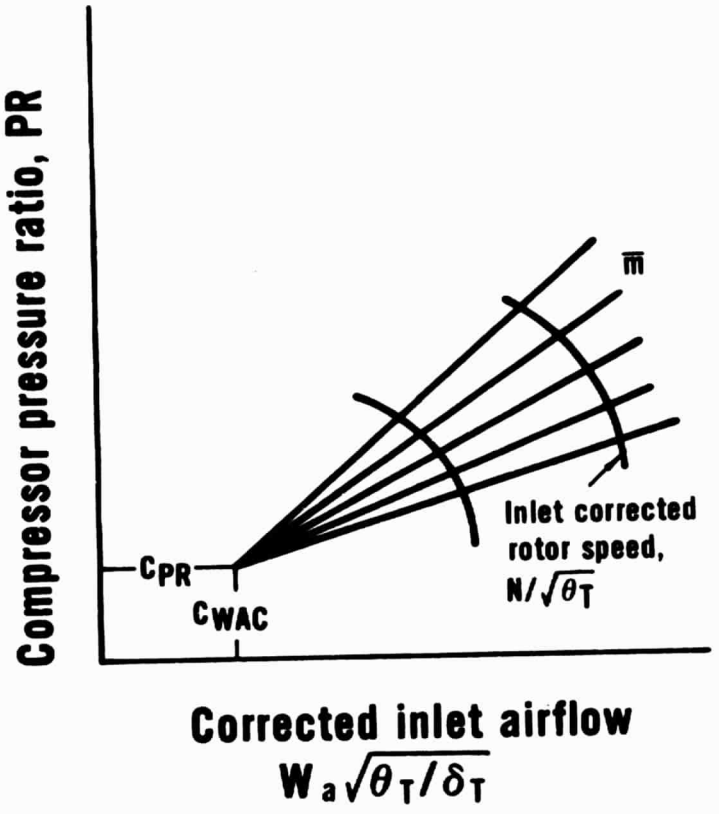

Figure 5 *Compressor Pressure Ratio Map*

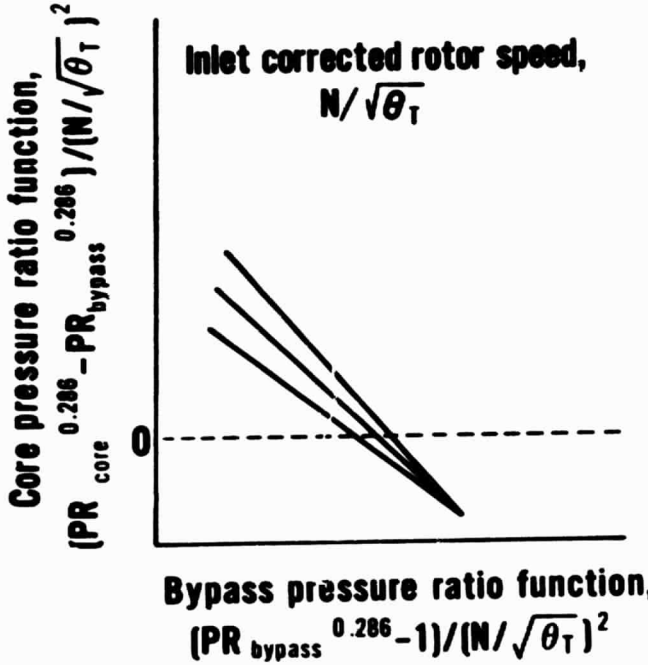

Figure 6 *Fan Core Pressure Ratio Map*

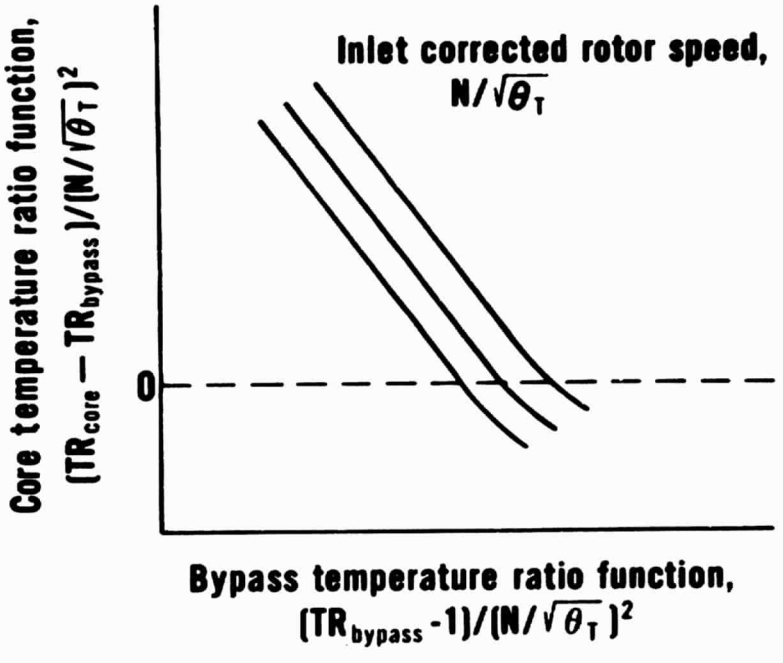

Figure 7 *Fan Core Temperature Ratio Map*

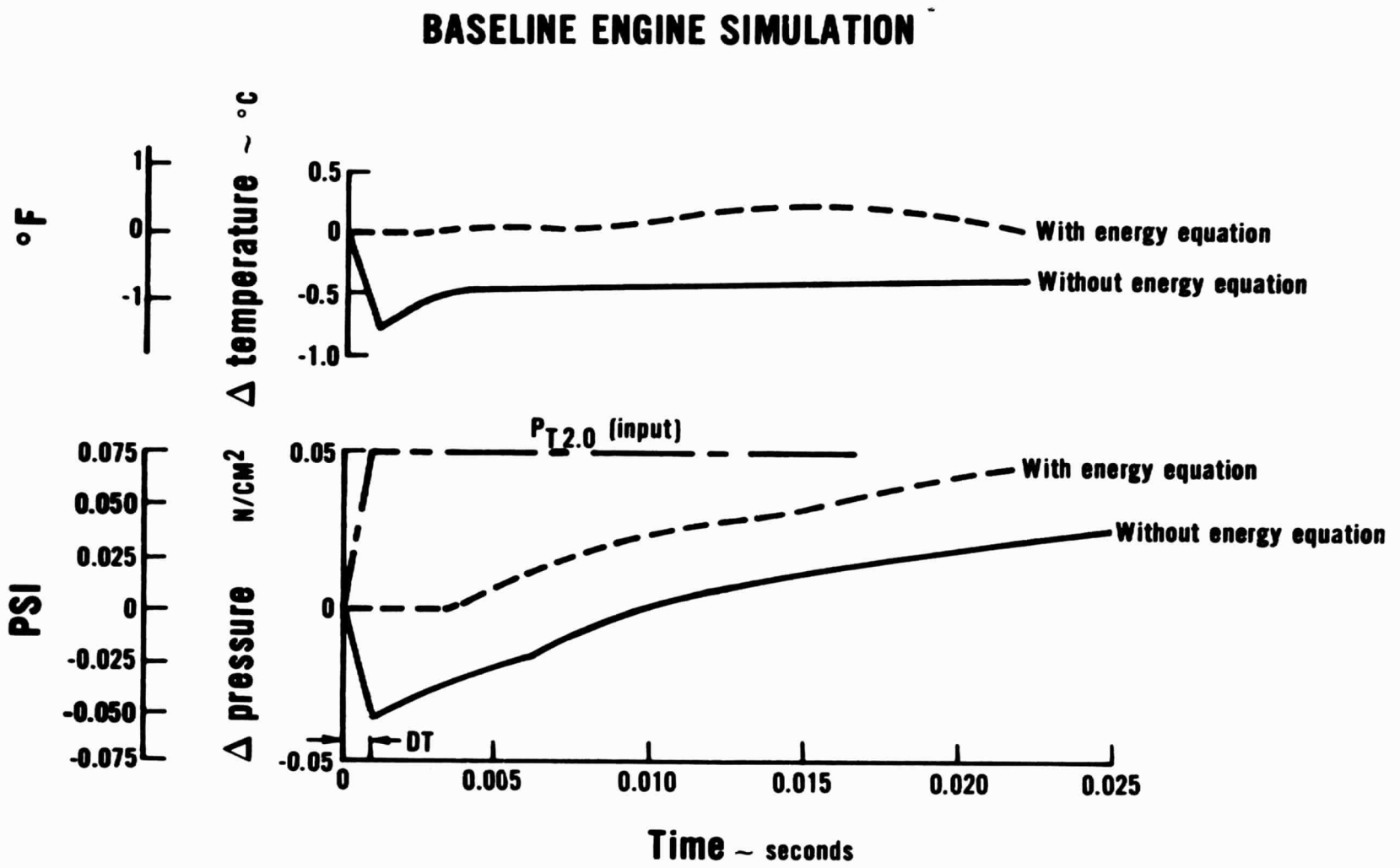

Figure 8 *Effect of Energy Equation on Station 7.0F Pressure and Temperature Response to a Step in Inlet Pressure*

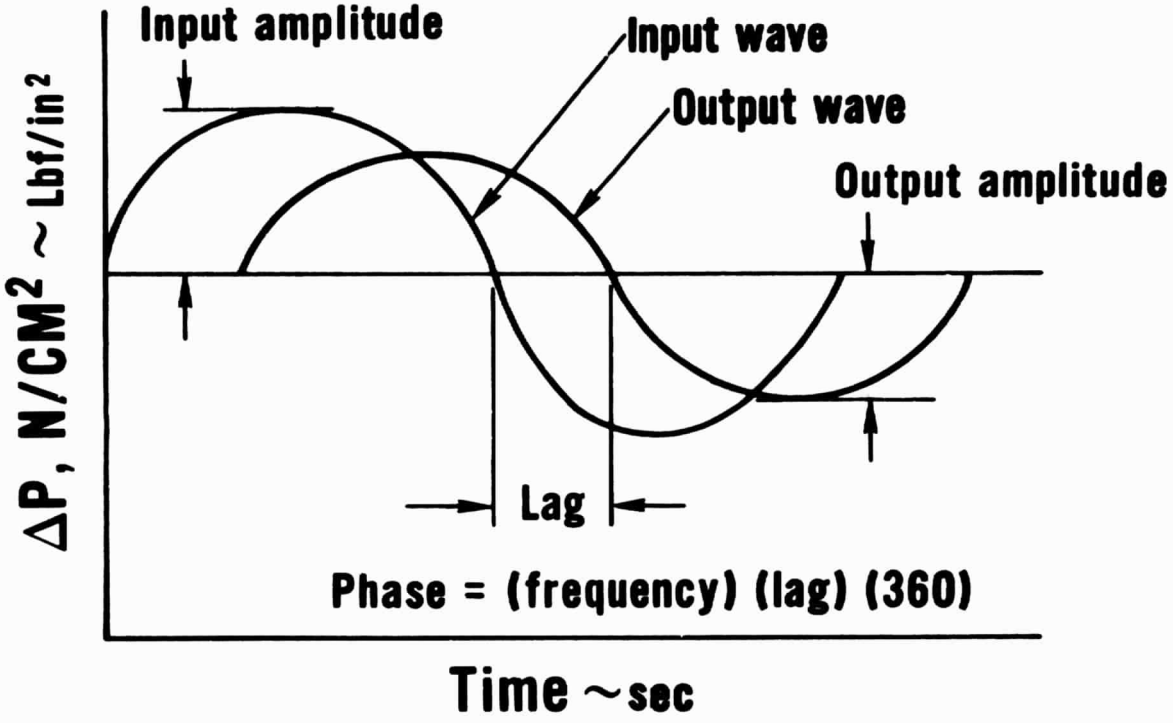

Figure 9 *Illustration of Wave Analysis for Evaluation of Gain and Phase*

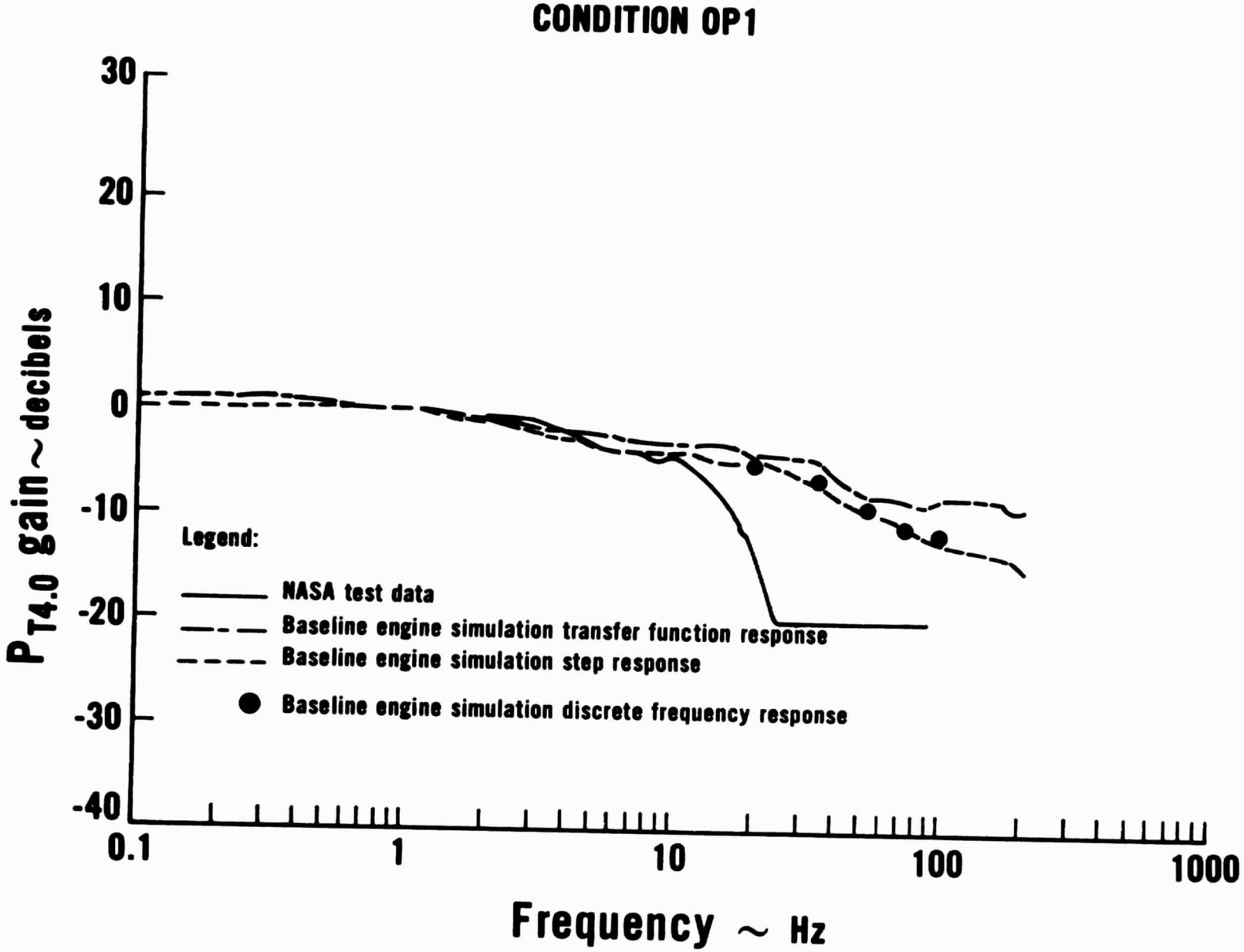

Figure 10 High Compressure Gain at Station 4.0

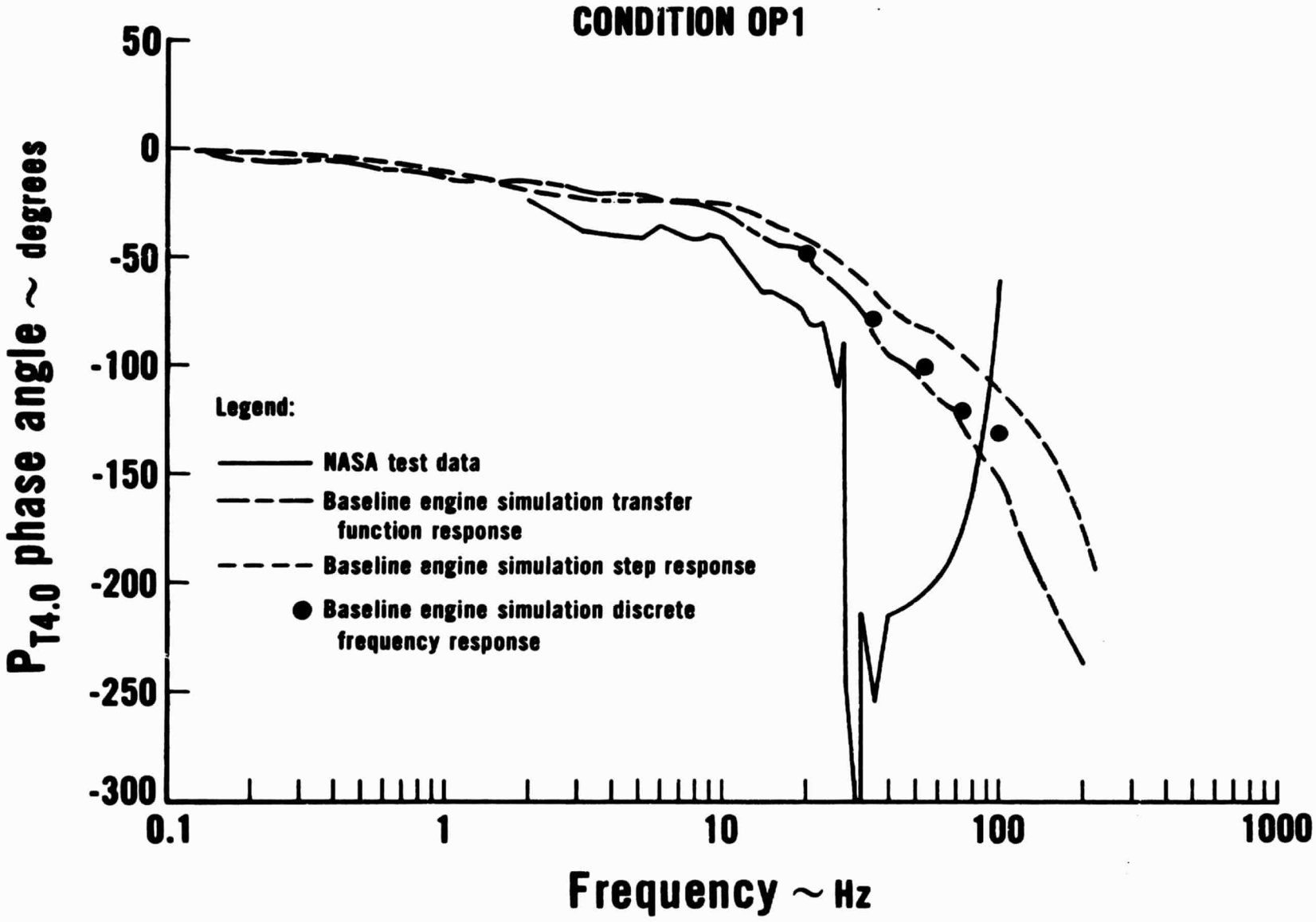

Figure 11 High Compressor Phase at Station 4.0

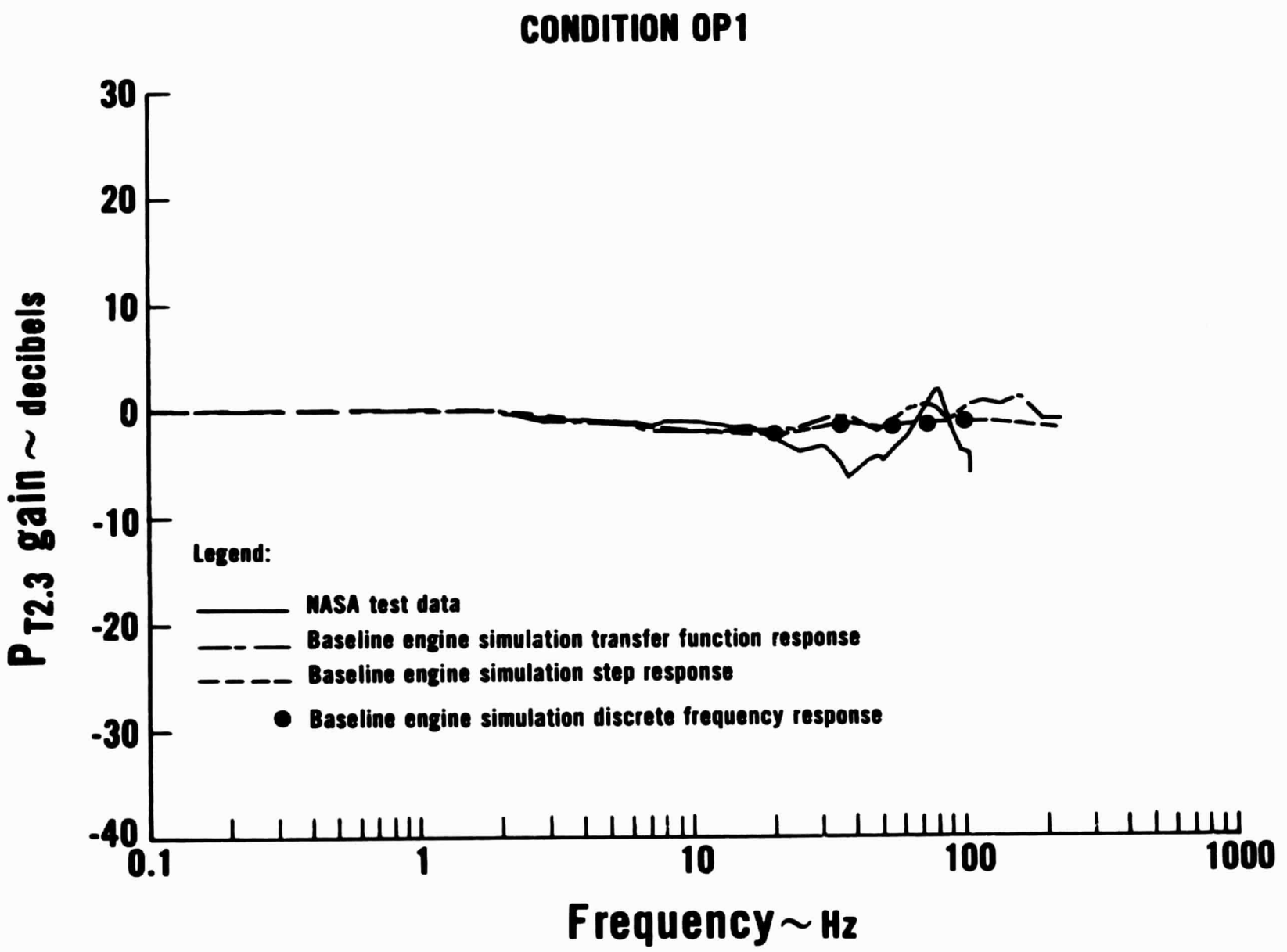

Figure 12 Fan Core Stream Gain at Station 2.3

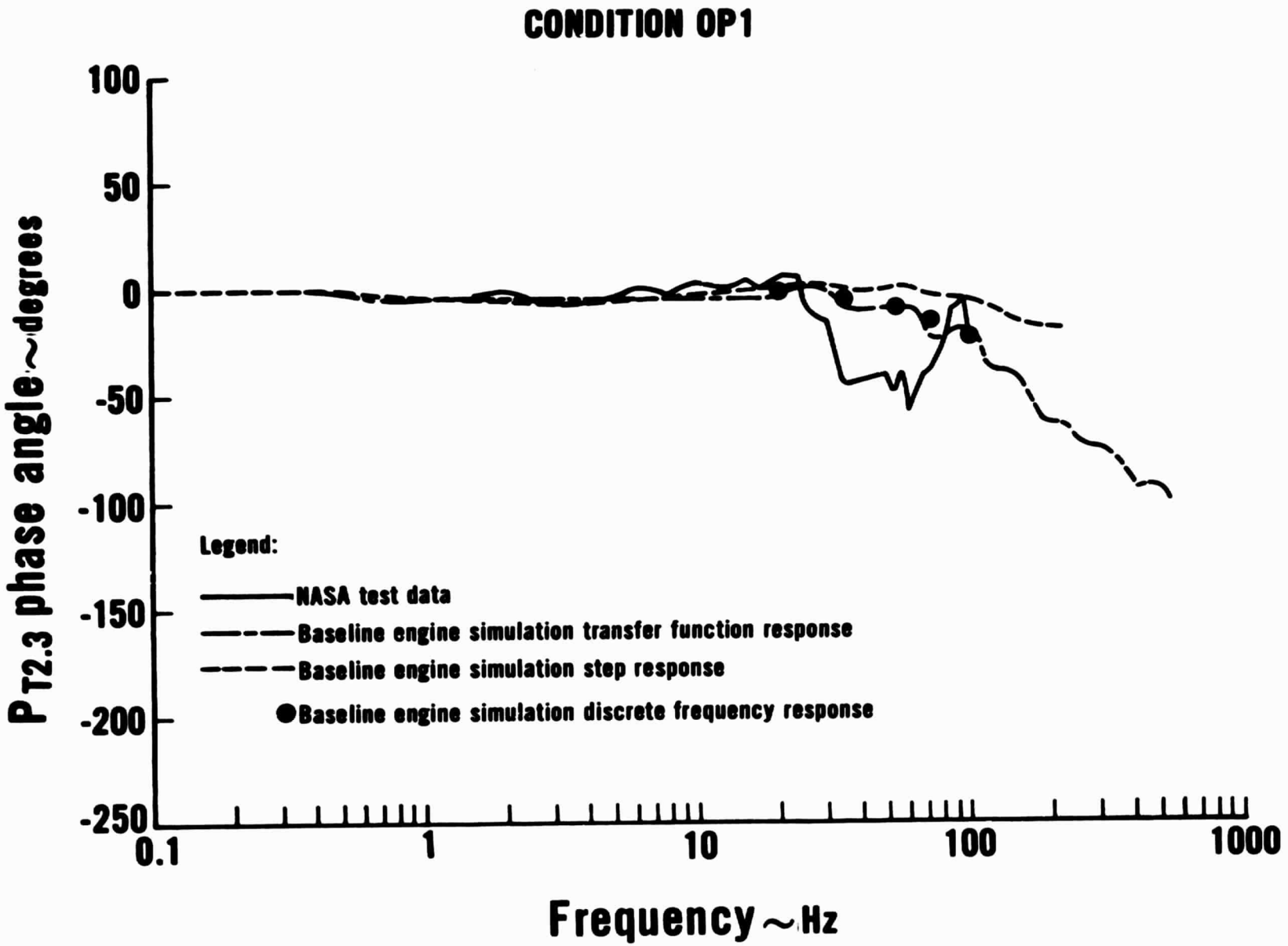

Figure 13 Fan Core Stream Phase at Station 2.3

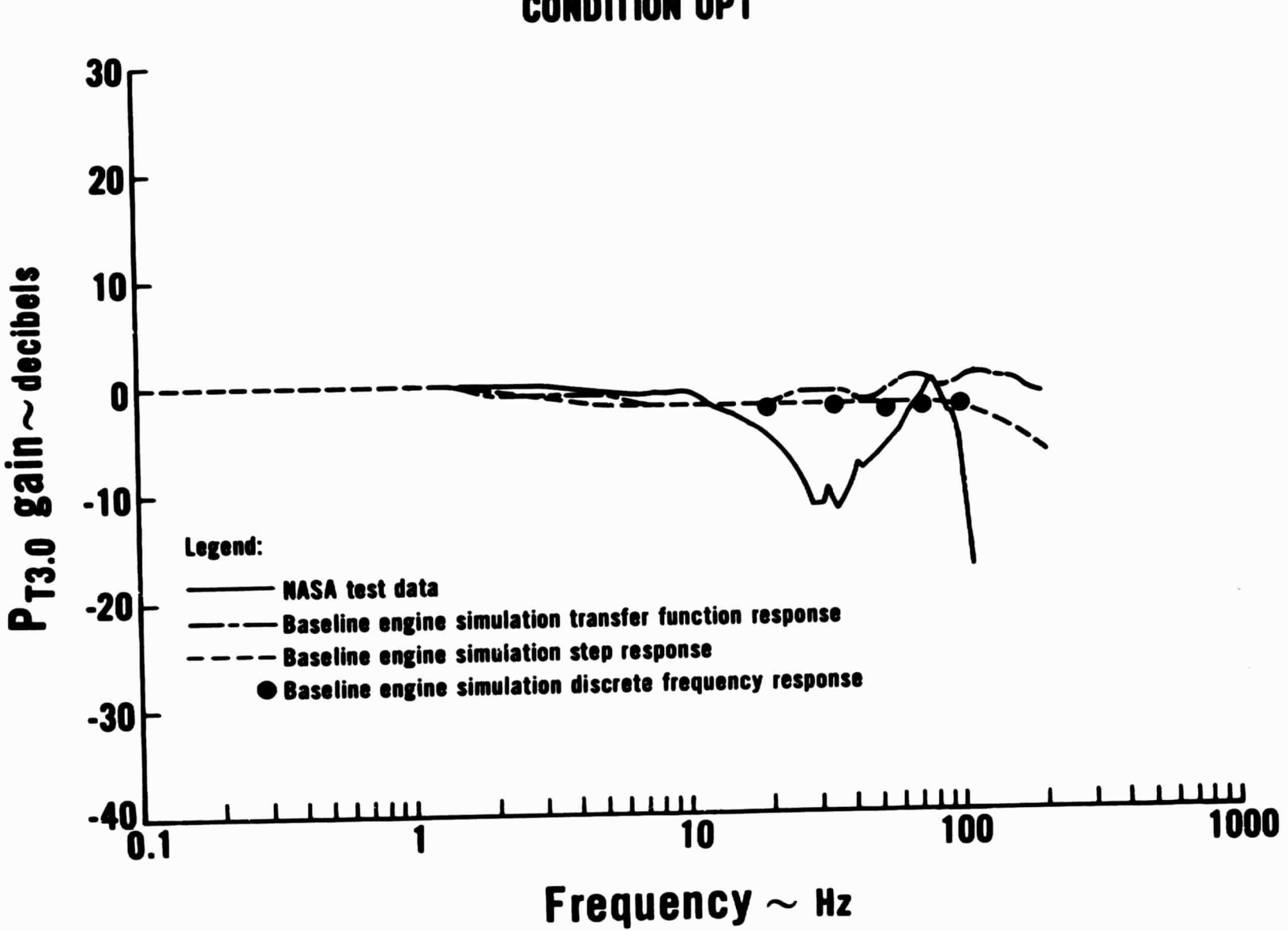

Figure 14 Low Compressor Gain at Station 3.0

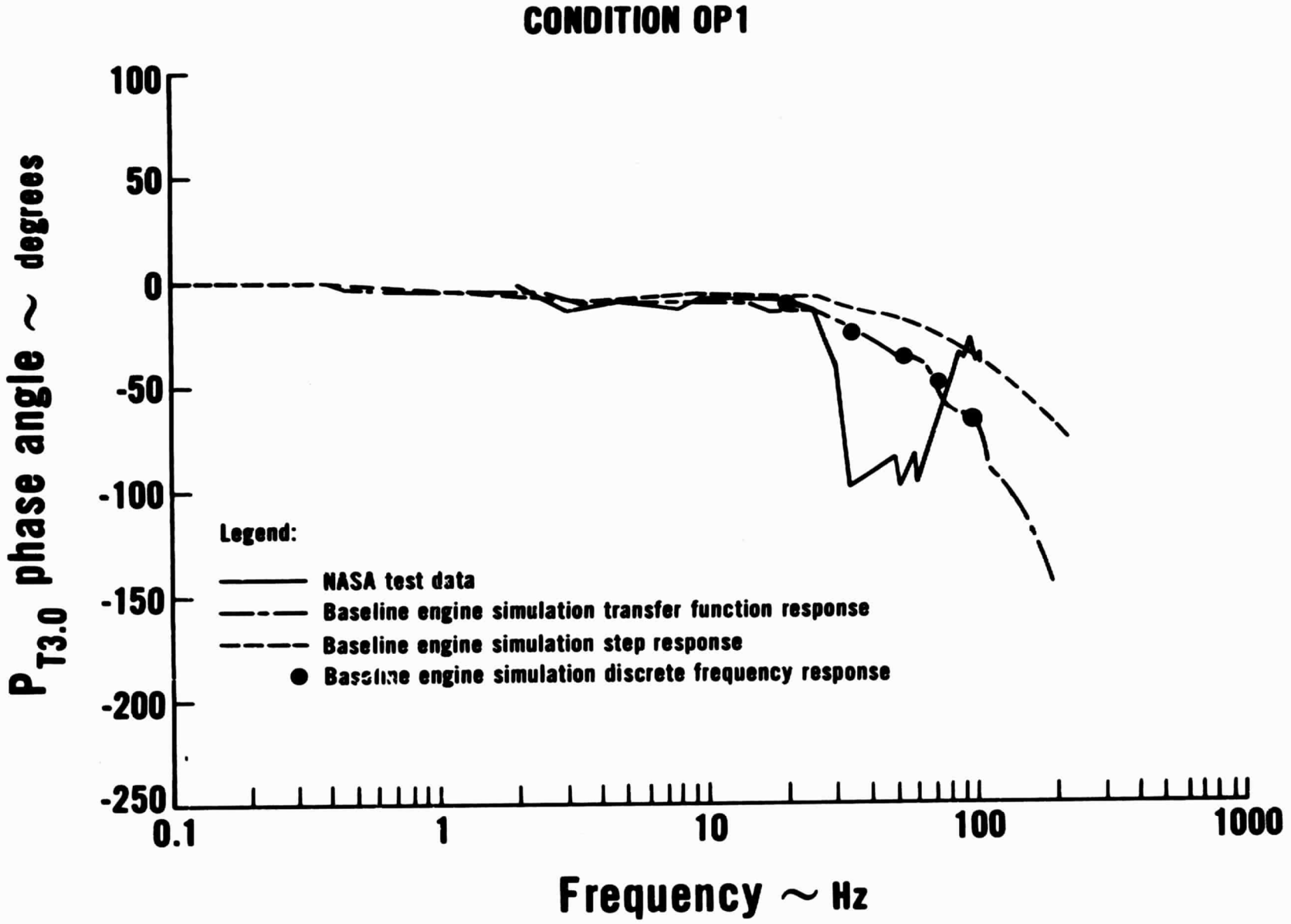

Figure 15 Low Compressor Phase at Station 3.0

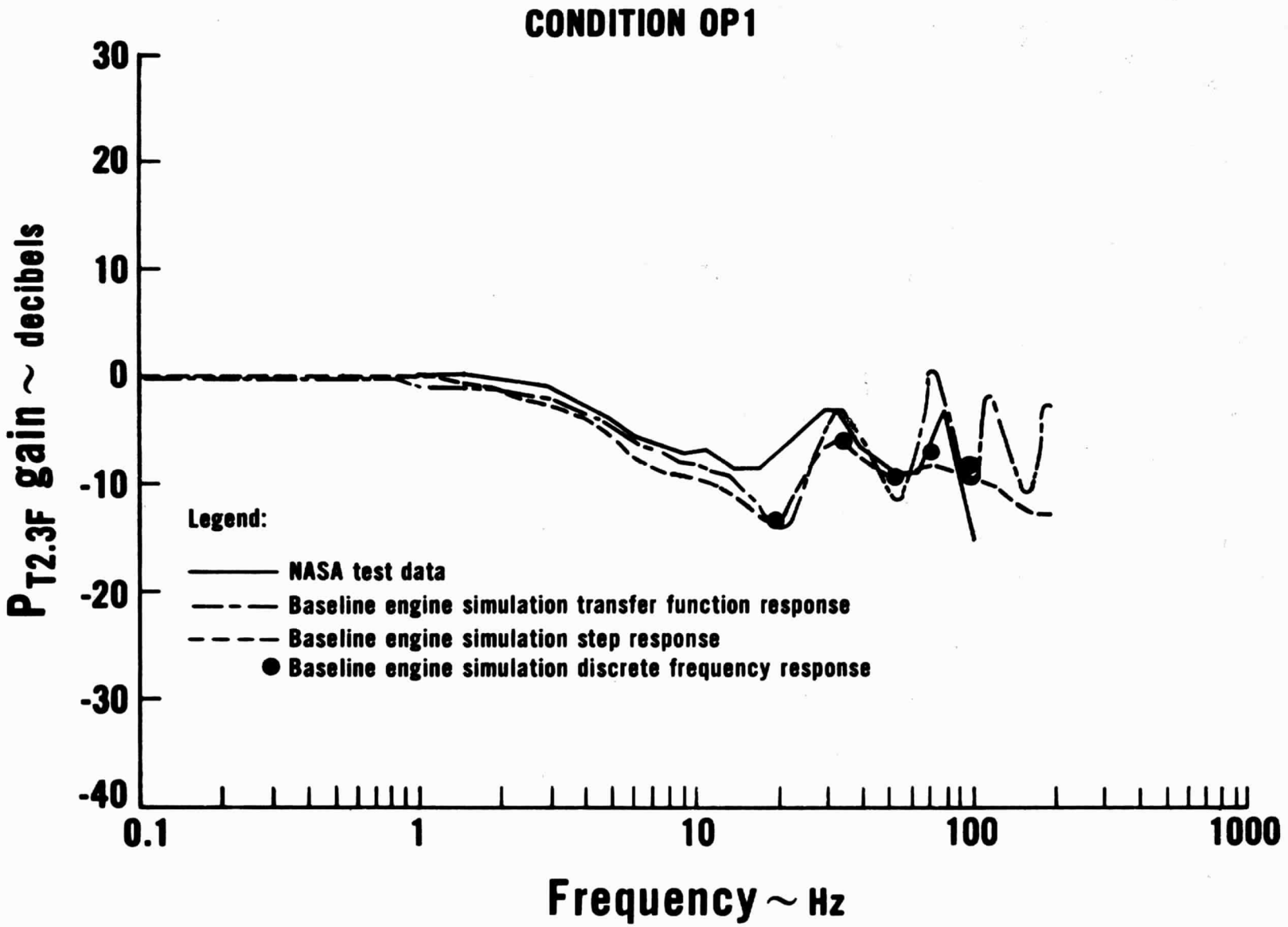

Figure 16 Fan Bypass Stream Gain at Station 2.3F

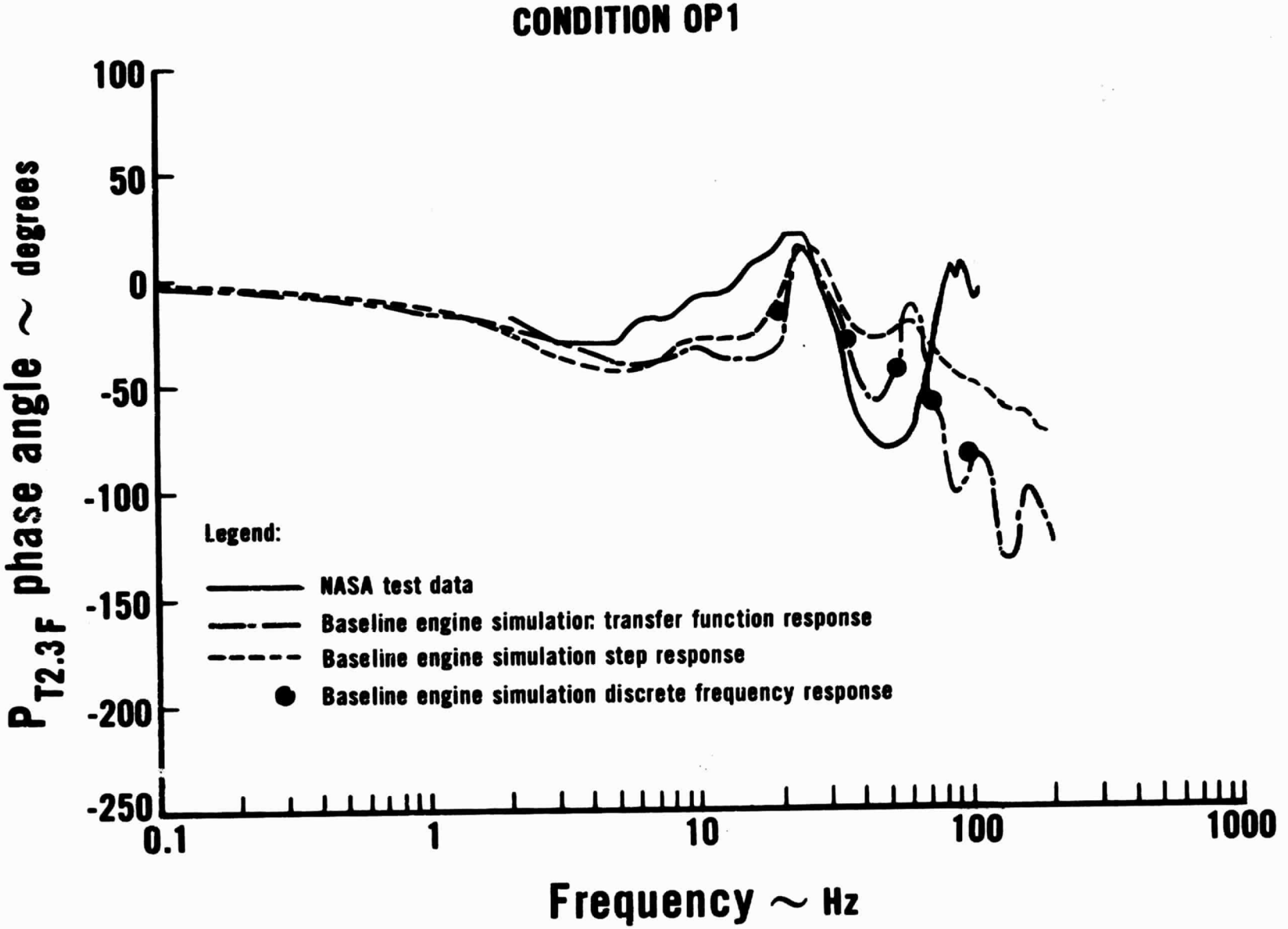

Figure 17 Fan Bypass Stream Phase at Station 2.3F

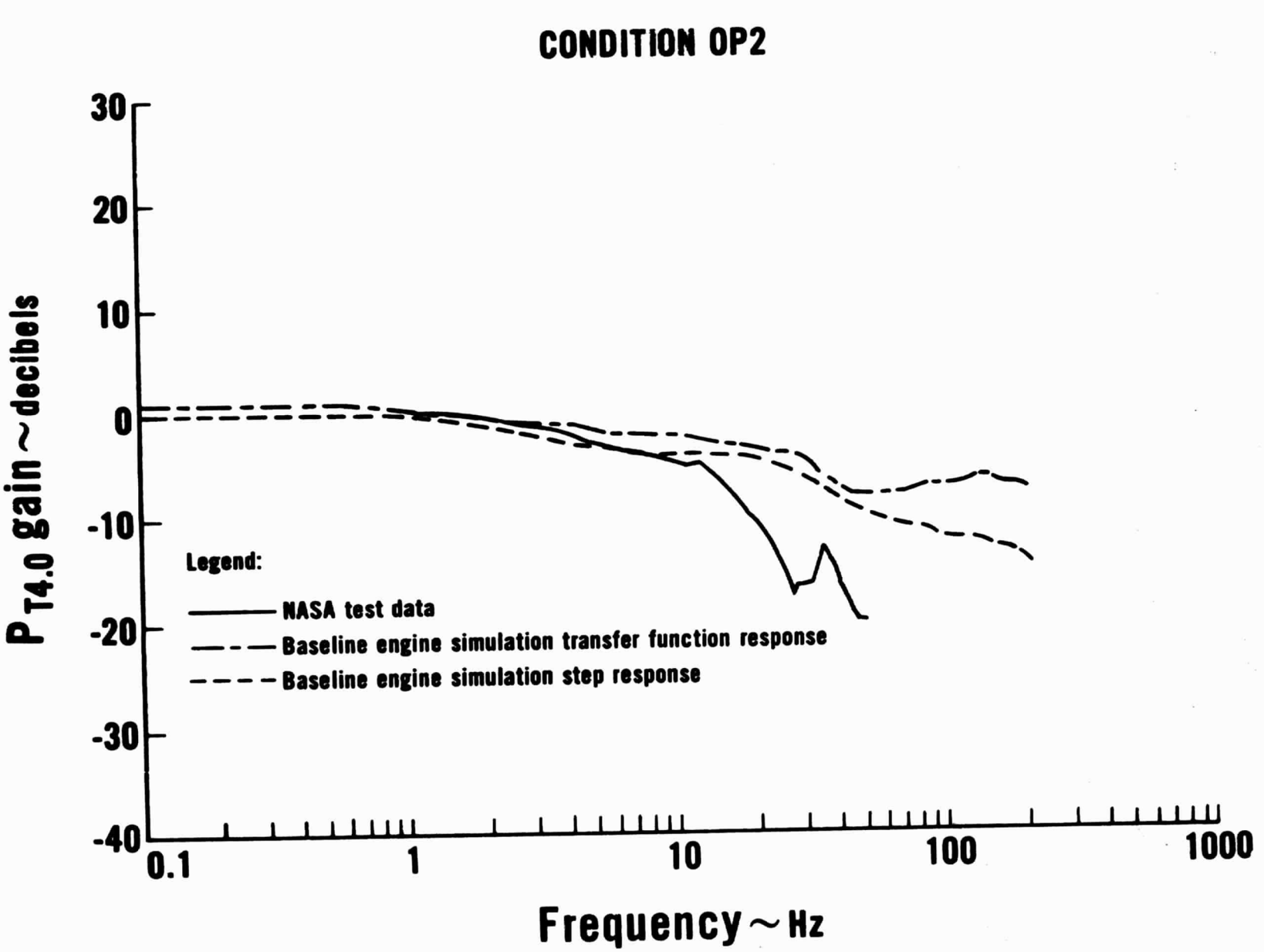

Figure 18 High Compressor Gain at Station 4.0

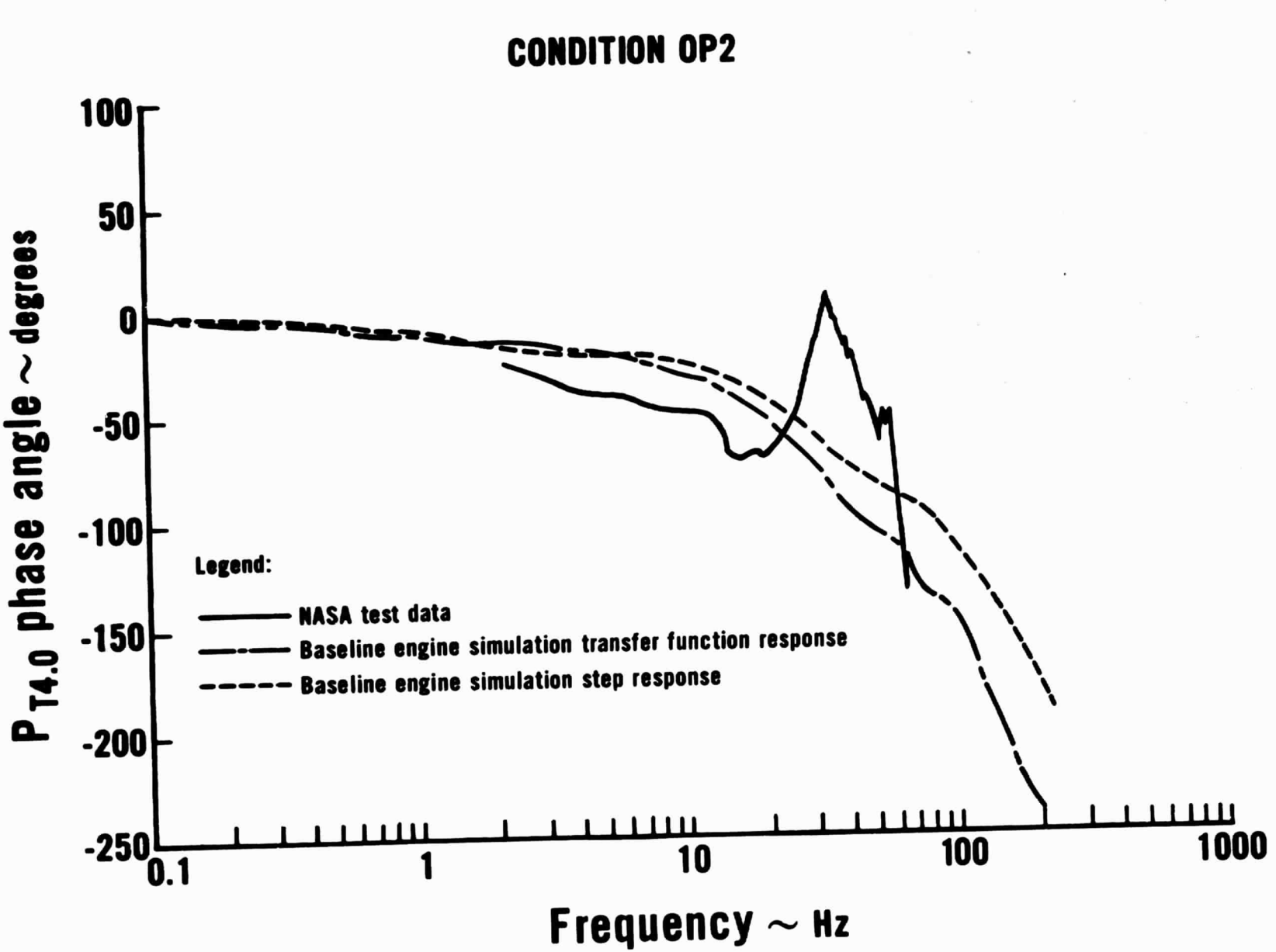

Figure 19 High Compressor Phase at Station 4.0

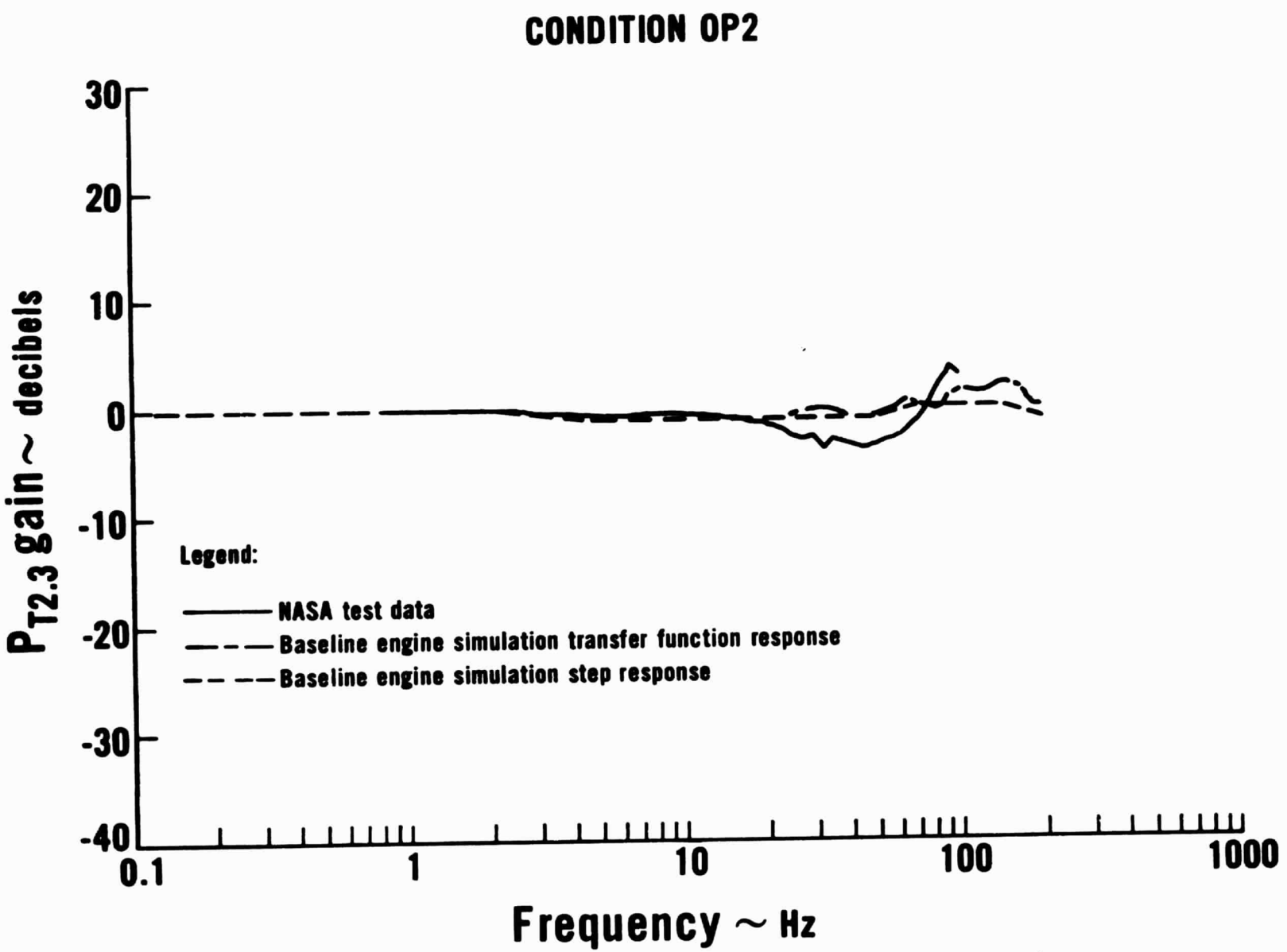

Figure 20 Fan Core Stream Gain at Station 2.3

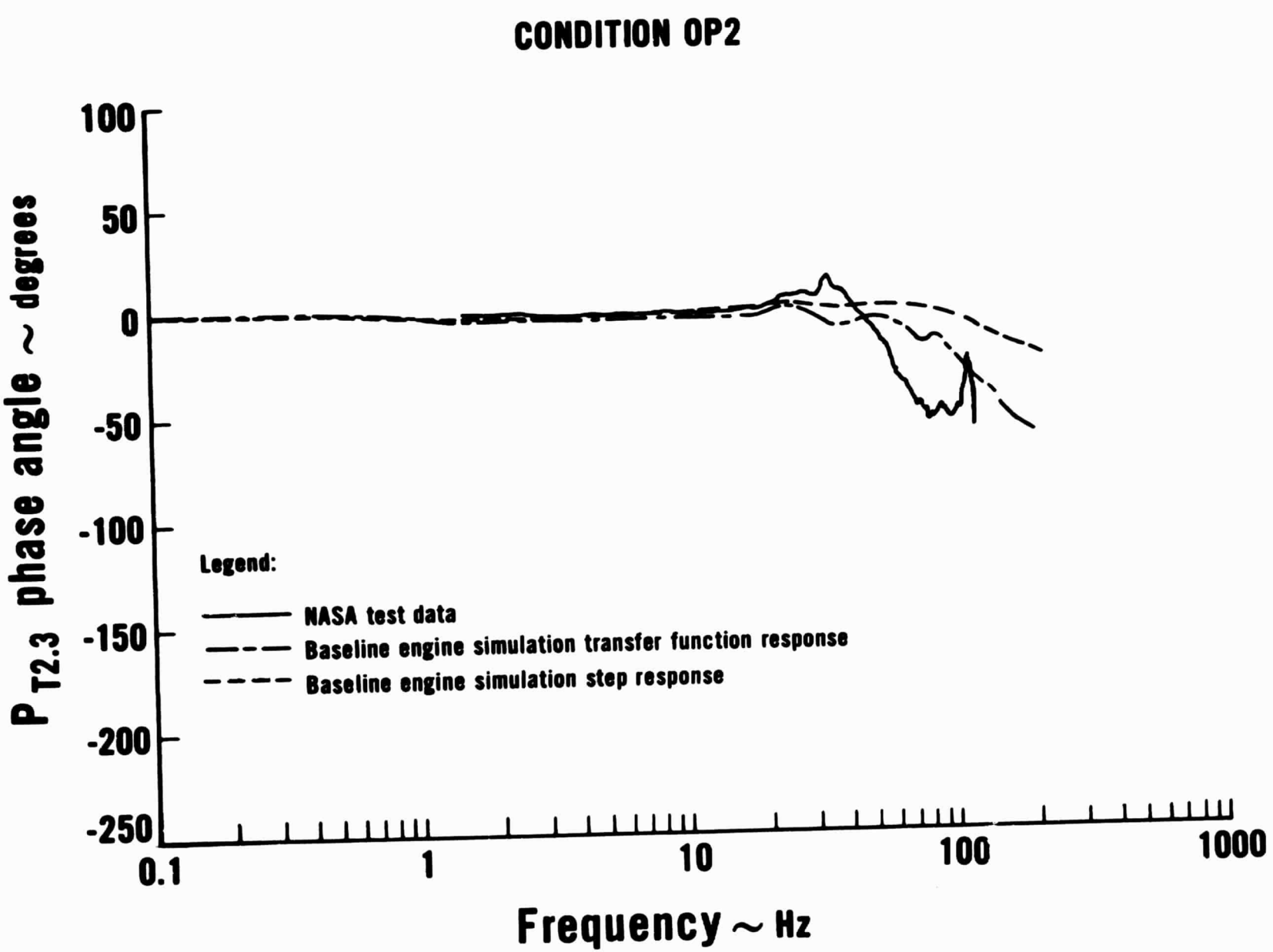

Figure 21 Fan Core Stream Phase at Station 2.3

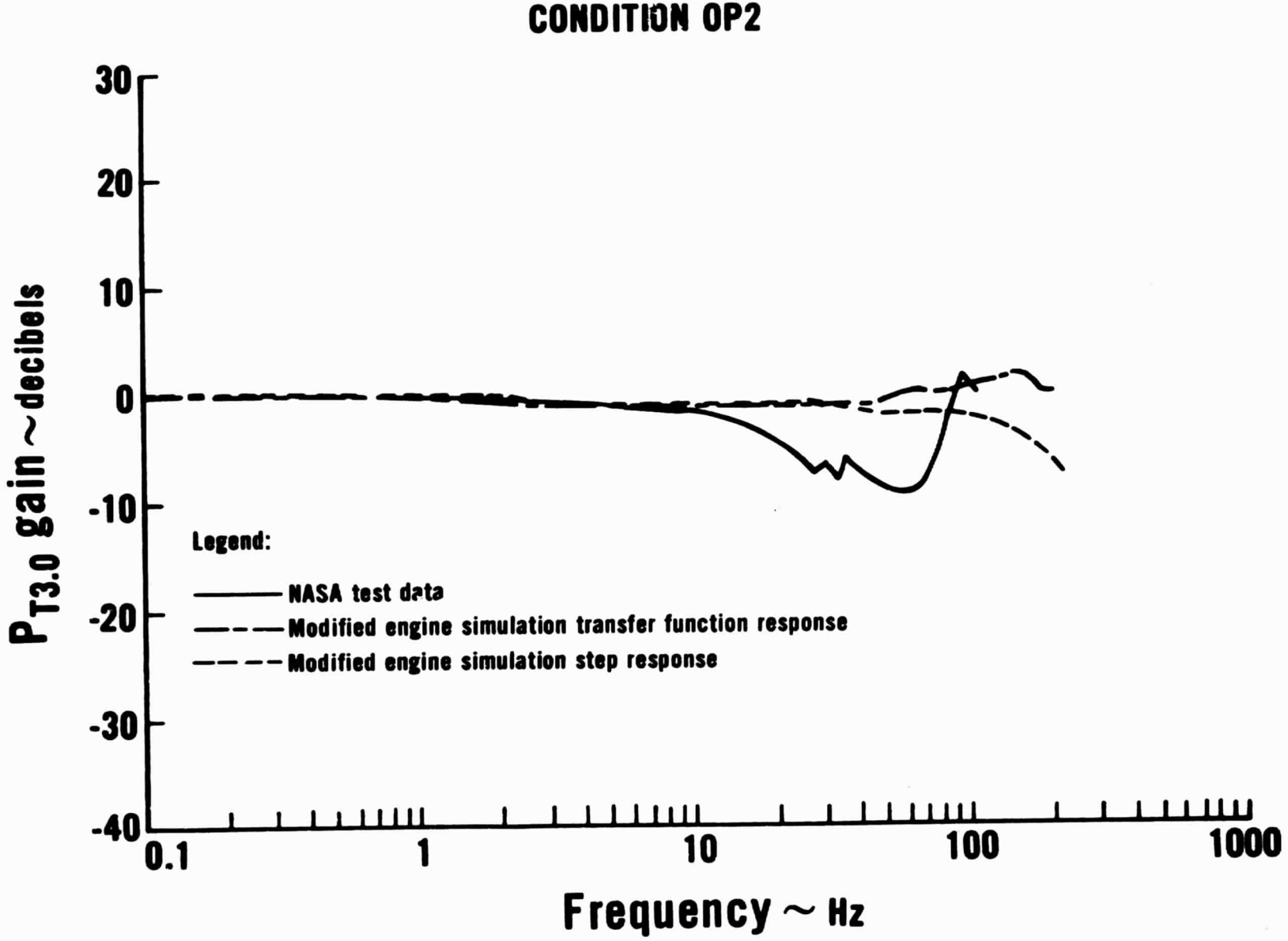

Figure 22 Low Compressor Gain at Station 3.0

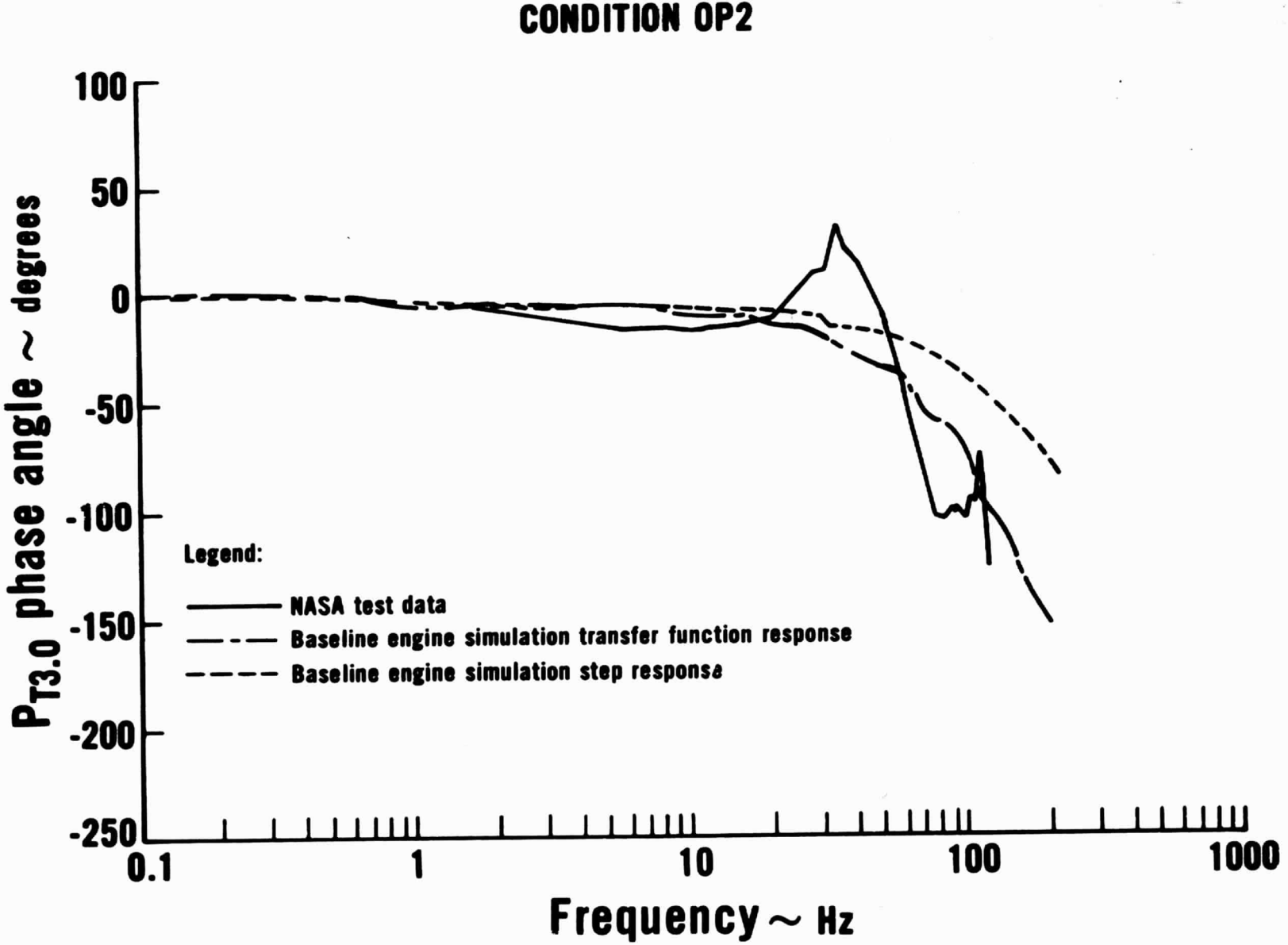

Figure 23 Low Compressor Phase at Station 3.0

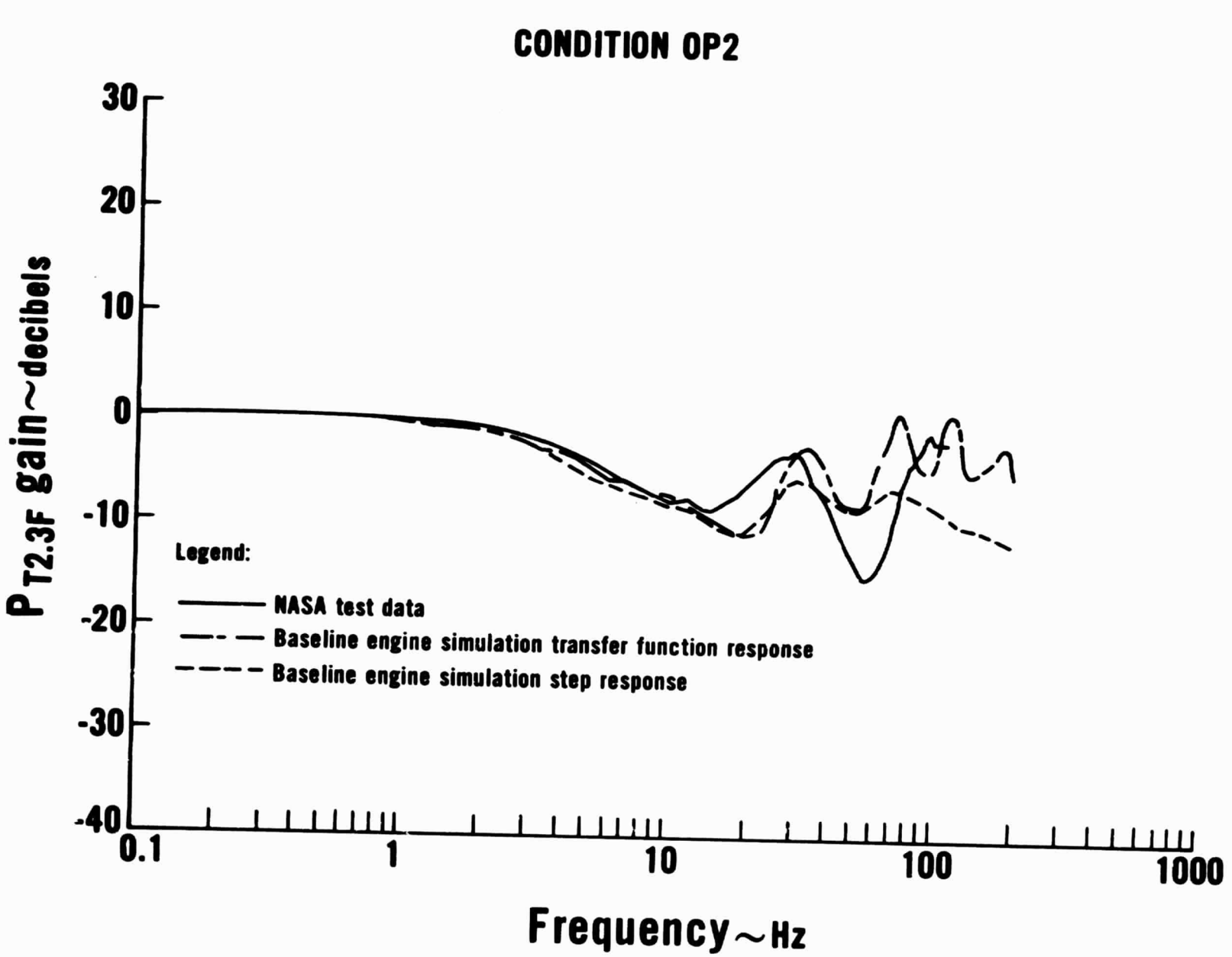

Figure 24 Fan Bypass Stream Gain at Station 2.3F

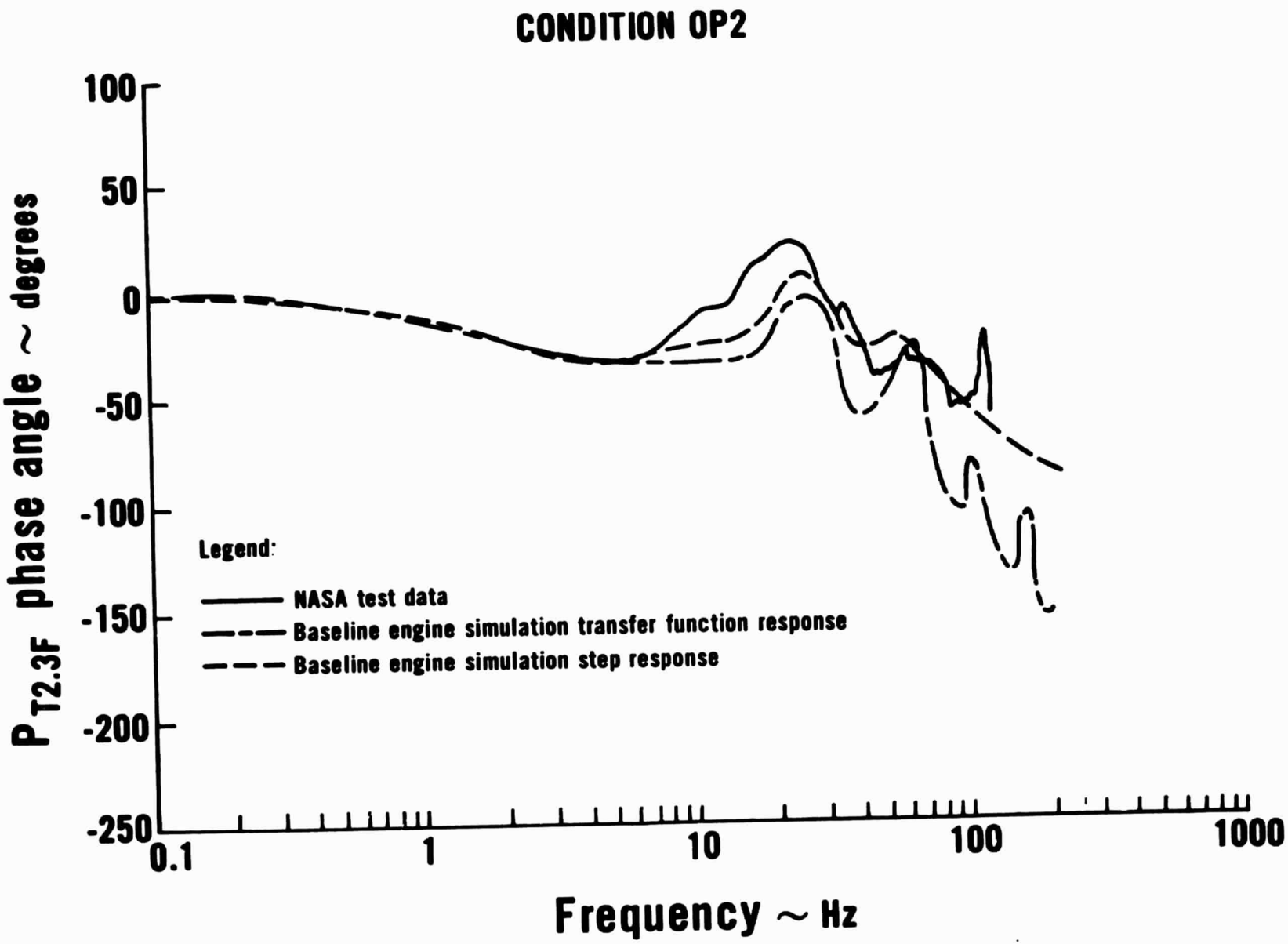

Figure 25 Fan Bypass Stream Phase at Station 2.3F

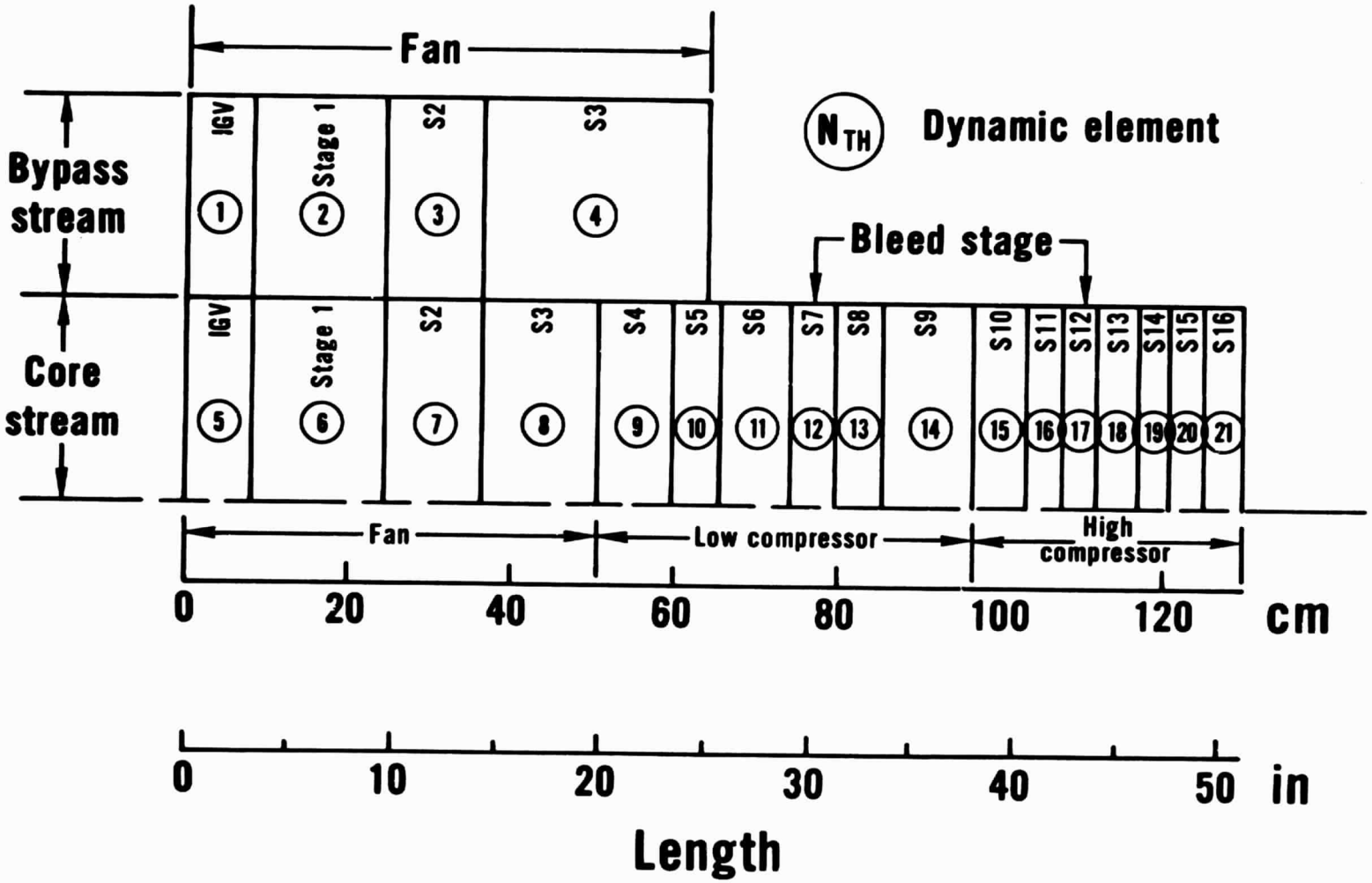

Figure 26 Compression System Simulation, Stage-By-Stage Configuration

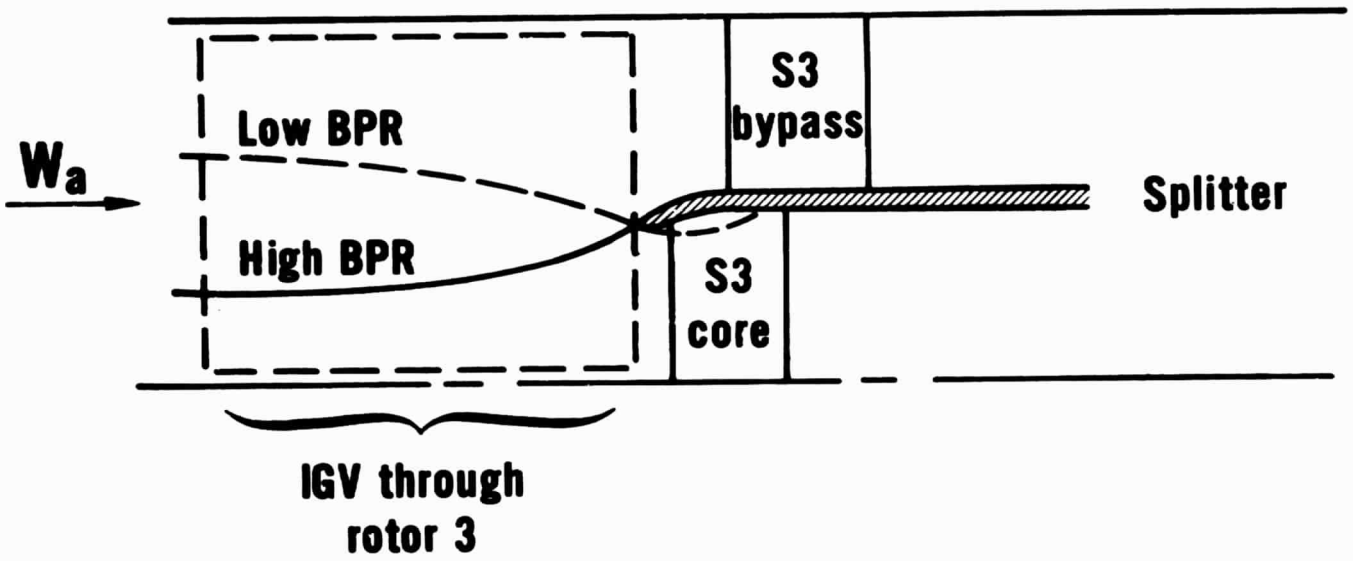

Figure 27 *Bypass Ratio Effects on Dividing Streamline Location and Core Stream Stator Operation*

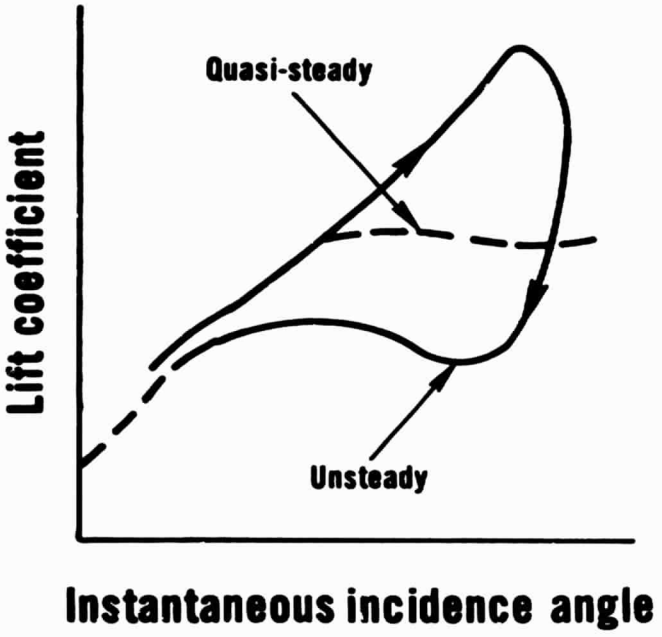

Figure 28 Airfoil Lift Characteristics

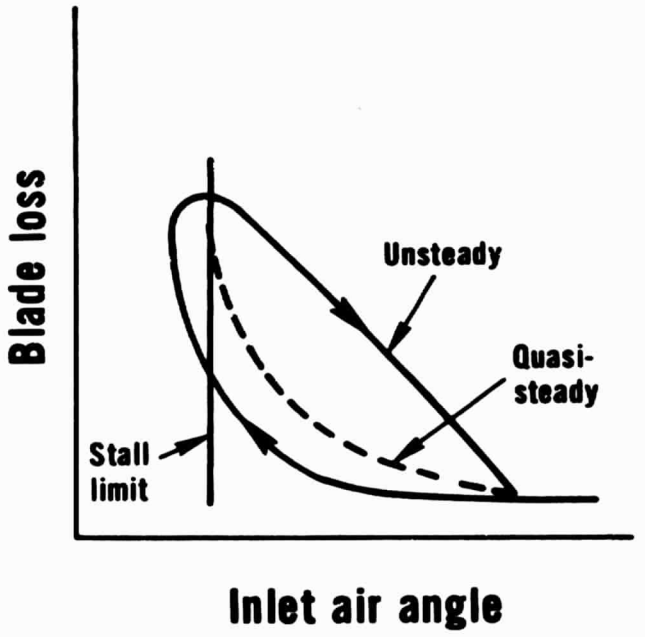

Figure 29 Compressor Airfoil Loss Characteristics

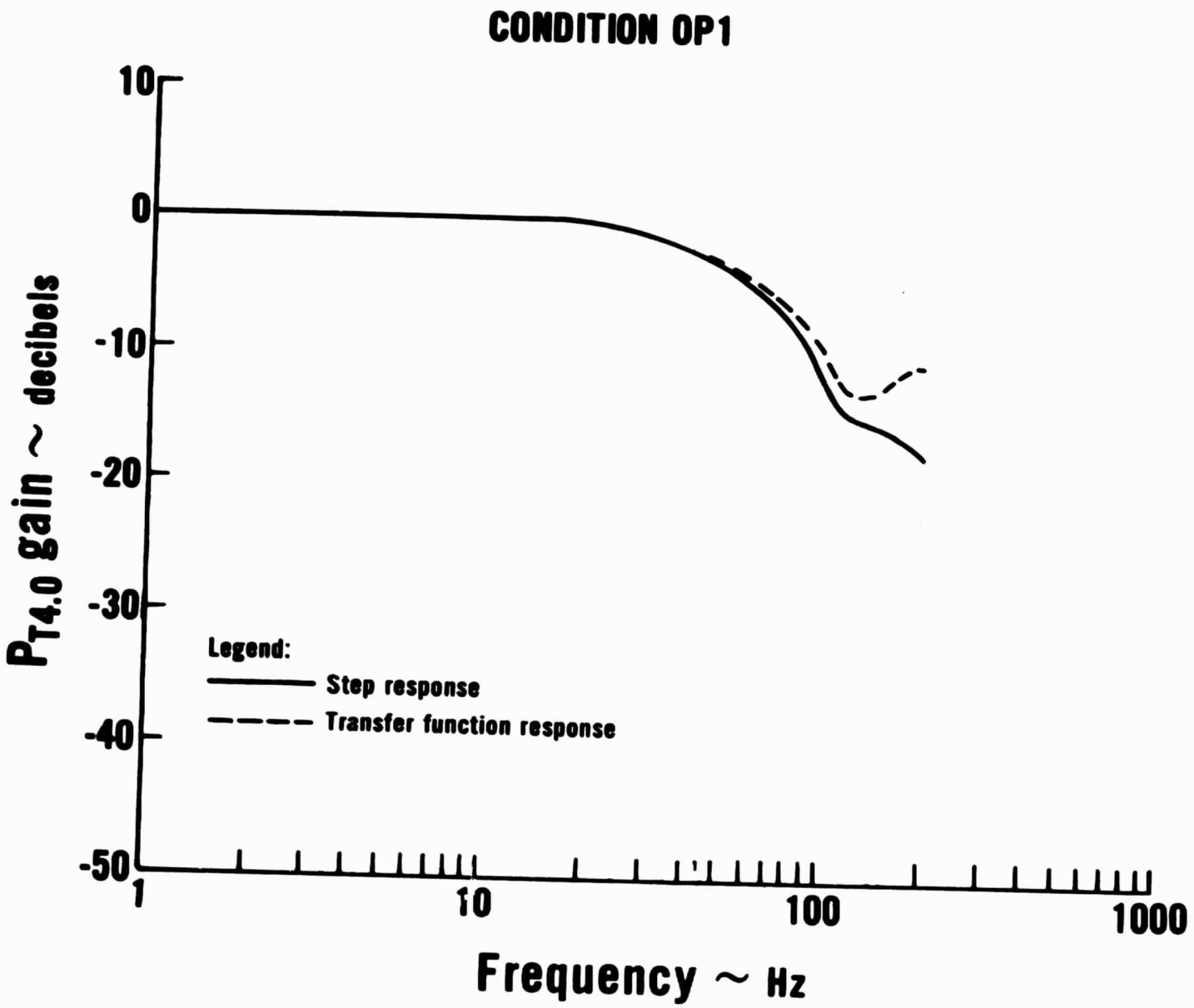

Figure 30 Stage-By-Stage Compression System Simulation Gain at Station 4.0

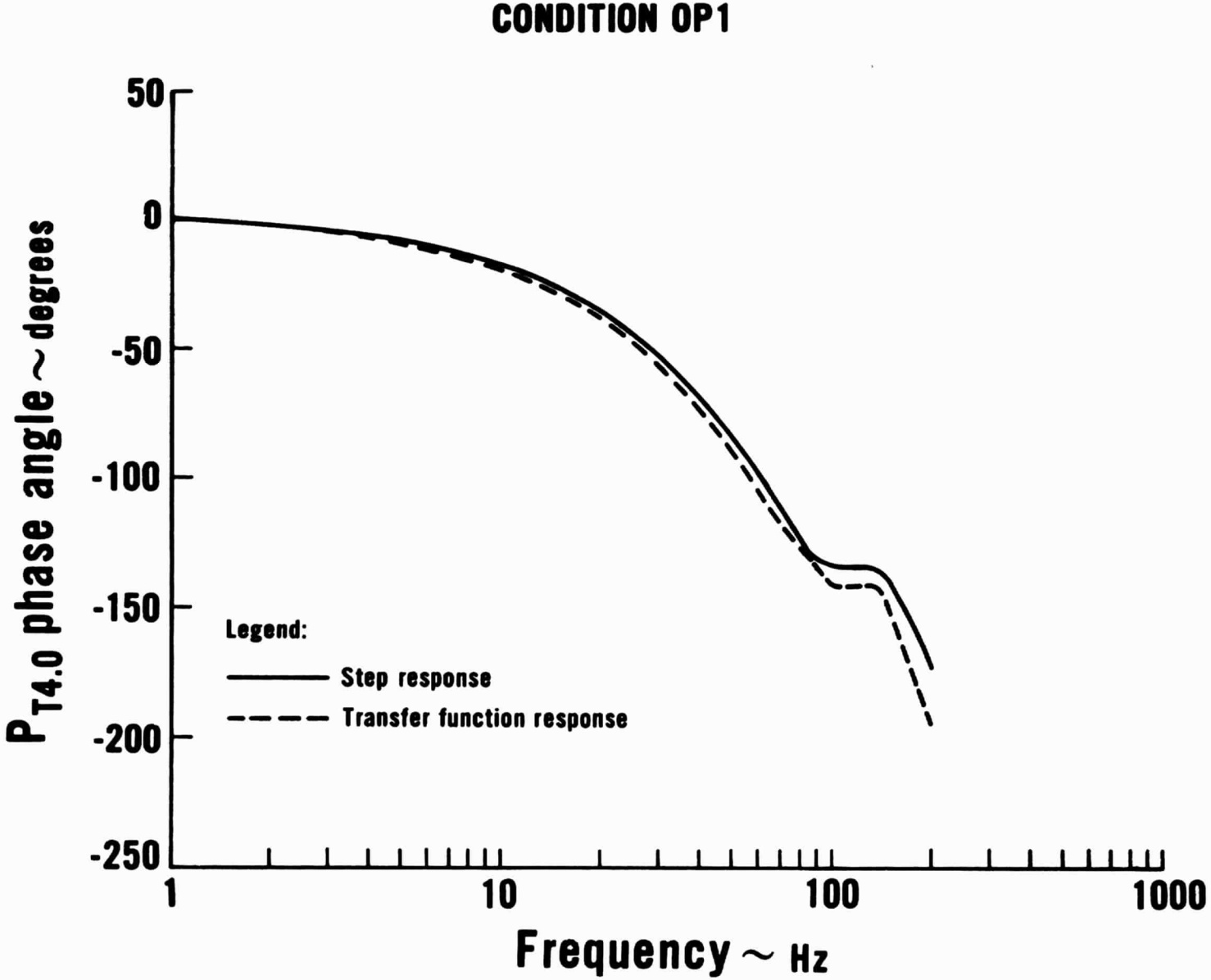

Figure 31 Stage-By-Stage Compression System Simulation Phase at Station 4.0

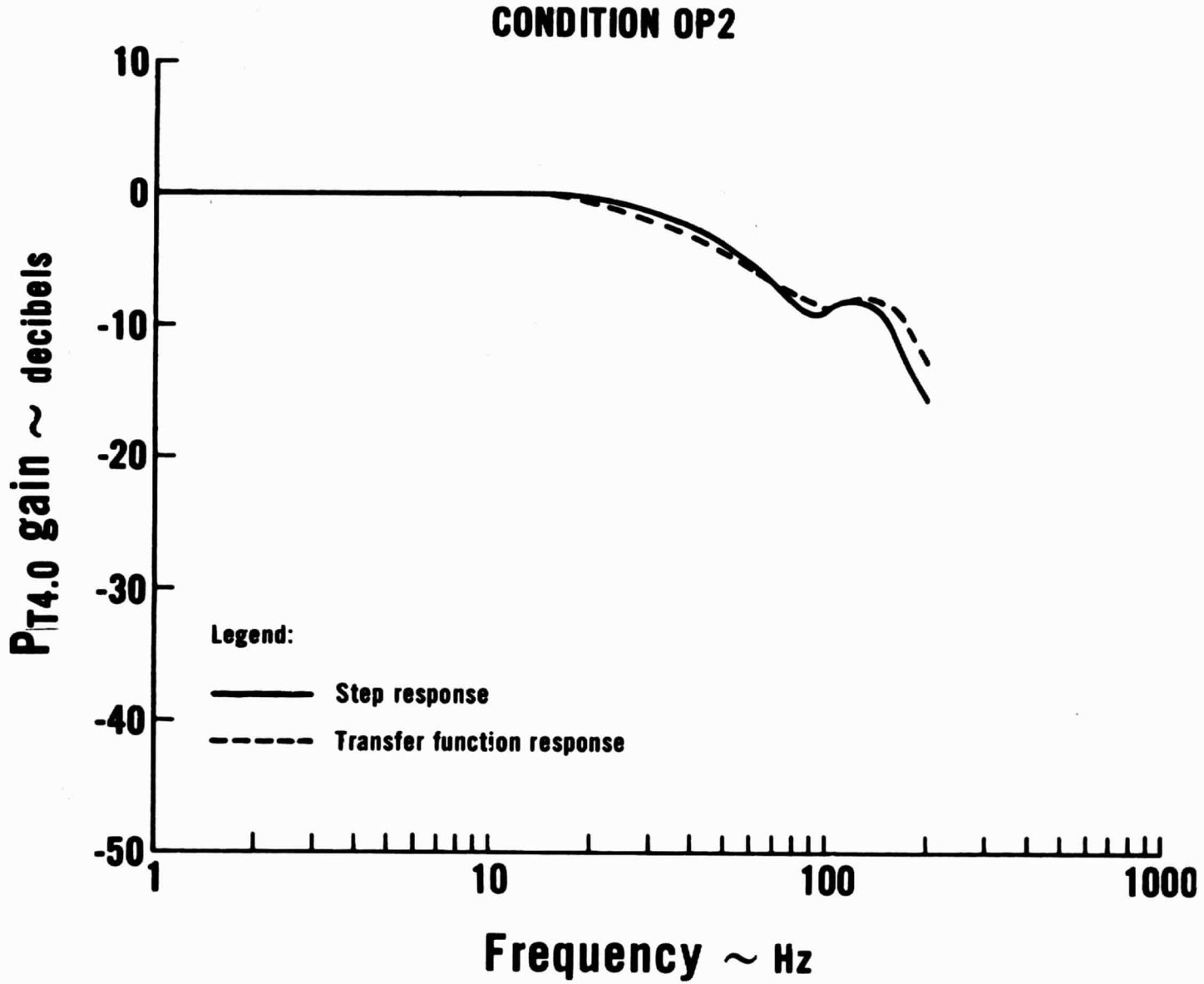

Figure 32 Stage-By-Stage Compression System Simulation Gain at Station 4.0

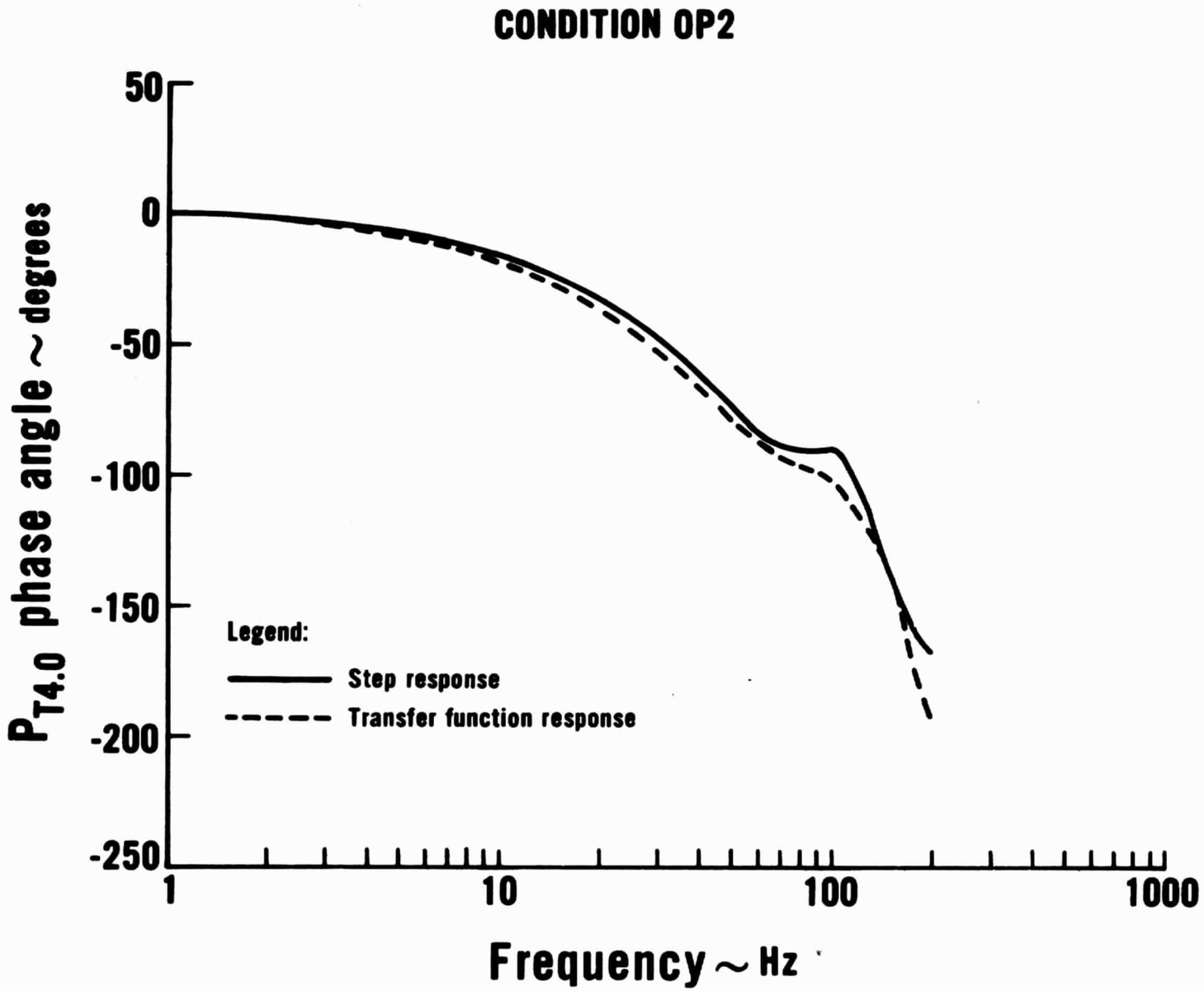

Figure 33 Stage-By-Stage Compression System Simulation Phase at Station 4.0

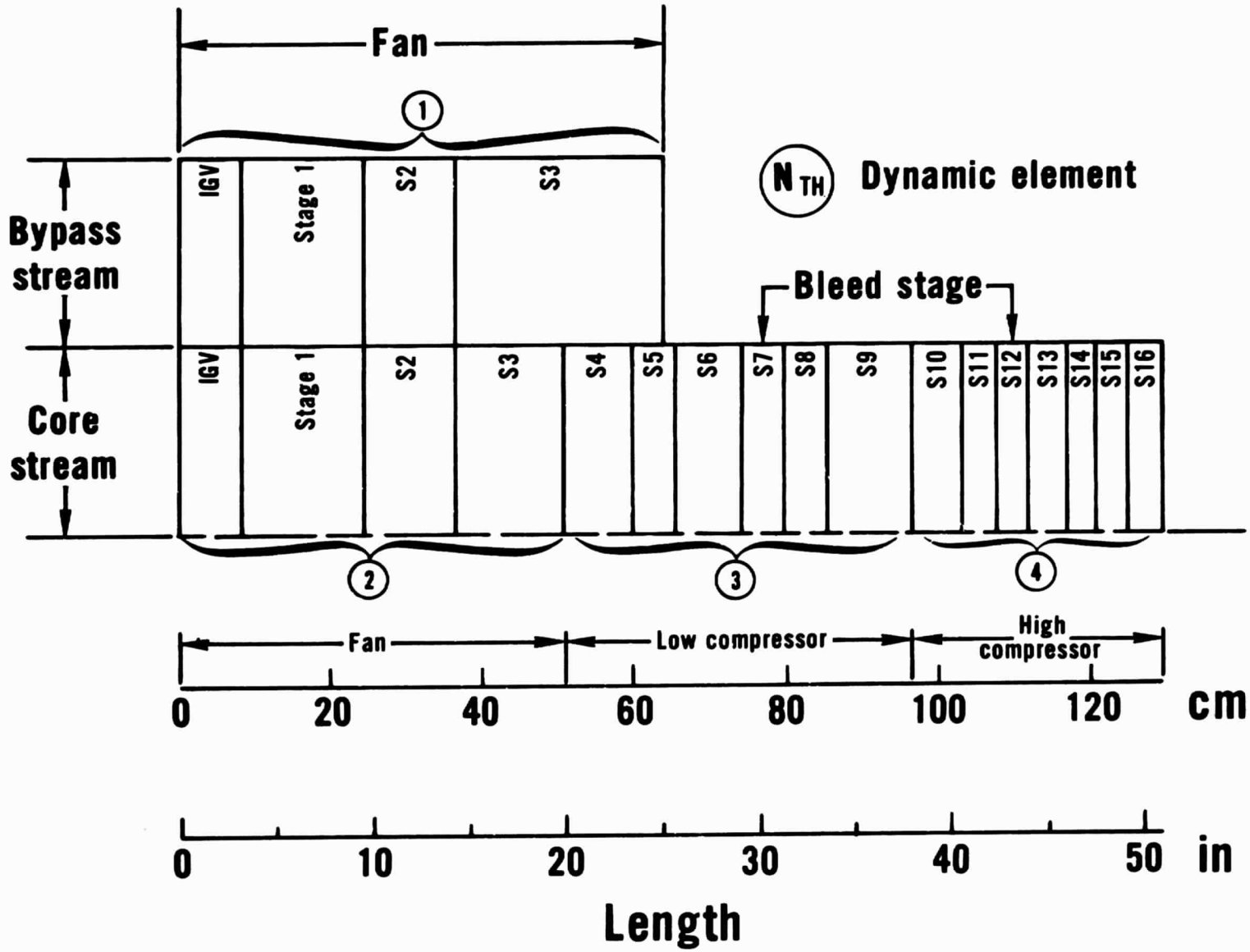

Figure 34 *Reduced Order Compression System Simulation, Fan/Low/High Lumped Configuration.*

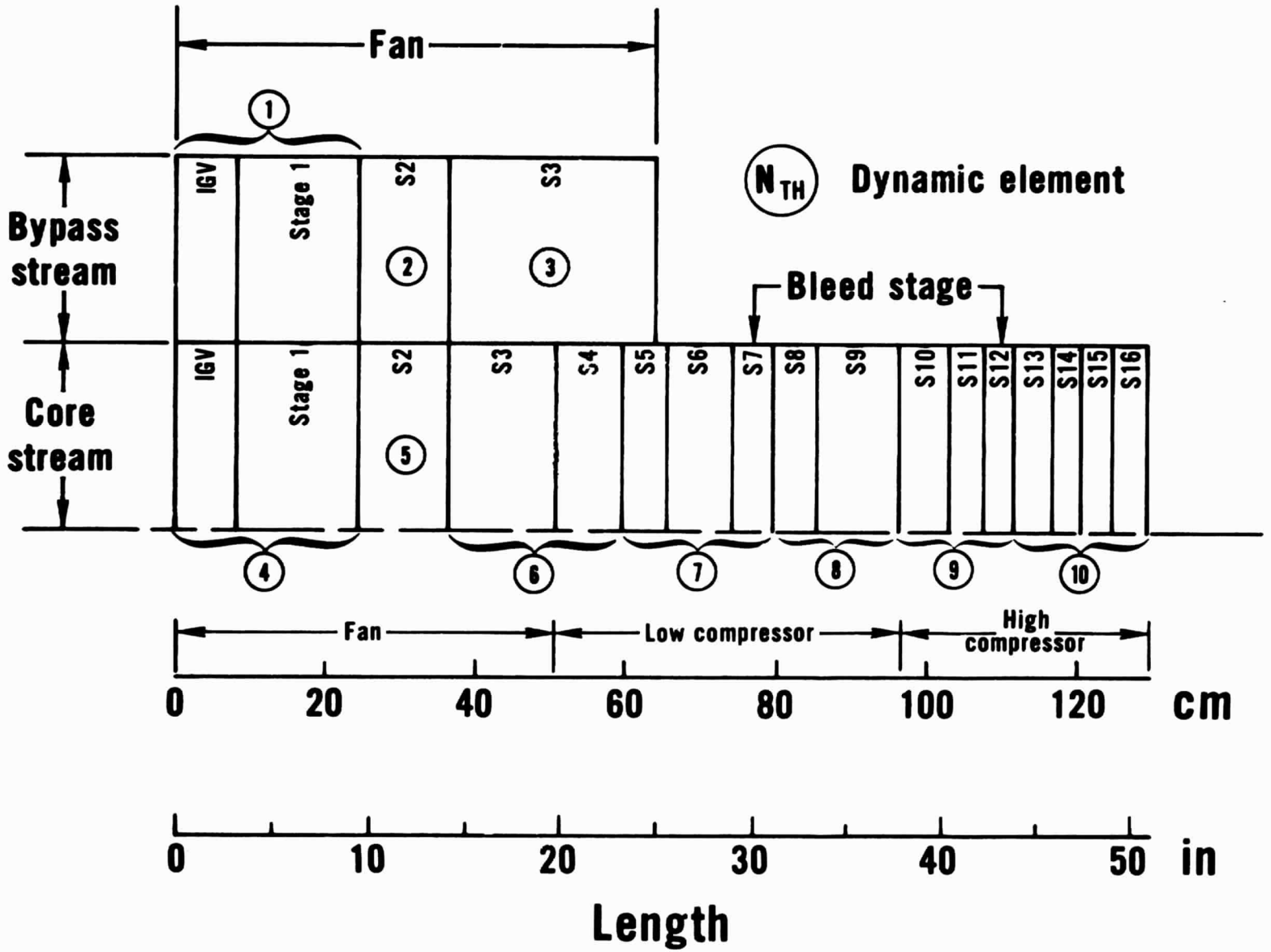

Figure 35 Reduced Order Compression System Simulation, Ten Element Configuration

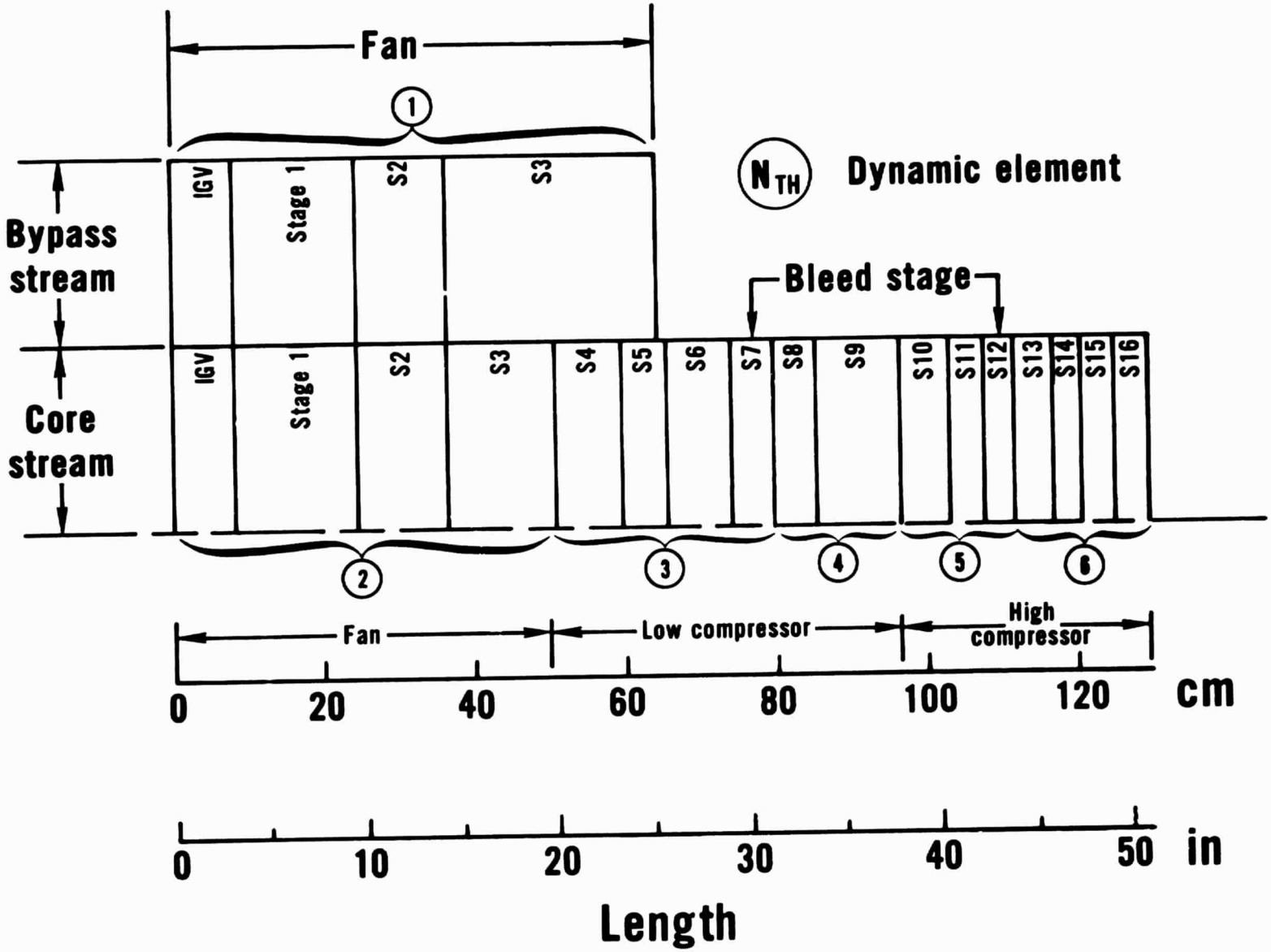

Figure 36 Reduced Order Compression System Simulation, Bleed Configuration

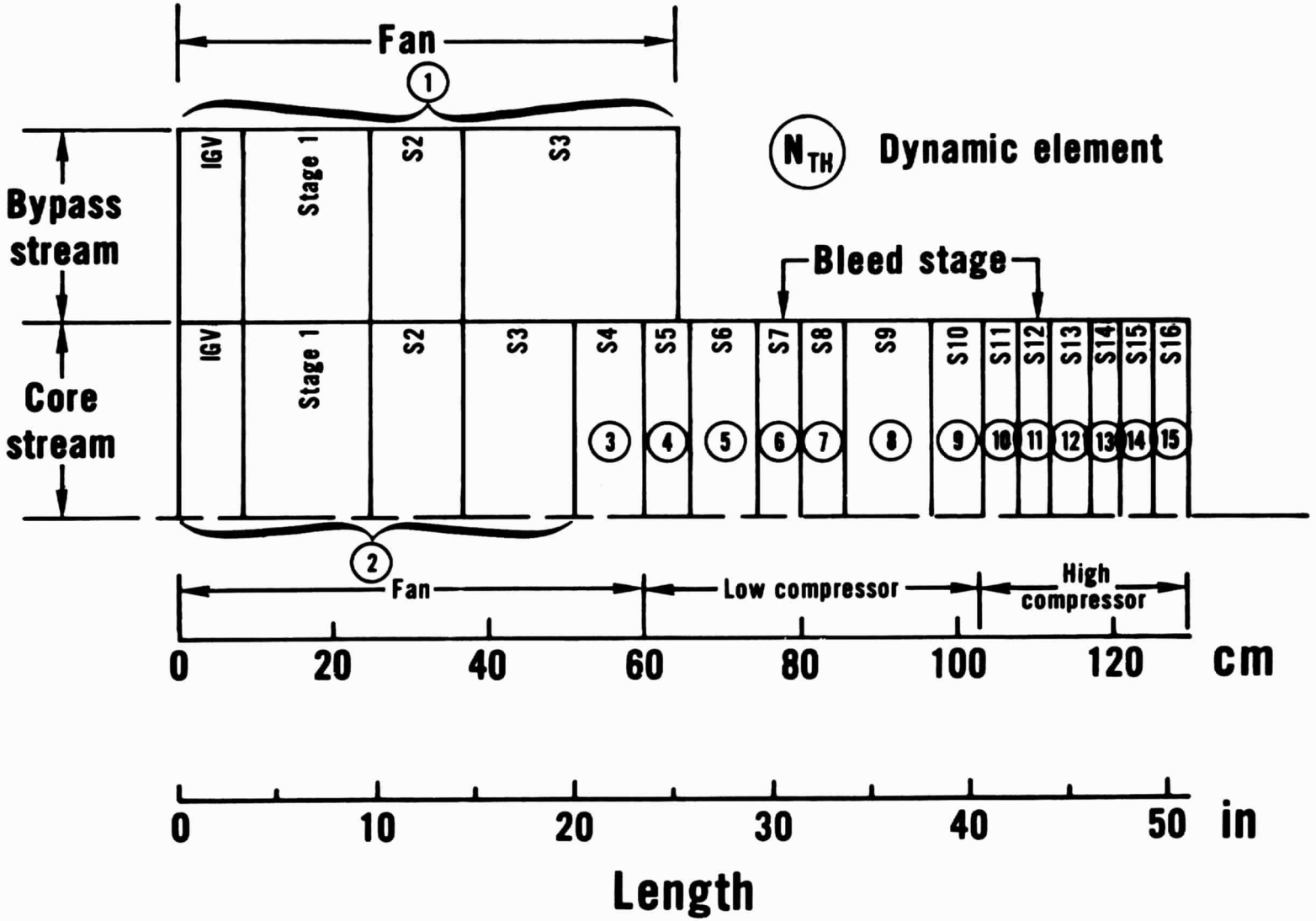

Figure 37 Reduced Order Compression System Simulation, Fan Lumped/Compressors Staged Configuration

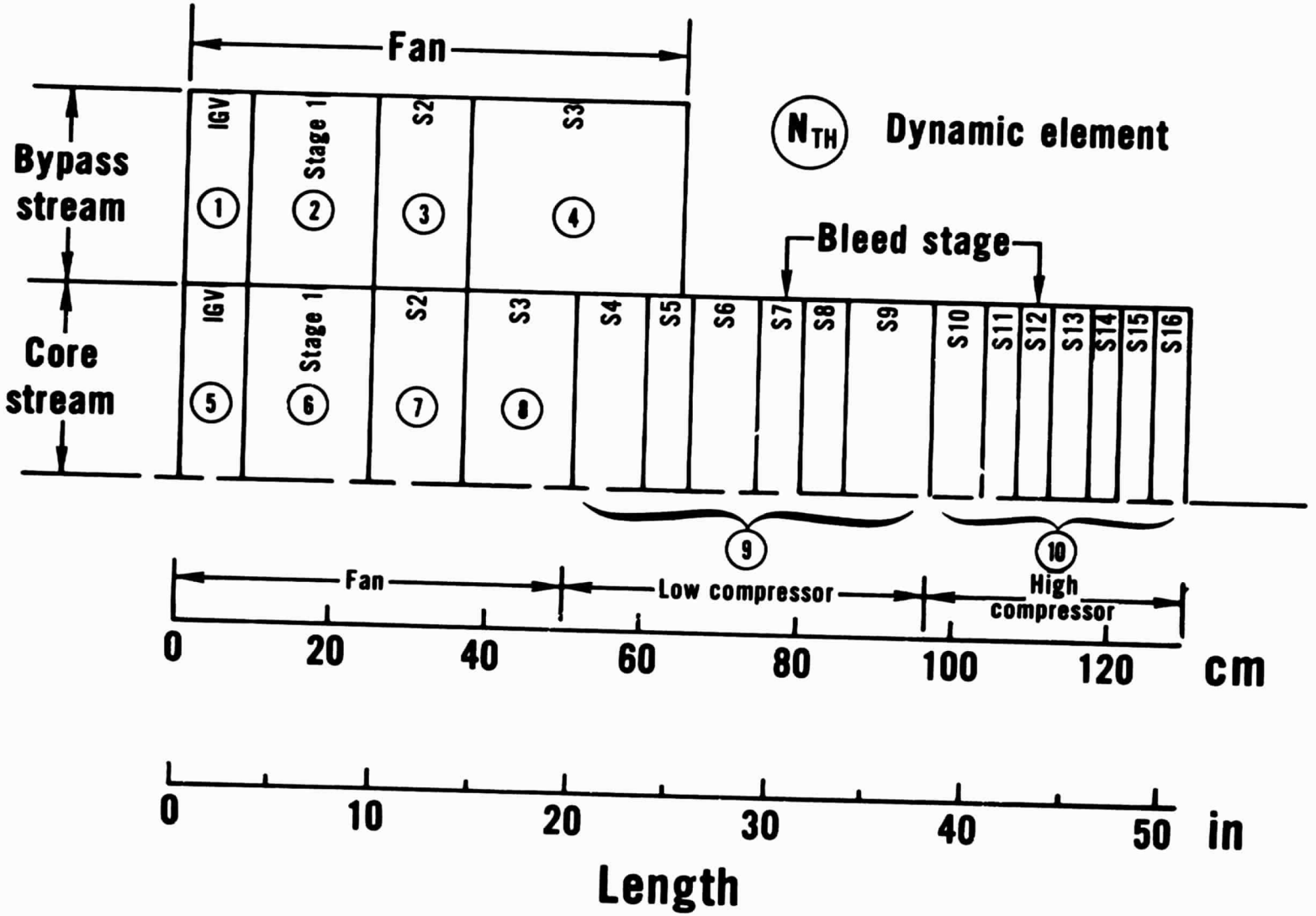

Figure 38 *Reduced Order Compression System Simulation, Fan Staged/Compressors Lumped Configuration*

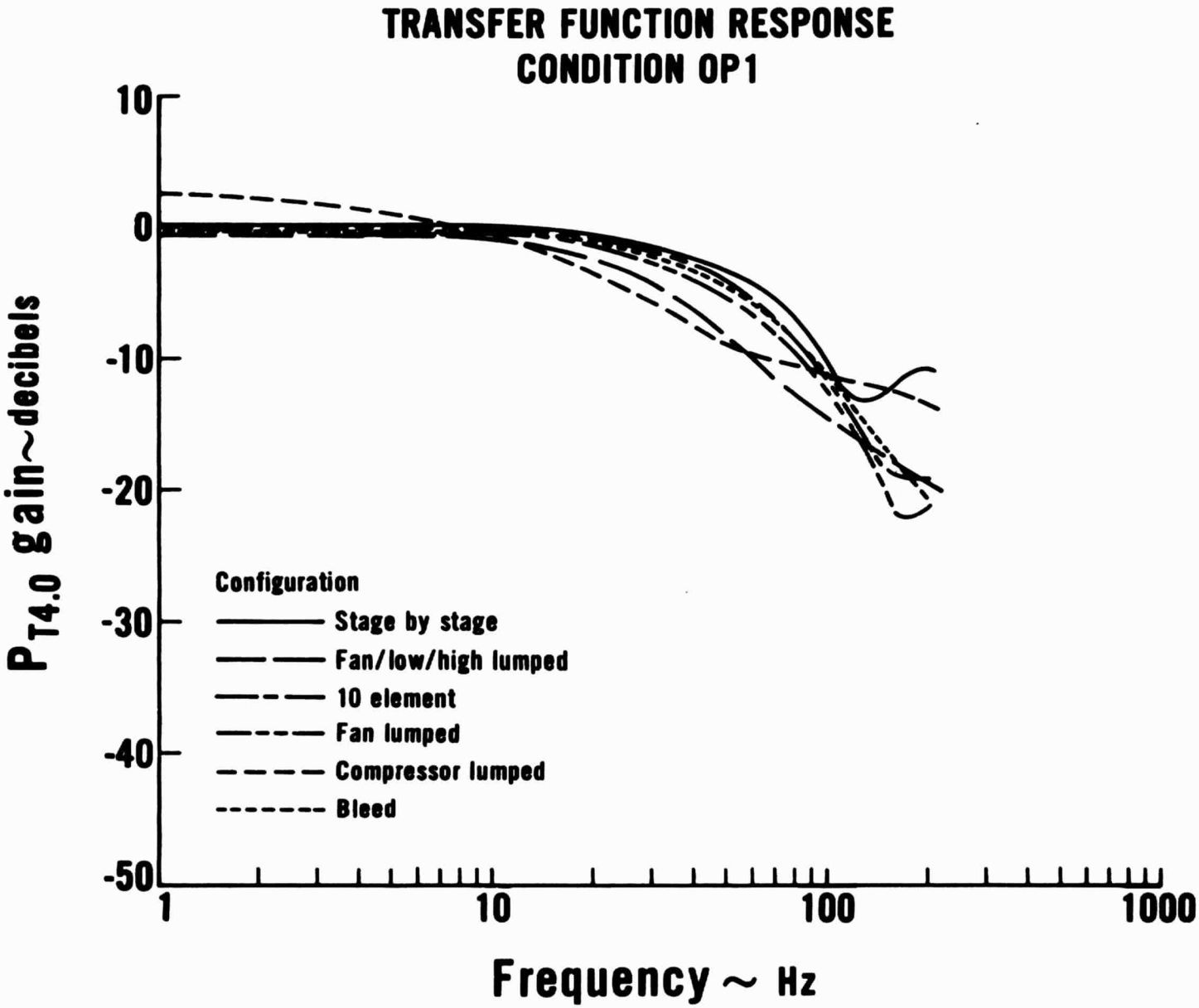

Figure 39 Compression System Simulation Gain at Station 4.0

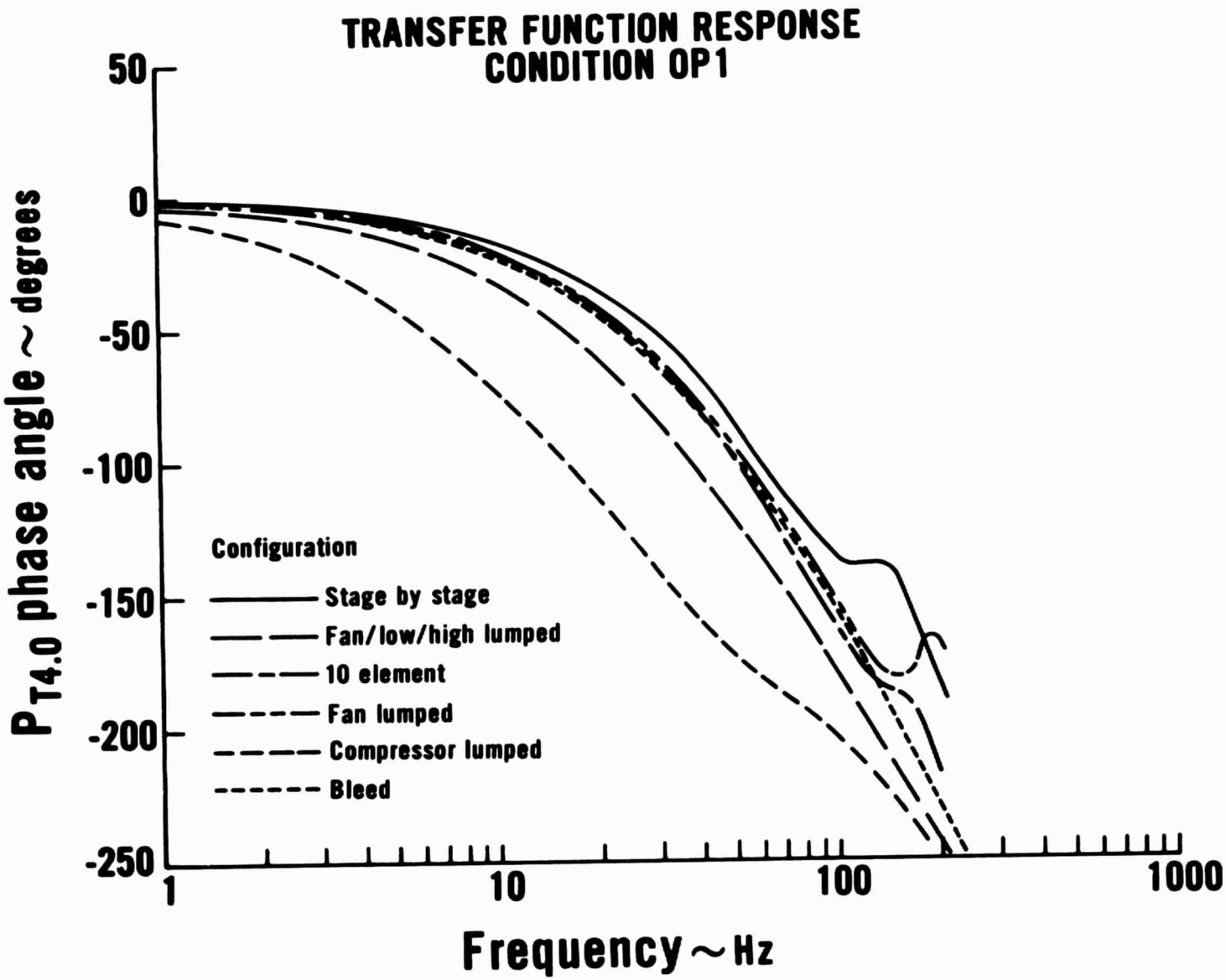

Figure 40 Compression System Simulation Phase at Station 4.0

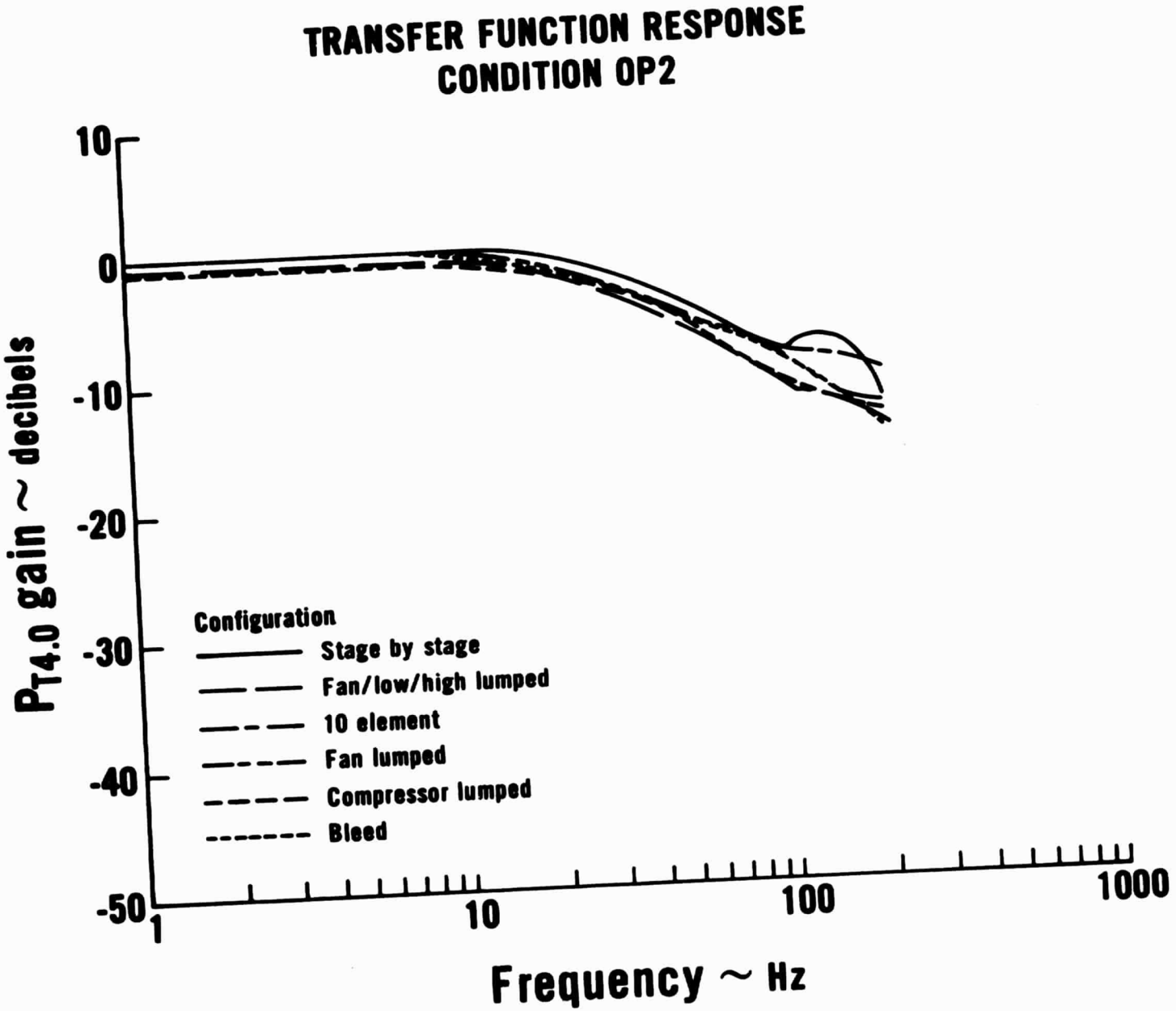

Figure 41 Compression System Simulation Gain at Station 4.0

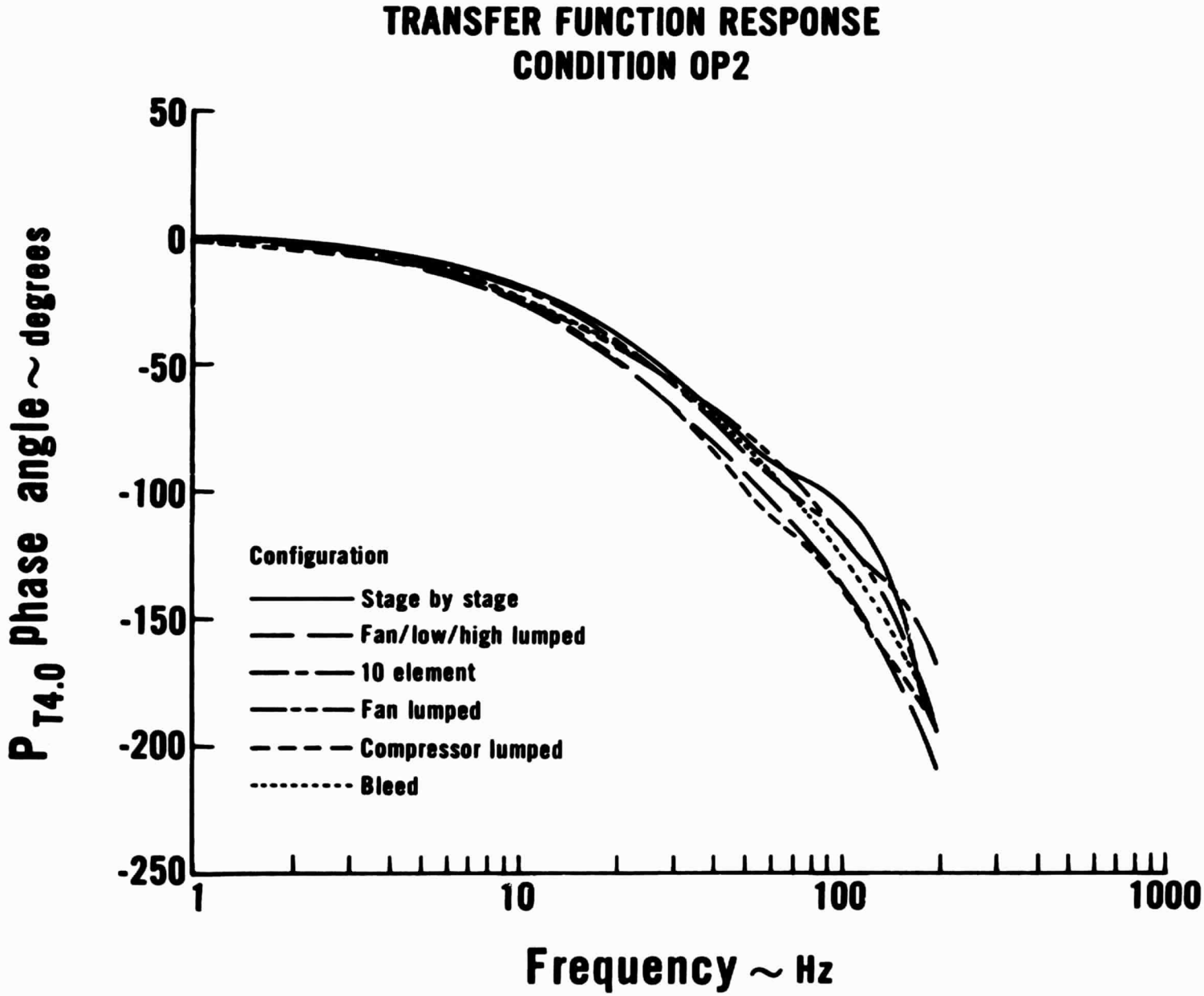

Figure 42 Compression System Simulation Phase at Station 4.0

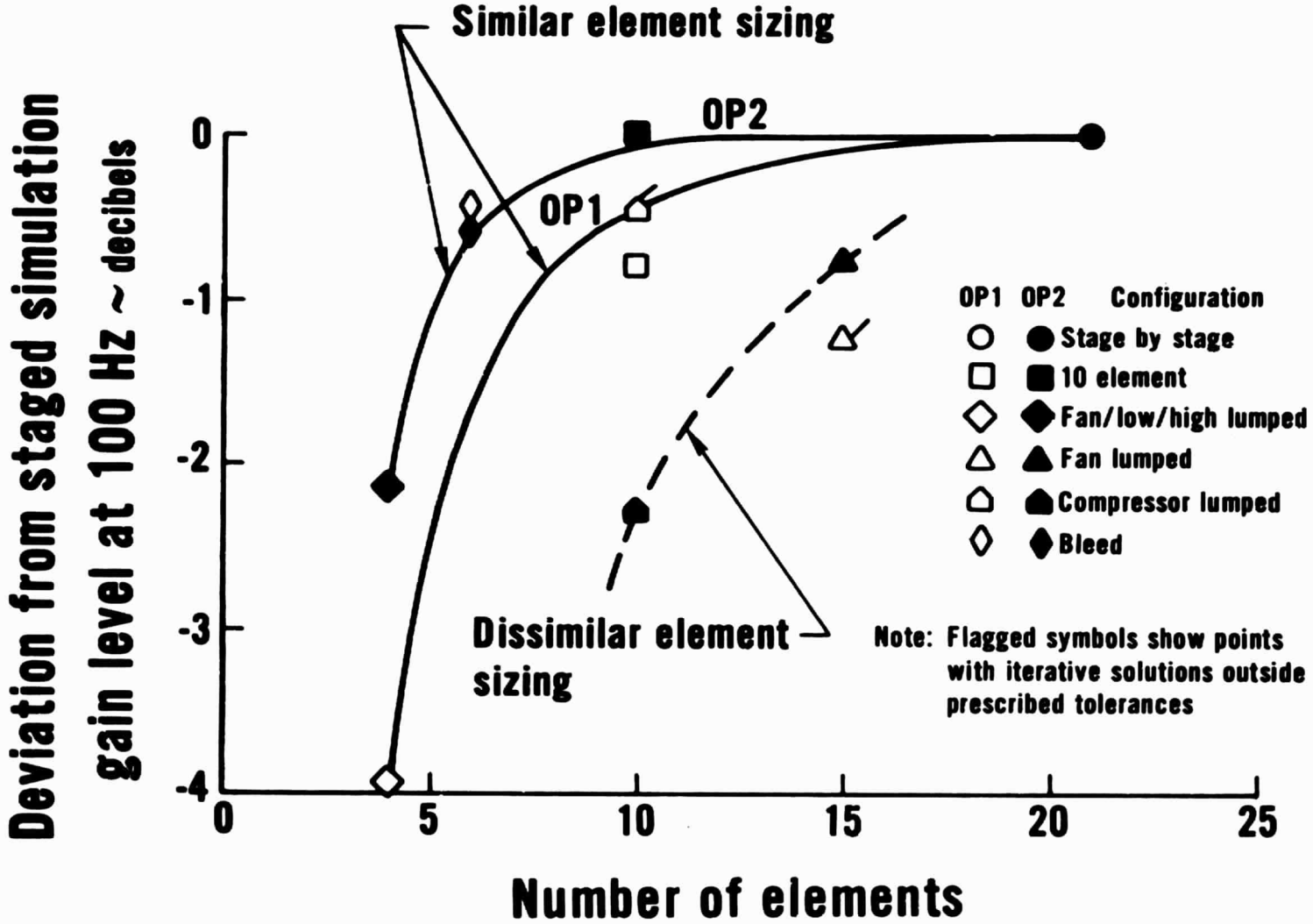

Figure 43 Correlation of Compression System Gain With Number of Dynamic Elements

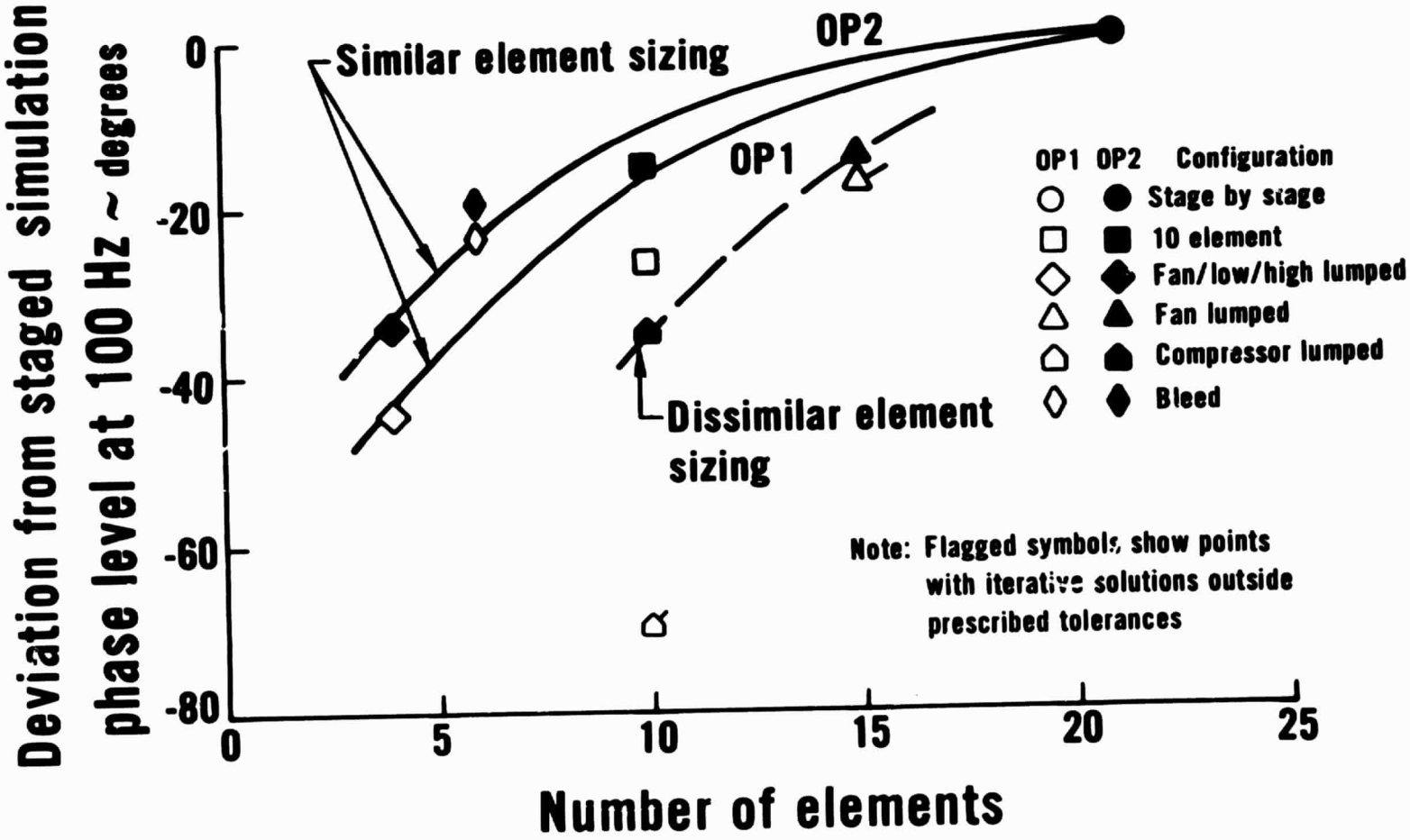

Figure 44 Correlation of Compression System Phase With Number of Dynamic Elements

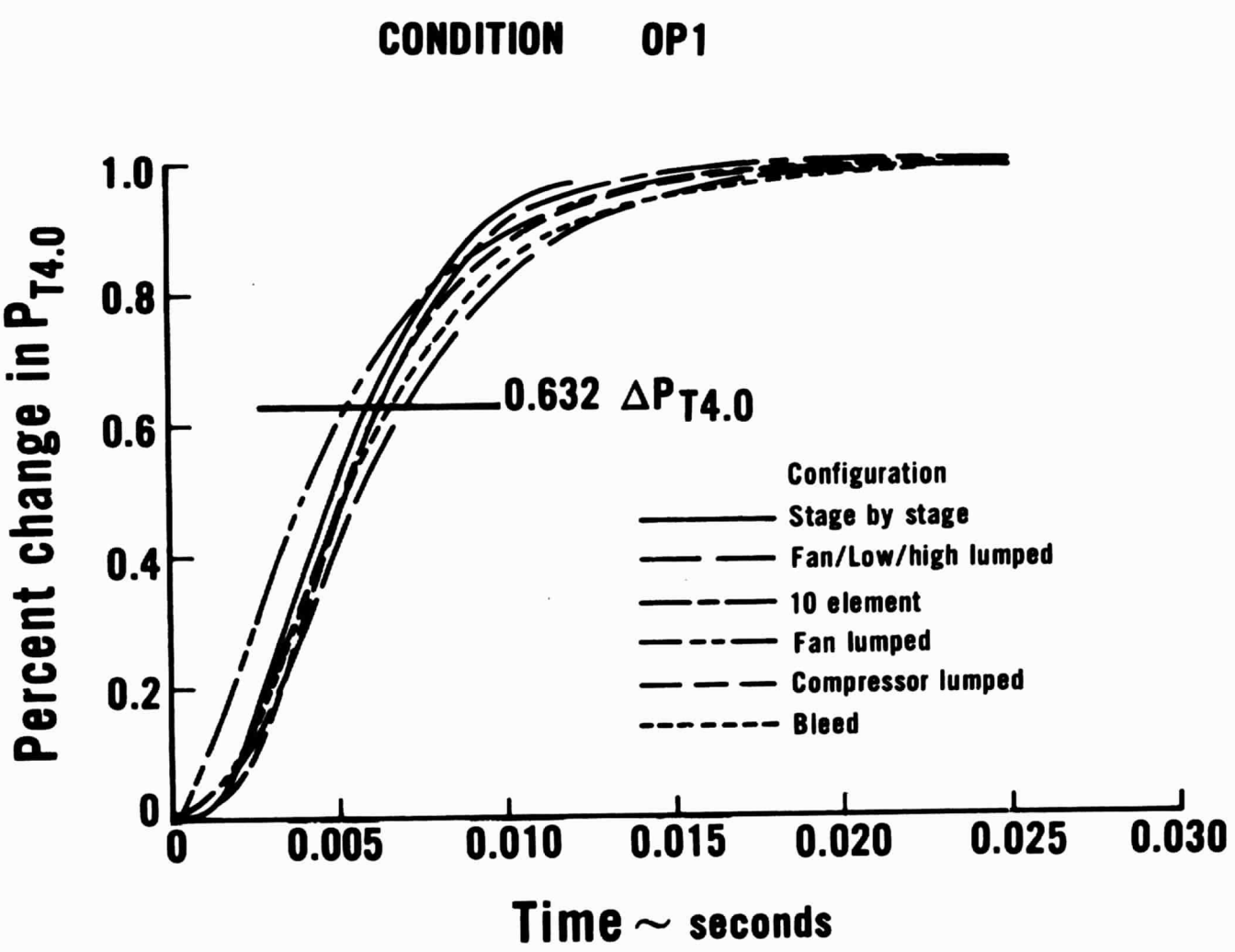

Figure 45 High Compressor Pressure-Time History of Response to a 1.0% Step in Inlet Pressure

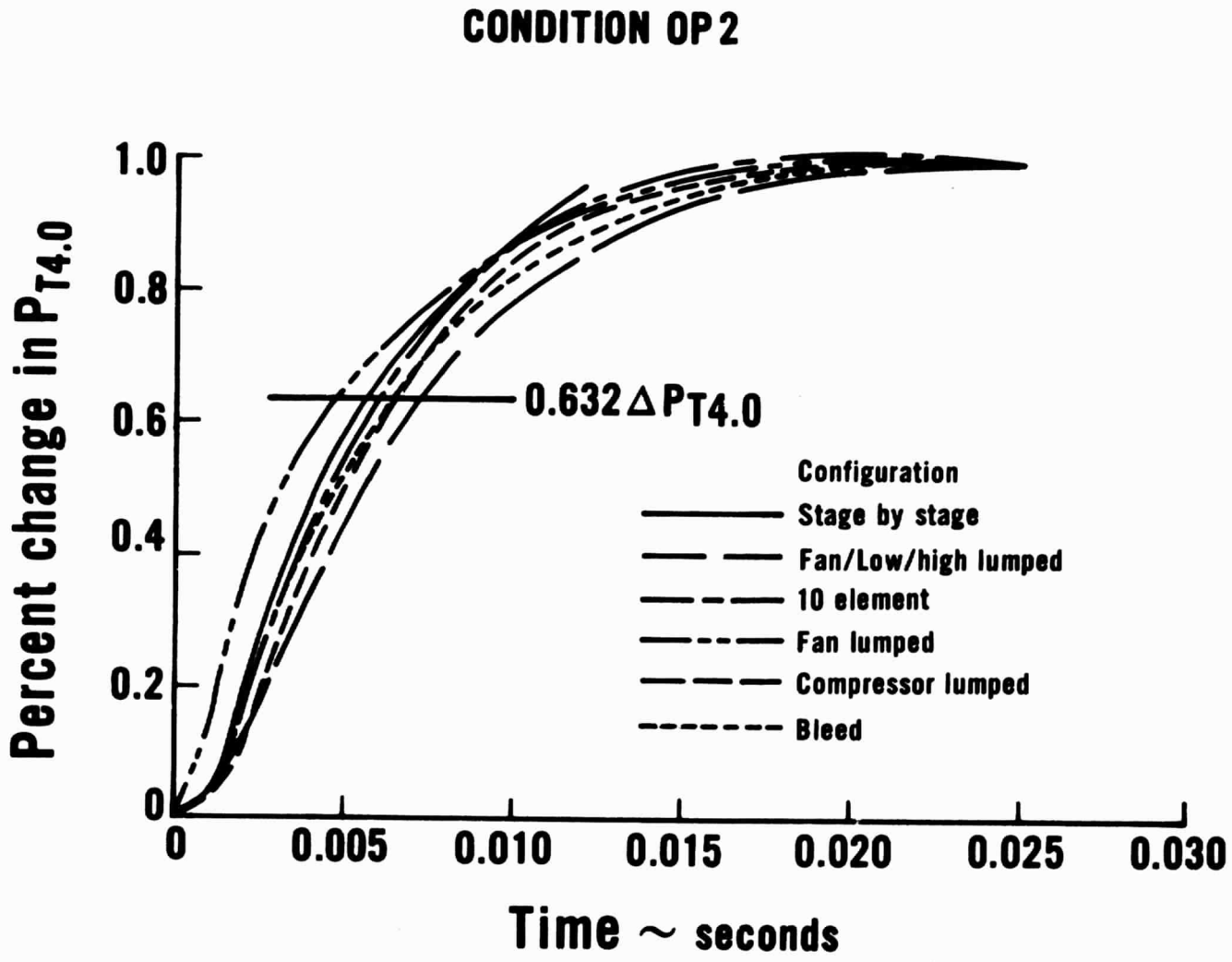

Figure 46 High Compressor Pressure - Time History of Response to a 1.0% Step in Inlet Pressure

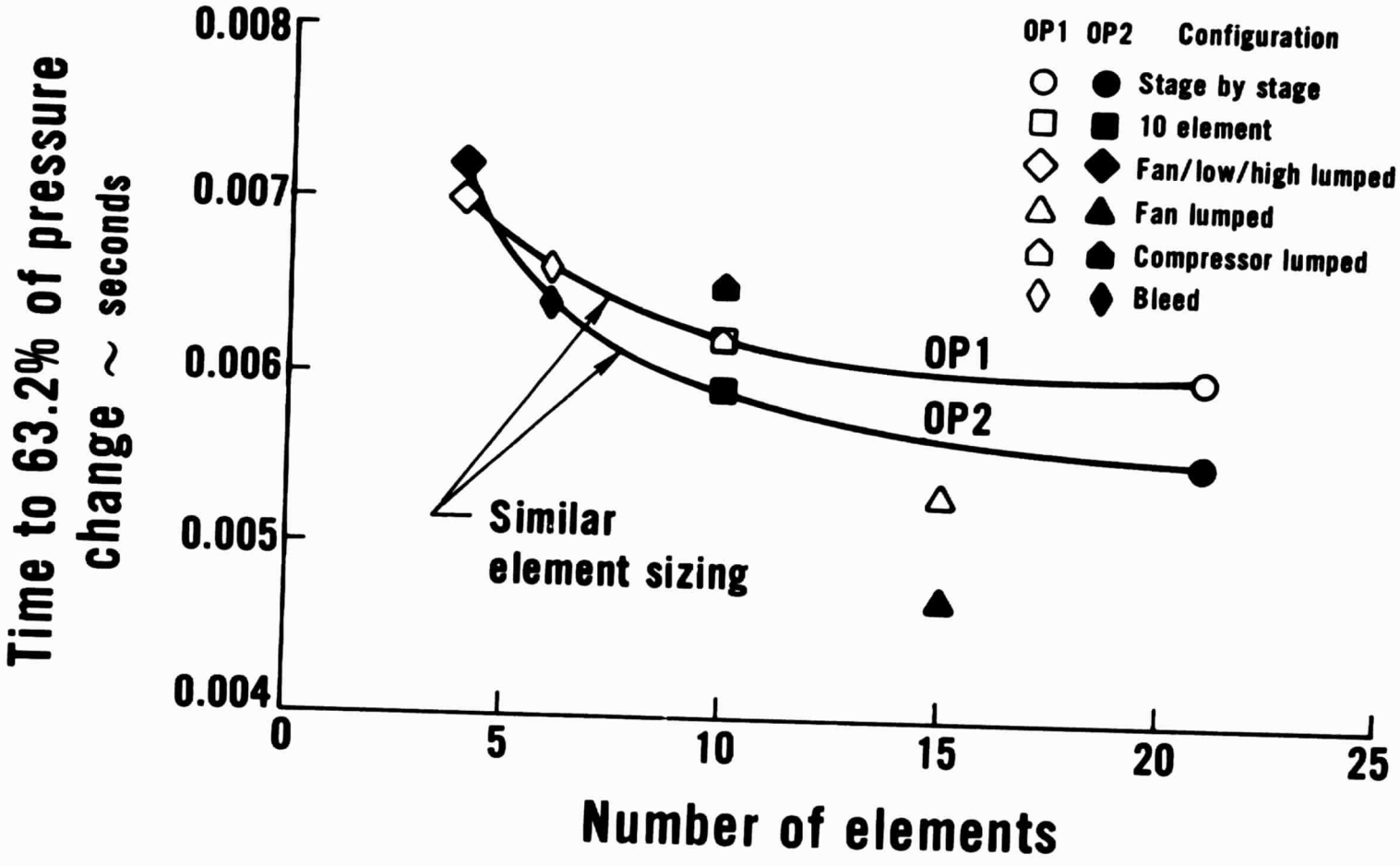

Figure 47 *Correlation of Compression System Response Time With Number of Dynamic Elements*

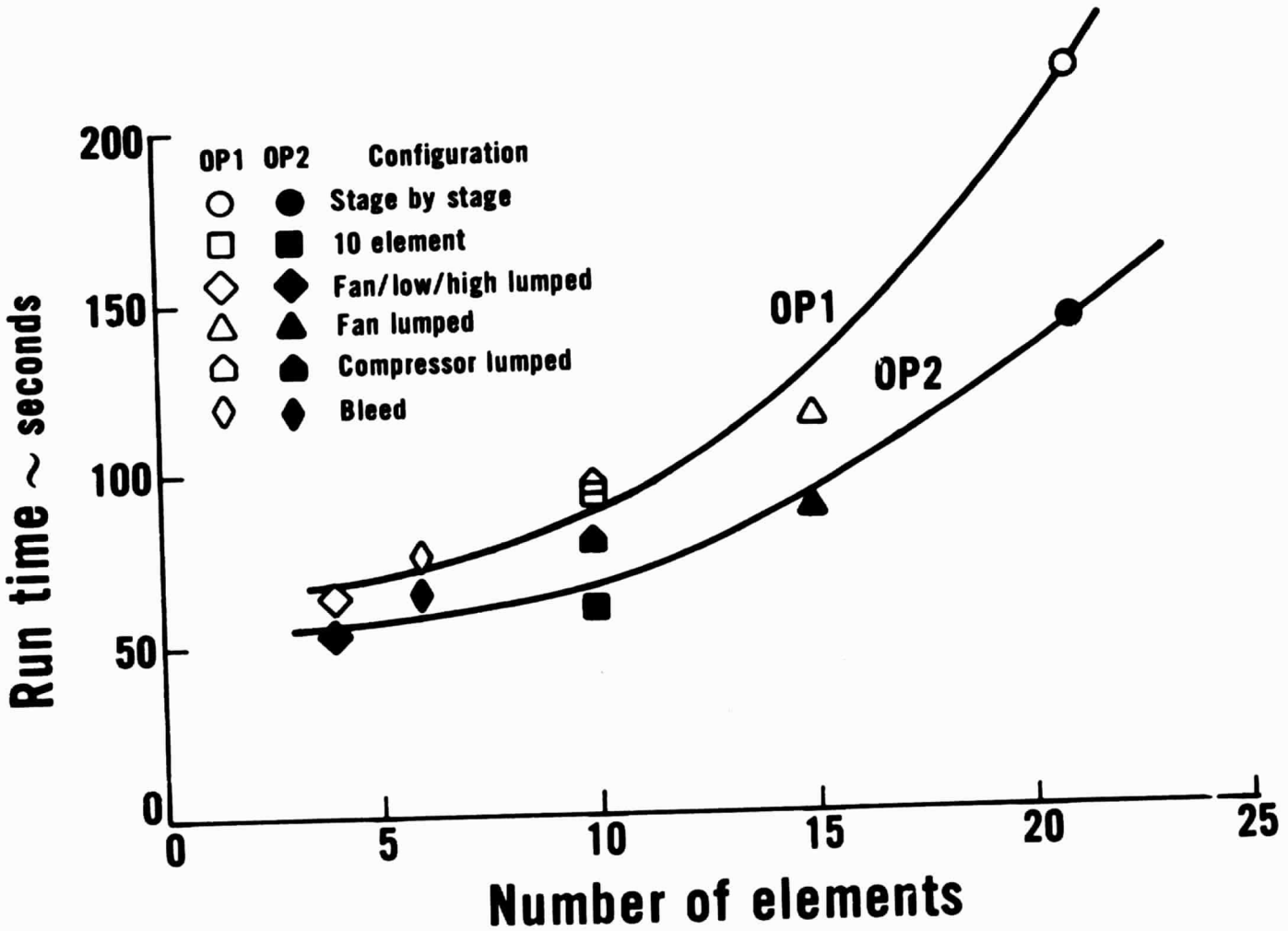

Figure 48 *Compression System Simulation Computer Run Time for 0.025 Second $P_{T2.0}$ Step Transient*

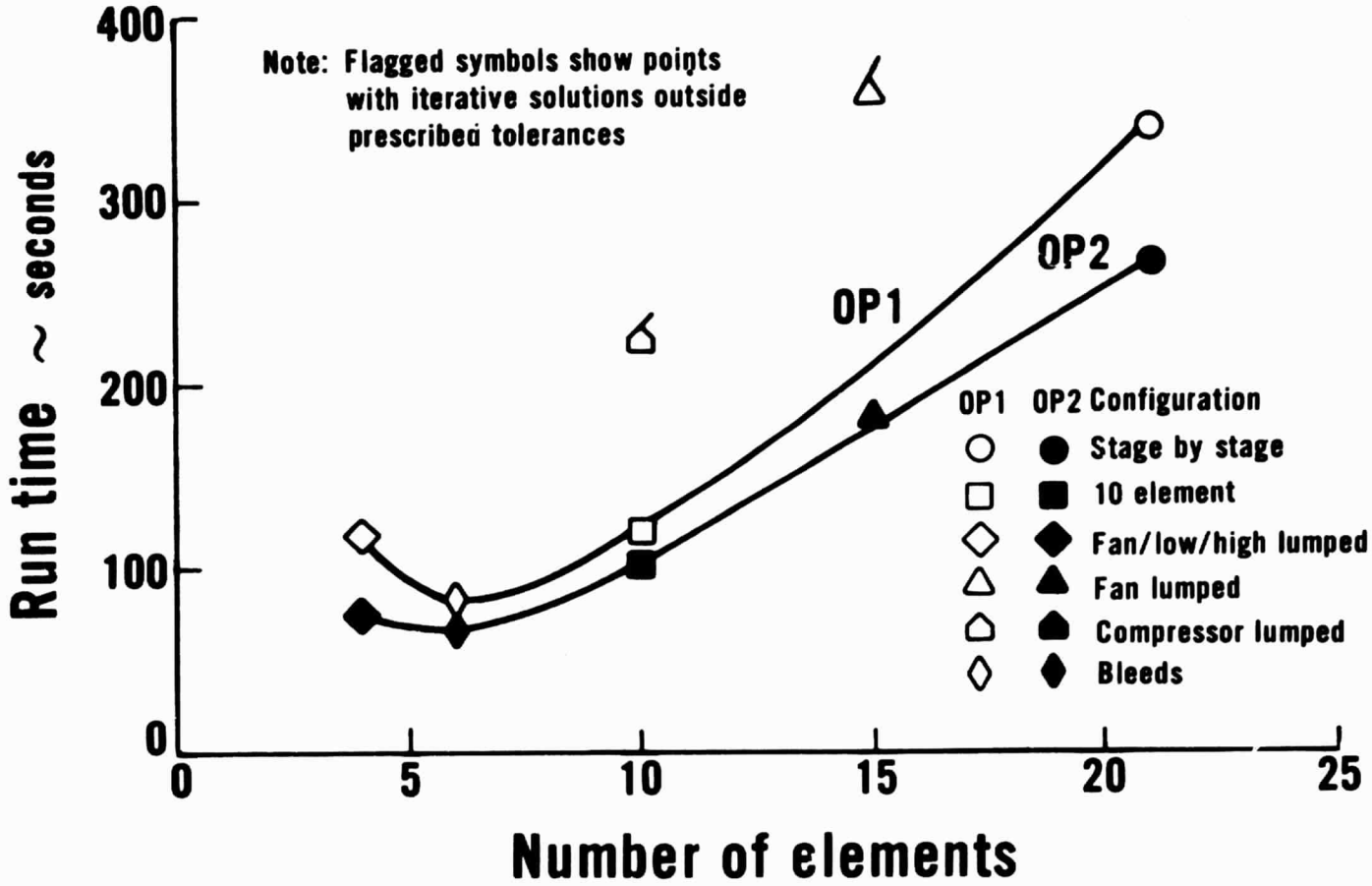

Figure 49 *Compression System Simulation Computer Run Time for Transfer Function Calculation*

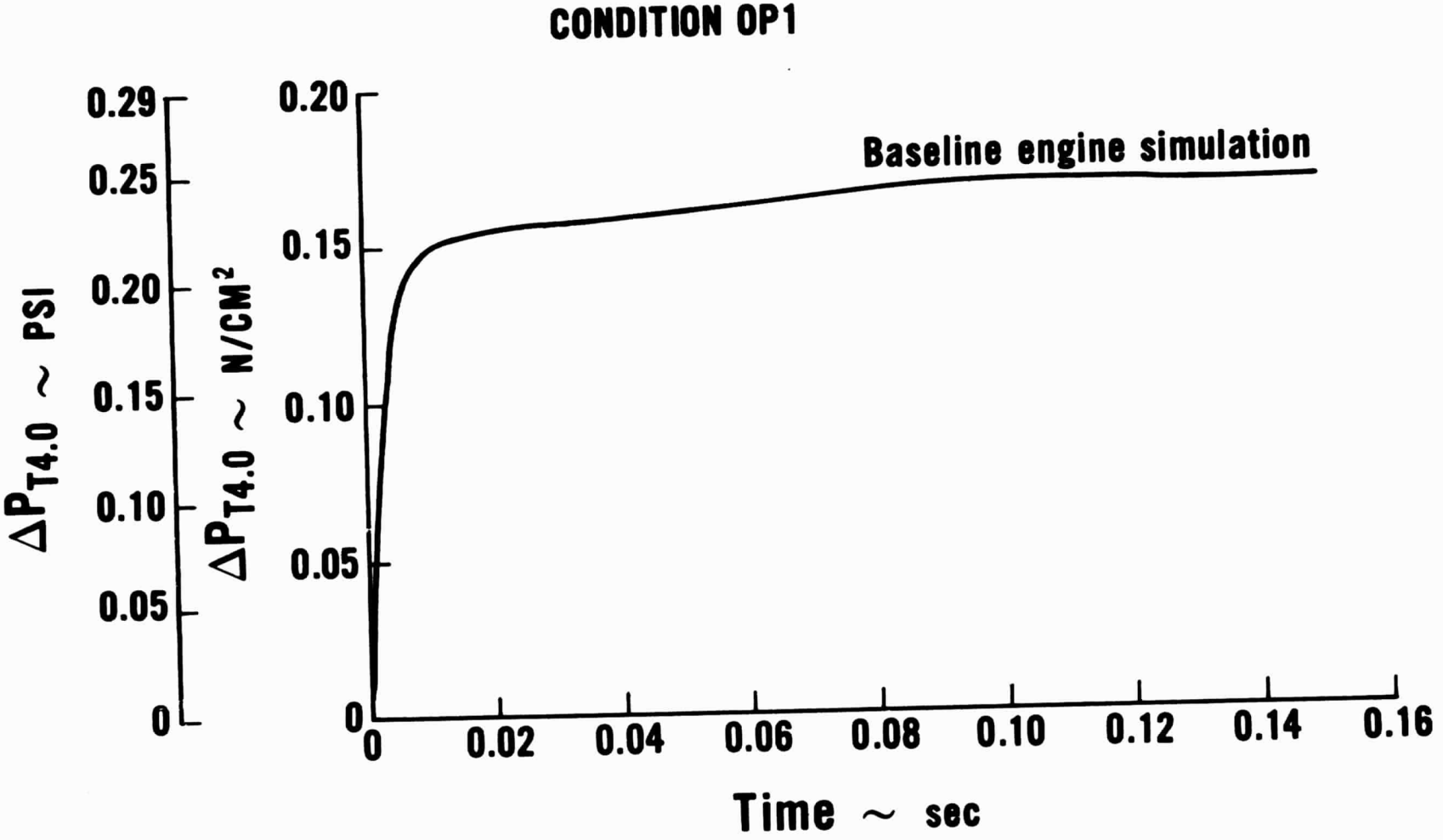

Figure 50 $P_{T4.0}$ *Response to a Step in Fuel Flow*

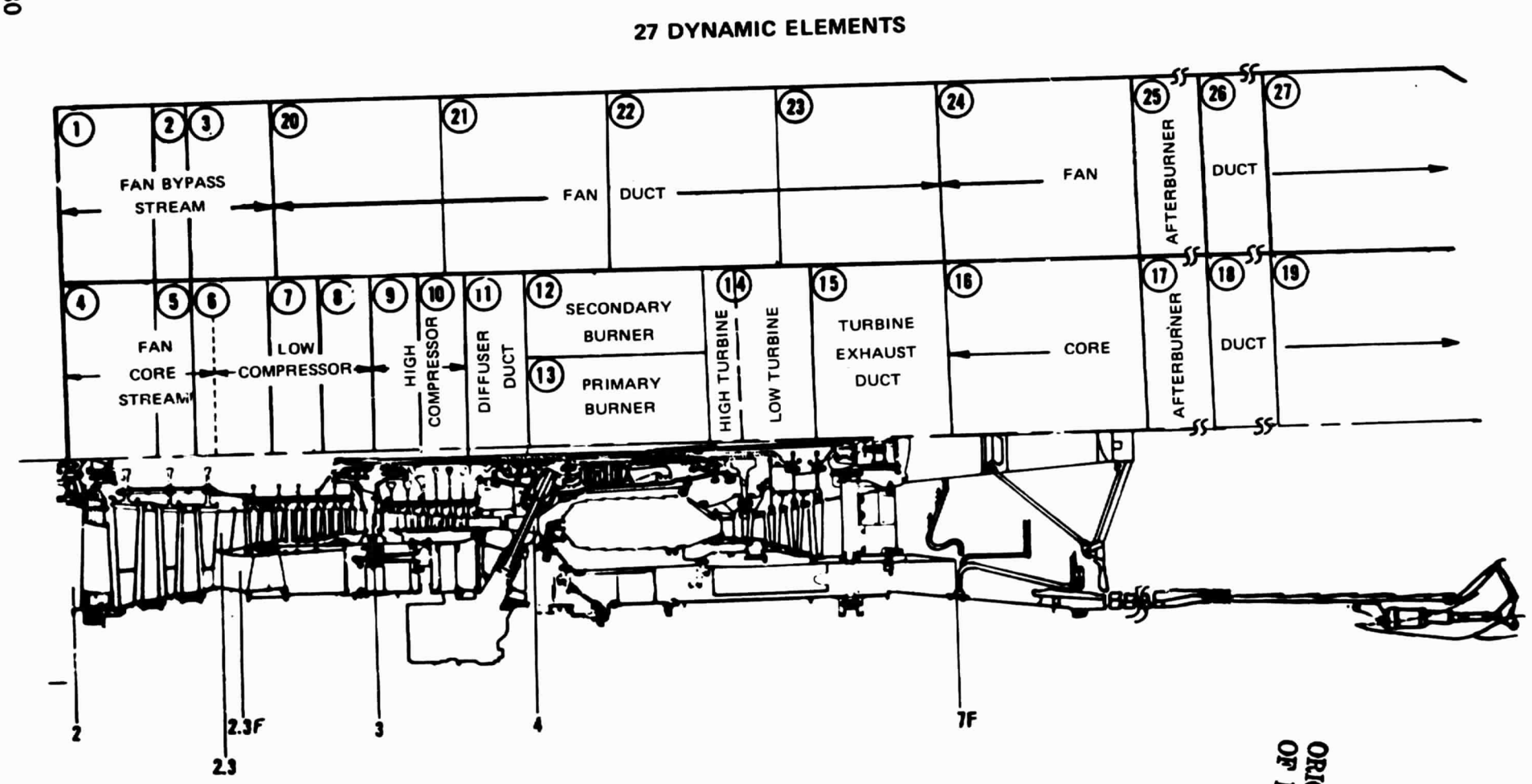

Figure 51 Configuration of Modified Engine Simulation

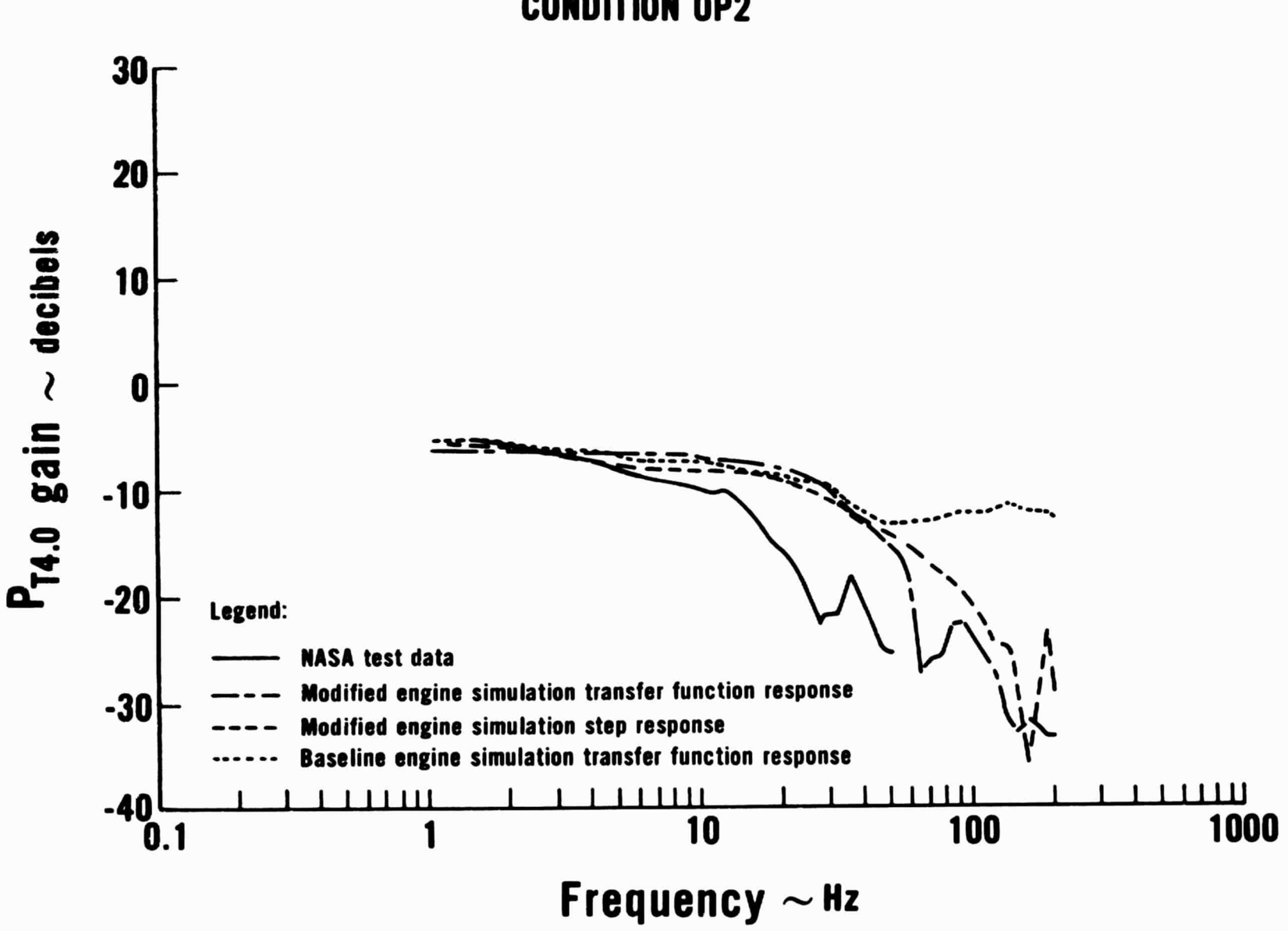

Figure 52 High Compressor Gain at Station 4.0

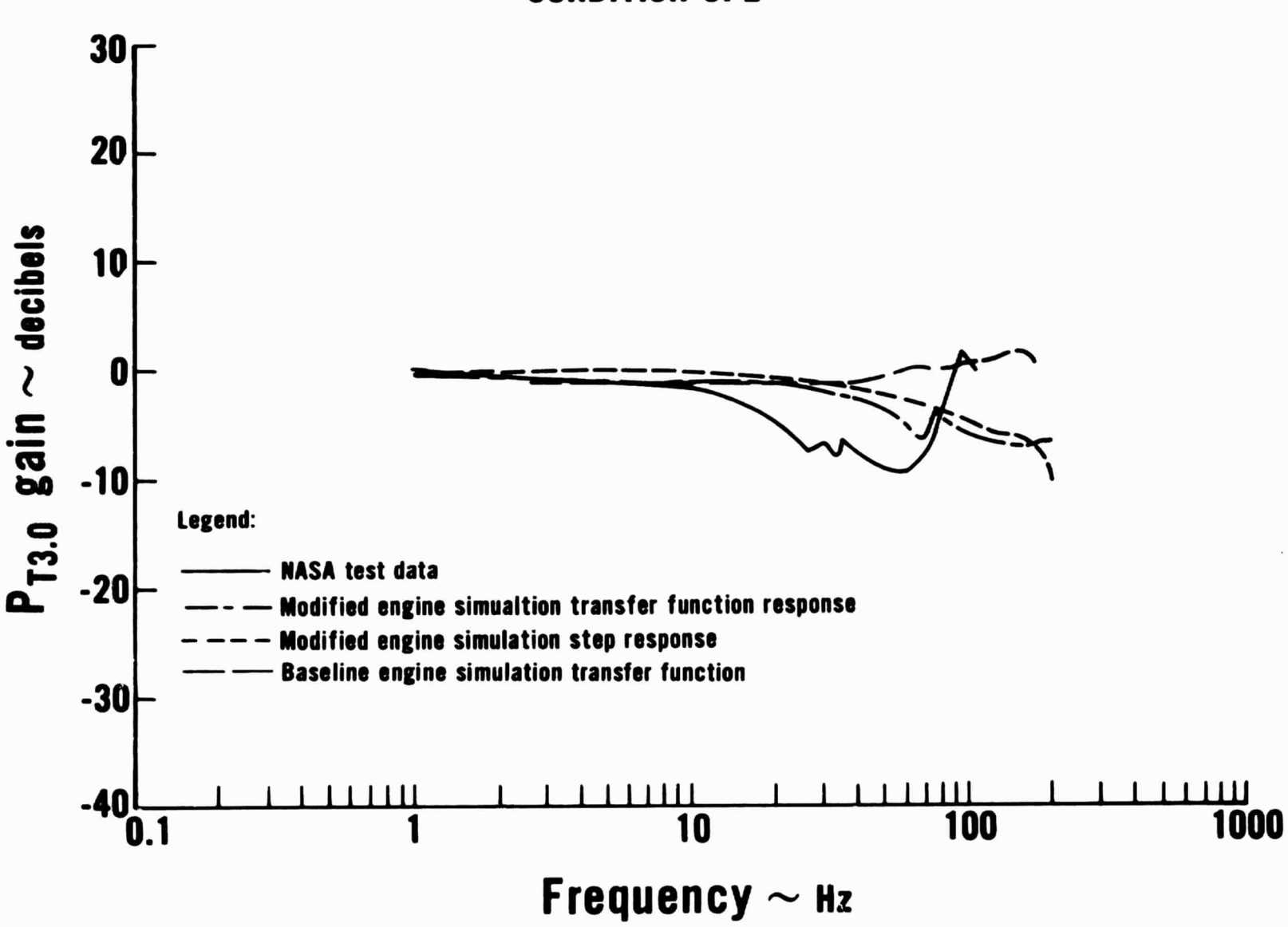

Figure 53 Low Compressor Gain at Station 3.0

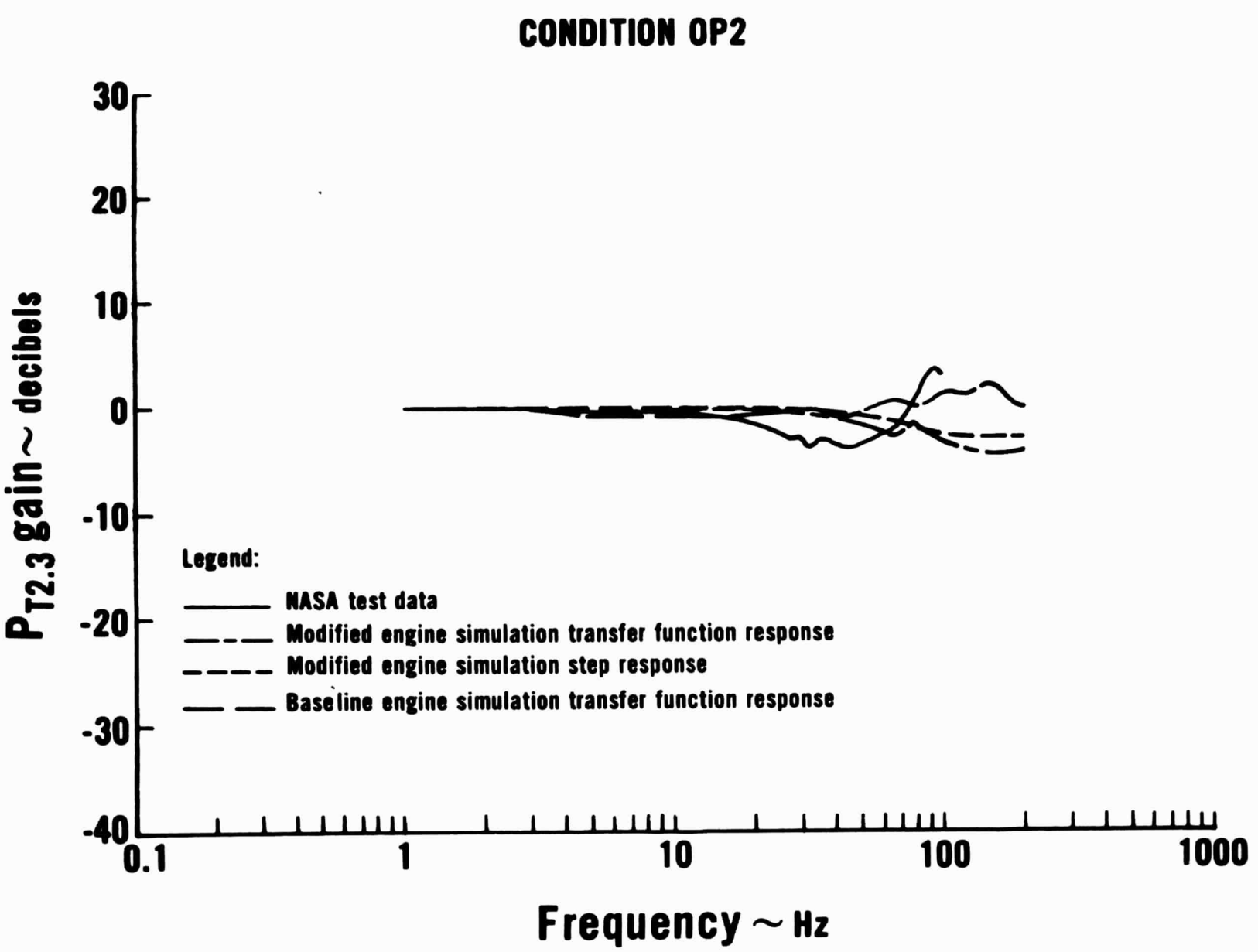

Figure 54 Fan Core Stream Gain at Station 2.3

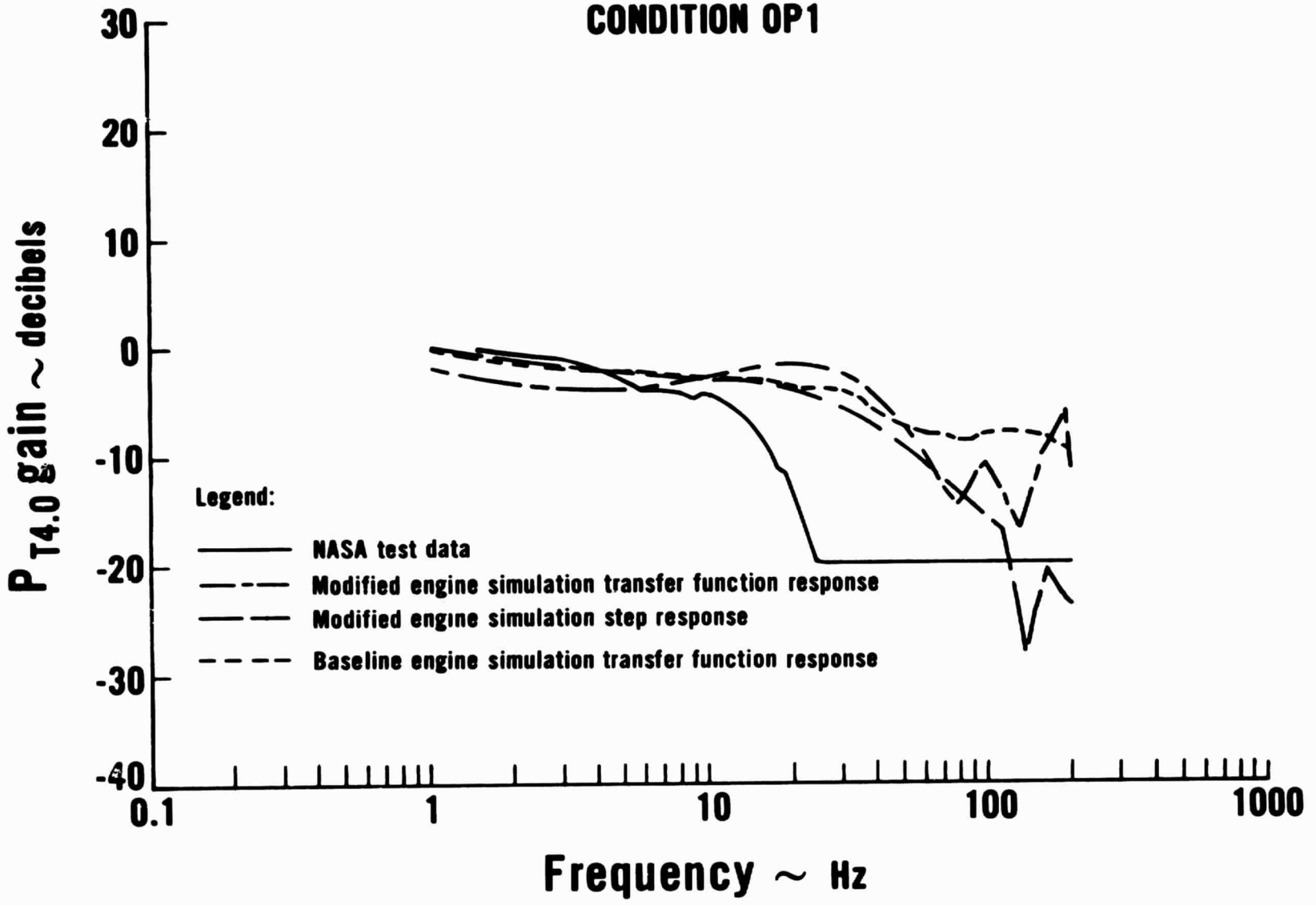

Figure 55 High Compressor Gain at Station 4.0

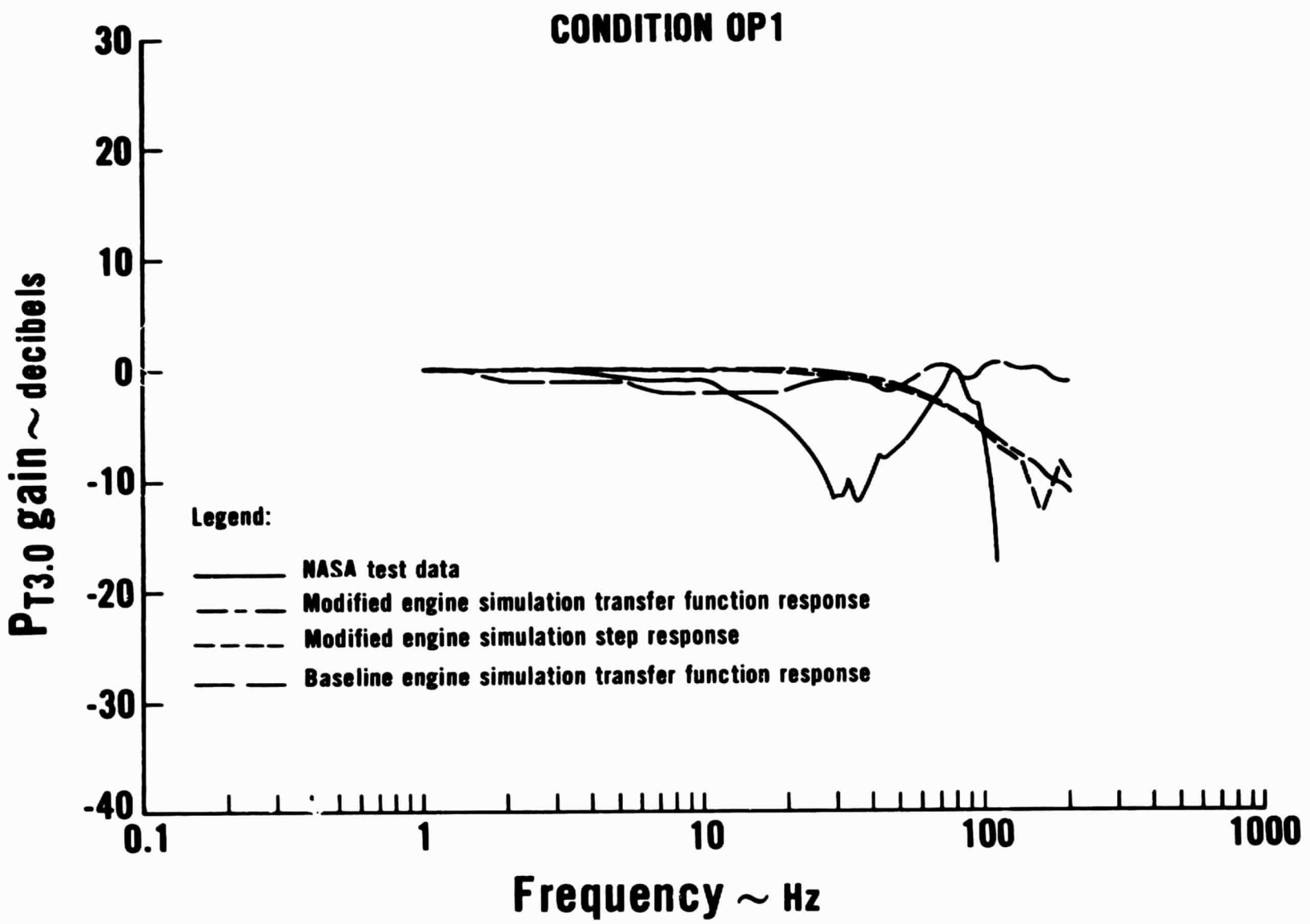

Figure 56 Low Compressor Gain at Station 3.0

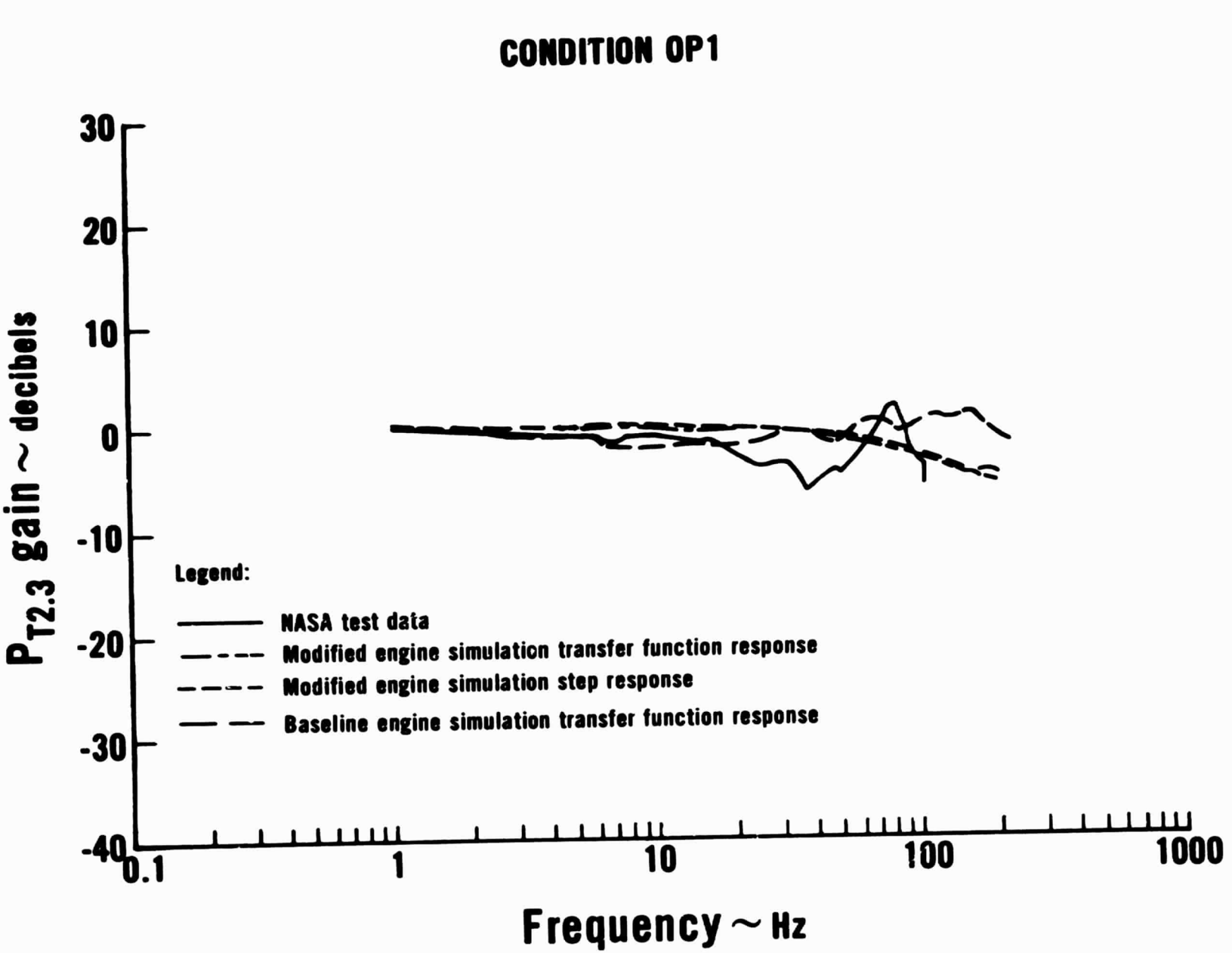

Figure 57 Fan Core Stream Gain at Station 2.3

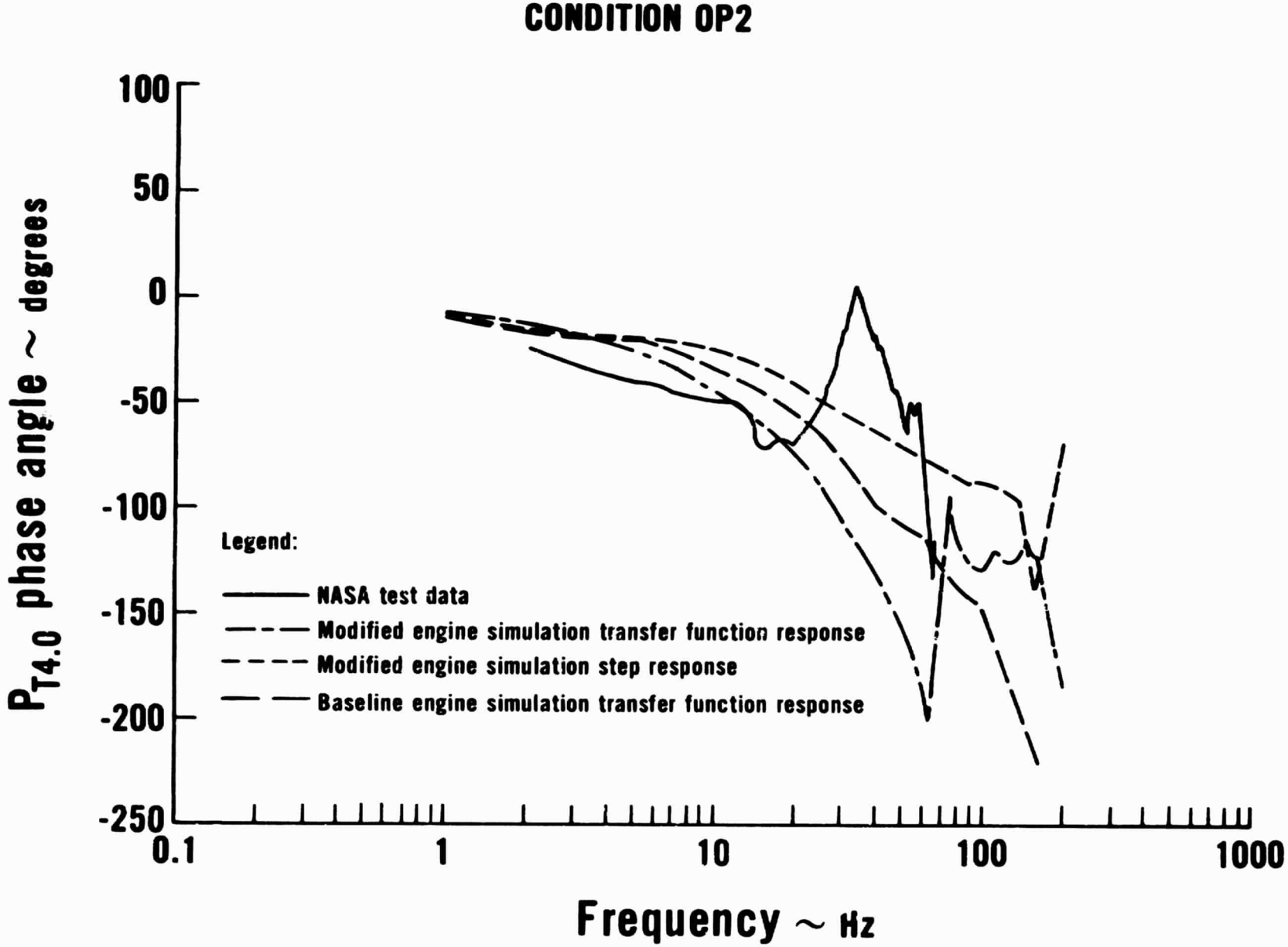

Figure 58 High Compre. or Phase at Station 4.0

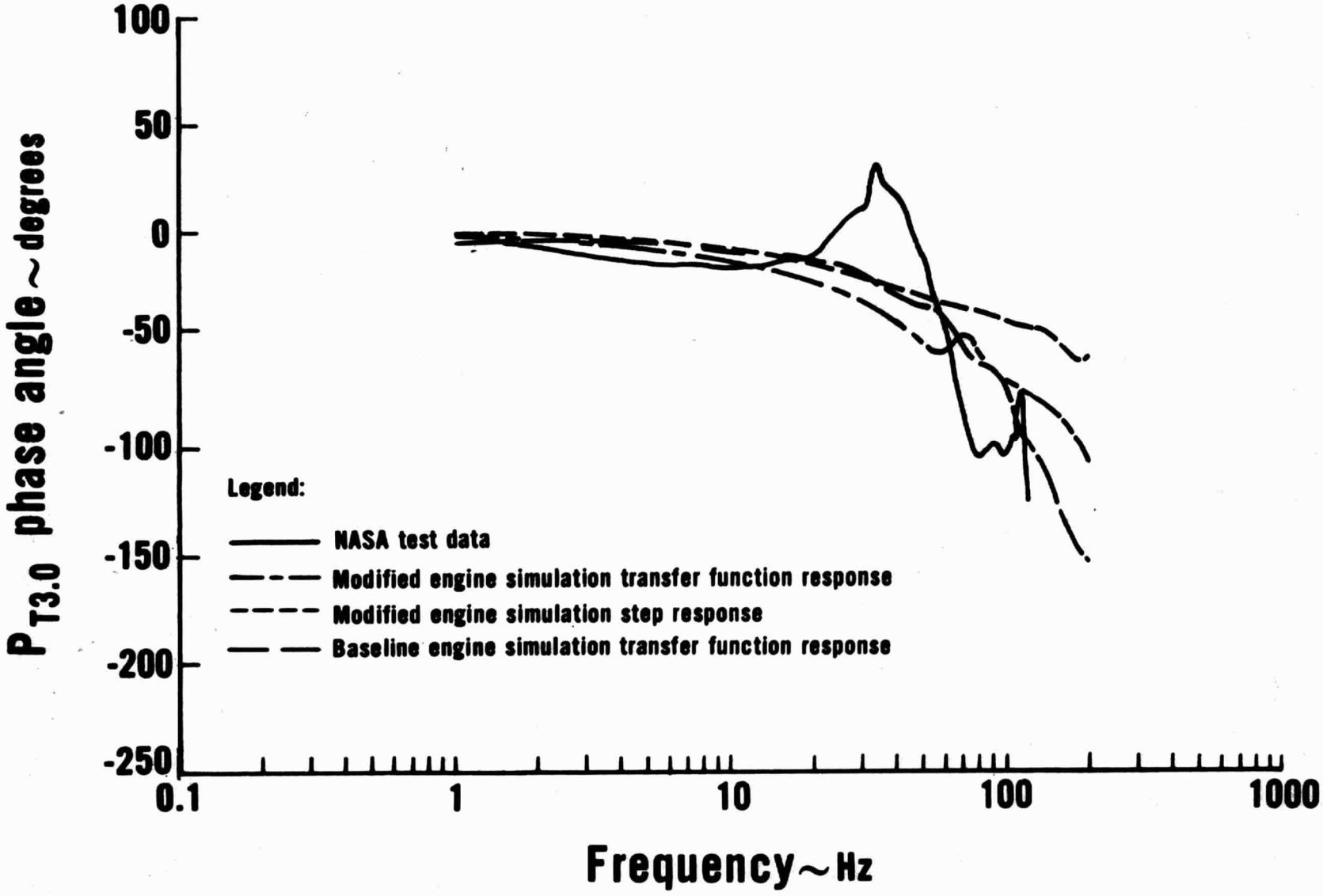

Figure 59 Low Compressor Phase at Station 3.0

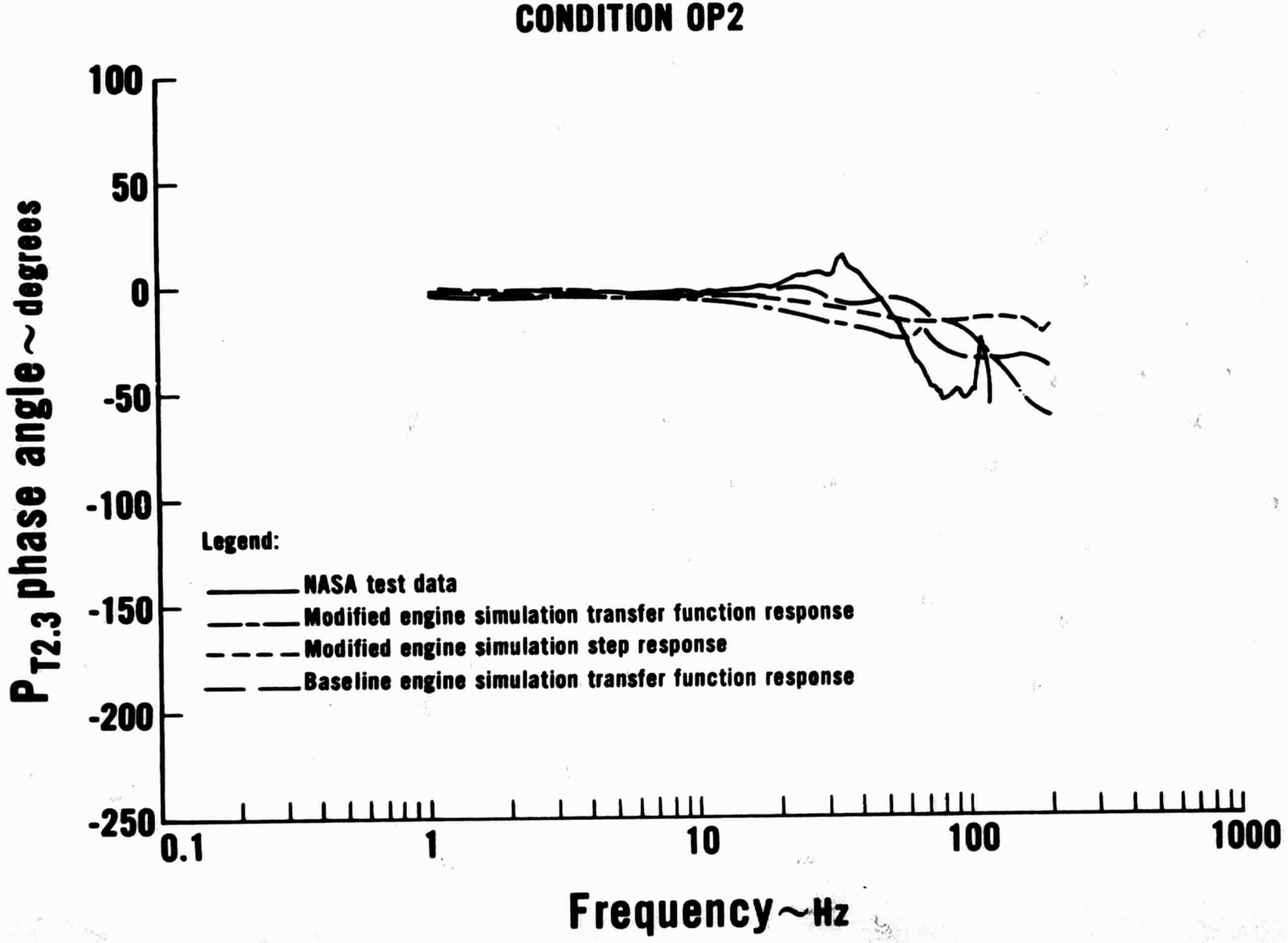

Figure 60 Fan Core Stream Phase at Station 2.3

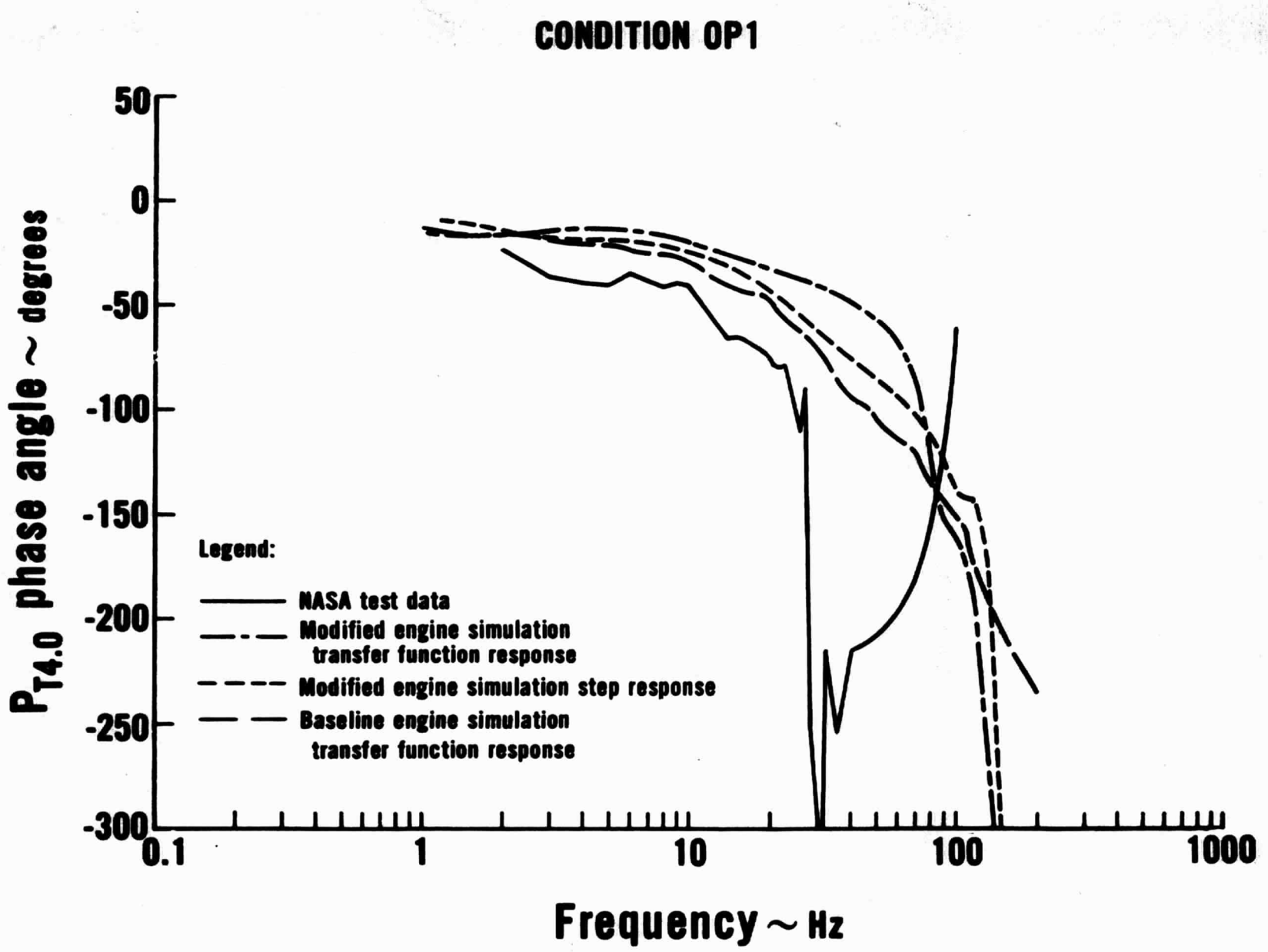

Figure 61 High Compressor Phase at Station 4.0

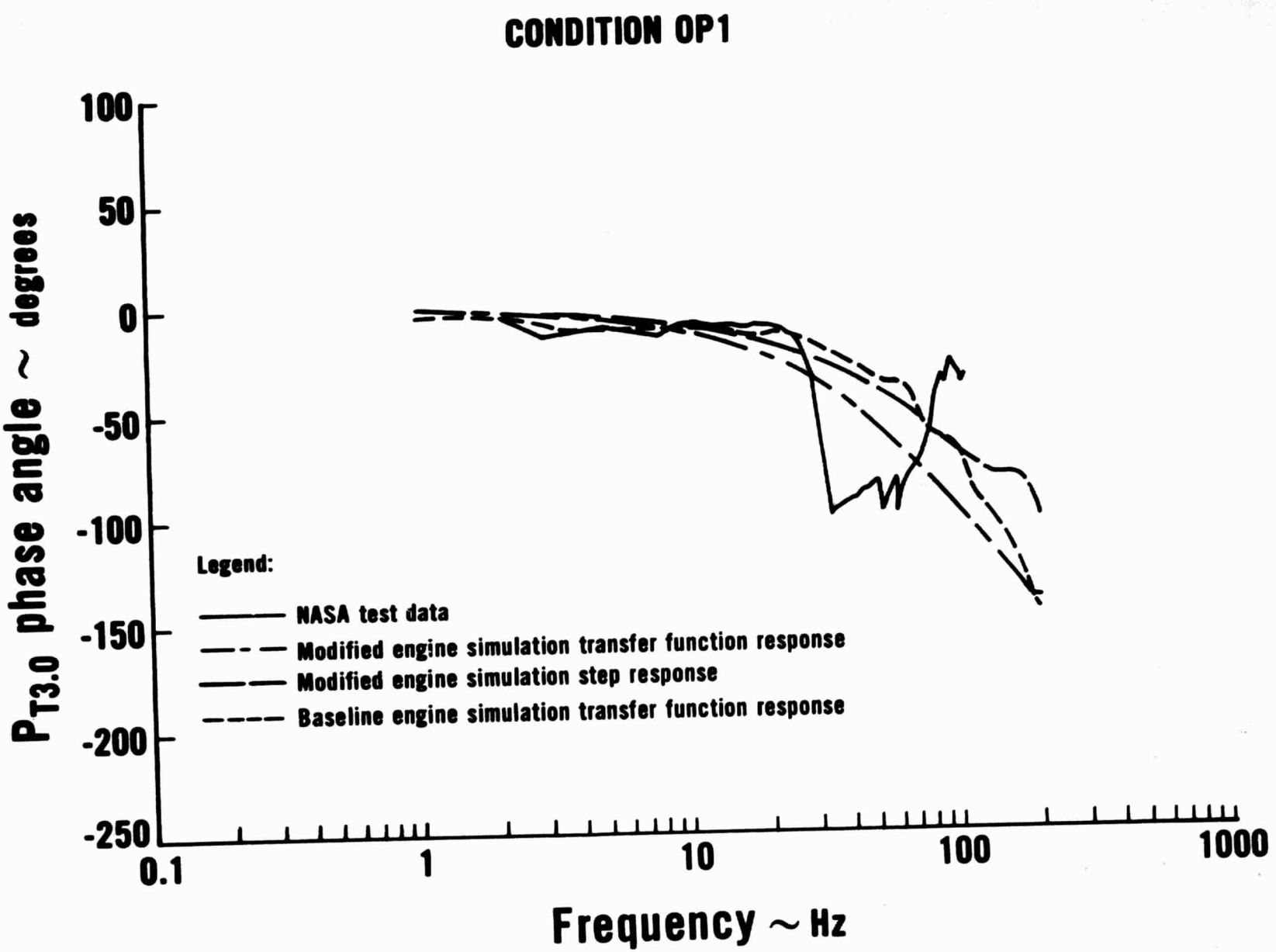

Figure 62 Low Compressor Phase at Station 3.0

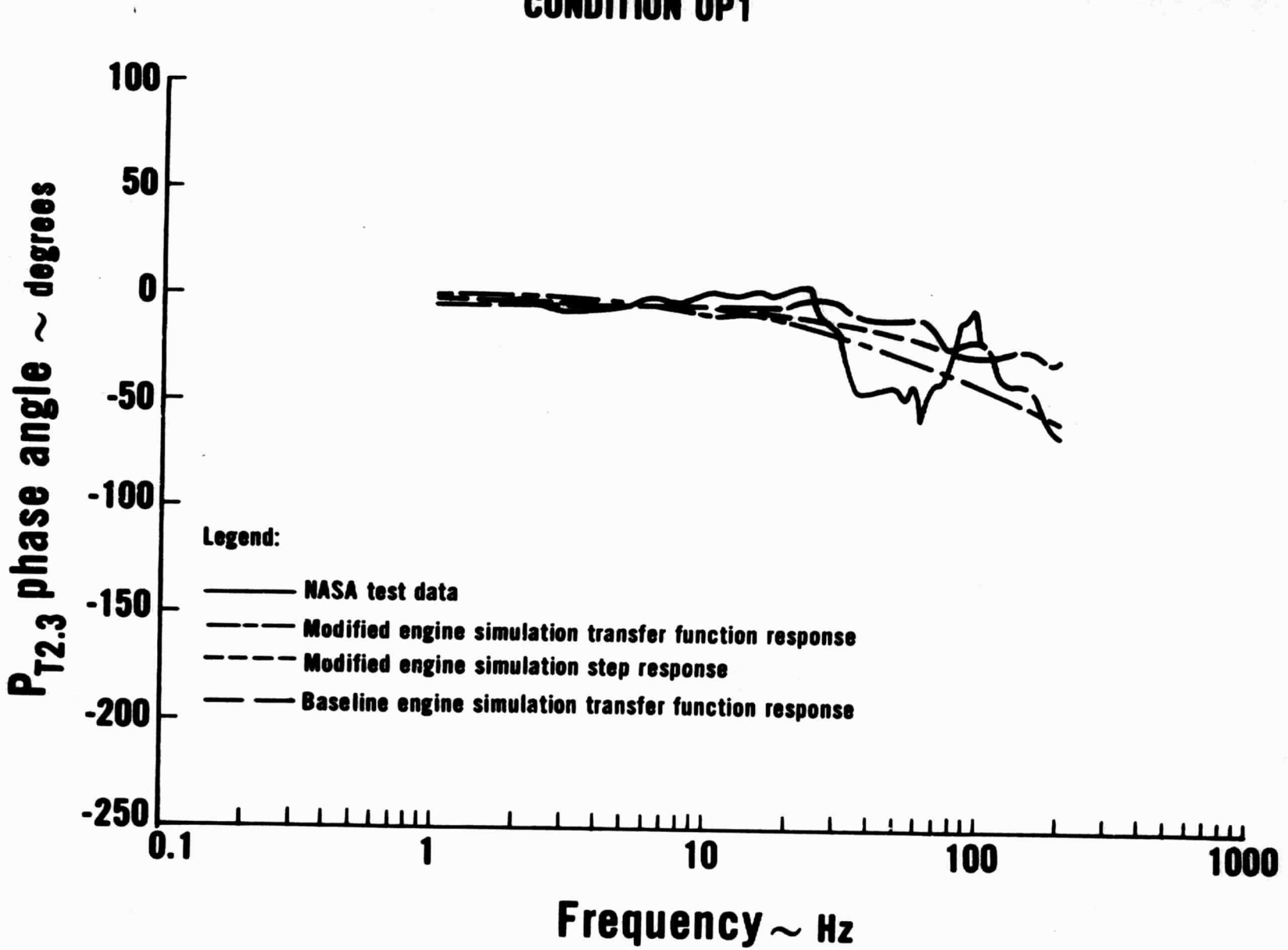

Figure 63 Fan Core Stream Phase at Station 2.3

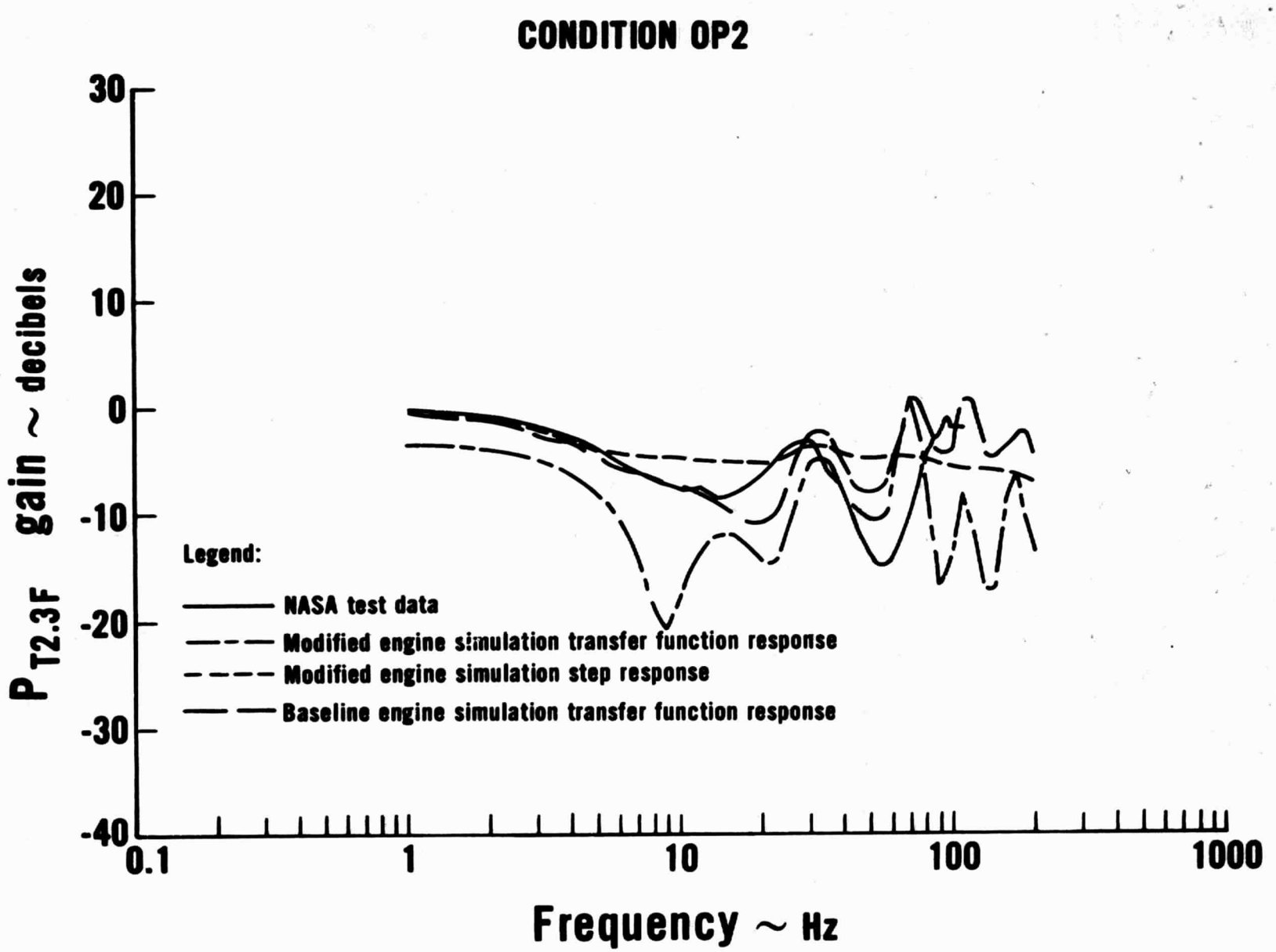

Figure 64 Fan Bypass Stream Gain at Station 2.3F

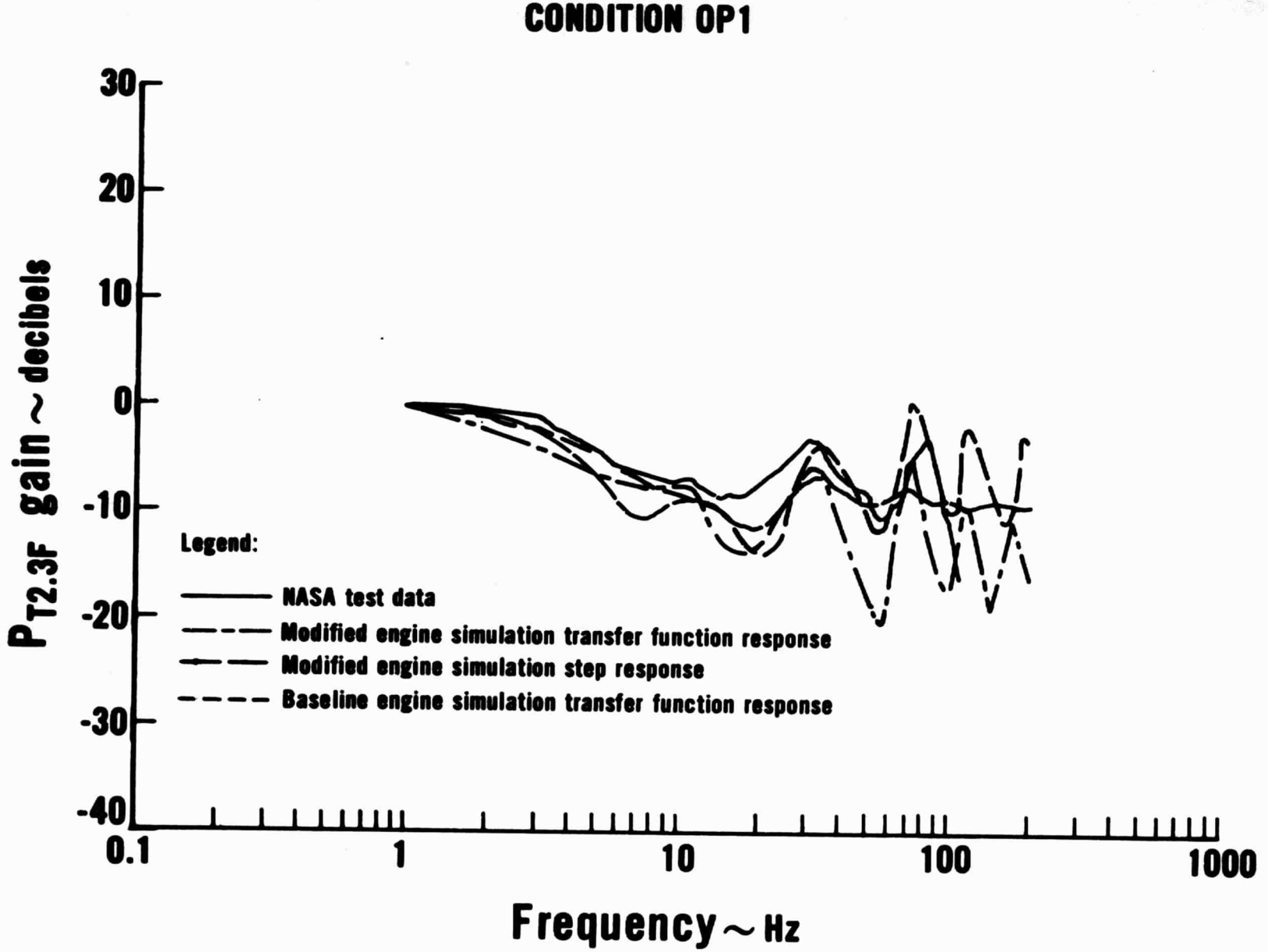

Figure 65 Fan Bypass Stream Gain at Station 2.3F

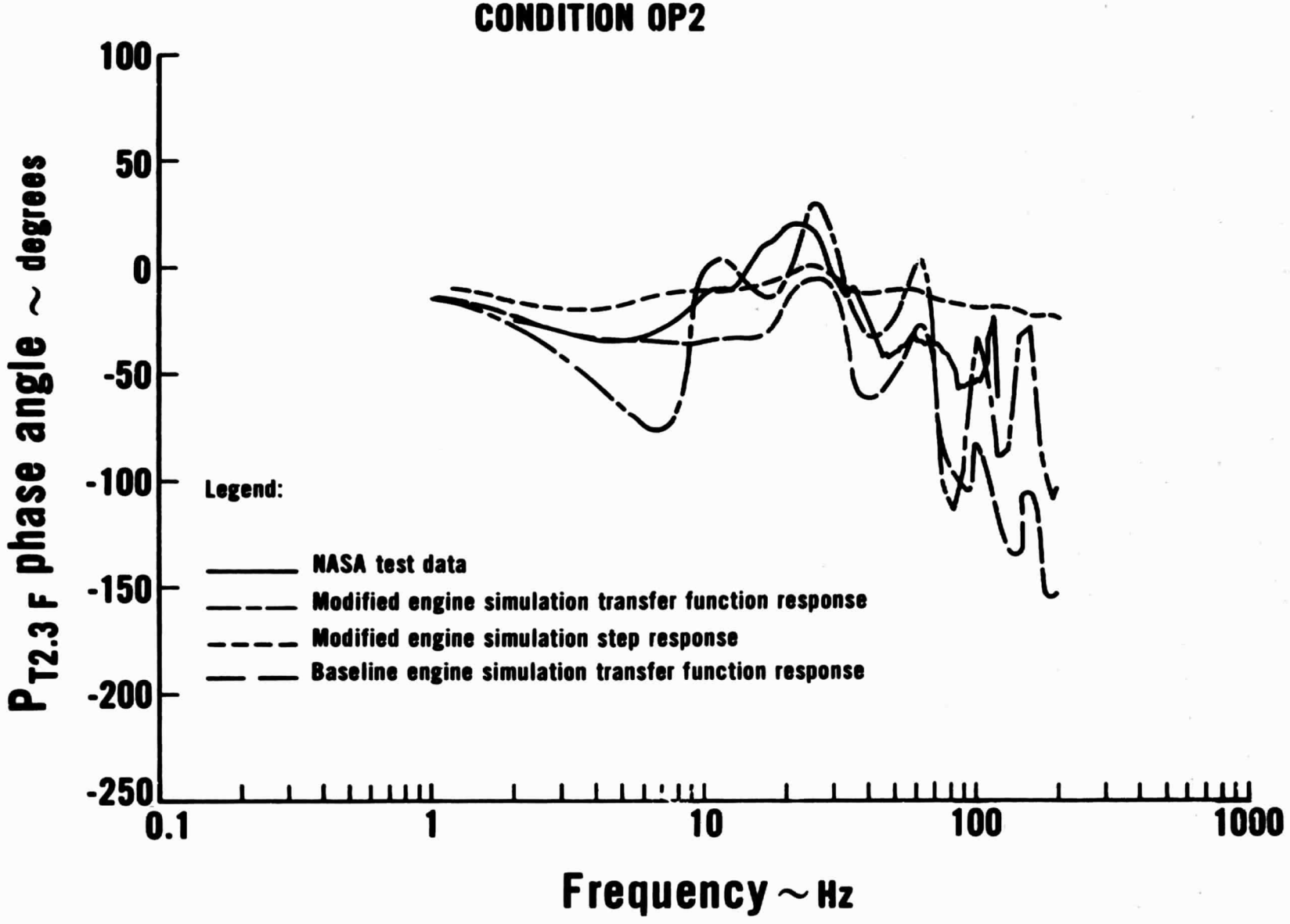

Figure 66 Fan Bypass Stream Phase at Station 2.3F

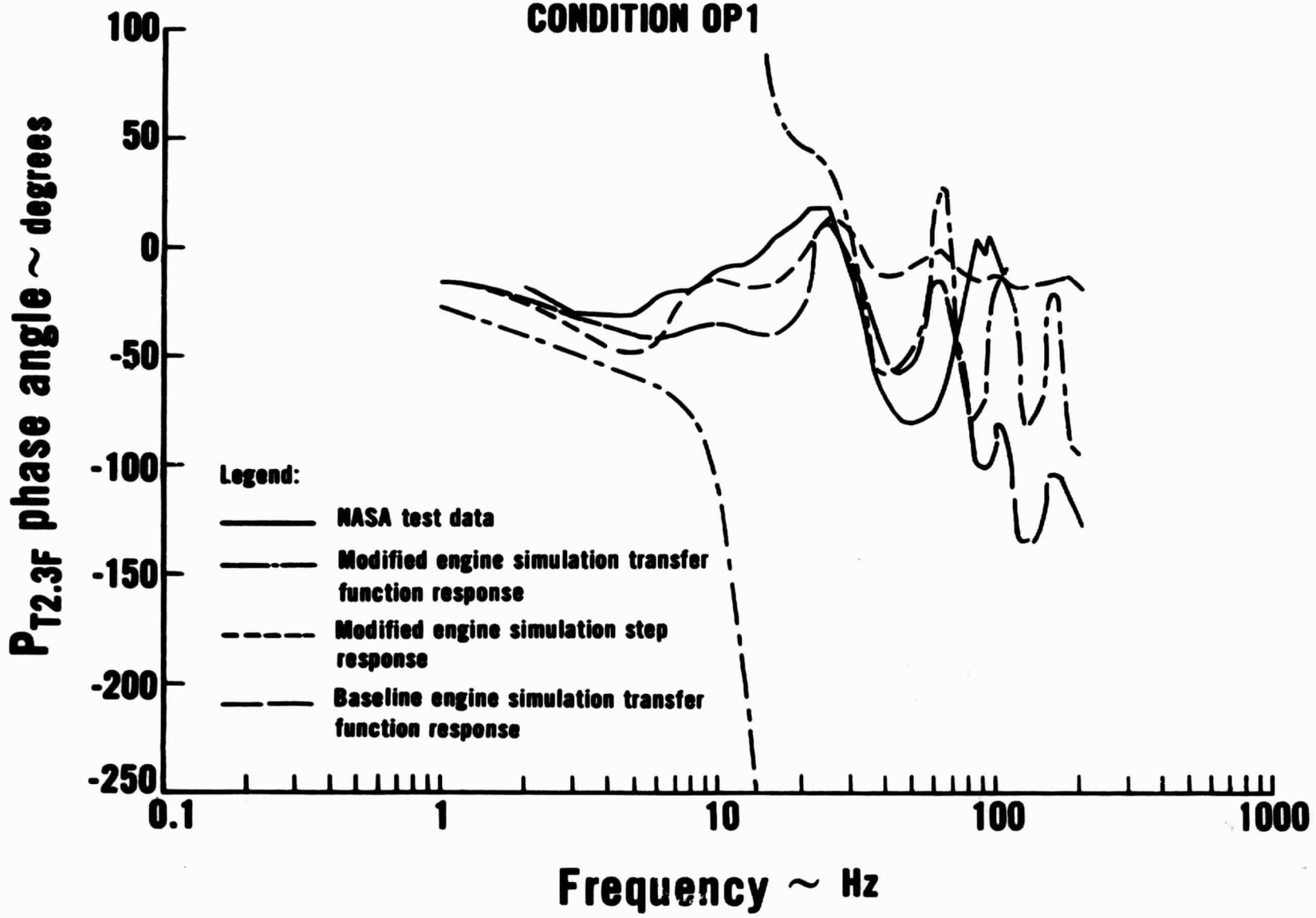

Figure 67 Fan Bypass Stream Phase at Station 2.3F

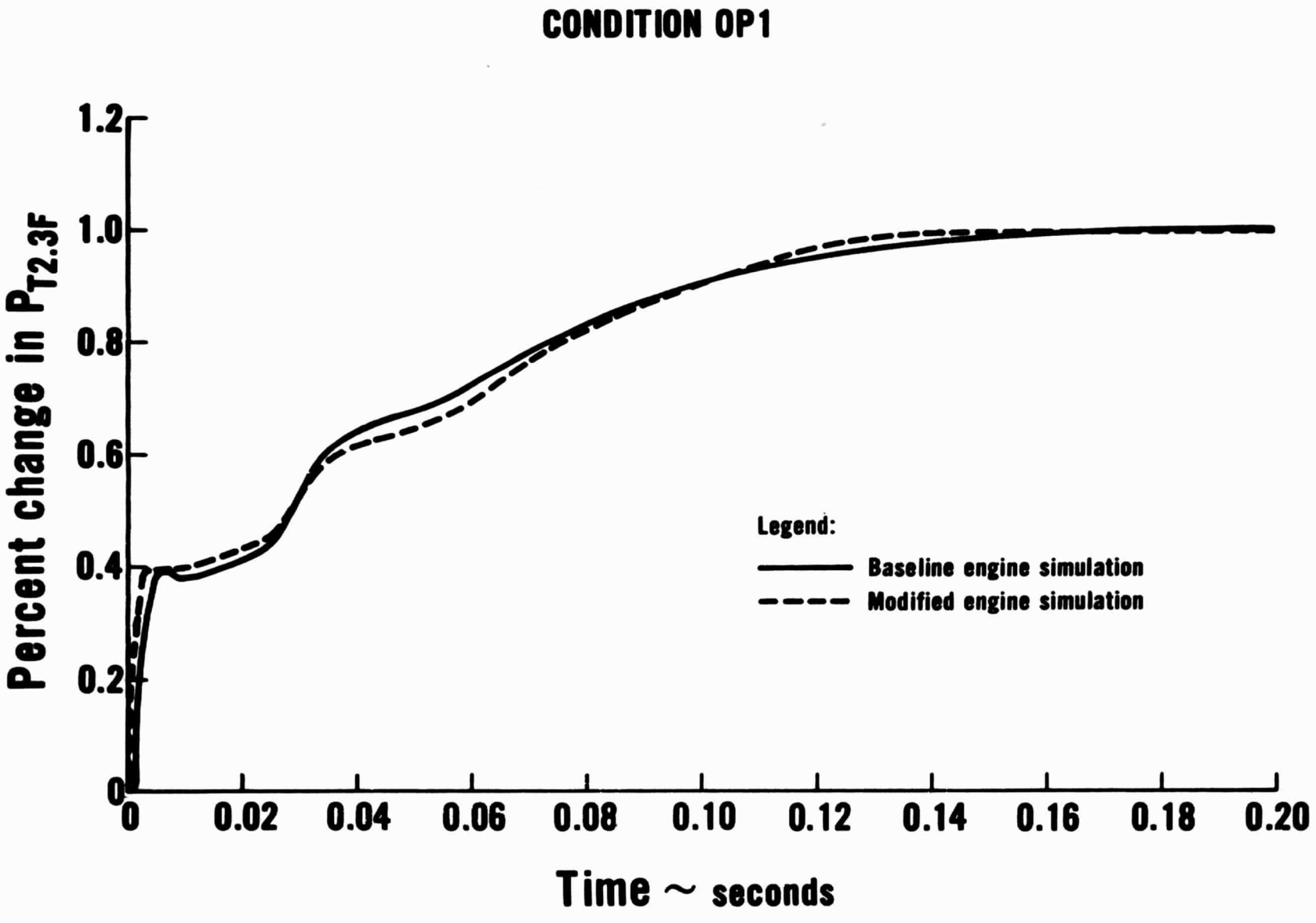

Figure 68 Fan Bypass Stream Pressure - Time History of Response to a 1.0% Inlet Pressure Step

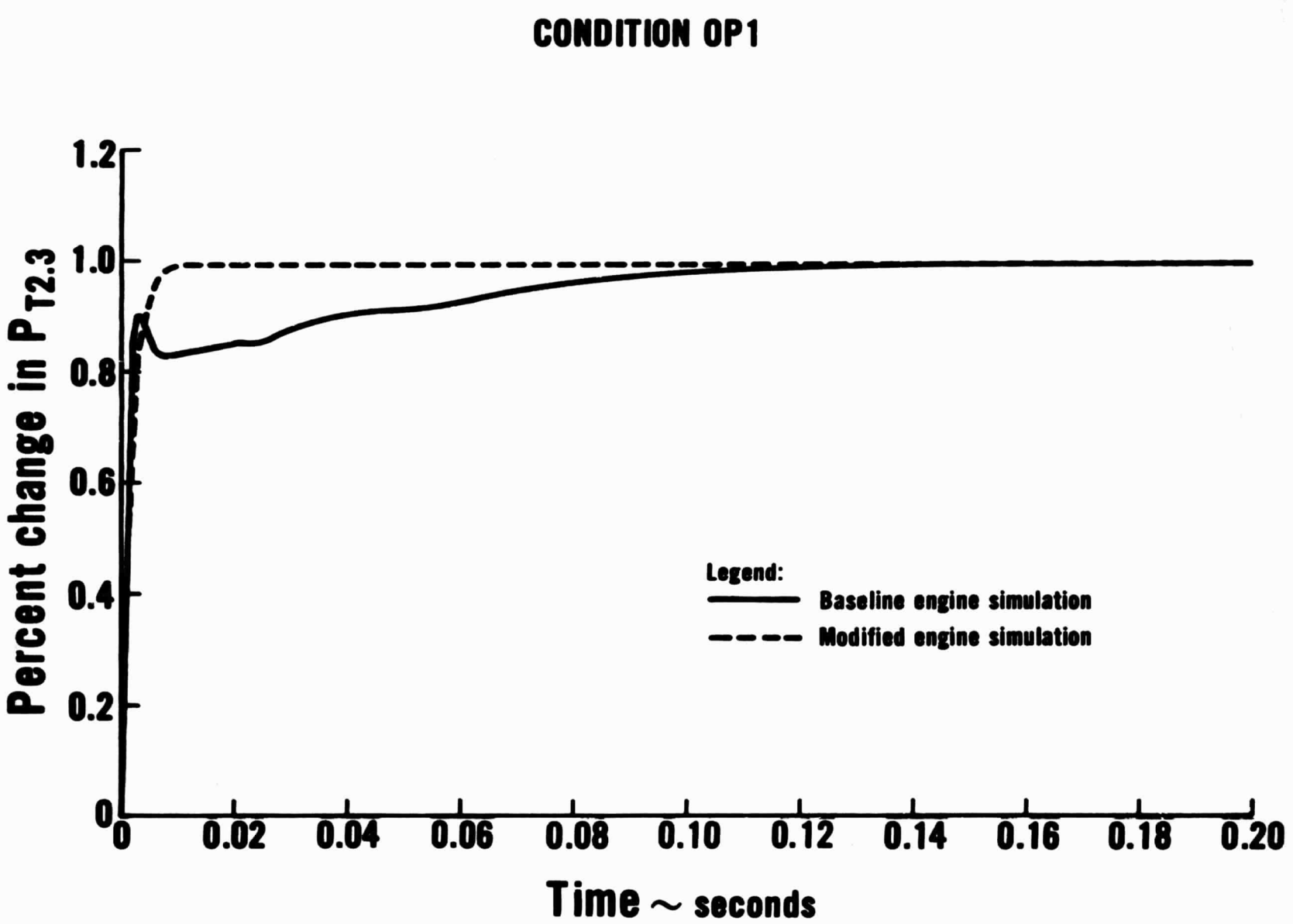

Figure 69 *Fan Core Stream Pressure - Time History of Response to a 1.0% Inlet Pressure Step*

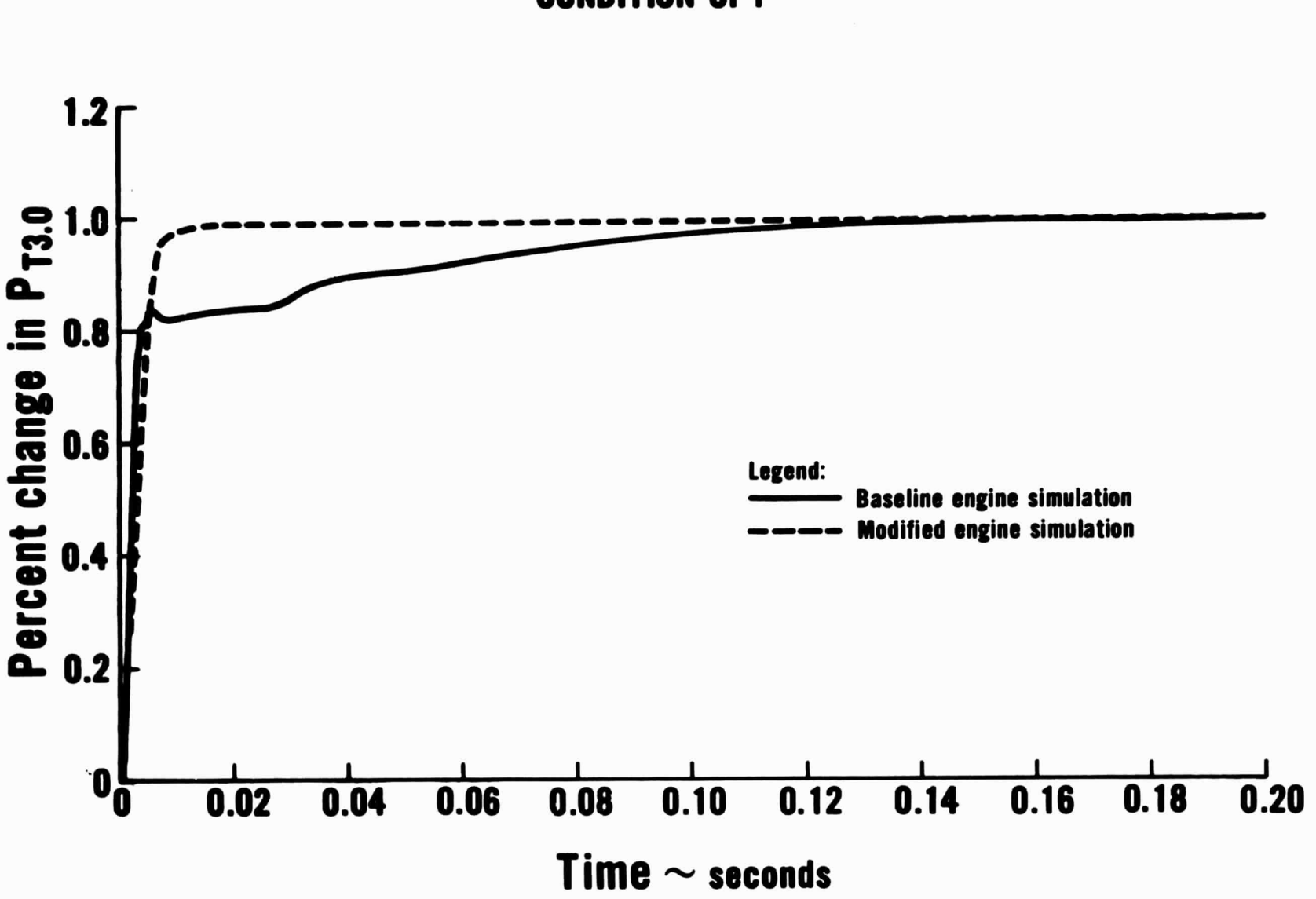

Figure 70 Low Compressor Pressure - Time History of Response to a 1.0% Inlet Pressure Step

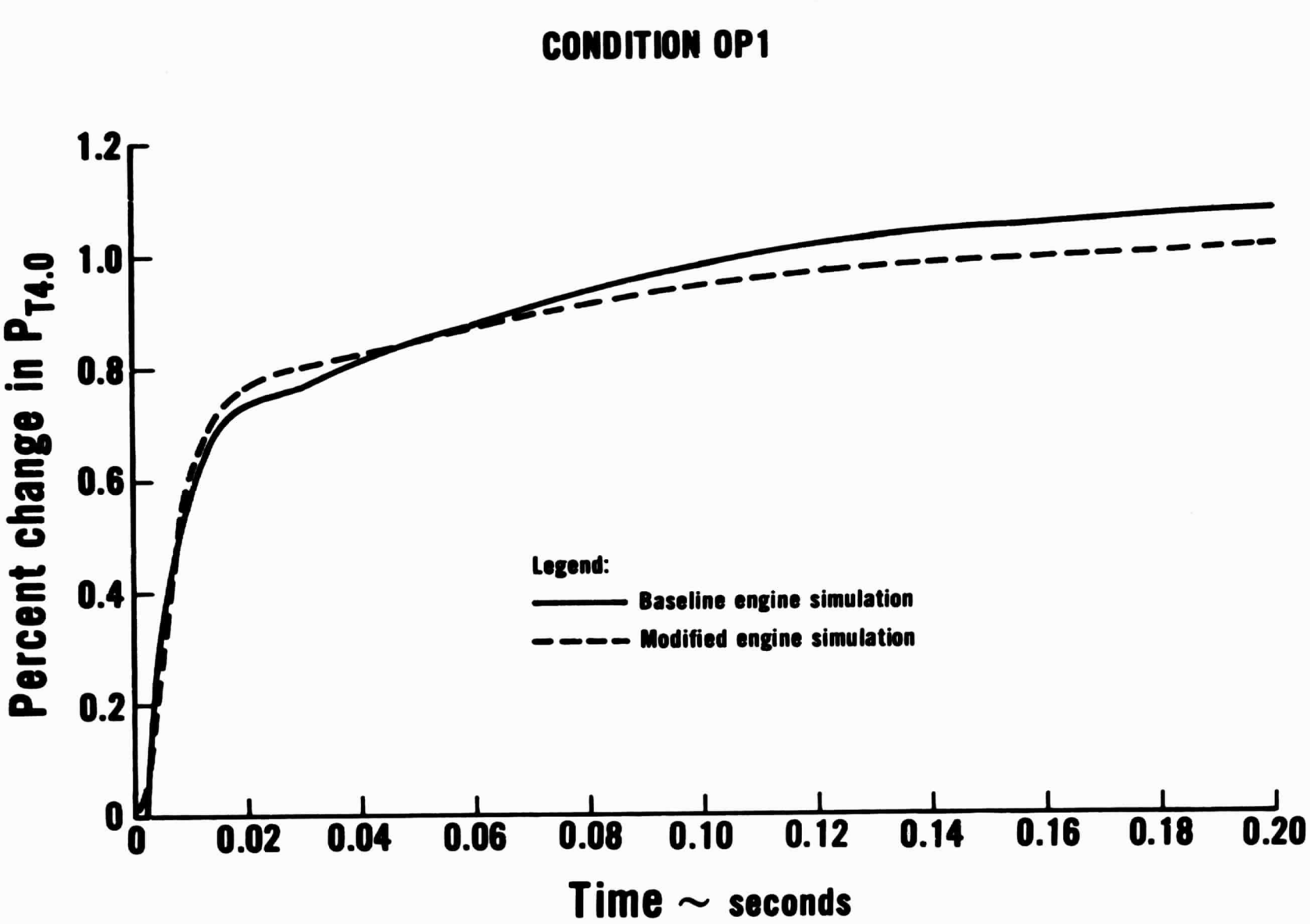

Figure 71 *High Compressor Pressure - Time History of Response to a 1.0% Inlet Pressure Step*

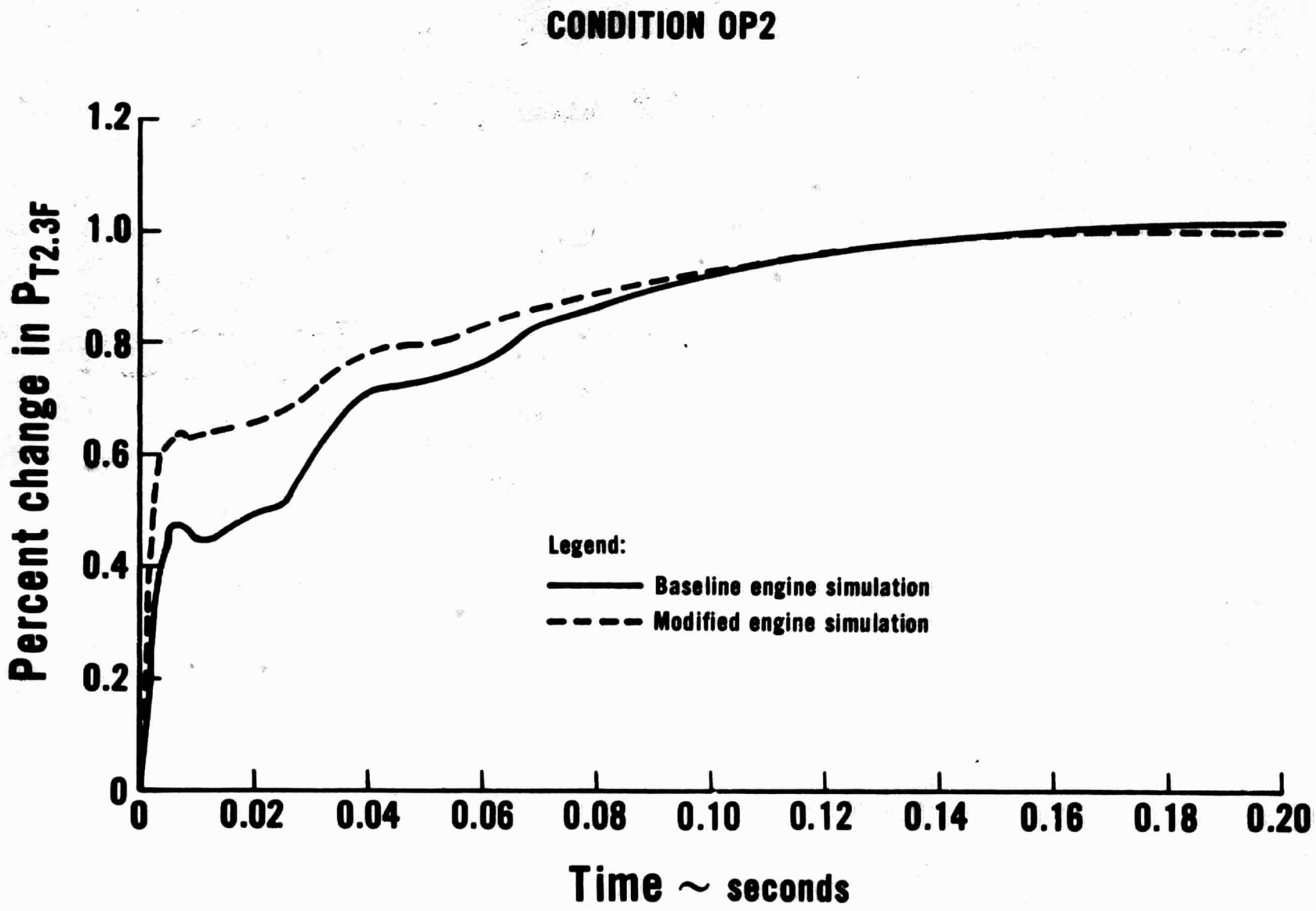

Figure 72 Fan Bypass Stream Pressure - Time History of Response to a 1.0% Inlet Pressure Step

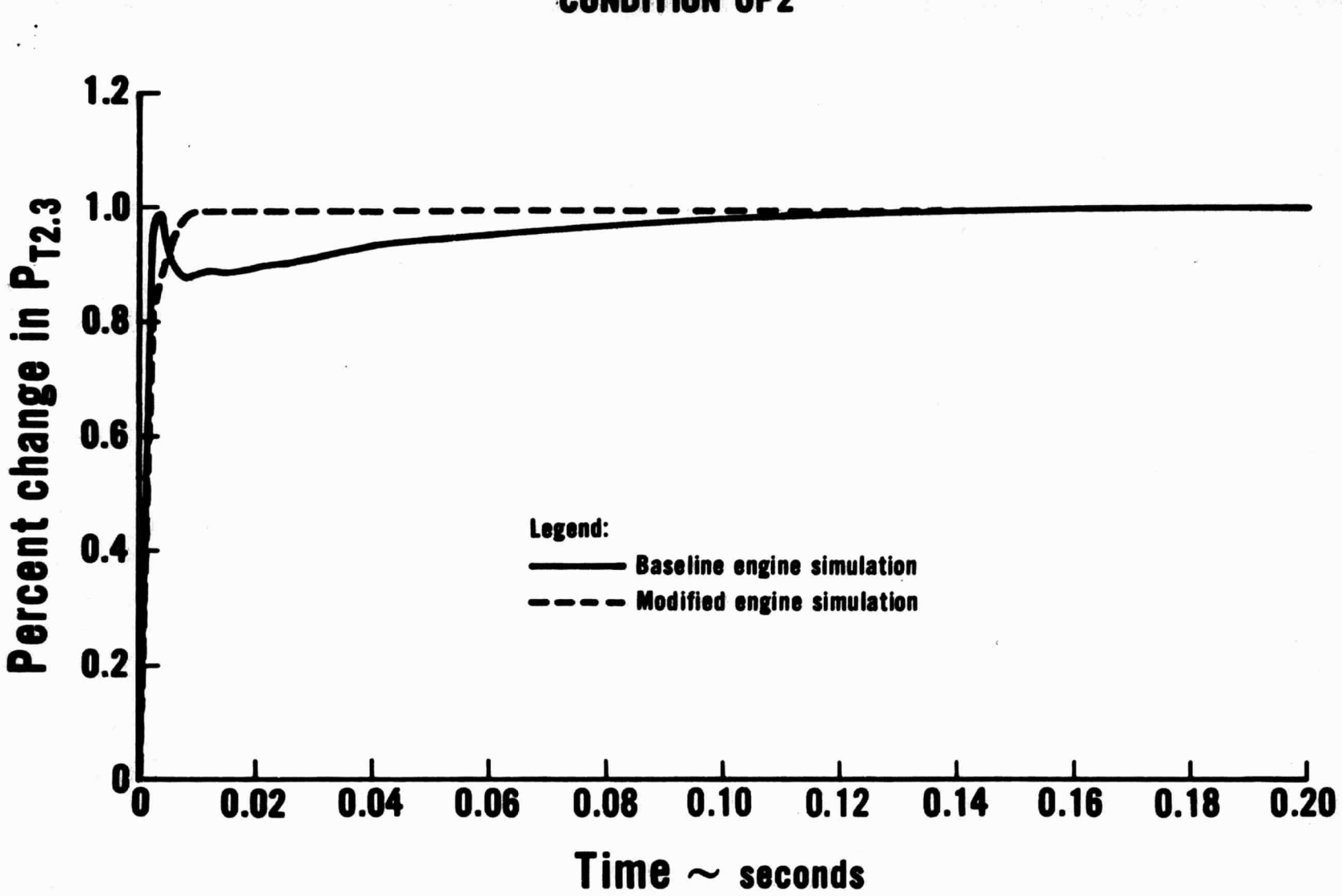

Figure 73 *Fan Core Stream Pressure - Time History of Response to a 1.0% Inlet Pressure Step*

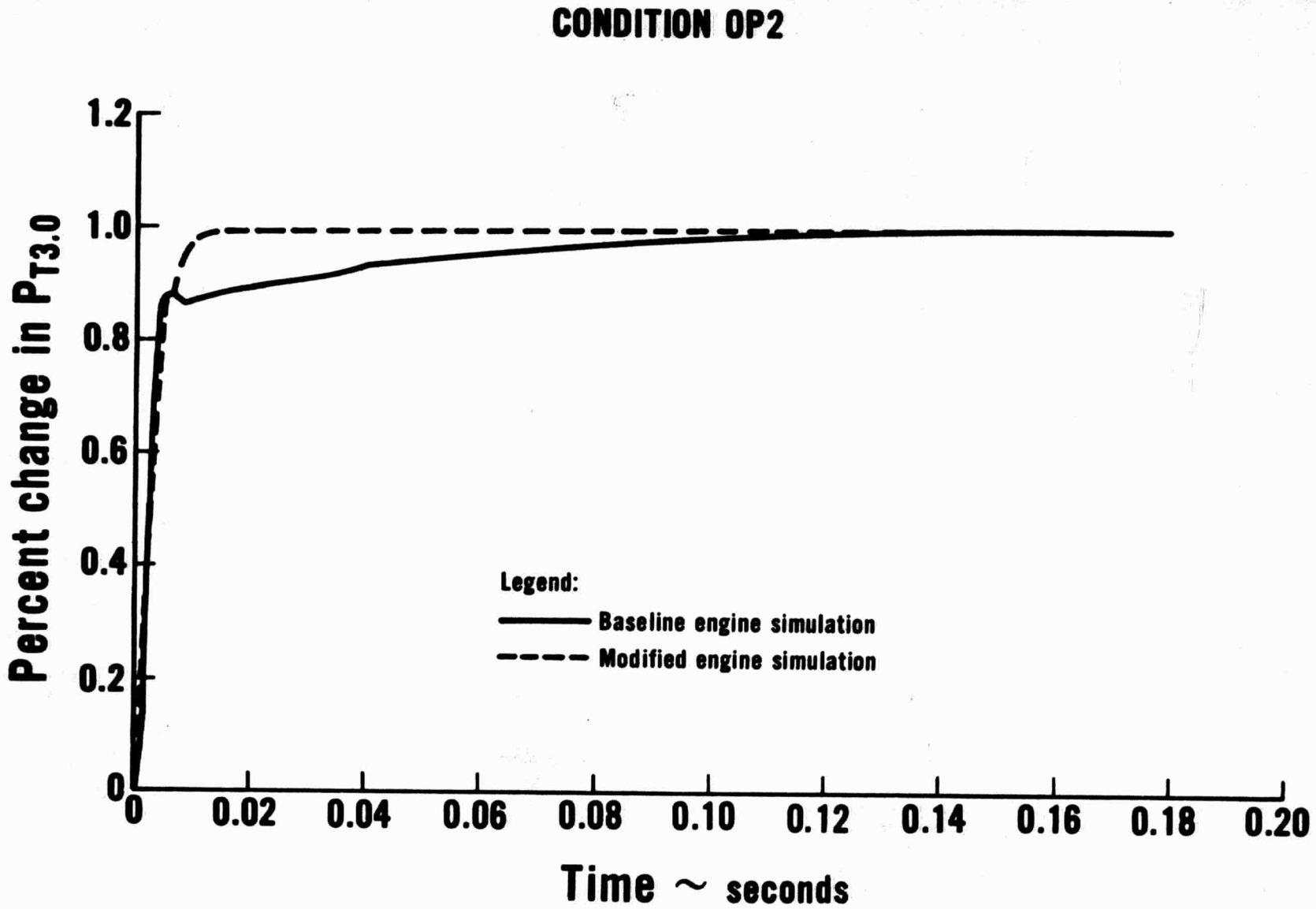

Figure 74 *Low Compressor Pressure - Time History of Response to a 1.0% Inlet Pressure Step*

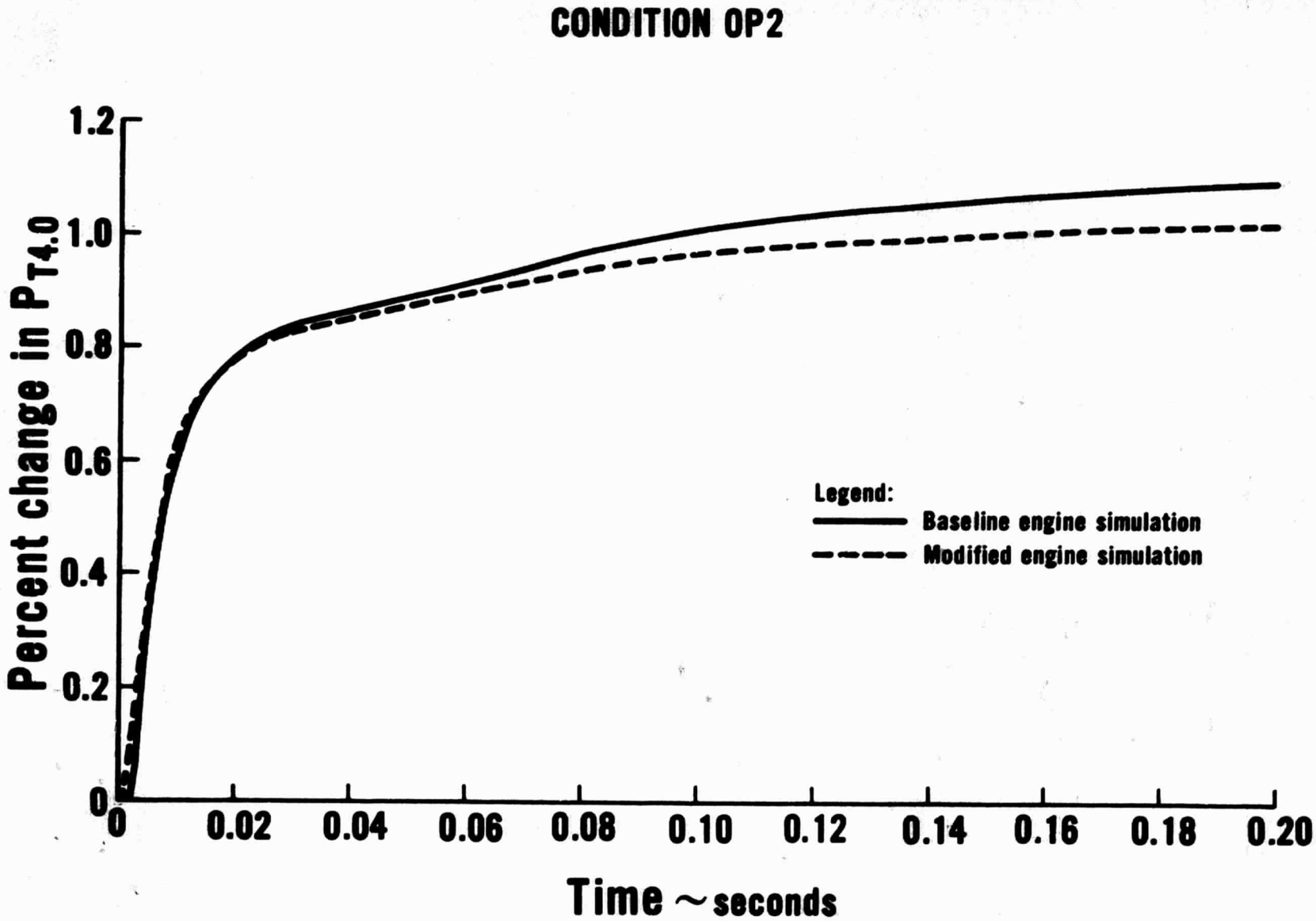

Figur. 75 High Compressor Pressure - Time History of Response to a 1.0% Inlet Pressure Step

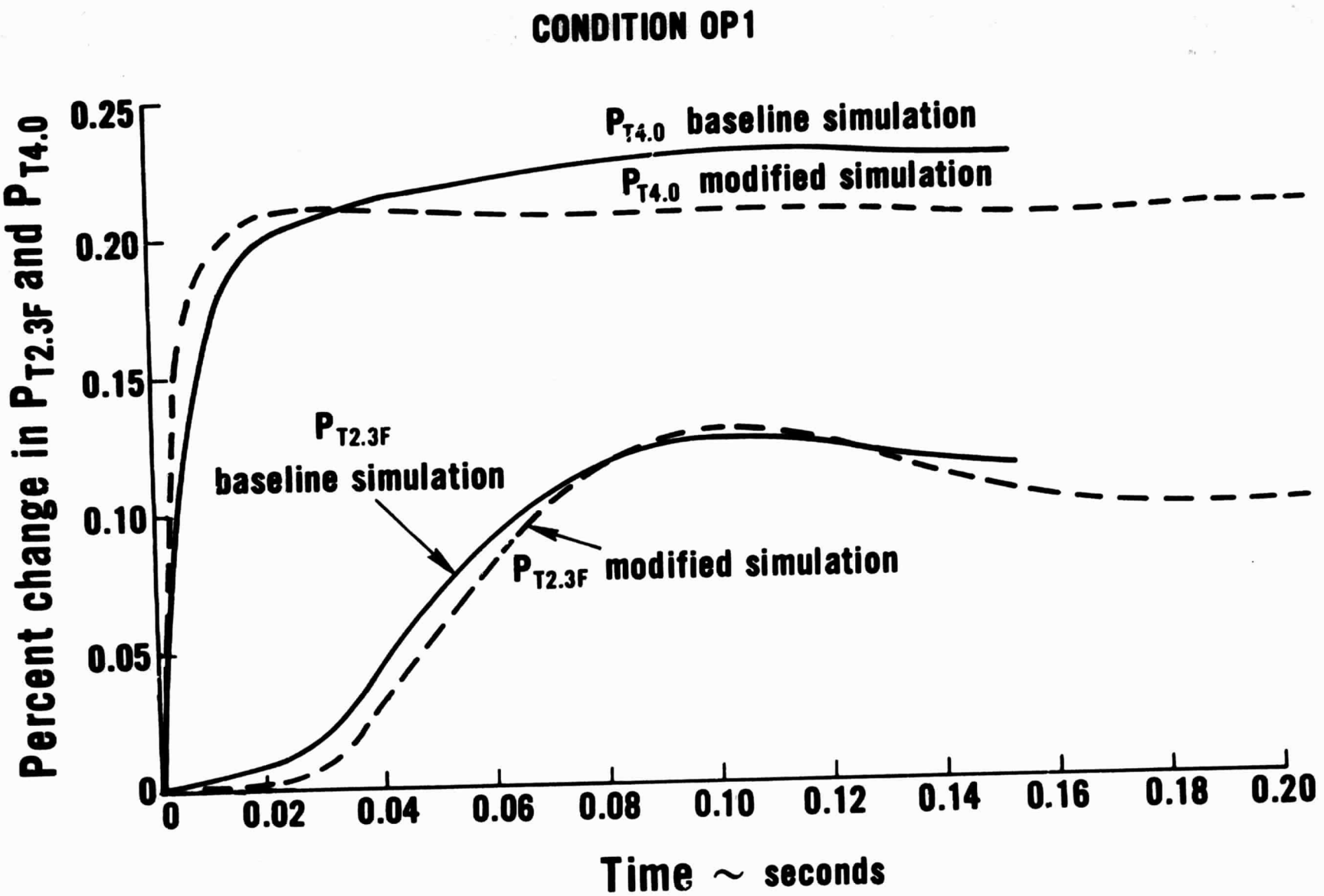

Figure 76 *Fan Bypass Stream and High Compressor Pressure - Time Histories of Response to a 1.0% Fuel Flow Step*

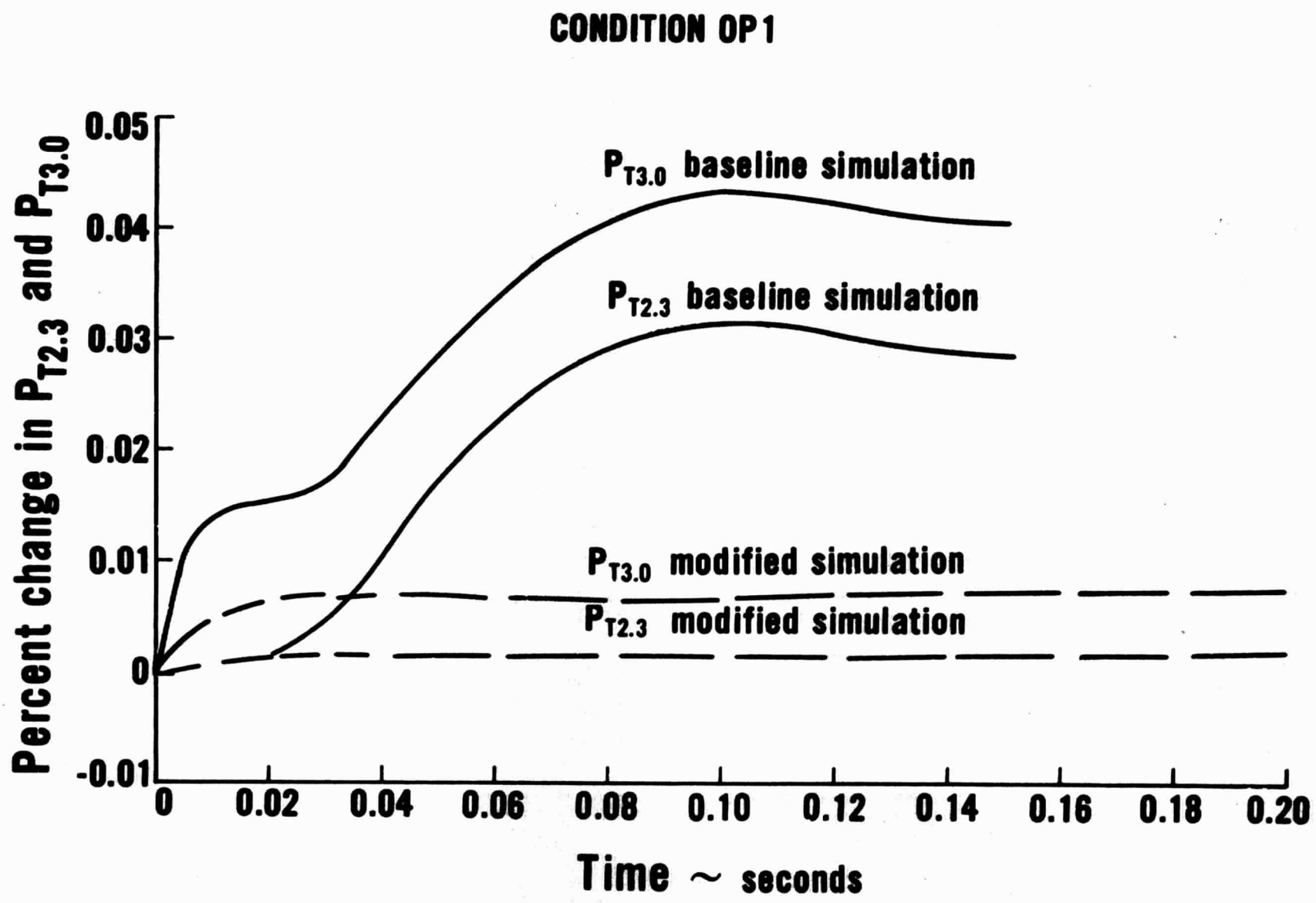

Figure 77 Fan Core Stream and Low Compressor Pressure - Time Histories of Response to a 1.0% Fuel Flow Step

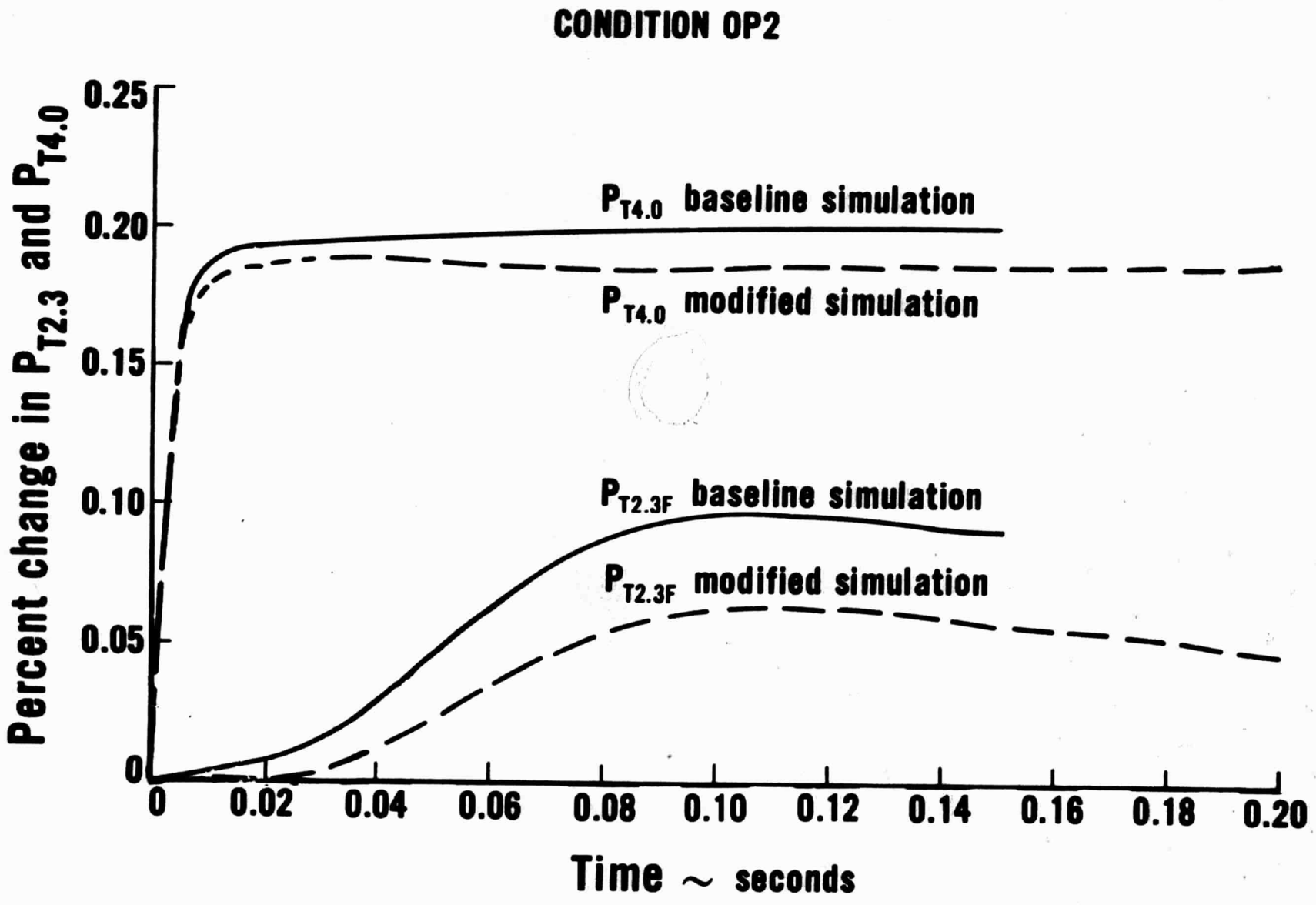

Figure 78 *Fan Bypass Stream and High Compressor Pressure - Time Histories of Response to a 1.0% Fuel Flow Step*

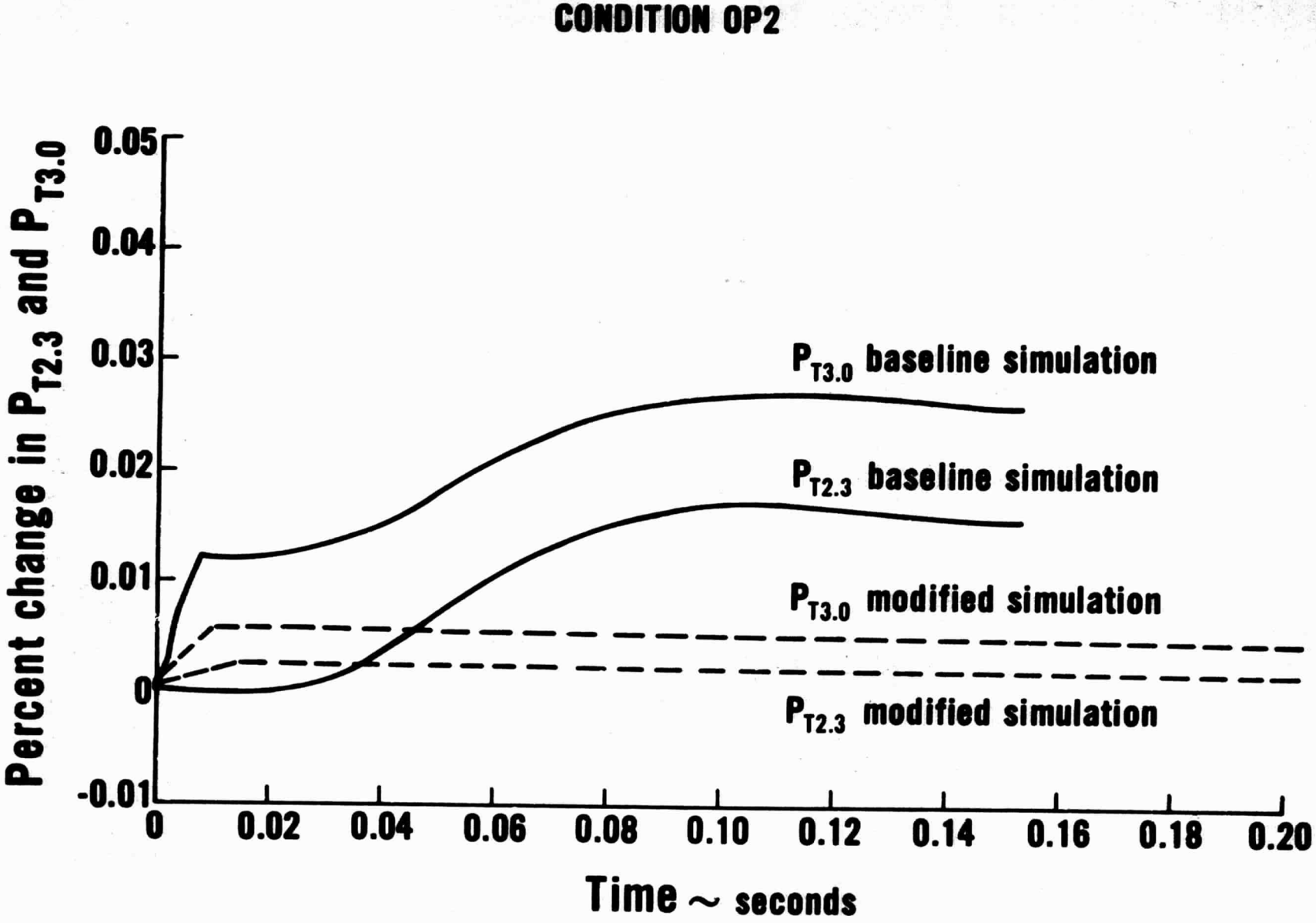

Figure 79 *Fan Core Stream and Low Compressor Pressure - Time Histories of Response to a 1.0% Fuel Flow Step*

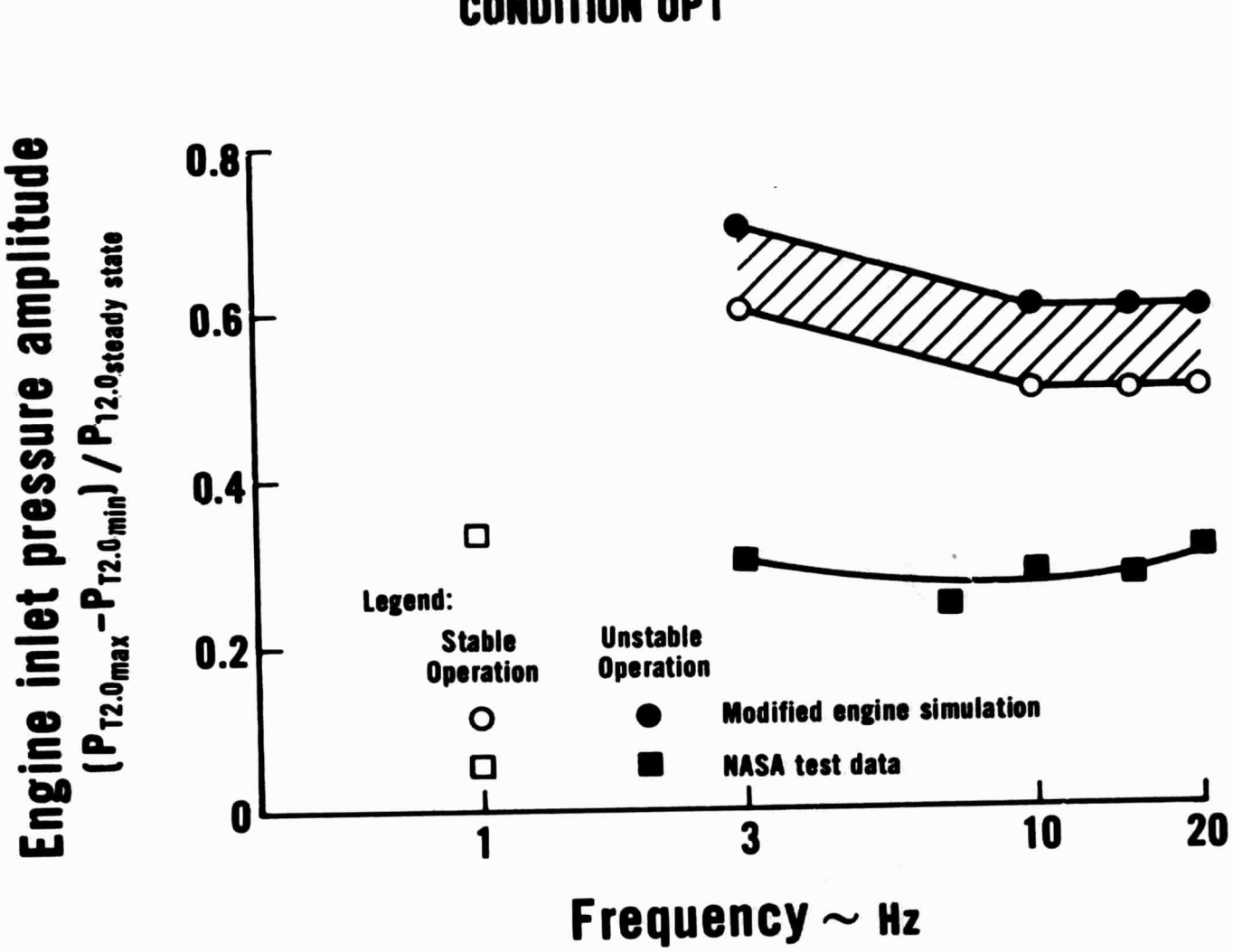

Figure 80 *Comparison of Modified Engine Simulation Stability Limits and Engine Surge Data*

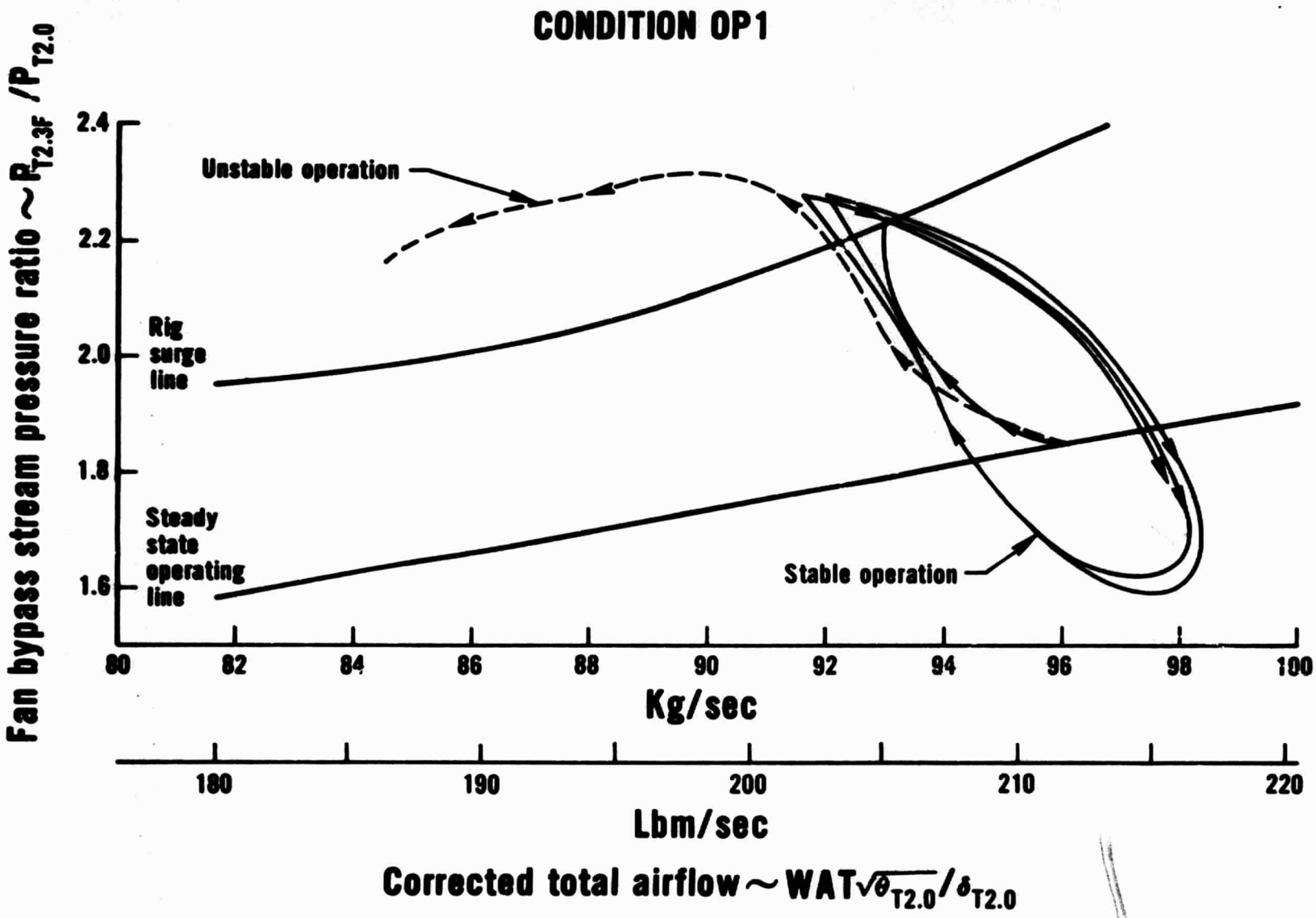

Figure 81 *Fan Operation Predicted by Modified Engine Simulation with 10 Hz Cyclic Inlet Pressure Variation*

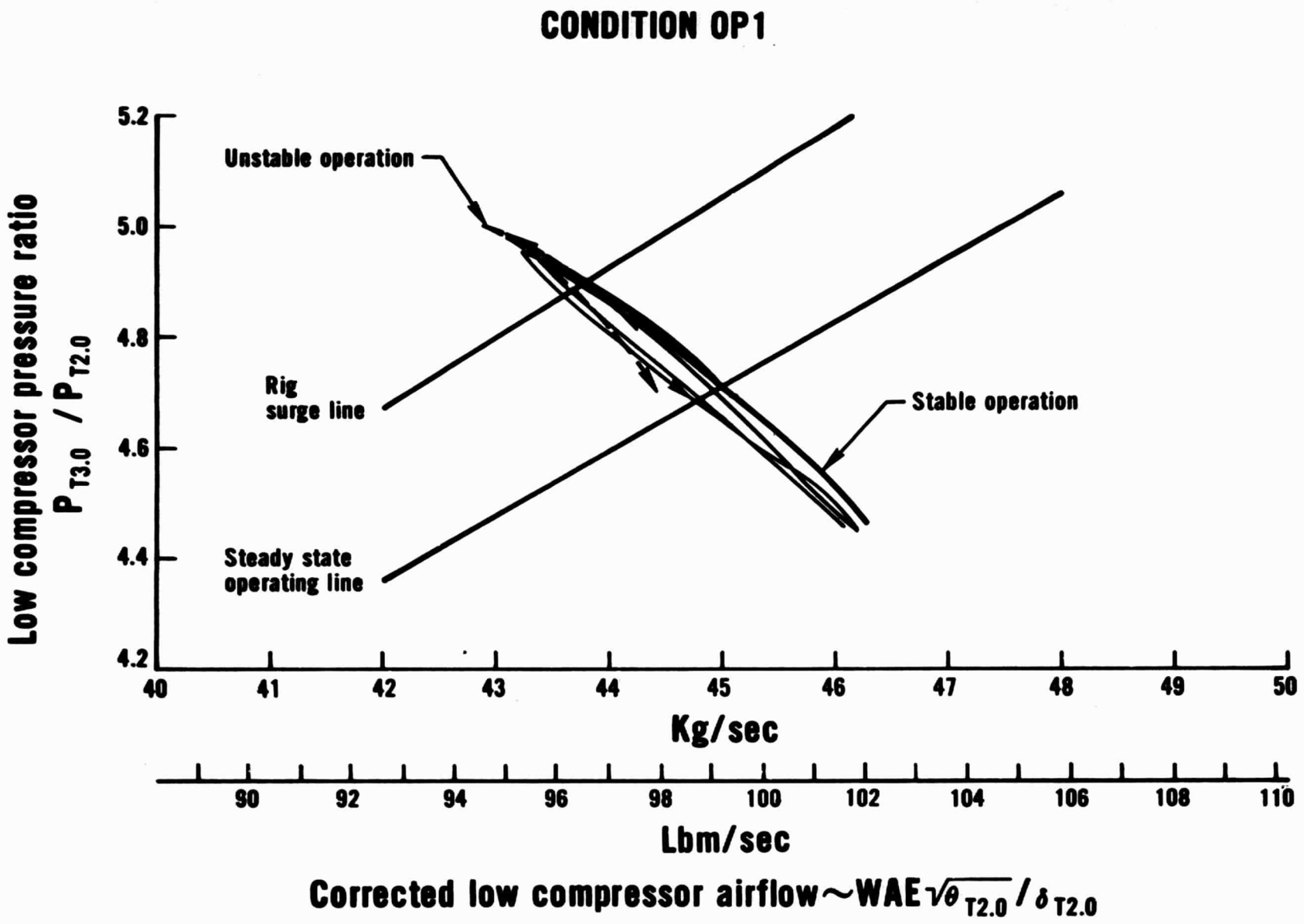

Figure 82 *Low Compressor Operation Predicted by Modified Engine Simulation with a 10 Hz Cyclic Inlet Pressure Variation*

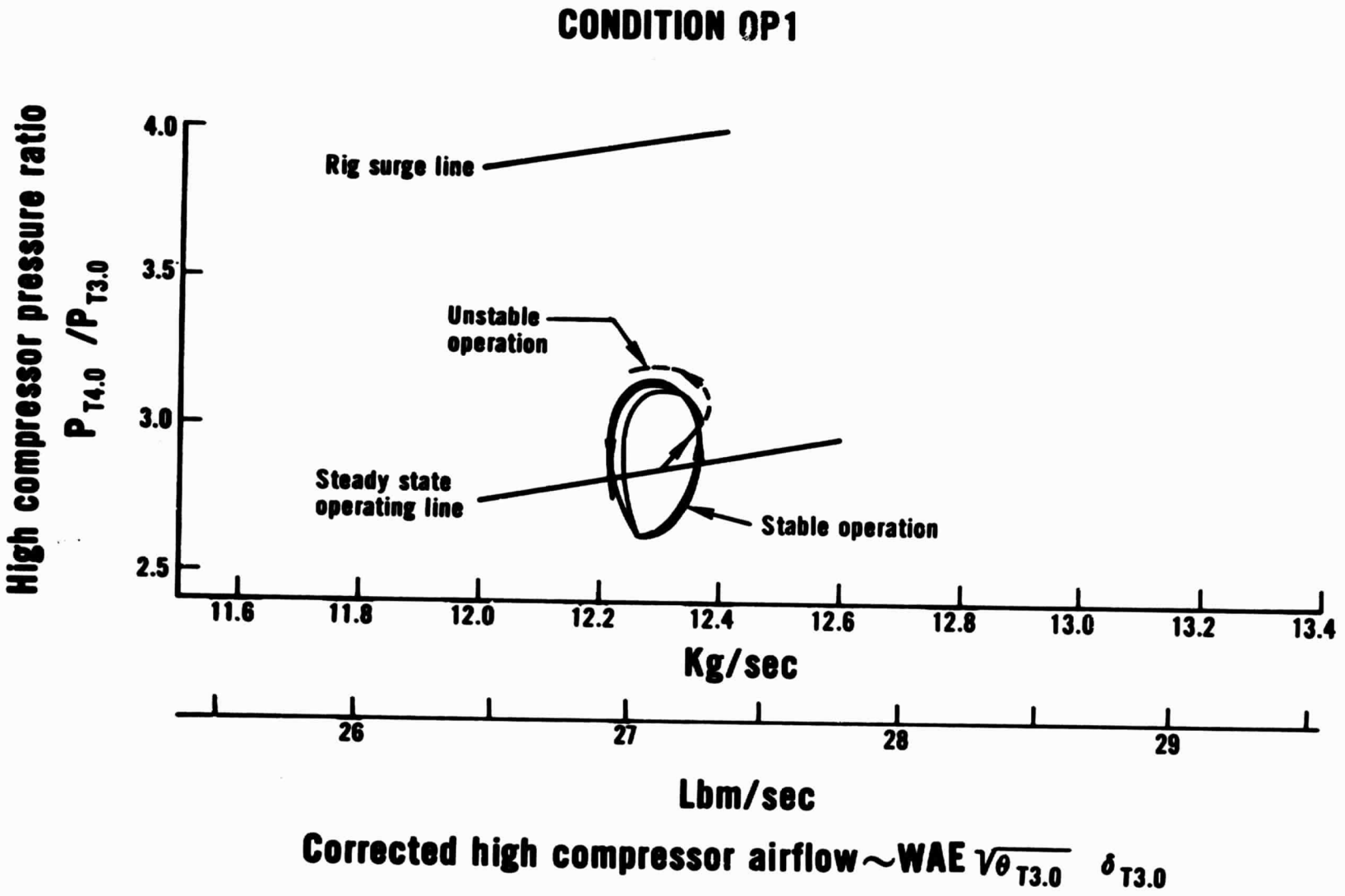

Figure 83 *High Compressor Operation Predicted by Modified Engine Simulation With a 10 Hz Cyclic Inlet Pressure Variation*

APPENDIX A
DESCRIPTION OF MODIFIED ENGINE SIMULATION

INTRODUCTION

This appendix describes the modified dynamic engine simulation evaluated during this program. This appendix is divided into three sections which are 1) performance characteristics used to simulate each component, 2) dynamic equations employed, and 3) a discussion of the program solution techniques.

The method of defining performance characteristics of each engine component is described in the Component Performance Characteristics section. The components described are the compressor, burner, turbine, ducts, exhaust nozzle and the control. The individual component characteristics describe the steady state operation of each component.

The Dynamic Equation section describes the method of simulating the dynamic characteristics of each component. The method uses dynamic forms of the continuity, momentum, and energy equations. The form of the equations used in the simulation is presented. Two dynamic computations, rotor dynamics and dynamic mixing, do not directly use the three basic equations to describe engine operation. The method of implementing rotor dynamics and dynamic mixing is also presented. The use of the dynamic equations in conjunction with the steady state performance characteristics is described.

The Solution Techniques section discusses the methods used to solve the simulation equations. The form of the simulation equations is implicit and iterative (relaxation) methods are used to arrive at solutions.

COMPONENT PERFORMANCE CHARACTERISTICS

Compressor

Description

The TF30-P-3 compression system consists of a three stage fan, a six stage low pressure compressor and a seven stage high pressure compressor. Figure A-1 presents a cross section of the TF30-P-3 compression system where key stages have been identified. The fan compresses all of the air coming into the engine. Part of the air flows through the core, i.e., into the low and high compressors, to be compressed to a higher pressure. The remaining flow goes only through the fan and is bypassed around the core. The ratio of the bypass flow to the core flow is the bypass ratio.

The compression system used in the modified engine simulation was based on individual row performance characteristics. A row consisted of either a rotor or a stator and a gap behind the rotor or stator. The rows were interconnected to form the entire compression system.

The compression system pressure and temperature change were defined through the use of characteristic maps for each individual row. The temperature rise was calculated from total temperature maps and the pressure change from static pressure maps. Total and static pressures in each row were related by standard compressible flow relationships.

Mathematical Model

In a row-by-row model, parameters are computed at the entrance to each stator or rotor and at the entrance to the gap (exit of the rotor or stator). The exit performance parameters of each row becomes the entrance conditions of the following row. Performance modifiers are used at various places in the compression system to account for off design operation of the system. These include:

1. Modification of the fan bypass stream and fan core stream performance characteristics to account for bypass ratio changes. The characteristic maps for the fan are determined for a design bypass ratio (BPR). The modifier allows calculation of fan performance parameters at bypass ratios other than design.

2. Modification of the performance characteristics in the vicinity of the splitter to account for flow separation at the splitter and the resulting change in flow angle.

Inlet Guide Vane

The normal simulation input parameters at the engine entrance are total pressure, total temperature and air flow. The row performance characteristics are based on static pressure therefore a static pressure must be calculated prior to starting the first row (inlet guide vane) computation. To determine the static pressure from the given parameters, a flow parameter is calculated as

$$FP_{ENTRANCE} = \frac{W_{a\ ENTRANCE}\sqrt{T_{T\ ENTRANCE}}}{P_{T\ ENTRANCE}\ A_{ENTRANCE}} \qquad (A1)$$

The static to total pressure ratio is determined from the compressible flow relationship shown in Figure A-2.

The static pressure is calculated as

$$P_{S\ ENTRANCE} = \frac{P_{T\ ENTRANCE}}{\left(P_{T\ ENTRANCE}/P_{S\ ENTRANCE}\right)} \tag{A2}$$

Row Computations

The entrance conditions to each row are obtained from the exit of the previous row or from the inlet guide vane entrance calculations. The rows are interconnected, or stacked, to provide a simulation of the complete compression system. The computations performed in each component of the row are diagrammed in Figure A-3. The remainder of this section is a presentation of the formulas which are used in the calculation of the thermodynamic properties through the compressor row.

The compressor row characteristics are presented as pressure and temperature functions which are correlated with a flow function and the row inlet corrected speed. The flow function for a given row is

$$\phi_n = \left[\frac{W_{ag\ n-1}\sqrt{T_{Tg\ n-1}/T_{STAND}}}{\left(P_{Tg\ n-1}/P_{STAND}\right)A_n}\right]\left[\frac{\left(N/\sqrt{T_{Tg\ n-1}/T_{STAND}}\right)_{DES\ n}}{\left(N/\sqrt{T_{Tg\ n-1}/T_{STAND}}\right)_n}\right]\left[\frac{MOD\ 1}{MOD\ 2}\right] \tag{A3}$$

$$\text{Where } \left(N/\sqrt{T_{Tg\ n-1}/T_{STAND}}\right)_{DES\ n} \tag{A4}$$

is the design speed for each row and is a constant value determined when the row characteristics are generated from test data.

MOD1 in equation (A3) is a modification applied to

$$\frac{\left(N/\sqrt{T_{Tg\ n-1}/T_{STAND}}\right)_{DES\ n}}{\left(N/\sqrt{T_{Tg\ n-1}/T_{STAND}}\right)_n} \tag{A5}$$

of the fan rows from station 2.0 to station 2.3 and 2.3F shown in Figure A-1. The modification is an equation which is a function of the geometric fan dimensions and the bypass ratio. The modification for the core stream is

$$MOD1 = \left[\frac{(OD_n^2 + 3ID_n^2)(1 + BPR)}{2(OD_n^2 + (1 + 2BPR)ID_n^2)}\right]^{1/2} \quad (A6)$$

The modification for the bypass stream is

$$MOD1 = \left[\frac{(3\,OD_n^2 + ID_n^2)(1 + BPR)}{2\left((2 + BPR)OD_n^2 + ID_n^2\right)}\right]^{1/2} \quad (A7)$$

This modification is made to allow use of the row characteristics at a bypass ratio other than the bypass ratio at which the characteristics were generated. The characteristics are generated for a given position of the streamline separating the bypass flow and the core flow which is a function of the bypass ratio. However, when the bypass ratio changes, the streamline between the bypass and the core stream moves which in turn changes the effective rotor or stator length. The change in effective rotor or stator length in turn effects the average wheel speed. The flow velocities through the rows are proportional to wheel speed and MOD1 can therefore be applied to the speed ratio term of the flow function ϕ_n to the account for the effective length variations.

MOD2 is a modification of the area at core stator 3 shown in Figure A-1. The modification is applied at low bypass ratios to account for a reduction in the flow area when flow separation exists at the splitter. The modification is

$$MOD2 = 0.38462\,BPR + 0.51538 \quad (A8)$$

and is limited to a maximum value of 1.0.

The pressure function (ψ) and the temperature function (λ) are determined from the row characteristic maps shown schematically in Figures A-4 and A-5, respectively.

The stator exit total temperature is assumed to be equal to the stator entrance total temperature because no work is input to the flow through the stators.

The rotor exit total temperature is computed using the relationship

$$T_{Tc\,n} = T_{Tg\,n-1}\left\{1.0 + \frac{\lambda_n}{MOD\,1}\left[\frac{\left(N/\sqrt{T_{Tg\,n-1}/T_{STAND}}\right)_n}{\left(N/\sqrt{T_{Tg\,n-1}/T_{STAND}}\right)_{DES\,n}}\right]^2\right\} \tag{A9}$$

The rotor and stator exit static pressure is computed using the relationship

$$P_{Sc\,n} = P_{Sg\,n-1}\left\{1.0 + \left[\frac{\psi_n + MOD\,3}{MOD\,1}\right]\left[\frac{\left(N/\sqrt{T_{Tg\,n-1}/T_{STAND}}\right)_n}{\left(N/\sqrt{T_{Tg\,n-1}/T_{STAND}}\right)_{DES\,n}}\right]^2\right\} \tag{A10}$$

where MOD1 is the same value and applied at the same location as the ϕ_n calculation. MOD3 is applied to the bypass stream rotor 3, core stream rotor 3 and core stream stator 3. These locations are identified on Figure A-1. This modification is applied to account for the radial bending of the streamlines in the vicinity of the splitter.

MOD3 is a dimensionless parameter defined as

$$MOD3 = [MOD1]\left[\frac{K_M \cdot \alpha_n M^2_{zg\,n-1}}{1.0 - M^2_{zg\,n-1}}\right]\left[\frac{\left(N/\sqrt{T_{Tg\,n-1}/T_{STAND}}\right)_{DES\,n}}{\left(N/\sqrt{T_{Tg\,n-1}/T_{STAND}}\right)_n}\right]^2 \tag{A11}$$

where K_M is defined in a different manner for each of the three locations where MOD3 is applied.

For bypass stream rotor 3

$$K_M = \left[\frac{A_{S3\,BYPASS}/A_{S3\,CORE}}{BPR_{R3}}\right]\left[\frac{1.0 + BPR_{R3}}{1.0 + (A_{S3\,BYPASS}/A_{S3\,CORE})}\right] \tag{A12}$$

$$X \left[\frac{A_{S3\,BYPASS} + A_{S3\,CORE}}{A_{R3\,BYPASS} + A_{R3\,CORE}}\right] - 1.0$$

For core stream rotor 3

$$K_M = \left[\frac{1 + BPR_{R3}}{1.0 + (A_{S3\ BYPASS}/A_{S3\ CORE})}\right]\left[\frac{A_{S3\ BYPASS} + A_{S3\ CORE}}{A_{R3\ BYPASS} + A_{R3\ CORE}}\right] - 1.0 \tag{A13}$$

For core stream stator 3

$$K_M = \frac{A_{R4} - A_{S3\ CORE}}{A_{S3\ CORE}} \tag{A14}$$

Two values of mach number are calculated in each row. The axial mach number is the mach number in a direction parallel to the centerline of the compression system. To determine the total pressure in each row, the mach number in the direction of the flow must be determined. The axial mach number is determined from the isentropic flow relationship

$$M_{yc\,n} = \left[\frac{\sqrt{1.0 + [W_{ac\,n}/P_{Sc\,n} A_n\ MOD2]^2\ [2.0\ (\gamma_n - 1.0) R\ T_{Tc\,n}/g\ \gamma_n]} - 1.0}{\gamma_n - 1.0}\right]^{0.5} \tag{A15}$$

The flow direction Mach number (M_z) is a function of the axial Mach number and flow angle (α). A schematic of the flow angles is shown in Figure A-6.

The flow angle at the exit of a stator is assumed to be the stator exit metal angle and is a constant value. The flow angle at the exit of a rotor is influenced by the rotational speed of the rotor and therefore must be calculated. The method of computation is

$$V_{yc\,n} = \frac{\sqrt{\gamma_n R g T_{Tc\,n}}}{\sqrt{(1.0/M^2_{yc\,n}) + (\gamma_n - 1.0)/2.0 \sin^2 \alpha_{c\,n}}} \tag{A16}$$

and

$$\sin \alpha_{c\,n} = \frac{1.0}{\sqrt{1.0 + (U_n/V_{yc\,n} - 1.0/\tan \beta_{c\,n})^2}} \tag{A17}$$

$V_{ac\,n}$ is the axial flow velocity and $\beta_{c\,n}$ is the exit metal angle of the rotor. The relationship of these parameters is shown in Figure A-7.

Equations (A16) and (A17) are solved by substituting equation (A17) into equation (A16) which provides a quadratic equation to solve for $V_{ac\,n}$ and subsequent calculation of $\alpha_{c\,n}$.

The flow mach number is calculated from the axial mach number and the flow angle as

$$M_{zc\,n} = M_{yc\,n}/\sin \alpha_{c\,n} \tag{A18}$$

The compressor flow function (ϕ_n) contains a total pressure term which must be determined along the flow path. The total pressure is a function of the flow mach number and is related to the static pressure using the isentropic flow relationship

$$P_{Tc\,n} = P_{Sc\,n} \left[1.0 + \frac{(\gamma_n - 1.0)\, M^2_{zc\,n}}{2.0} \right]^{\frac{\gamma_n}{\gamma_n - 1.0}} \tag{A19}$$

The flow conditions across the gap are assumed to be constant with one exception. The static pressure and the flow angle, and therefore flow mach number and total pressure, are modified at the exit of core rotor 3, shown in Figure A-3. The modification is to account for the splitter flow separation at low bypass ratio.

The modifications are implemented through a change in the parameter β which is the core rotor 3 metal exit angle. The modified angle, $\beta_{g\,n}$, is defined as a function of bypass ratio. The value of $\beta_{g\,n}$ is

$$\beta_{g\,n} = 75.5277 - 14.3077\ BPR \tag{A20}$$

with a minimum limit of the actual core rotor 3 metal exit angle (57.5°).

The axial velocity at the gap exit is recalculated by

$$V_{yg\,n} = V_{yc\,n} \tan \beta_{g\,n}/\tan \beta_{c\,n} \tag{A21}$$

The static pressure at the exit of the gap is determined by

$$P_{Sg\,n} = P_{Sc\,n} + \left[\frac{2.0\, W_{ac\,n}}{A_{n\,g}} \right] \left[\frac{V_{yc\,n} - V_{yg\,n}}{1.0 + A_{n+1}\ MOD2/A_n} \right] \tag{A22}$$

MOD2 is the core stator 3 area modification presented previously.

The flow angle at the gap exit is recalculated as

$$\sin \alpha_{g\,n} = \frac{V_{yg\,n}/(U_n - V_{yc\,n}/\tan \beta_{c\,n})}{\sqrt{1.0 + [V_{yg\,n}/(U_n - V_{yc\,n}/\tan \beta_{c\,n})]^2}} \tag{A23}$$

The change in the axial velocity and the flow angle results in a change in the flow mach number which is determined by

$$M_{zg\,n} = \sqrt{\frac{V^2_{yg\,n}/\gamma_n\, Rg\, T_{Tc\,n} \sin^2 \alpha_{g\,n}}{1.0 - (\gamma_n - 1.0)\, V^2_{yg\,n}/2.0\, \gamma_n\, RgT_{Tc\,n} \sin^2 \alpha_{g\,n}}} \tag{A24}$$

The total pressure at the exit of the gap is calculated from the isentropic flow relationship

$$P_{Tg\,n} = P_{Sg\,n} \left(1.0 + \frac{(\gamma_n - 1.0)\, M^2_{zg\,n}}{2.0}\right)^{\frac{\gamma_n}{\gamma_n - 1.0}} \tag{A25}$$

Burner

Description

The TF30-P-3 combustor is composed of eight cans. Air discharged from the high compressor is divided into a primary and secondary zone. The primary air supports combustion and the secondary air provides cooling for the cans and dilution of the fuel-air mixture.

Simulation

The burner model used in the engine simulation was separated to simulate the dynamics of the hot combustion section and the cool bypass flow. Separation of the burner primary and secondary airflow was therefore necessary to simulate this operation. Two parallel airstreams were used to represent the primary and secondary zones, with the combustion calculations performed in the primary airstream. At the discharge plane of the burner, the primary and secondary streams were mixed to establish the inlet conditions to the turbine. The model of the primary zone of the burner accounted for combustion efficiency, heat addition, pressure losses, and mixing of the two zones. The secondary zone is represented as a duct, which is described under the section entitled "Ducts". The burner is shown in Figure A-1 where station 4.0 is the burner entrance and station 5.0 is the burner exit.

Efficiency

During the combustion process, all of the theoretical temperature rise is not obtained from the fuel-air mixture. The actual temperature rise is taken into account through use of an efficiency factor which is empirically derived from both rig and engine tests of the burner.

The efficiency characteristics used in the simulation were applied to the heat addition computations of the primary zone. The efficiency was described in curve form as illustrated schematically in Figure A-8 where

$$\eta_B = f(f/a, P_{T4.0}, T_{T4.0}, K_{B\ EFF}) \qquad \text{(A26)}$$

The burner efficiency constant $K_{B\ EFF}$ is equal to 1.7 and has been determined experimentally from engine data.

Heat Addition

The primary zone heat addition process was simulated in terms of temperature rise. The temperature rise in the burner is determined using the enthalpy of formation of a compound. The technique used for chemical reactions is to determine the enthalpy of the reacting components, fuel and air in the burner, at some reference state (25°C(77°F) and 1 atmosphere pressure). The enthalpy of combustion is the enthalpy change when combustion occurs and the state of the elements is changed from the reactants to the final combustion

products. Since initially the reactants are not at the reference state, a computation must be performed to determine the enthalpy change required to attain the reference state. After the combustion has occurred, the enthalpy change effects a temperature change in the final combustion products.

The basic method of implementing the temperature rise is

$$H_{REACTANTS} + Q_{REACTANTS} = H_{PRODUCTS} \tag{A27}$$

where $H_{REACTANTS}$ is the energy required to cool or heat the reactants to the reference state.

$$H_{REACTANTS} = H_{4.0\ PRI} - H_{REFERENCE\ STATE\ REACTANTS} \tag{A28}$$

The energy release due to the combustion of the fuel is determined from the enthalpy of combustion for the fuel ($\bar{h}_{COMBUSTION}$), the fuel flowrate and the burner efficiency

$$Q_{RELEASE} = \eta_B W_f \bar{h}_{COMBUSTION} \tag{A29}$$

The energy release plus the energy required to cool or heat the reactants is used to increase the temperature of the products of combustion. The enthalpy of the products can be determined by

$$H_{5.0\ PRI} = Q_{RELEASE} + H_{REACTANTS} + H_{REFERENCE\ STATE\ PRODUCTS} \tag{A30}$$

The temperature rise is determined from the enthalpy and the pressure specific heat coefficient for the products. The pressure specific heat coefficient is a function of temperature therefore an integration process must be used to determine the final temperature of the products of combustion as shown

$$h_{5.0\ PRI} = H_{5.0\ PRI}/(W_{a4.0\ PRI} + W_f) = \int_{25°C\ (77°)}^{T_{T5.0\ PRI}} CpdT \tag{A31}$$

where

$$Cp = f(T_{T5.0\ PRI}) \tag{A32}$$

An iteration is performed whereby a value of $T_{T5.0\ PRI}$ is determined such that the integrated enthalpy is equal to $h_{5.0\ PRI}$.

Pressure Drop

The total pressure drop through the primary side of the burner can be attributed to three sources. One is due to heat addition. The others can be attributed to friction losses and losses due to airflow through the burner liner. The entire pressure loss, however, is calculated through the use of one equation which is:

$$\Delta P_B = P_{T4.0}\, K_B \left(\frac{W_{a\ PRI}\sqrt{T_{T4.0}/T_{STAND}}}{P_{T4.0}/P_{STAND}} \right)^2 \qquad \text{(A33)}$$

The constant K_B is determined experimentally.

Mixing

The primary and secondary zones of the burner are mixed at the exit of the burner. The mixing routine assumes homogeneous mixing of the mass, momentum and energy. In equation form it is

mass $$W_{a\ PRI} + W_{a\ SEC} = W_{a5.0} \qquad \text{(A34)}$$

momentum

$$W_{a\ PRI}\, v_{PRI} + P_{S\ PRI}\, A_{PRI} + W_{a\ SEC}\, v_{SEC} + P_{S\ SEC}\, A_{SEC} = W_{a5.0}\, v_{5.0} + P_{S5.0}\, A_{5.0} \qquad \text{(A35)}$$

energy $$W_{a\ PRI}\, h_{B\ PRI} + W_{a\ SEC}\, h_{B\ SEC} = W_{a5.0}\, h_{B5.0} \qquad \text{(A36)}$$

A further constraint which must be satisfied is that the static pressures at the exit of the two streams to be mixed must be equal. That is

$$P_{S\ PRI} = P_{S\ SEC} \qquad \text{(A37)}$$

Turbine

Description

The TF30-P-3 engine uses a single stage high turbine to power the high compressor and a three stage turbine to power the fan-low compression system. The turbines are shown in Figure A-1 with the high turbine between stations 5.0 and 6.0 and the low turbine between stations 6.0 and 6.9.

Simulation

The performance of the low and high turbines is determined in the same manner. Individual stage characteristics for the turbines were not available, therefore it was necessary to represent each turbine from overall performance data. The turbine model accounted for the effects of efficiency, turbine cooling air, and power extraction.

The low and high turbine computations are the same therefore the following description will describe the high turbine performance but is applicable to the low turbine as well.

Efficiency

The required turbine shaft power is determined from the compressor requirement, power extracted for external uses, and power required for acceleration or deceleration of the rotor. The rotor acceleration or deceleration will be discussed under the section entitled "Rotor Dynamics". The required power can be summed up as

$$HP_{Tu} = HP_{COMPRESSOR} + HP_{EXTERNAL} + HP_{ROTOR} \qquad \text{(A38)}$$

The specific work requirement from the turbine is a function of the power and the turbine gas flow W_{Tu} as follows

$$\Delta h_{Tu} = \frac{K_{Tu}\, HP_{Tu}}{W_{Tu}} \qquad \text{(A39)}$$

where K_{Tu} is the conversion factor for converting power to an energy term.

The turbine gas flow is determined from the mixed burner exit flow and accounts for the turbine cooling air.

The efficiency computation uses an efficiency map for determining a reference efficiency and applies modifications to account for Reynolds effects and an efficiency scale factor.

A schematic of the efficiency map is shown in Figure A-9. The map is entered with an actual work term and a corrected speed term. The constants $C1_{Tu}$ and $C2_{Tu}$ in Figure A-9 are defined as

$$C1_{Tu} = \frac{(\Delta h/N^2)_{REFERENCE}}{(\Delta h/N^2)_{DESIGN}} \tag{A40}$$

and

$$C2_{Tu} = \frac{(N/\sqrt{T_{T5.0}})_{REFERENCE}}{(N/\sqrt{T_{T5.0}})_{DESIGN}} \tag{A41}$$

The efficiency map is a generalized map which can be used for a variety of engines. The reference values in equations (A40) and (A41) are a constant value for the generalized map and are determined when the map is generated. The design values are associated with the particular engine for which the generalized map is being used and allow the generalized map to be used for the TF30-P-3 simulation. In effect, the constants scale the efficiency map to simulate various turbine sizes.

The output of the reference efficiency map is an ideal work term which can be represented as shown in Figure A-9. The reference efficiency is

$$\eta_{Tu\ REF} = \frac{(C1_{Tu}\ \Delta h_{Tu}/N^2)_{ACTUAL}}{(C1_{Tu}\ \Delta h_{Tu}/N^2)_{IDEAL}} \tag{A42}$$

The efficiency correction for Reynolds effects and scaling are applied to the reference efficiency to determine the turbine efficiency

$$\eta_{Tu} = \eta_{Tu\ REF} + \Delta\eta_{Tu\ REYNOLDS} + \Delta\eta_{Tu\ SCALE\ FACTOR} \tag{A43}$$

Turbine Pressure Ratio

The turbine pressure ratio is determined from the enthalpy entering the turbine and the ideal power extracted from the turbine. The enthalpy at the high turbine entrance $h_{Tu5.0}$ is determined from the exit conditions of the burner. The ideal enthalpy at the exit of the turbine is determined from the enthalpy at the entrance, the actual enthalpy drop in the turbine, and the turbine efficiency.

$$(h_{Tu6.0})_{IDEAL} = h_{Tu5.0} - \Delta h_{Tu}/\eta_{Tu} \tag{A44}$$

The turbine pressure ratio is determined from the relative pressure at constant entropy at stations 5.0 and 6.0. The relative pressures are determined by

$$P_{RELATIVE\ 5.0} = f(h_{Tu5.0},\ f/a) \tag{A45}$$

$$P_{RELATIVE\ 6.0} = f\left[(h_{Tu6.0})_{IDEAL},\ f/a\right] \tag{A46}$$

The turbine pressure ratio is equal to the ratio of the relative pressures or

$$PR_{Tu} = \frac{P_{T5.0}}{P_{T6.0}} = \frac{P_{RELATIVE\ 5.0}}{P_{RELATIVE\ 6.0}} \tag{A47}$$

Turbine Area

The turbine area is calculated by

$$A_{Tu} = \left(\frac{W_{a5.0}\sqrt{T_{T5.0}}}{P_{T5.0}\,FP_{CRITICAL}}\right)\left(\frac{FP_{CRITICAL}}{FP}\right) \tag{A48}$$

The critical flow parameter, $FP_{CRITICAL}$, is determined from standard gas dynamic relationships for a choked nozzle. The ratio of critical flow parameter to turbine flow parameter is obtained from a flow parameter ratio map. A schematic of the map is presented in Figure A-10. The input to the map is a pressure ratio function and a speed function. The constants $C3_{Tu}$ and $C4_{Tu}$ are defined as

$$C3_{Tu} = \frac{(N/\sqrt{T_{T5.0}})_{REFERENCE}}{(N/\sqrt{T_{T5.0}})_{DESIGN}} \tag{A49}$$

and

$$C4_{Tu} = \frac{(1.0 - 1.0/PR_{Tu})_{REFERENCE}}{(1.0 - 1.0/PR_{Tu})_{DESIGN}} \tag{A50}$$

The definitions of the reference and design values for the flow parameter ratio map are the same as previously stated for the efficiency map.

Exhaust Nozzle

Description

The TF30-P-3 exhaust nozzle is a variable area device which is used to control the airflow through the engine. The nozzle is shown in Figure A-1. The nozzle can operate either choked or unchoked.

Simulation

Two curves are used to define the operation of the nozzle. The discharge coefficient (Cd) curve, shown schematically in Figure A-11, is a function of the nozzle pressure ratio. The discharge coefficient is defined as the ratio of the effective area to the geometric area. A flow parameter ratio curve, shown schematically in Figure A-12 is also a function of the nozzle pressure ratio. The geometric area is determined by

$$A_{10.0} = \frac{W_{a10.0}\sqrt{T_{T10.0}}}{Cd\ P_{T10.0}} \left(\frac{FP_{CRITICAL}}{FP}\right) \left(\frac{1.0}{FP_{CRITICAL}}\right) \qquad \text{(A51)}$$

where the critical flow parameter ($FP_{CRITICAL}$) is the flow parameter determined for a choked nozzle. The critical flow parameter is a function relationship as shown

$$FP_{CRITICAL} = f(R, \gamma_{10.0}) \qquad \text{(A52)}$$

Control

Description

The TF30-P-3 fuel control is a droop slope control which uses high rotor speed (N2), power lever angle (PLA), and burner pressure (P_B) to regulate the fuel flow (W_f) of the engine.

Simulation

The simulation of the control schedule uses a curve of the form shown in Figure A-13.

The PLA input determines the position of the droop slope. The N2 input determines the W_f/P_B output from the control along the droop slope. The W_f/P_B output is multiplied by P_B to obtain W_f output. If the fuel flow is more than required to operate the engine at steady state, excess power is available at the turbines and the engine accelerates. As the engine accelerates and N2 increases, W_f/P_B decreases along the droop slope until the steady state operating conditions are reached. Deceleration of the engine occurs if the W_f/P_B is too low for the N2 speed. The series of steady state operating points for different droop slopes defines a steady state operating line on the control schedule. An accel schedule is used to

limit the rate of acceleration of the engine and a deceleration schedule is used to limit the rate of deceleration of the engine. These limits are shown on Figure A-13.

Ducts

Description

Five sections of the flowpath in the engine are simulated. These are: the fan duct which extends from the fan bypass exit to the exhaust nozzle, the core duct which extends from the core splitter to the exhaust nozzle, the turbine exhaust duct which extends from the low turbine exit to the core splitter, the diffuser duct which extends from the high compressor exit to the burner entrance, and the secondary zone of the burner (burner bypass). No augmented operation was investigated during this program, therefore, only the pressure loss characteristics required simulation.

Simulation

The pressure loss was calculated as a function of the duct mach number as shown.

$$\frac{\Delta P_{DUCT}}{P_{DUCT}} = K_D M^2 \qquad \text{(A53)}$$

The constant K_D is a value which was determined from experimental data.

DYNAMIC EQUATIONS

This section describes the equations used to simulate dynamic operation of the engine. The equations describe the dynamics of rotor speed transients, exhaust stream mixing, unsteady compressor aerodynamics, and fluid flow.

Rotor Dynamics

Simulation of engine transient operation requires accounting of the effects of rotor dynamics. Acceleration or deceleration of the rotors exists when the turbine horsepower either exceeds or is less than the required steady state level.

The basic formula used to determine the rotor speed changes is

$$HP_{ROTOR} = \frac{NI\ (dN/dt)}{\left(\frac{60}{2\pi}\right)^2 K_R} \tag{A54}$$

or rearranging

$$\frac{dN}{dt} = \left(\frac{HP_{ROTOR}}{NI}\right)\left(\frac{60}{2\pi}\right)^2 K_R \tag{A55}$$

Dynamic Mixing

Mixed flow turbofan engine simulations can use a mixing routine which forces an axial static pressure balance between airstreams at the exhaust mixing plane. Experience at Pratt & Whitney Aircraft indicates that this approach is sufficiently accurate for simulation of steady state operation and engine power transients.

Simulation of engine high frequency operation requires a dynamic mixing routine. The dynamic mixing routine used in the modified engine simulation assumes that the inertial and viscous characteristics of the gas flow induce a lag in the static pressure balance at the mixing plane. At the mixing plane, the dynamic mixing routine separates the duct and core airstreams. A static pressure imbalance is allowed to occur between the two airstreams during a transient. The pressure imbalance changes the area split at the exit of the two streams in a direction which tends to equalize the pressures. The exit area of each airstream and the static pressure imbalance are related by the following equations:

$$A_{bypass} = A_{bypass\ initial\ value} + GAIN \int (P_{S\ bypass} - P_{S\ core})\, dt \tag{A56}$$

$$A_{core} = A_{total} - A_{bypass} \tag{A57}$$

The magnitude of the gain level in the above equation was emperically set to give frequency response characteristics similar to engine test results.

Unsteady Compressor Aerodynamics

The compressor unsteady aerodynamics account for deviations in rotor and stator lift characteristics which occur during operation in a dynamic flow field. The unsteady effects are computed by applying a first order lag to the quasi steady entropy change across the rotor or stator. The quasi steady entropy change is computed from the equation.

$$\Delta s = \frac{\gamma}{\gamma - 1} R \ell n TR_T - R \ell n PR_T \tag{A58}$$

where TR_T and PR_T are the total temperature and total pressure ratios defined by the rotor or stator characteristics. The quasi steady entropy change is modified by a time constant which is a function of the rotor or stator chord length and the axial velocity at the stator or rotor exit.

$$\tau = \frac{\text{chord length}}{\text{Axial velocity}} \tag{A59}$$

The dynamic entropy change is obtained by applying the time constant as shown below.

$$\Delta s \rightarrow \boxed{\frac{1}{\tau s + 1}} \rightarrow \Delta s' \tag{A60}$$

Equation (A58) is rewritten to solve for the dynamic pressure ratio

$$PR'_T = e^{\left(\frac{\gamma}{\gamma - 1} \ell n TR_T - \frac{\Delta s'}{R}\right)} \tag{A61}$$

where the temperature ratio is held constant at the quasi steady value.

Fluid Flow Dynamic Equations

The general relationships which describe one-dimensional fluid flow phenomena recognize three basic properties. These are the mass of the fluid, its momentum and its energy. These properties are conservative in that a change to any of them within the boundaries of a system must be the result of quantities passing through the boundaries. In the most basic terms, then, the relationships can be expressed as:

$$\Delta \text{Mass}_{CV} = \text{Mass}_{in} - \text{Mass}_{out} \tag{A62}$$

$$\Delta \text{Momentum}_{CV} = \text{Momentum}_{in} - \text{Momentum}_{out} \tag{A63}$$

$$\Delta \text{Energy}_{CV} = \text{Energy}_{in} - \text{Energy}_{out} \tag{A64}$$

where:

CV refers to a bounded system known as a control volume or finite element; in, refers to quantities entering the finite element; out, to quantities leaving the finite element.

Δ refers to an incremental change

The introduction of the independent variable time (t), allows the formulation of equations that describe the properties within the finite element at a particular value of time.

$$m_t = \text{Mass}_t = \dot{\text{Mass}}_{t-\Delta t} + \frac{\Delta \text{Mass}_{in}\,\Delta t}{\Delta t} - \frac{\Delta\ \text{Mass}_{out}\ \Delta t}{\Delta t} \tag{A65}$$

$$P_t = \text{Momentum}_t = \text{Momentum}_{t-\Delta t} + \frac{\Delta \text{Momentum}_{in}\,\Delta t}{\Delta t} - \frac{\Delta \text{Momentum}_{out}\,\Delta t}{\Delta t} \tag{A66}$$

$$E_t = \text{Energy}_t = \text{Energy}_{t-\Delta t} + \frac{\Delta \text{Energy}_{in}\,\Delta t}{\Delta t} - \frac{\Delta \text{Energy}_{out}\,\Delta t}{\Delta t} \tag{A67}$$

As Δt approaches zero, the right hand sides of these equations are the integrals with respect to time of the time derivatives of the incoming and outgoing properties. These are expressed as follows:

$$m = \int \partial m / \partial_t \bullet\ dt \tag{A68}$$

$$P = \int \partial P / \partial_t \bullet dt \tag{A69}$$

$$E = \int \partial E / \partial_t \bullet dt \tag{A70}$$

At this point, it is recognized that the solutions obtained must be in terms of the parameters with which fluid systems are normally identified. These are pressure, temperature, density and velocity. First, formulas are presented for the time derivatives of the three basic properties at the boundaries of the system. This will be followed by formulas for the quantities of the properties within the finite element at a particular time.

With reference to Figure A-14, a representation of the geometry of a typical finite element, the time derivatives of the properties, either incoming and outgoing, are given by:

$$\frac{\partial m}{\partial t} = \rho A v \equiv W \tag{A71}$$

$$\frac{\partial P}{\partial t} = \frac{\partial (mv)}{\partial t} = \frac{v\partial m}{\partial t} + \frac{m\partial v}{\partial t} = vW + \Sigma F \tag{A72}$$

$$\frac{\partial E}{\partial t} = h_T W \tag{A73}$$

where:

$$h_T = \int Cp\, dT + 0.5\, \rho v^2 = \int Cp\, dT_T \tag{A74}$$

The mass derivative is the density times the area perpendicular to the flow direction times the distance travelled by the fluid per time differential. This latter quantity is the velocity of the fluid. The time rate of change of momentum consists of two terms, the first one describing the change in momentum due to mass transfer and the second one consisting of the summation of forces on the fluid in the direction of the flow. The second term represents the application of Newton's second law to the finite element. The energy derivative is expressed in terms of the total enthalpy which is the sum of the specific kinetic energy of the fluid and the specific potential, or thermal, energy contained within the fluid. The specific enthalpy is multiplied by the flow to obtain the time rate of change of energy at the boundary.

At this point, the time derivatives of mass, momentum and energy have been identified in terms of the parameters usually associated with fluid flow. In particular, these quantities have been defined at the boundaries of a finite element or control volume assuming that the flow field is one-dimensional. Spatial integrals which define the quantities of mass, momentum and energy which lie within the boundaries of a finite element are given by:

$$m = \int_{CV} \rho dV = \int \rho A dL \tag{A75}$$

$$P = \int_{CV} \rho v dV = \int \rho A v dL \tag{A76}$$

$$E = \int_{CV} 0.5 \rho v^2 dV + \int_{CV} \rho Cv T dV = \int [0.5\, v^2 + Cv\, T]\, \rho A dL \tag{A77}$$

A basic assumption of our implementation of the finite element technique is that the parameters of the element vary in a linear fashion from one side to the other. These formula for the spatial variations in the general parameter are:

$$p = p_{in} + \left(\frac{p_{out} - p_{in}}{\Delta L}\right) L \qquad \text{(A78)}$$

where L varies from 0 to ΔL across the element. This formula is applied to the variations in pressure, temperature, density, area and velocity across the element.

Substitution of these equations into the spatial integrals allow their evaluation yielding the following functions for the properties within the finite element.

$$m = f(\rho, A, \Delta L) \qquad \text{(A79)}$$

$$P = f(\rho, A, v, \Delta L) \qquad \text{(A80)}$$

$$E = f(\rho, A, v, T, \Delta L) \qquad \text{(A81)}$$

One item must still be defined. That is the sum of the forces on the fluid exerted by its surroundings in the flow direction (ΣF), which appears in the equation for the time rate of change of momentum. Again with reference to Figure A-14, it can be seen that the geometry of the finite element plays a role in the assessment of the forces exerted on the fluid. The boundaries through which flow passes are assumed to be perpendicular to the flow direction. The walls of the duct form the other boundary of the element. The total force consists of two parts; the force exerted by the fluid outside of the element and the force exerted by the walls on the fluid inside the element. The first term is simply the pressure times the flow area at the boundary. In the absence of any area variation across the element or friction, there are no body forces exerted by the walls in the flow direction.

The sum of forces on the fluid within the finite element is then:

$$\Sigma F = P_{in} A_{in} - P_{out} A_{out} \qquad \text{(A82)}$$

Up to this point, the discussion has been limited to one-dimensional flow in ducts without considering the changes to the properties imposed by external mechanisms; in particular, changes due to the forces on the fluid exerted by the turbo-machinery and the rate of energy transfer to the fluid in the form of mechanical work. Denoting these parameters as:

F' - force on the fluid due to the mechanical components

$\frac{dW}{dt}$ - rate of mechanical work performed on the fluid by the mechanical components

the spatial integrals of Equations A75 through A77, define the three equations which govern the fluid flow within a one dimensional finite element. These equations can be written as:

$$m = (2\rho_{in} A_{in} + 2\rho_{out} A_{out} + \rho_{in} A_{out} + \rho_{out} A_{in})\,\Delta L/6 = \int (W_{in} - W_{out})\,dt \tag{A83}$$

$$P = [(3A_{in} + A_{out})\rho_{in} v_{in} + (A_{in} + 3A_{out})\rho_{out} v_{out} + (A_{in} + A_{out})(\rho_{in} v_{out} + \rho_{out} v_{in})]\,\Delta L/12 = \int (W_{in} v_{in} - W_{out} v_{out} + P_{in} A_{in} - P_{out} A_{out} + F')\,dt \tag{A84}$$

$$E = [v_{in}^2 (A_{in}(\rho_{in}/5 + \rho_{out}/20) + A_{out}(\rho_{in}/20 + \rho_{out}/30)) + v_{out}^2 (A_{in}(\rho_{in}/30 + \rho_{out}/20) + A_{out}(\rho_{in}/20 + \rho_{out}/5)) + v_{in} v_{out} (A_{in}(\rho_{in}/10 + \rho_{out}/15) + A_{out}(\rho_{in}/15 + \rho_{out}/10))]\,\Delta L/2 + Cv[(3A_{in} + A_{out})\rho_{in} T_{in} + (A_{in} + 3A_{out})\rho_{out} T_{out} + (A_{in} + A_{out})(\rho_{in} T_{out} + \rho_{out} T_{in})]\,\Delta L/12 = \int [h_{T\,in} W_{in} - h_{T\,out} W_{out} + \frac{dW}{dt}]\,dt \tag{A85}$$

In evaluating the external force and energy derivative inputs to a finite element, a concept known as the actuator disc is employed. In this model, the turbomachinery is represented by a series of discs of negligible length across which total pressure and temperature change as a function of a specific component characteristic. The effect of these changes on the momentum and energy flux at the incoming boundary of the finite element is included by utilizing the parameters that result from the component characteristics in the calculation of the incoming momentum and energy derivatives. This concept is shown schematically in Figure A-15. The "in" station represents the inlet to the component while, at the "in'" station, conditions that would exist at the component exit in steady-state are assumed. Momentum and energy derivatives computed as a function of conditions at "in'" will include the effects of the turbomachinery components. On this basis, the expressions for the time derivatives of momentum and energy given in Equations (A84) and (A85) can be modified in the following manner:

$$W_{in'} v_{in'} + P_{in'} A_{in} \equiv W_{in} v_{in} + P_{in} A_{in} + F' \tag{A86}$$

$$h_{T\,in'} W_{in'} \equiv h_{T_{in}} W_{in} + \frac{dW}{dt} \tag{A87}$$

The modified engine simulation described the compressor characteristics on a row by row basis. Dynamically, the compressor operation was described using ten finite elements. The finite element configuration required that row performance characteristics be combined algebraically to establish the properties associated with the finite element actuator disc.

SOLUTION TECHNIQUE

Three ordinary differential equations (ODE's) which are applicable to a single finite element within an arbitrary flow field were defined in the previous section. This set can be applied to each of the elements of the system and results in a set of equations which, when solved simultaneously, will describe the flow field at any point in time, given the time history of the field up to that point and its current boundary conditions. The simulated response of the system is composed of a series of solutions at the discrete values of time required by the particular problem being studied. It must commence with a steady state solution which provides the required initial values of the properties.

The transient solution technique applies implicit solution methods directly to the ODE's. A simple trapezoidal numerical integration scheme is applied to the time derivatives of the properties (Equation A71-A73). This results in a set of non-linear algebraic equations which yield solutions at discrete values of time in an iterative manner.

The concept referred to above is generally known as a relaxation method. Relaxation methods rely on solving a set of implicitly defined relationships in an iterative manner. The solution method uses a set of independent variables which will permit computation of both the right hand and left hand sides of the set of governing equations (Equations A83 - A85). A solution is obtained when, for a particular set of boundary conditions, the value of all independent variables satisfy the equations.

In applying this method to the set of non-linear algebraic equations which are used to model the dynamic behavior of the flow field described by an arbitrary set of finite elements, a set of three variables describing conditions at the exit of each element must be chosen. Two of these must describe the state of fluid while the third must describe its motion. Pressure and temperature, either static or total, are chosen for the first two while mass flow or velocity is used for the third. This set of variables is sufficient to explicitly calculate both sides of the three equations and, hence, the three error terms associated with them. Additional pairs of independent variables and errors are used to implicitly define boundary conditions or constraints of the system that cannot be expressed explicitly. These include the flow areas in the turbines and at the exhaust nozzle. A sophisticated non-linear equation solver, utilizing a modified Newton-Raphson approach, operates on this set of independent variables and errors to achieve the required solutions.

There are several advantages associated with the use of implicit solution techniques. The most important of these is the improvement in execution time possible relative to explicit numerical integration techniques. In finite element models, the degree of improvement is a function of the number of elements used to represent the system. Explicit techniques require a time increment which approaches an order of magnitude smaller than the time to propagate a signal across the element. Implicit methods, because of their intrinsic computational stability, can tolerate any value of time increment. The selection of the proper one

is based purely on the required frequency content of the results. Typically, implicitly defined models achieve execution times ten times faster than their explicit counterparts for comparable accuracy.

Another significant, although often overlooked, advantage to implicit solution techniques is the ability to easily modify the boundary conditions of the problem. For instance, steady-state solutions are easily obtained by forcing the time derivatives of the fluid properties to zero. This is accomplished by automatically specifying the time derivatives to be the error terms. The set of independent variables remains unchanged. In a similar manner, the linearized partial derivatives used in the transfer function calculations are obtained by holding the fluid properties (Mass, Momentum and Energy) constant at their given base values while each of them are perturbated in turn. In this case, the error terms are the difference between the given values of the properties and those calculated from the model. Non-zero time derivatives result from each perturbation solution and are used to compute the required partial derivatives. The importance of this capability lies in the fact that the same computer program can be used for all of the different requirements without resorting to expensive and time-consuming recoding.

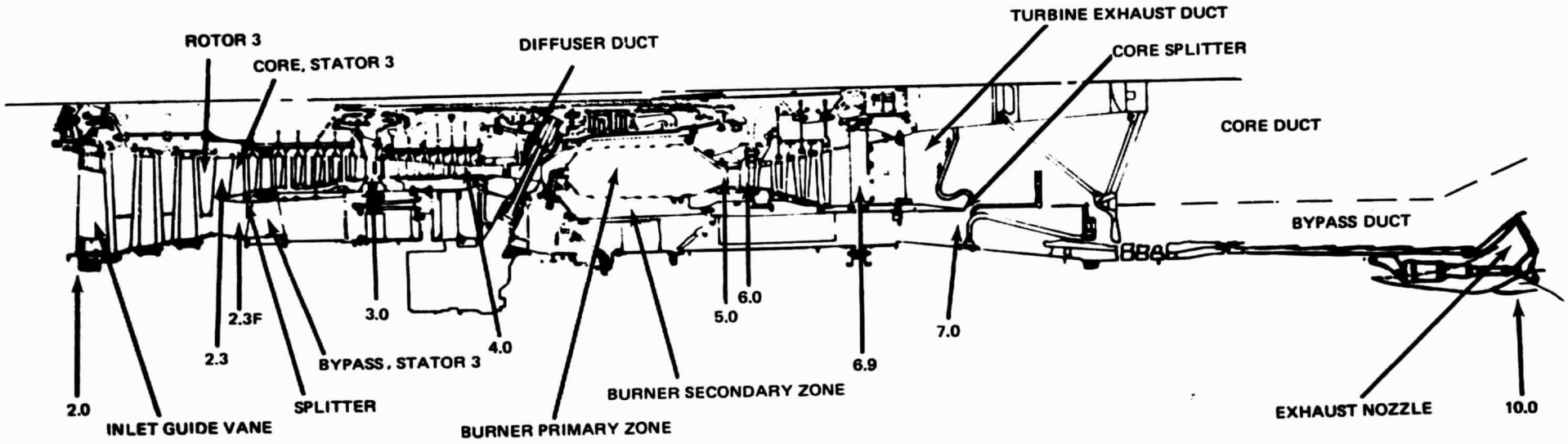

Figure A-1 Engine Station and Component Identification

Figure A-2 Flow Parameter Curve

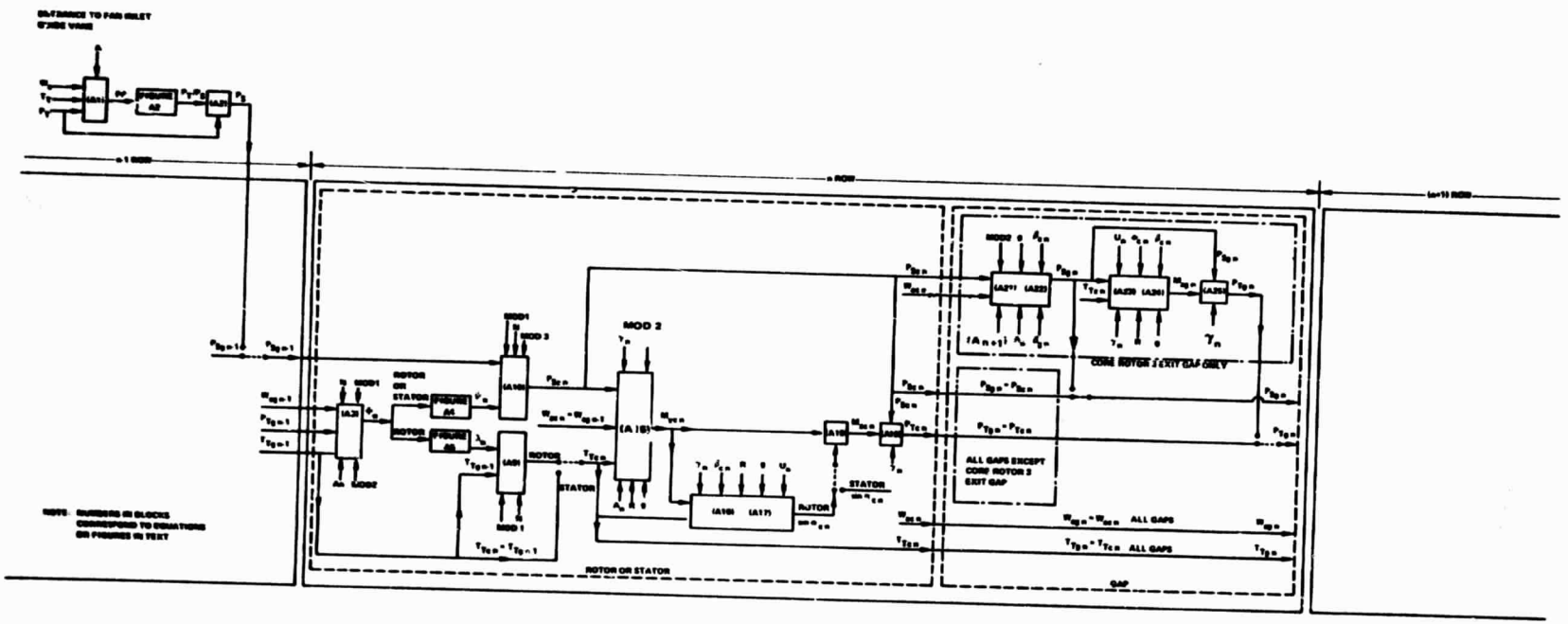

Figure A-3 Block Diagram for Simulation of Nth Compressor Row Steady State Performance

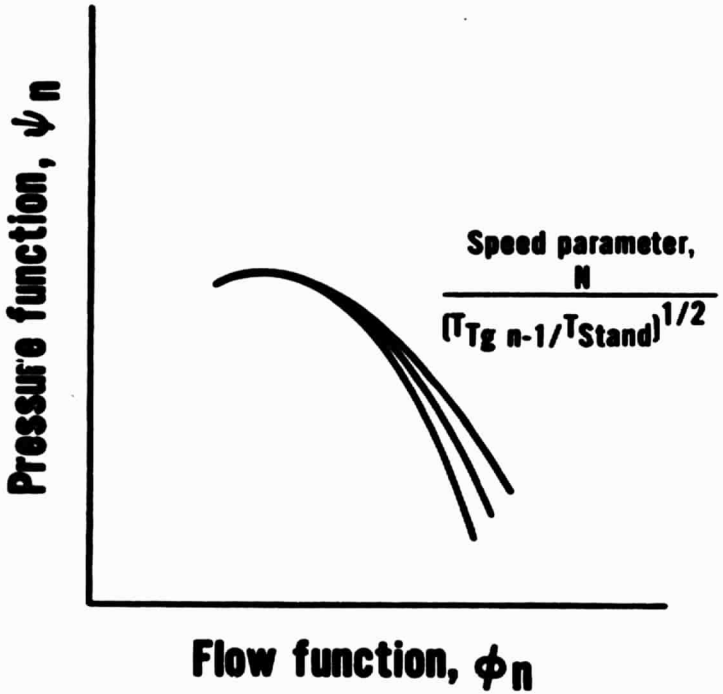

Figure A-4 Rotor and Stator Static Pressure Characteristics

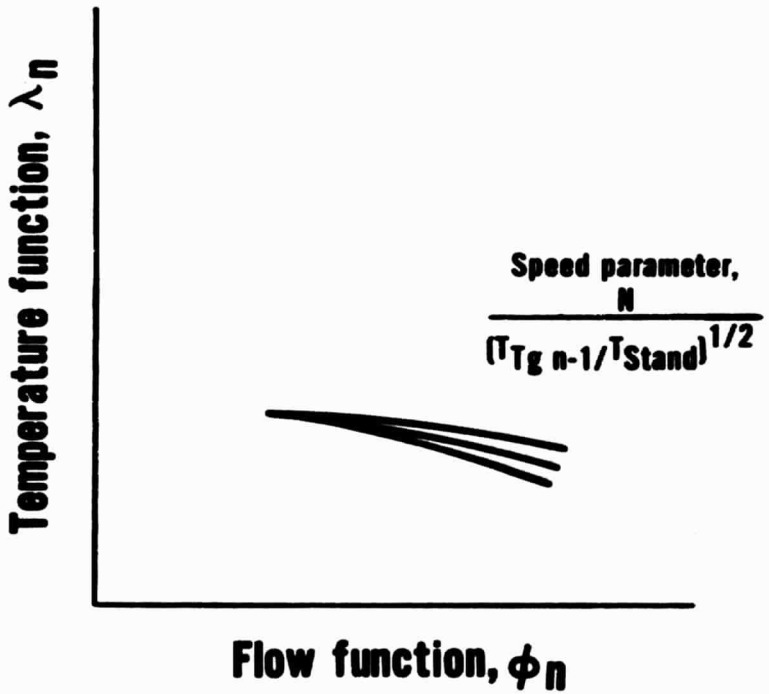

Figure A-5 Rotor Total Temperature Characteristics

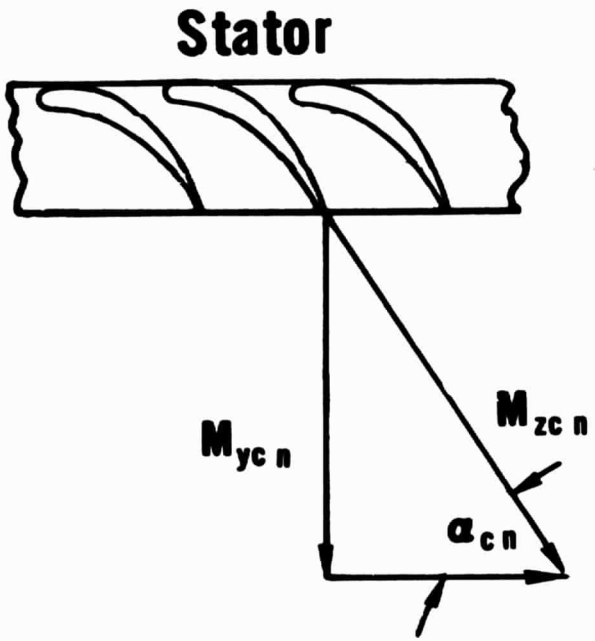

Figure A-6 Stator Exit Velocity Triangle

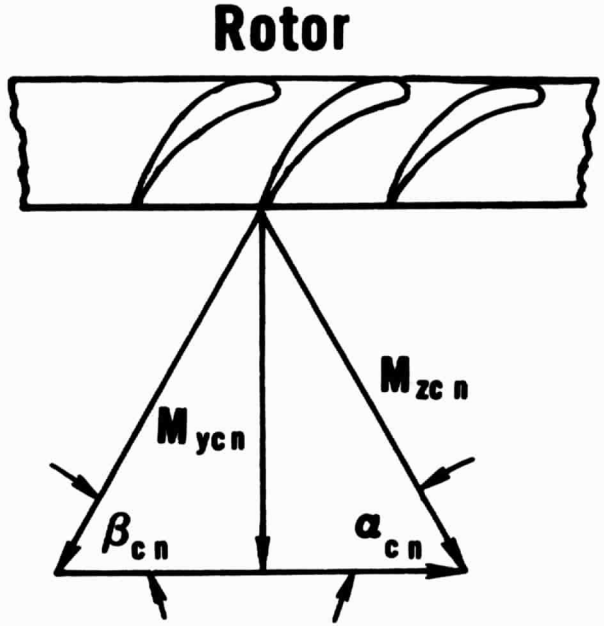

Figure A-7 Rotor Exit Velocity Triangle

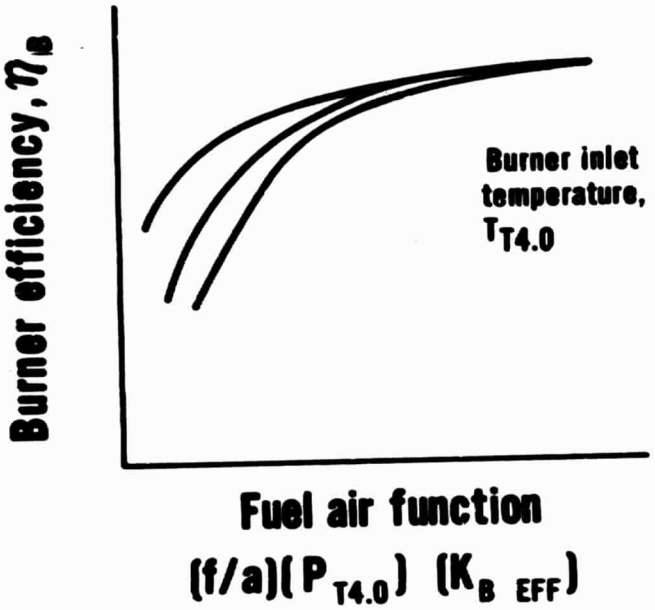

Figure A-8 Burner Efficiency Map

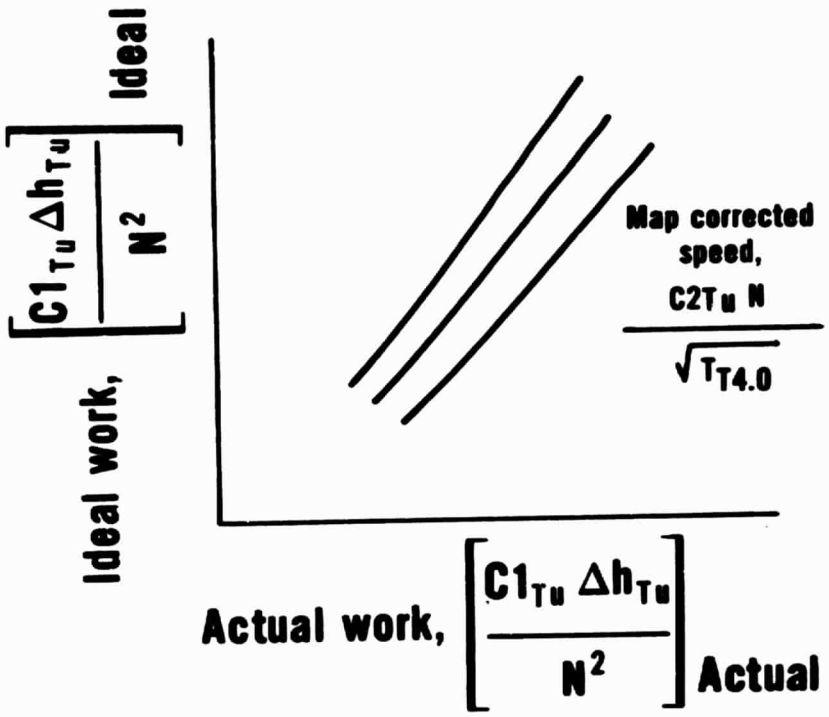

Figure A-9 Turbine Efficiency Map

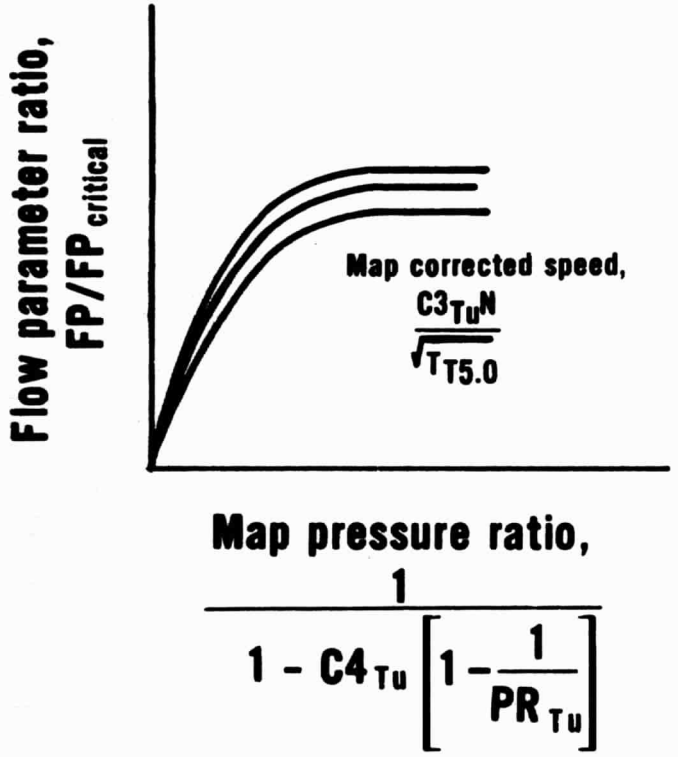

Figure A-10 Turbine Flow Parameter Map

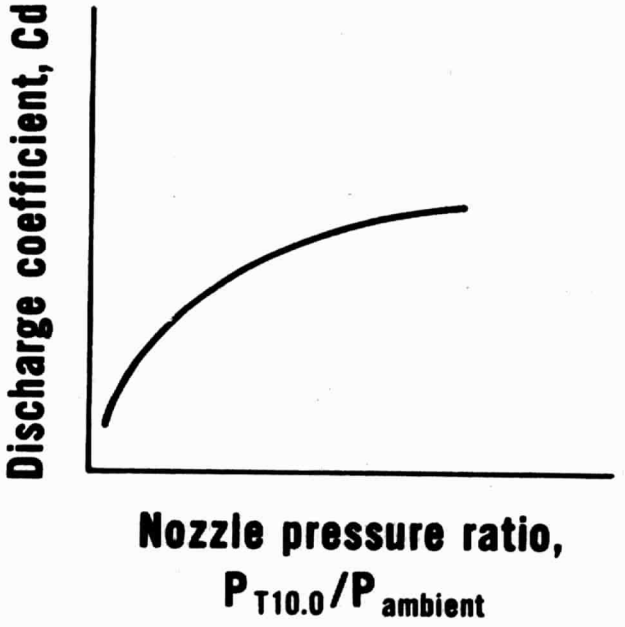

Figure A-11 Exhaust Nozzle Discharge Coefficient

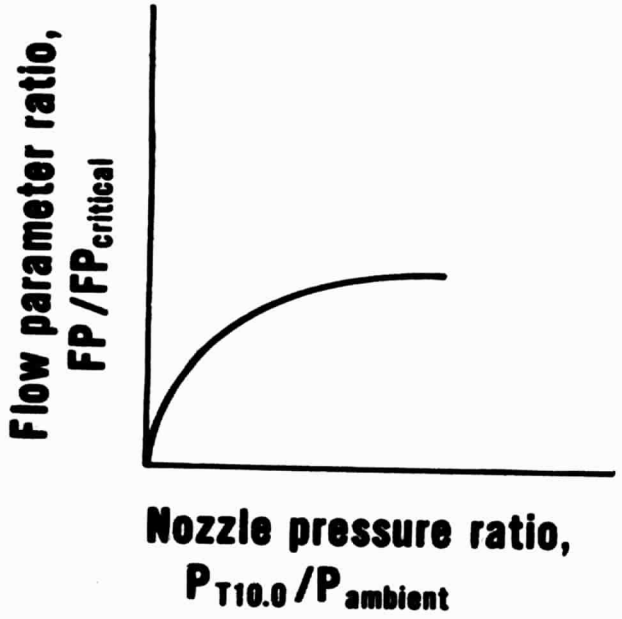

Figure A-12 Exhaust Nozzle Flow Parameter

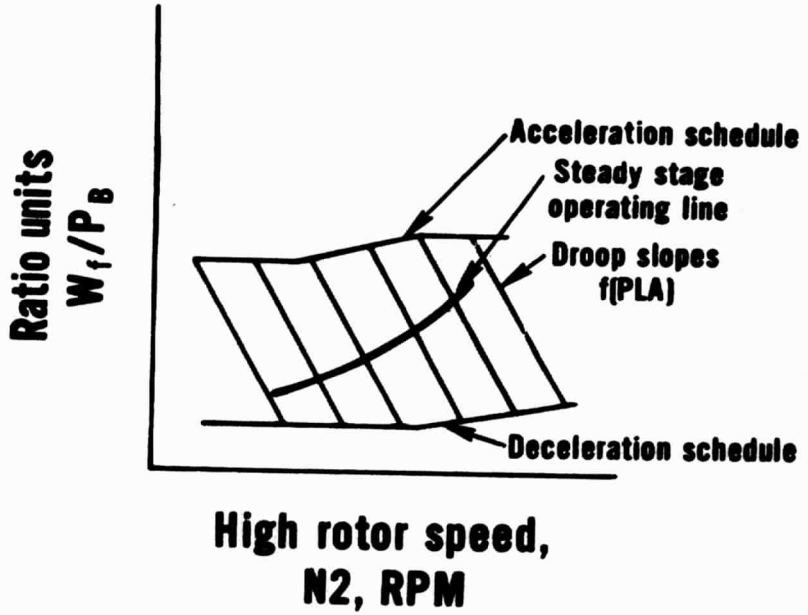

Figure A-13 Engine Control Schedules

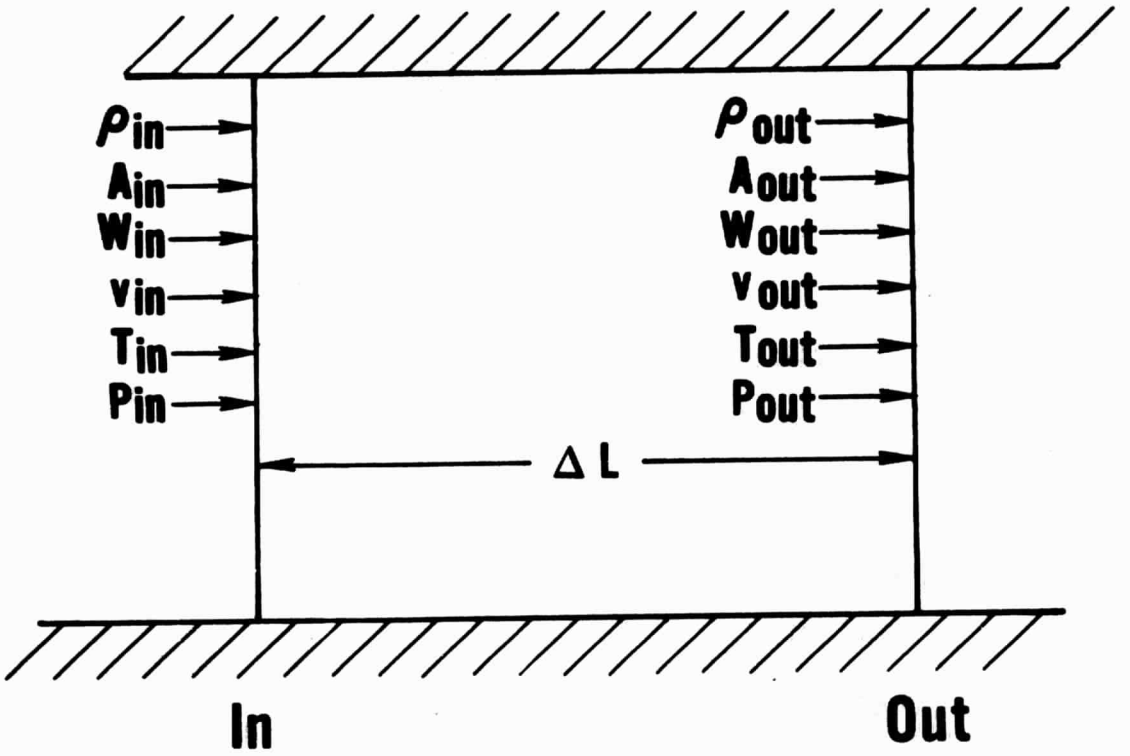

Figure A-14 Finite Element Representation

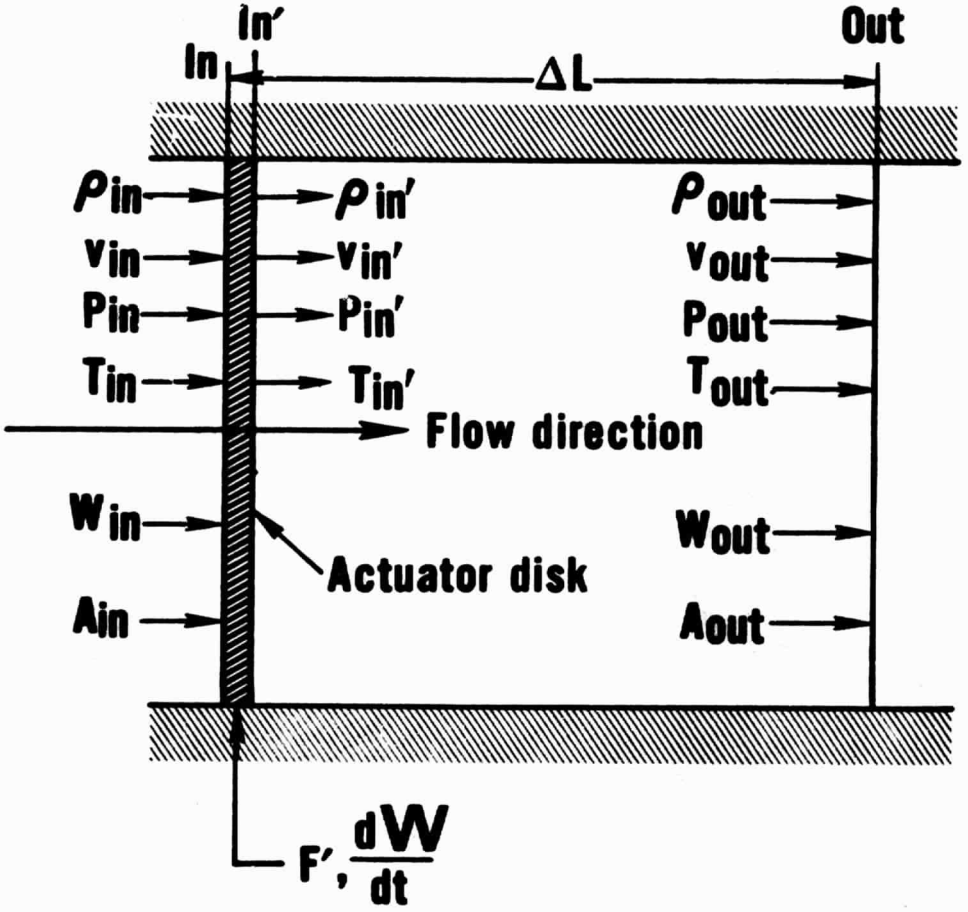

Figure A-15 Finite Element Representation Showing the Actuator Disc Concept

APPENDIX B

SIMULATION FREQUENCY RESPONSE

Frequency response characteristics were established for the engine and compression system simulations for the purpose of evaluating simulation dynamic characteristics. Three methods were used to determine the phase and gain characteristics of the simulations. These were: 1) linearized transfer functions, 2) step response and 3) discrete frequency response. In general, results obtained by analysis of simulation transients (step and discrete frequency) may differ from those obtained from transfer functions. Assuming that transients are confined to the linear range of the simulation, the difference is attributable to the nature of transfer function and transient solutions. Transfer function results are obtained from explicit solution of the system of linear equations derived from the simulation. The transfer function solution is exact in the sense that it contains no errors associated with numerical integration. Transient results do include the errors associated with numerical integration. The differences in results can be viewed as a measure of how well the transients reflect the dynamic characteristics of the simulation transfer functions.

In the process of obtaining the matrices of linear coefficients which were used to compute transfer functions, some observations were made which bear discussion. It was found that the transfer function frequency response results were sensitive to program iteration tolerances and the perturbation size of the input and state variables. The sensitivity was shown by large offsets in the frequency response curves, especially at the low frequency end of the spectrum. The offsets were essentially eliminated by perturbing the variables in both a positive and negative direction, instead of just one direction.A possible explanation for the improved results is that the errors associated with the iteration tolerances tended to cancel with the two directionally opposed perturbations. In addition, the directionally opposed perturbation effectively doubled the perturbation size at a fixed level of iteration tolerances.

The linear matrix coefficients derived from two cases using different perturbation sizes were examined and revealed that, although the frequency response characteristics were in agreement, the values of the coefficients were different. This indicated the relative consistency of the coefficients was more important than the levels. As a corollary, the low frequency effects noted above appeared to be a function of the relative values of the entire set of coefficients.

A study of the effects of iteration tolerance and pertubation size on frequency response accuracy and program execution time was made using the compression system simulation. The results of the study are shown on Figure B-1. The figure shows the effects of tolerance size and perturbation size in terms of the percentage error in gain at 0.1 hertz and case execution time in units of minutes and seconds. The ratio of perturbation to tolerance size is also shown for each case. Three trends in results are shown by the figure. First, the program execution time increases as the iteration tolerances are reduced. This results from the requirement to make more iterative passes to satisfy solution tolerances. Second, the

frequency response accuracy improves as the perturbation to tolerance ratio increases. As the ratio increases, the influence of the errors introduced by iteration tolerances is dimished-ed. Third the perturbation size reaches as optimum with respect to frequency response accuracy. The perturbation size must be large enough to resolve the characteristics of the system, but small enough to remain within the linear range of the system.

A final observation is made on the basis of experience gained from computing transfer functions for the compression system and engine simulations. The difficulty of computing transfer functions appeared to correlate with the non uniformity of dynamic element sizing. Results of the reduced order compression system investigation showed two cases where not all of the iterations were completed within the ranges of input tolerances. The dynamic configuration for both cases contained elements of non uniform sizing. The computation of transfer functions for the modified engine simulation was also found to be difficult and required linearization of the performance characteristics and scaling of tolerances to obtain marginally satisfactory results. The engine simulation was again non-uniform in element sizing. The non uniformity was a consequence of introducing the modified compression system model into the engine simulation.

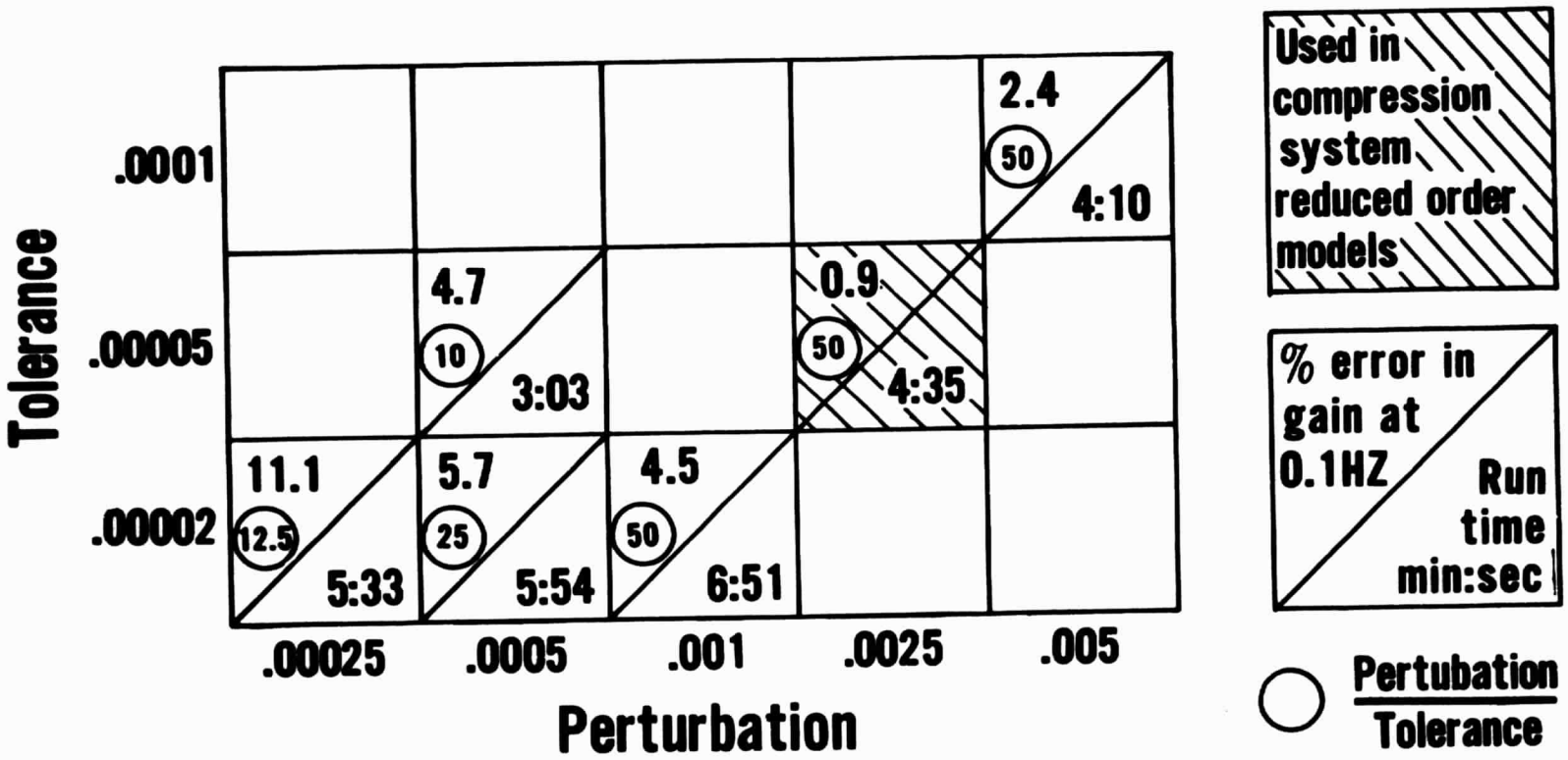

Figure B-1 Summary of Transfer Function Pertubation Size and Tolerance Study

LIST OF SYMBOLS

a	Constant
A	Area, cm^2; in^2
A	System matrix
b	Constant
B	Input matrix
BPR	Bypass Ratio, bypass airflow/core airflow
c	Constant
C	Output matrix
C1, C2, C3, C4	Constants
Cd	Exhaust nozzle discharge coefficient
Cp	Specific heat at constant pressure, J/(kg)(K); Btu/(lbm) (°R)
C_{PR}	Compressor map pressure ratio at intersection of $\overline{m}$ lines
Cv	Specific heat at constant volume, J/(kg)(K); Btu/(lbm) (°R)
C_{WAC}	Compressor map corrected airflow at intersection of $\overline{m}$ lines
db	Decibels, 20 log (output/input)
DT	Computer simulation time increment, seconds
D	Output/input direct coupling matrix
e	Base of natural system of logarithms
E	Energy, (kg) $(cm^2)/sec^2$; (lbm) $(in^2)/sec^2$
f/a	Fuel-air ratio
F	Forces, N; lbf
F′	Mechanical forces, N; lbf
FP	Flow parameters, (Kg) $(K)^{1/2}/(sec^2)$ (N); (lbm)$(°R)^{1/2}$/(sec)(lbf)
g	Gravitational constant, 1(Kg)(m)/(N)(sec^2); 32.17(lbm)(ft)/(lbf)(sec^2)
h	Specific enthalpy, J/Kg; Btu/lbm
H	Total enthalpy; J/sec; Btu/sec
HP	Power, W; Horsepower
K_B	Burner pressure loss coefficient, sec^2/Kg^2; sec^2/lbm^2
K_D	Duct pressure loss coefficient
I	Moment of inertia, (N)(m)(sec^2); (lbf)(Ft)(sec^2)
ID	Inside diameter, cm; in

LIST OF SYMBOLS (Cont'd)

IGV	Inlet guide vane
K_m	Compressor modifier coefficient
K_R	Conversion constant, 1(N)(m)/(sec)(W); 550(ft)(lbf)/(sec) (horsepower)
K_{Tu}	Horsepower to energy conversion factor, 1J/sec; 0.707 Btu/sec
L	Distance, cm; in
ΔL	Element length, cm; in
m	Mass, Kg; lbm
$\bar{m}$	Compressor map "m" line
M	Mach number
n	Stage number designation
N	Rotational speed, RPM
N1	Low rotor speed, RPM
N2	High rotor speed, RPM
OD	Outside diameter, cm; in
ODE	Ordinary differential equation
OP1	Operating point at $N1/\sqrt{\theta_{T2.0}}$ approximately equal to 8600 RPM
OP2	Operating point at $N1/\sqrt{\theta_{T2.0}}$ approximately equal to 7600 RPM
p	General designation of finite element parameter
P	Pressure, N/cm^2; lbf/in^2
P	Momentum, (Kg)(cm)/sec; (ft)(lbm)/sec
PLA	Power lever angle, degrees
PR	Pressure Ratio
P_{STAND}	Standard pressure, 10.1325 N/cm^2; 14.696 lbf/in^2
Q	Energy, J/sec; Btu/sec
R	Gas constant, 287 (N)(m)/(Kg)(K); 53.3 (lbf)(ft)/(lbm)(°R)
R3	Rotor three
s	Entropy, J/g; Btu/lbm
s	LaPlace Operator
S3	Stator three
t	Time, seconds

LIST OF SYMBOLS (CONT'D)

T	Temperature, K; °R
TR	Temperature ratio
T_{STAND}	Standard temperature, 288.2K; 518.7°R
u	Input vector
U	Mean rotor speed, cm/sec; in/sec
v	Velocity, cm/sec; in/sec
V	Volume, cm^3; in^3
W	Weight flow, Kg/sec; lbm/sec
W	Work, J; Btu
WAC	Corrected airflow, Kg/sec; lbm/sec
WAE	Engine core airflow, Kg/sec; lbm/sec
WAT	Total airflow, Kg/sec; lbm/sec
x	State vector
$\dot{x}$	dx/dt
X	Independant variable
y	Output vector
α	Flow angle, degrees
β	Rotor metal exit angle, degrees
Δ	Incremental change
δ	Ratio of total pressure to standard pressure
η	Efficiency
γ	Specific heat ratio
λ	Temperature function
π	3.14159
ϕ	Flow function Kg/(sec)(cm^2); lbm/(sec)(in^2)
ψ	Pressure function
ρ	Density, Kg/cm^3; lbm/ft^3
τ	Time constant, sec
θ	Ratio of total temperature to standard temperature

LIST OF SYMBOLS (CONT'D)

Subscripts

a	Airflow
B	Burner
c	Compressor stator or rotor exit
CV	Control volume
D	Duct
DES	Design
EFF	Efficiency
f	Fuel
g	Compressor gap exit
in	Entrance of finite dynamic element
in′	Exit of actuator disk
n	Stage number designation
out	Exit of finite dynamic element
PRI	Primary
ΔP	Pressure loss
R	Rotor
REF	Reference
S	Static
STAND	Standard
SEC	Secondary
T	Total
Tu	Turbine
t	Time
y	Axial direction
z	Flow direction
1	Time designation, seconds
2	Time designation, seconds
3	Time designation, seconds
2.0	Engine inlet
2.1	Fan first stator passage
2.3	Fan core exit
2.3F	Fan bypass exit

LIST OF SYMBOLS (CONT'D)

3.0	Low compressor exit
3.12	Twelfth stage stator passage
4.0	High compressor exit
5.0	Burner exit
6.0	High turbine exit
6.9	Low turbine exit
7.0	Turbine diffuser duct exit
7.0F	Fan bypass duct exit
10.0	Exhaust nozzle

REFERENCES

1) J.E. McAuley, "Effect of Dynamic Variations in Engine - Inlet Pressure on the Compressor System of a Twin - Spool Turbofan Engine," NASA TMX-2081, September 1970.

2) Robert C. Seidel, "Computer Programs for Calculation of Matrix Stability and Frequency Response from a State-Space System Description," NASA TMX-71581, July 1974.

3) Donald G. Shultz and James L. Melsa, "State Functions and Linear Control Systems," McGraw-Hill, Inc., Copywright 1967.

4) J.B. Kidd, T.E. Edgerton, C.F. Chen, "Transfer Function Synthesis in the Time Domain - An Extension of Levy's Method," IEEE Transactions on Education, June - September 1965.

5) R.W. King, J.A. Schuerman, and R.G. Muller, "Analysis of Distortion Data from TF30-P-3 Mixed Compression Inlet Test," NASA CR-2686, June 1976.